UNIVERSIDAD NACIONAL DE GENERAL SAN MARTIN
COMISION NACIONAL DE ENERGIA ATOMICA
INSTITUTO DE TECNOLOGIA
Prof. Jorge A. Sábato

Dinámica y conversión de energía en sistemas cuánticos forzados lentamente[(*)]

por Lic. Pablo G. Terrén Alonso

Directora

Prof. Dra. Liliana Arrachea

[(*)] **Tesis para optar al título de *Doctor en Ciencia y Tecnología mención Física***

República Argentina

2023

UNIVERSIDAD NACIONAL DE GENERAL SAN MARTIN
COMISION NACIONAL DE ENERGIA ATOMICA
INSTITUTO DE TECNOLOGIA
Prof. Jorge A. Sábato

Energy dynamics and energy conversion in quantum systems under slow driving[(*)]

by Lic. Pablo G. Terrén Alonso

Advisor

Prof. Dra. Liliana Arrachea

[(*)] Thesis submitted for the degree of Doctor in Science and Technology, Physics

República Argentina

2023

Contents

Chapter 1

Abstract

This thesis is about transport phenomena along tiny electronic devices in the quantum regime. More specifically, we study few-level quantum systems driven out of equilibrium by the effect of t-dependent forces and coupled to one or more macroscopic reservoirs kept at different temperatures and possibly at different chemical potentials. The field of study of these type of systems is sometimes referred to as "quantum thermodynamics" [1, 2, 3, 4, 5, 6, 7, 8]. The aim of this chapter is to provide a short conceptual map of the context in which this work is developed. General remarks about pump effects, quantum thermal machines and the link to geometry are presented.

Thermodynamics in quantum nanoscale systems has been a rapidly growing research topic for some years now, emerging at the intersection of statistical mechanics, nanoscience, quantum information, as well as atomic and molecular physics. A paradigmatic goal in this field is to conceive and realize thermal machines in the quantum realm, which, like the classical thermodynamic cycles, transform heat to useful work or use work to refrigerate [9, 10, 11, 12, 13, 14, 15, 16, 17, 18, 19, 20, 21]. The development of efficient thermal machines operating in the quantum realm is, in fact, of paramount importance also for quantum technologies. Numerous theoretical proposals [22, 23, 24, 25, 26, 27, 28, 29, 30, 31, 32] stimulated experimental efforts on several platforms [33, 34, 35], including solid-state electronics [36, 37, 38, 39] and nanomechanical systems [40, 41, 42, 43, 44], as well as cold atoms and trapped ions [45, 46, 47, 48, 49]. In this work we will consider a particular class of thermal machines: those for which the external parameters controlling the microscopic state of the working substance change slowly in time. Consequently, the internal state of the system will stay close to the thermal equilibrium. This condition will be very useful for the evaluation of the energy dynamics, and will give us an interesting geometric structure that we will take advantage of. Starting from the seminal works of Aharonov and Bohm [50] as well as Berry [51], geometric effects have pervaded many areas of physics. In quantum transport, distinct contributions of geometric origin affect charge and energy currents. For a typical setup consisting of a central quantum system coupled to macroscopic reservoirs, the pumped charge in a periodically driven system was shown to be of geometric origin [52, 53, 54, 55, 56, 57], akin to the Berry phase [51]. This transport effect can be expressed in terms of a closed-path integral in the driving parameter space and is independent of the presence of an additional dc bias. A similar approach was adopted to analyze heat transport in a driven two-level system weakly coupled to bosonic baths [58]. Closely related to these ideas is the geometric description of driving-induced forces [59, 60, 61, 62, 63, 64, 65, 66, 67], including geometric magnetism [68, 69], with the extension of geometric response functions to open systems also being discussed in relation to Cooper pair pumping [70].

Dissipative effects are a fundamental feature of finite-time thermodynamic processes. An interesting approach linking dissipation to geometry was developed some decades ago for macroscopic systems in the slow driving regime [71, 72, 73, 74, 75]. More recently these ideas were generalized to the quantum case [76, 77, 78, 79], and in particular using linear response theory

for systems coupled to macroscopic baths, near equilibrium [69, 80, 81]. Geometric concepts like *thermodynamic metric* and *thermodynamic length* were recently introduced as promising tools to characterize the dissipated energy and to design optimal driving protocols [82, 83, 84, 81, 85, 86].

This large body of work linking geometry to transport naturally hints at similar connections for thermal machines. First, thermal machines involve periodic variations of parameters and one may naturally expect geometric effects in the sense of Berry to play an important role. Second, the efficiency with which thermal machines operate is reduced by dissipation, and thus geometry enters the physics of thermal machines also in a second rather distinct way through the concept of thermodynamic length.

In Chapters 5 and 6, under quite general assumptions, we will show that the operation of quantum thermal machines and the underlying heat-work conversion is fundamentally tied to such geometric effects. The heat–work conversion and dissipation mechanisms can be respectively described by different components of a single *thermal geometric tensor*. As said before, heat–work conversion component can be expressed in terms of a Berry-type phase, which has an associated Berry-type curvature [51] (similar ideas can be found in Refs. [87, 88]). Besides, it is well known that dissipation and entropy production admit a geometric description in terms of the concept of thermodynamic length [71, 72, 73, 74, 75, 89, 90, 91, 69, 92]. This geometric approach has proven useful to optimize finite-time thermodynamic processes (examples can be found in [83, 93, 94, 95] for classical and [96, 81, 97] for quantum systems), including the finite-time Carnot cycle [86, 97] and slowly driven engines [98, 99, 100, 101, 102]. However, these cycles are characterized by the WS being coupled to a single reservoir or completely decoupled from reservoirs. In this work we will generalize this definition of a length and an area in the parameter space, to include machines whose cycles are constantly attached to two or more thermal reservoirs. In addition, we will see that these geometric concepts are very useful to search for optimal drivings.

An important case that we address in this work is the quantum RC circuit of Section 2.4, which is coupled to a single fermionic reservoir. Treated as an adiabatic machine, the effect of the time-dependent driving translates into a net charge accumulation in the capacitor. In complete analogy with the pumping effect, the latter has a geometric nature. Furthermore, the energy dynamics is fully dissipative and can be characterized through the same concept of thermodynamic length.

In Chapter 2 we summarize and motivate the specific physical configurations in which we will embody the general concepts to be developed along the thesis. These are essentially quantum bits and quantum dots, considered in different regimes.

Chapter 3 is devoted to the discussion of the theoretical tools and methods that we use to obtain the results from the models. We review the formulation of the adiabatic dynamics as proposed by Ref. [80], similar to the Kubo formula applied to slow-driving forces. We include a general introduction to a quantum master equation approach for weak coupled systems as developed in Ref. [103]. We also review the equilibrium many body Green's function method and the numerical renormalization group approach for the Anderson impurity model.

In Chapter 4 we consider a slowly driven quantum dot with local Coulomb interaction, coupled to a single fermionic reservoir at $T = 0$. We compute the adiabatic dynamics of the charge, spin and energy, considering the system as a generalized realization of a quantum capacitor. We show that the non-equilibrium accumulation of charge has a geometric nature and that the dissipation takes place in the form of an instantaneous Joule law. The latter lead to generalized fluctuation-dissipation relations.

In Chapter 5 we apply the adiabatic dynamics results for a particular (but wide) class of Hamiltonians. We take advantage of the emergent mathematical structure of this approach to develop a general theoretical framework, useful to characterize quantum thermal machines in the slow-driving regime. We define the so called thermal geometric tensor and derive expressions of

the important features of heat engines and refrigerators (e.g. heat-work conversion, dissipation, efficiencies) in terms of this tensor. We also exemplify the developed concepts trough an explicit example, a driven quantum dot connected to two fermionic reservoirs.

In Chapter 6 we return to some of the results obtained in Chapter 5 to address the problem of finding optimal driving protocols for a given thermal machine. The power generation of a heat engine and the efficiency of both the heat engine and refrigerator operational modes is reduced to an isoperimetric problem with nontrivial underlying metrics and curvature. We illustrate the procedure in a qubit coupled to two reservoirs, again operating as a thermal machine by means of an adiabatic protocol.

Finally, in Chapter 7 we summarize the results of the present thesis and we give a future perspective on how this work could be continued.

Resumen

En esta tesis analizamos fenómenos de transporte a lo largo de dispositivos electrónicos pequeños en el régimen cuántico. Más específicamente, estudiamos sistemas cuánticos de pocos niveles desplazados del equilibrio por el efecto de fuerzas dependientes del tiempo y acoplados a uno o más reservorios macroscópicos mantenidos a diferentes temperaturas y posiblemente a diferentes potenciales químicos. El campo de estudio de este tipo de sistemas a veces se denomina "termodinámica cuántica" [1, 2, 3, 4, 5, 6, 7, 8]. El objetivo de este capítulo es proporcionar un breve mapa conceptual del contexto en el que se desarrolla este trabajo. Se presentan consideraciones generales sobre efectos de bombeo, máquinas térmicas cuánticas y su relación con conceptos geométricos. La termodinámica en sistemas cuánticos en la nanoescala ha sido un tema de investigación de rápido crecimiento en los últimos años, surgiendo en la intersección de la mecánica estadística, la nanociencia, la información cuántica, así como la física atómica y molecular. Un objetivo paradigmático en este campo es concebir y realizar máquinas térmicas en el dominio cuántico que, al igual que los ciclos termodinámicos clásicos, transformen calor en trabajo útil o utilicen trabajo para refrigerar [9, 10, 11, 12, 13, 14, 15, 16, 17, 18, 19, 20, 21]. The development of efficient thermal machines operating in the quantum realm is, in fact, of paramount importance also for quantum technologies. El desarrollo de máquinas térmicas eficientes que operen en el régimen cuántico es, a su vez, de gran relevancia para las tecnologías cuánticas. Numerosas propuestas teóricas [22, 23, 24, 25, 26, 27, 28, 29, 30, 31, 32] han estimulado esfuerzos en diversas plataformas experimentales [33, 34, 35], incluyendo dispositivos de estado sólido [36, 37, 38, 39] y sistemas nanomecánicos [40, 41, 42, 43, 44], así como también en experimentos de átomos fríos y trampas de iones [45, 46, 47, 48, 49]. En este trabajo consideraremos una clase particular de máquinas térmicas: aquellas para las cuales los parámetros externos que controlan el estado microscópico de la sustancia de trabajo cambian lentamente en el tiempo. Como consecuencia, el estado interno del sistema será muy parecido al estado de equilibrio térmico. Esta condición resulta de gran utilidad para evaluar la dinámica de la energía y nos proporciona una interesante estructura geométrica de la que sacar provecho. A partir de los trabajos seminales de Aharonov y Bohm [50], así como de Berry [51], los efectos geométricos han atravesado muchas áreas de la física. En el transporte cuántico, distintas contribuciones de origen geométrico afectan las corrientes de carga y energía. Para una configuración típica que consta de un sistema cuántico central acoplado a reservorios macroscópicos, se demostró que la carga bombeada en un sistema accionado periódicamente tiene un origen geométrico [52, 53, 54, 55, 56, 57], similar a la fase de Berry [51]. Este efecto de transporte se puede expresar en términos de una integral de línea cerrada en el espacio de parámetros forzantes y es independiente de la presencia de una diferencia de potencial externo. Un enfoque similar se adoptó para analizar el transporte de calor en un sistema paramétrico de dos niveles débilmente acoplado a baños bosónicos [58]. La descripción geométrica de las fuerzas inducidas por parámetros externos [59, 60, 61, 62, 63, 64, 65, 66, 67] está estrechamente relacionada con estas ideas, incluyendo el magnetismo geométrico [68, 69] con la extensión de las funciones de respuesta geométrica a sistemas abiertos y discutiéndose en relación con el bombeo de pares de Cooper [70].

Los efectos disipativos son una característica fundamental de los procesos termodinámicos

de tiempo finito. Hace algunas décadas se desarrolló un enfoque interesante que vincula la disipación con la geometría para sistemas macroscópicos forzados lentamente [71, 72, 73, 74, 75]. Más recientemente, estas ideas se generalizaron al caso cuántico [76, 77, 78, 79], y en particular para sistemas acoplados a baños macroscópicos cerca del equilibrio [69, 80, 81] usando la teoría de respuesta lineal. Conceptos geométricos como la *métrica termodinámica* y la *longitud termodinámica* fueron introducidos recientemente como herramientas prometedoras para caracterizar la energía disipada y diseñar protocolos óptimos [**miller2019dic**, 82, 83, 84, 81, 86].

Este vasto volumen de investigación que vincula la geometría con el transporte sugiere naturalmente conexiones similares para las máquinas térmicas. En primer lugar, las máquinas térmicas requieren de variaciones periódicas de parámetros de control, por lo que es esperable que los efectos geométricos (en el sentido de Berry) desempeñen un papel importante. Por otro lado, la eficiencia con la que operan estos sistemas se reduce a causa de la disipación. En este caso, la geometría entra en la física a través de un concepto diferente: la longitud termodinámica.

En los Capítulos 5 y 6, bajo suposiciones bastante generales, mostraremos que el funcionamiento de las máquinas térmicas cuánticas y la conversión subyacente de calor en trabajo está fundamentalmente ligado a tales efectos geométricos. Los mecanismos de conversión y disipación pueden ser respectivamente descriptos por diferentes componentes de un solo *tensor geométrico térmico*. Como se dijo anteriormente, la componente de conversión calor-trabajo se puede expresar en términos de una fase de tipo Berry, que tiene una curvatura de tipo Berry asociada [51] (ideas similares se pueden encontrar en Refs. [87, 88]).

Además, es sabido que la disipación y la producción de entropía admiten una descripción geométrica en términos del concepto de longitud termodinámica [71, 72, 73, 74, 75, 89, 90, 91, 69, 92]. Este enfoque geométrico ha demostrado ser útil para optimizar procesos termodinámicos de tiempo finito (se pueden encontrar ejemplos en [83, 93, 94, 95] para sistemas clásicos y [96, 81, 97] para sistemas cuánticos), incluyendo el ciclo de Carnot de tiempo finito [86, 97] y motores forzados lentamente [98, 99, 100, 101, 102]. Sin embargo, estos ciclos se caracterizan por tener la sustancia de trabajo acoplada a un solo reservorio, o completamente desacoplada de los reservorios. En este trabajo generalizaremos esta definición de longitud y área en el espacio de parámetros para incluir máquinas que se mantienen acopladas a los reservorios a lo largo de todo el ciclo. Además, veremos que estos conceptos geométricos son muy útiles para buscar parametrizaciones óptimas.

Un caso importante que abordamos en este trabajo es el circuito RC cuántico de la Sección 2.4, el cual está acoplado a un solo reservorio fermiónico. Tratada como una máquina adiabática, el efecto del forzado dependiente del tiempo se traduce en una acumulación de carga neta en el capacitor. En analogía con el efecto de bombeo, este último tiene una naturaleza geométrica. Además, la dinámica de la energía es totalmente disipativa y se puede caracterizar mediante el mismo concepto de longitud termodinámica.

En el Capítulo 2 resumiremos y motivaremos los sistemas físicos específicos en los que aplicaremos los conceptos generales a desarrollar a lo largo de la tesis. Se trata esencialmente de bits cuánticos y puntos cuánticos, considerados en diferentes regímenes.

El capítulo 3 está dedicado a la discusión de las herramientas y métodos teóricos que utilizamos para obtener los resultados de los modelos. Revisamos la formulación de la dinámica adiabática propuesta por Ref. [80], similar a la fórmula de Kubo, en este caso realizando una expansión en la velocidad de los parámetros forzantes. Incluimos una introducción general de ecuaciones maestras cuánticas aplicadas a sistemas débilmente acoplados como se desarrolla en Ref. [103]. También revisamos el método de funciones de Green de muchos cuerpos (en equilibrio) y la técnica de grupo de renormalización numérica (NRG) para el modelo de impurezas de Anderson.

En el Capítulo 4 consideramos un punto cuántico forzado lentamente con interacción local de

Coulomb, acoplado a un solo reservorio fermiónico a $T = 0$. Calculamos la dinámica adiabática de carga, el espín y la energía, considerando el sistema como una realización generalizada de un capacitor cuántico. Mostramos que la acumulación de carga fuera de equilibrio tiene una naturaleza geométrica y que la disipación tiene la forma de una ley de Joule instantánea. Esto último conduce a relaciones generalizadas de fluctuación-disipación.

En el Capítulo 5 aplicamos los resultados de la dinámica adiabática para una clase particular (pero amplia) de Hamiltonianos. Aprovechamos la estructura matemática emergente de este enfoque para desarrollar un marco teórico general, útil para caracterizar las máquinas térmicas cuánticas en el régimen de forzado lento. Definimos el llamado tensor geométrico térmico y derivamos expresiones para caracterizar las cualidades importantes de los motores térmicos y refrigeradores (por ejemplo, conversión de calor en trabajo, disipación, eficiencias) en términos de este tensor. También ejemplificamos los conceptos desarrollados a través de un ejemplo explícito: un punto cuántico forzado conectado a dos reservorios fermiónicos.

En el Capítulo 6 retomamos algunos de los resultados obtenidos en el Capítulo 5 para abordar el problema de encontrar protocolos óptimos para una máquina térmica dada. La potencia de un motor térmico y la eficiencia de los modos operativos de motor y refrigerador se reducen a un problema isoperimétrico con métricas y curvaturas subyacentes no triviales. Ilustramos el procedimiento en un bit cuántico acoplado a dos reservorios, nuevamente operando como una máquina térmica mediante un protocolo adiabático.

Finalmente, en el Capítulo 7 resumimos los resultados de la presente tesis y damos una perspectiva futura sobre cómo podría continuarse este trabajo.

Chapter 2

Physical systems motivating this thesis, and its models

2.1 Generic Hamiltonian description

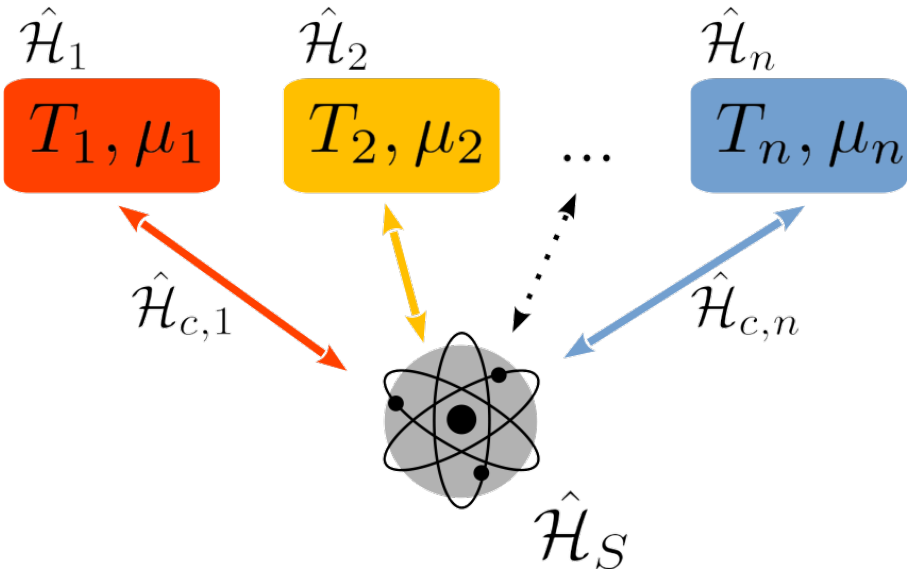

Figure 2.1: Schematic representation of Eq. (2.1). A quantum system $\hat{\mathcal{H}}_S$ is coupled to one or more macroscopic baths $\hat{\mathcal{H}}_\alpha$ at thermodynamic equilibrium (environment) through the contacts $\hat{\mathcal{H}}_{c,\alpha}$.

The class of systems considered in this work can be summarized using a prototypical Hamiltonian of the form,

$$\hat{\mathcal{H}}(t) = \hat{\mathcal{H}}_S(t) + \left(\sum_{\alpha=1}^{n} \hat{\mathcal{H}}_\alpha + \hat{\mathcal{H}}_{c,\alpha} \right) \tag{2.1}$$

where we distinguish three parts:

- the term $\hat{\mathcal{H}}_S(t)$ describes a low-dimensional, few-level quantum system S. We include the explicit temporal dependence as a general feature, since in most cases S is taken to be an externally driven system.
- the $\hat{\mathcal{H}}_\alpha$ terms describe reservoirs of free particles with a very large number of degrees of freedom. We may refer to them indistinctly as reservoirs or baths, and with no further clarification are assumed to be held at fixed temperatures and chemical potentials.

- finally, the connection between S and the reservoirs is contained in the hybridization terms $\hat{\mathcal{H}}_{c,\alpha}$.

In this description the system S is regarded as open, with the macroscopic baths representing the environment. Schematically the situation is depicted in Fig. 2.1. Throughout the thesis we will consider some particular realizations of the Hamiltonian Eq. (2.1) in different scenarios and conditions. Despite we will focus in configurations with $n = 1$ or 2 baths, in many cases the generalization to arbitrary n is quite straightforward. The next sections are devoted to describe each one of the considered systems, motivate their use and state some of their basic physical properties.

2.2 Quantum dots

Quantum dots are small conducting regions created in semiconducting structures. Due to the small dimensions of these devices, the electronic behaviour display energy and charge quantization, similar to what is found in atomic systems. For this reason they are usually referred to as artificial atoms. Very importantly, quantum dots properties, such as geometry, coupling to the reservoirs or the number of confined electrons can be accurately tuned through the use of gates. This flexibility allows the design of interesting experiments in the mesoscale and fundamental physical phenomena as well. A remarkable example is the Kondo effect.

An electronic microscopy image of a quantum dot is presented in Fig. 2.2. The indicated gate voltages can be used to modify the properties of the electronic box (the "QD" region), and a pair of quantum point contacts (indicated as "QPC") regulates the interaction with the external reservoirs.

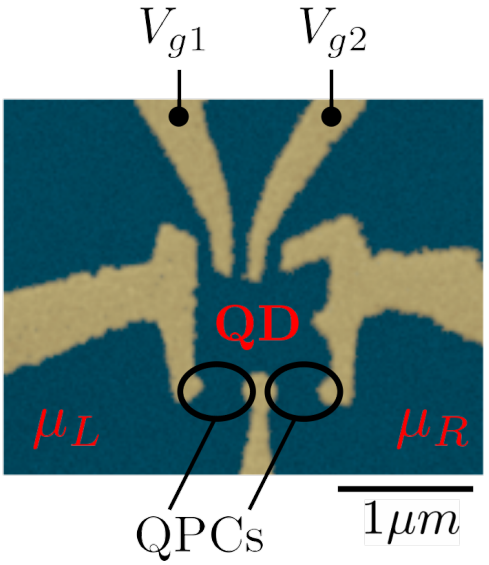

Figure 2.2: Lateral quantum dots are 2D electron gas (2DEG) confined to a small region using electrical gates, fabricated through lithography. Micrograph image taken from [104].

In Fig. 2.3 a simplified sketch of a quantum dot coupled to a left and right reservoir is shown. The dot presents a discrete spectrum ε_n with energy levels separated by a gap $\Delta\varepsilon$, roughly given by the dimensions of the quantum box and Coulomb's repulsion between confined electrons. A voltage gate V_g allows a rigid displacement in the energy levels of the dot. The reservoirs are considered in thermal equilibrium with a bias voltage difference $\mu_L - \mu_R = \Delta\mu$. Electrons can tunnel back and forth from the reservoirs to the dot trough the QPCs.

For sufficiently low temperatures it is possible to adjust the occupation number of the dot using the voltage gate V_g with high precision. If $k_BT << \Delta E$, then this can be done one

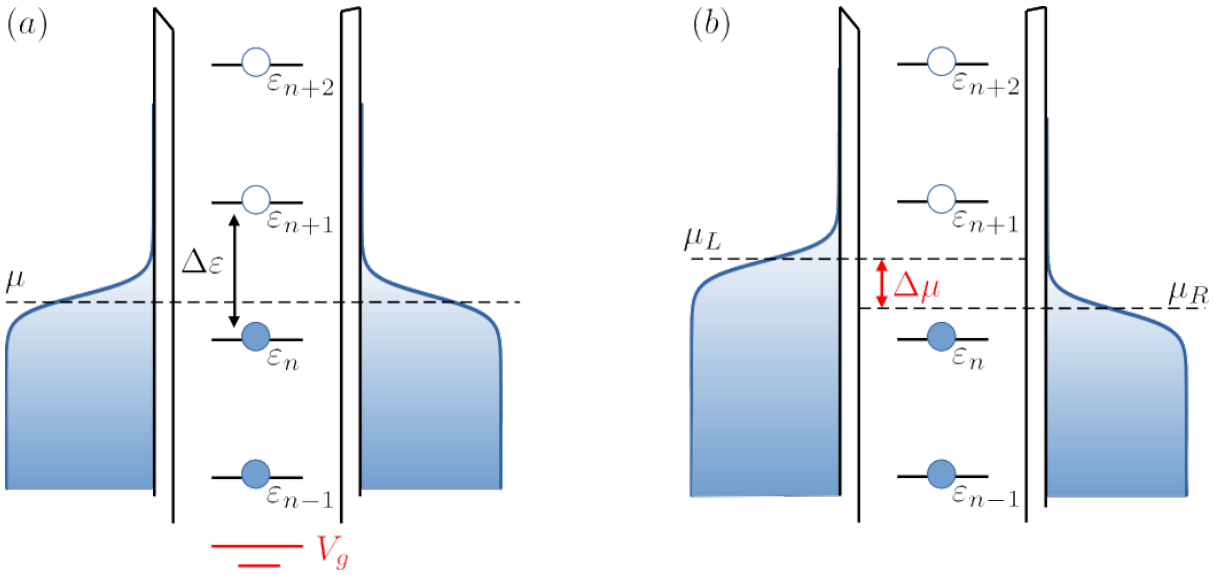

Figure 2.3: (a) Lowering the gate voltage V_g such that $\varepsilon_{n+1} \approx \mu$ allows an extra electron to jump into the dot. (b) In the Coulomb blockade regime the transport window lies between two levels.

electron at a time. Furthermore, if the bias voltage also fulfills the condition $\Delta\mu << \Delta E$ and the conduction window lies entirely inside a gap, then transport is blocked. Usually, the different levels are originated due to the Coulomb repulsion inside the quantum dot and this effect is named Coulomb blockade.

It becomes clear that quantum dots can be tuned to confine an odd number of electrons. In such a case the total spin of the dot is (at least) $S = 1/2$, known as the local moment regime (LMR). Due to the similarities regarding magnetic impurities in a metallic environment, in this regime the system develops a non trivial many-body phenomena: the Kondo resonance (predicted in 1988[105, 106] and first observed in 1998[107] in this system). Although the Kondo physics will not play a significant role in the thesis, it is necessary to understand the basic ideas to interpret the presence of the Kondo resonance in the DoS of the dot. More details will be given in Chapter 4, where we study the charge and energy dynamics of a quantum RC circuit including many body effects.

2.2.1 Single Impurity Anderson Model (SIAM)

In the context of magnetic impurities in a host metal, a model was proposed by Anderson in 1961 to describe the interaction between the localized magnetic moment at the impurity site and the electron spins of the metal.

The impurity induces localized states of energy $\varepsilon_{dj\sigma}$ that couples to the conduction band $c_{k,\sigma}$ of the host. In its simplest form, a single level is considered ($j = 1$), and the Hamiltonian for the impurity plus the coupling is written as:

$$\mathcal{H}_{SIAM} = \underbrace{\sum_{\sigma} \epsilon_{d,\sigma}\hat{n}_{d,\sigma} + U\hat{n}_{d,\uparrow}\hat{n}_{d,\downarrow}}_{\mathcal{H}_S} + \sum_{\vec{k},\sigma} \underbrace{\left(V_{\vec{k}}\hat{c}^{\dagger}_{d,\sigma}\hat{c}_{\vec{k},\sigma} + V^{*}_{\vec{k}}\hat{c}^{\dagger}_{\vec{k},\sigma}\hat{c}_{d,\sigma}\right)}_{\mathcal{H}_{c,\alpha=\vec{k}\sigma}} + \sum_{k\sigma} \underbrace{\varepsilon_{\vec{k}}c^{\dagger}_{\vec{k}\sigma}c_{\vec{k}\sigma}}_{\mathcal{H}_{\alpha=\vec{k}\sigma}} \tag{2.2}$$

where $\hat{n}_{d,\sigma} = d^{\dagger}_{\sigma}d_{\sigma}$ is the (impurity site) occupation number operator, and U is the local Coulomb repulsion between the electrons at the impurity. In terms of Fig. 2.1 the central system corresponds to the impurity site and is modelled as $\mathcal{H}_S = \sum_{\sigma} \epsilon_{d,\sigma}\hat{n}_{d,\sigma} + U\hat{n}_{d,\uparrow}\hat{n}_{d,\downarrow}$. The

Anderson model is very well suited to describe the physics of the quantum dot, identifying the impurity site with the dot and the electrons of the reservoirs with the conduction band. Despite its simplicity, the SIAM model is capable of developing the Kondo resonance. A more detailed analysis of the SIAM model and the relation with the experimental parameters can be found in Section 3.3.2 where we solve the problem of a single resonant level coupled to the continuum (corresponding to the simplest case of $U = 0$). Also in Chapter 4, where the full many-body problem is considered and treated by a numerical approach.

2.3 Qubits

The simplest physical system capable of displaying quantum effects is the two-level system. In general we can label the two states $|g\rangle$ (for ground) and $|e\rangle$ (for excited). Any arbitrary state will be a linear combination of those:

$$|\alpha\rangle = c_g\,|g\rangle + c_e\,|e\rangle \tag{2.3}$$

with c_g and c_e complex numbers satisfying $|c_g|^2+|c_e|^2 = 1$. In a strict sense a qubit is a two-level system. However, when referring to qubits, a high degree of control over the quantum state of the system is assumed. With the increased interest in the family of quantum technologies (q. computing, q. communications, q. sensing, etc.) over the past years, a big number of qubit hardware realizations have begun to be developed. Among the solid state devices, we find qubits based on nitrogen-vacancy centers, quantum dots, topological devices or superconducting circuits[108]. Other prominent platforms include ion traps, NMR and photonics.

Within these many platforms, our interest is mostly in the circuit quantum electrodynamics (c-QED), which is a highly promising family of devices for the experimental realization of quantum heat engines and refrigerators. In the last decades the c-QED has seen a great advance in the fabrication, characterization and range of applications[109, 110, 111], including the integration of these devices to dissipative elements and thermal reservoirs, allowing experimental studies on quantum heat transport[112, 113] and thermometry[114].

At the simplest level a superconducting qubit is a nonlinear resonant LC circuit consisting of a capacitance in series with a Josephson junction [115]. Let ω_r be the typical resonant frequency of the circuit. At sufficiently low temperature, $k_BT << \omega_r$ and dissipation (level broadening $<< \omega_r$) the resonator acts as a quantum harmonic oscillator with quantized energy levels. The qubit is defined using two levels of the harmonic oscillator (usually the ground state for $|g\rangle$ and the first excited for $|e\rangle$). From a practical point of view, one must include the non-linear element to the circuit (Josephson junction) in order to introduce an energy-dependent level spacing in the resonator. This is useful both for controlling transitions one by one, and suppress undesired excitations to the upper levels. In Fig. 2.4 we show a schematic representation of a basic superconducting qubit. The main parameters are the capacitance C, the non-linear inductance L_J and the phase difference across the junction ϕ.

The two main designs of qubits based of tunnel junctions are the *charge qubits* [116] (also known as Cooper-pair box) and the *flux qubits* [117, 118]. In the charge qubits a superconducting island is coupled to a larger superconducting reservoir using a Josephson junction. The junction acts as a valve for Cooper pairs between the reservoir and the island. The qubit energy gap is controlled by a capacitive gate voltage used to adjust the charge on the island (in a similar way to the quantum dot system of the previous section). Finally, the qubit states are represented by the number of Cooper pairs in the island (e.g. $|g\rangle = |N\rangle$ and $|e\rangle = |N+1\rangle$).

In the flux qubit design the states are assigned to a clockwise or counter-clockwise currents flowing around the circuit. In this case the junction acts as a valve for quanta of magnetic flux and is controlled externally by an applied magnetic field.

In this work we will consider qubit systems weakly coupled to thermal baths (see Chapter 6). The description of the system will be presented in terms of a master equation for the reduced

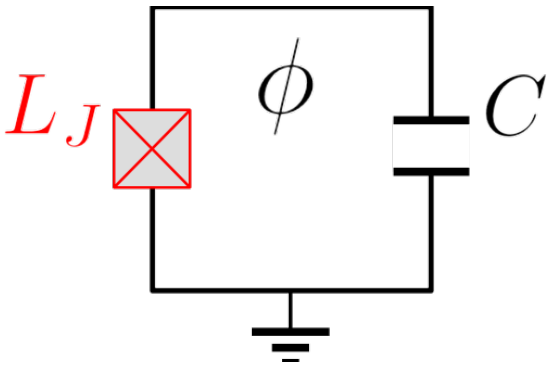

Figure 2.4: Schematic representation of a transmon: a superconducting Josephson junction qubit.

density matrix of the qubit, $\hat{\rho}_S = \mathrm{Tr}_\mathrm{B}[\hat{\rho}]$. We describe in detail how we arrive to the master equation in Section 3.4. In principle, the effect of the environment with a temperature T over an initial state of the qubit is to thermalize the state to a Gibbs distribution,

$$\hat{\rho}_{S,\mathrm{eq}} = \frac{1}{\mathcal{Z}}\left(e^{-\varepsilon_g/k_BT}|g\rangle\langle g| + e^{-\varepsilon_e/k_BT}|e\rangle\langle e|\right) \tag{2.4}$$

with ε_g and ε_e the energies of the ground and excited state, respectively. The relaxation time τ_R to the equilibrium state will depend on the rate coefficients of the resulting master equation[119]. Since we will be interested in the slow driving dynamics of the qubit, we expect that the density matrix at any time to be close to Eq. (2.4). This means that τ_R defines the timescale for which the slow dynamics (or adiabatic approximation) results break.

2.3.1 The qubit-boson model

Following the sketch of Fig. 2.1 let us consider a single qubit asymmetrically coupled to two bosonic baths, L and R:

$$\mathcal{H}_{qubit} = \vec{B}\cdot\hat{\vec{\sigma}} + \sum_{k_\alpha}\omega_{k_\alpha}b^\dagger_{k_\alpha}b_{k_\alpha} + \sum_{k_\alpha}V_{k_\alpha}\left(b^\dagger_{k_\alpha} + b_{k_\alpha}\right)\hat{\sigma}_\alpha, \tag{2.5}$$

where, according to the notation of Eq. (2.1), $\mathcal{H}_S = \vec{B}\cdot\hat{\vec{\sigma}}$ is the qubit Hamiltonian, which depends on the external parameter $\vec{B}$, and $\alpha = L, R$ are the bath's labels. In cQED setups, the type of coupling can be engineered. In this thesis, we will consider a configuration where the coupling breaks $L \leftrightarrow R$ symmetry. Concretely, we consider the simplest case where $\omega_{k_L} = \omega_{k_R}$ and $V_{k_L} = V_{k_R}$. Thus the coupling asymmetry arise from the different choice for σ_L and σ_R. In Chapter 6 we will consider the setup with $\sigma_L = \sigma_x$ and $\sigma_R = \sigma_z$.

Our interest in this system comes from the possibility of the qubit to parametrically couple and decouple from the reservoirs. This can be seen by choosing a particular value for $\vec{B}$, for example we may take $\vec{B} = (B_x, 0, 0)$. Writing the evolution equation in the Heisenberg representation, for the L bath we find that:

$$\begin{aligned}\left\langle\frac{d\left(\mathcal{H}_L + \mathcal{H}_{c,L}\right)}{dt}\right\rangle &= -i/\hbar\left\langle\left[\left(\mathcal{H}_L + \mathcal{H}_{c,L}\right), \mathcal{H}\right]\right\rangle \\ &= -i/\hbar\left\langle[\mathcal{H}_L, \mathcal{H}_{c,L}] + [\mathcal{H}_{c,L}, \mathcal{H}_L]\right\rangle \\ &= 0\end{aligned} \tag{2.6}$$

where we have used that $[\mathcal{H}_{c,L}, \mathcal{H}_S] = 0$ because $\sigma_L = \sigma_x$, meaning that no energy flux is allowed between the left bath and the qubit although dephasing may take place [120]). In other words,

when $\vec{B}$ is aligned in the x direction energy can only flow from (or to) the R reservoir. The opposite happens when $\vec{B}$ aligns to the z direction.

Applying this philosophy to a more general case, we will consider a time dependent parameter $\vec{B} \equiv \vec{B}(t)$. If we consider the situation where the thermalization times of the system are fast with respect to the changes on the $\vec{B}$ parameter, then $\mathcal{H}_S(\vec{B}(t))$ is a realization of the adiabatic thermal machine as described in 2.6. We will perform a detailed study of this particular machine in the heat engine mode, in the search of optimal driving protocols.

2.4 Quantum capacitors

In the last decades there has been a growing interest in the generation and control of coherent electronic currents, in part motivated by the strong analogy with many photonic experiments in the field of quantum information. In solid state devices, however, the environment imposes many challenges to the preservation of the quantum coherence. Interactions with other electrons, impurities in the sample and the phononic scattering determines a typical length, below which the propagating electrons keep their coherence, and thus defining the limits of the *mesoscale*. Advances in technology lead to the fabrication of cleaner samples and the ability to reach lower temperatures, reducing much of these undesired interactions while electron-electron interactions remain a more fundamental problem to address.

In this context, the quantum RC circuit is a prominent platform to investigate the dynamics of single electrons in quantum coherent devices. The *mesoscopic capacitor*, as first considered in the seminal papers of Refs. [121, 122, 123] is the quantum analog of a classical RC circuit, which operates under the driving induced by *ac* voltage. From the experimental side, a first implementation was presented in Ref. [124]. The device consists of a two-dimensional electron gas in the integer quantum Hall regime. A quantum point contact allows the edge states of the sample to coherently tunnel back and forth to a quantum dot, which is precisely the capacitive element. Finally, a metallic voltage gate is placed on top of the quantum dot, capacitively coupling to it. In Fig. 2.5 (taken from Ref. [124]) a diagram of the device is shown. The transmission of the quantum point contact is controlled through the V_g gates, while the V_{ac} gate is used to inject *ac* current to the circuit.

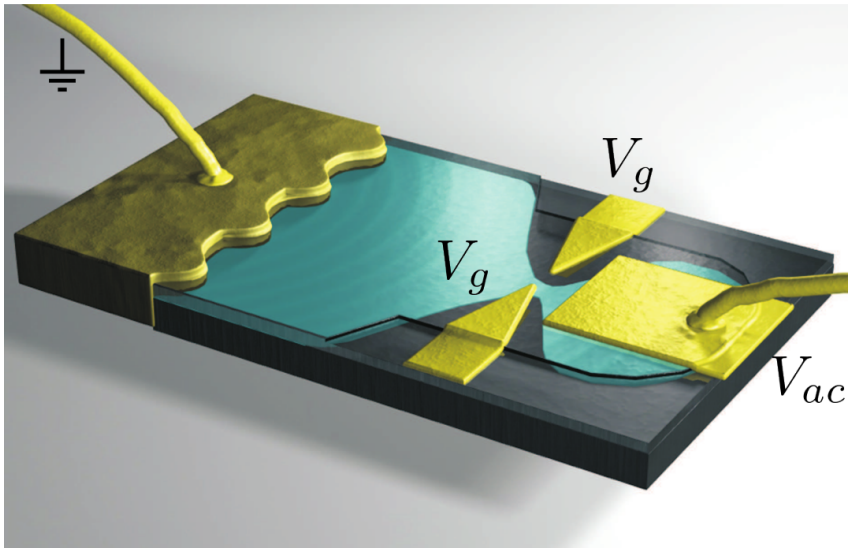

Figure 2.5: The minimal RC circuit. A 2D electron gas (in blue) is allowed to coherently interact with a quantum dot through a quantum point contact. The resistive element is the point contact with the fermionic reservoir and the quantum capacitance is given by the quantum dot. Figure taken from Ref. [124]

The system had been already predicted to display non-trivial properties [121, 122, 123] such as an universal quantized resistance $R_0 = h/2e^2$ at the point contact, and a quantum capacitance term of the form $C_0 = e^2\gamma(E_F)$ proportional to the local density of states γ of the quantum dot at the Fermi energy E_F. In the subsequent years the charge dynamics of this circuit under *ac* driving has been the subject of several experimental [125, 126, 127] and theoretical [128, 129, 130, 131, 132, 133, 134, 135, 136, 137, 138, 139, 140, 141, 142, 143, 144, 145, 146, 147, 148, 149] studies in the linear and non-linear regimes.

Not only the charge but also the energy dynamics in this system deserves attention. In fact, this is the minimal electronic system to address fundamental questions on the energy transport and heat production in the quantum regime, which is a subject under active investigation across the areas of statistical mechanics, condensed matter, cold atoms and quantum information. In this work we intend to contribute to the understanding of the quantum RC circuit in the presence of many-body interactions, and the inclusion of a time-dependent Zeeman field applied to the dot. As we will see in Chapter 4 interesting mechanisms take place, like the net exchange of work between the two types of forces and the non-equilibrium accumulation of charge with different spin orientations. We will see that even in the case of including a time-dependent magnetic field, the dissipation takes place in the form of an instantaneous Joule law with the universal resistance R_0, which is a step further in the line of work of Refs. [132, 149].

2.5 Adiabatic quantum pumps

The idea of the adiabatic pump mechanism was first introduced by Thouless [150] for a closed system at zero temperature. Further extensions were made for open systems by Spivak et al [151] some years later. Traditionally, quantum pumps are linked to the generation of *dc* particle currents in nanostructures via the time-periodic modulation of two or more system parameters. In this thesis we consider an extended definition to include heat transport as well, while retaining the basic idea of controlling the transport (completely or partially) through the external, time-dependent potentials. With "adiabatic" we mean that the modulation of the control parameters is performed at a timescale much bigger than the relaxation time of the system (i.e. very slowly). The adiabatic energy pump will have a prominent importance throughout this work, since it will be a necessary ingredient for the heat-work conversion and refrigeration mechanism in the machines that we consider. In addition, it will be directly linked to the geometric concepts developed in the next chapters.

One of the first experimental realizations of this concept is the single-electron pump devised by Pothier et al. [152, 35], which is an analogue to a peristaltic bomb for electrons, also know as a "turnstile pump".

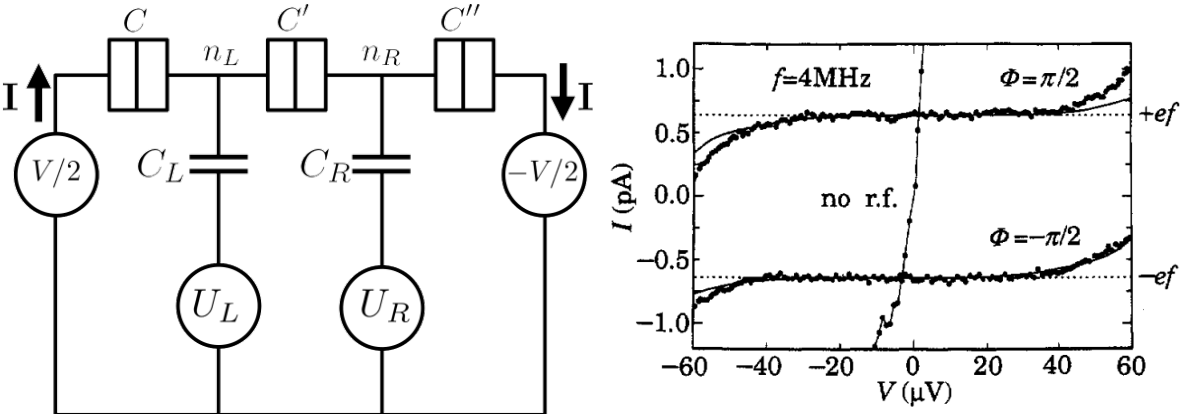

Figure 2.6: Pothier's single-electron pump. Left: Schematic picture of the setup. Right: $I - V$ curve of the device. Figures taken from Ref. [35].

Pothier's device consists of a linear array of three tunnel junctions C, C', C'' and two QDs -both set in the Coulomb-blockade regime- placed in between each connected junction, as depicted in Fig. 2.6 (left). The energy of the QDs is controlled by two voltage gates U_L and U_R respectively, and therefore the number of electrons in the QDs, n_L and n_R can be independently adjusted one at a time. When a small bias voltage V is applied to the ends of the circuit, charge transport is blocked by the presence of the electrons occupying the dots. The gates U_L and U_R act as a precise mechanism of flow control, allowing the pull or push of the electrons from the adjacent reservoirs.

The setup allows to perform a single-electron transport using a suitable sequential change in the voltage gates: An electron can tunnel from the left reservoir to the left dot, then jump to the right dot and finally to the rigth reservoir. As an illustrative example, consider the energy of the QDs set by the dephased *ac* votages $U_L(t) \propto \sin(2\pi f t)$ and $U_R(t) \propto \sin(2\pi f t + \Phi)$. Fig. 2.6 (right, extracted from Ref. [35]) shows the $I-V$ curve of the device for a fixed frequency f and the two values of the phase lag, $\Phi = \pi/2$ and $\Phi = -\pi/2$. For each cycle of the configuration of the gate, an electron flows from one reservoir to the other, so the net electrical current is measured to be exactly ef. The phase Φ allows the control of the direction of the current. The pumping effect is reversible, and the change on sign of Φ has the effect of reversing the mechanism of the pump. As said before, it is important to observe that the charge pump can occur in the case of zero bias voltage ($V = 0$), indicating that the effect is purely due to the change of the external potentials.

Notice that Pothier's pump is ultimately a classical device: QDs are mostly isolated from the reservoirs due the effect of the potential barriers, and at a first approximation, no quantum correlation is present during the cycle. In more general conditions, the adiabatic pumping can be driven by any cyclic changes in the parameters of the system, like the shape of the confining potentials, the connection to the reservoirs or any field modifying the interference pattern of the coherent electrons in the device. An early experimental work intended to take advantage of the quantum properties of the electrons was presented by Switkes et al. [104]. The device consist on a single QD whose shape is controlled by a pair of gate voltages. The pump effect is obtained as a consequence of the modulation of the quantum mechanical wavefunction of the electrons inside the dot. See Ref. [104] and Ref. [153] for a detailed discussion.

Using the Landauer-Büttiker scattering matrix theory, Brouwer [52] developed a description of the pump effect in terms of the S matrix of the system. Here we review some of the important results of Ref. [52].

Consider a central system connected to two particle reservoirs ($m = 1, 2$). The central system is driven by time-dependent potentials $X_j(t)$, $j = 1, 2$. A scattering matrix S is defined to describe the instantaneous transport properties, which is a function of X_1 and X_2 only. If we take a closed curve $\vec{X}(t) = (X_1(t), X_2(t))$ of total duration τ to drive the central system, the net charge flowing from the m reservoir for a cycle is found to be:

$$Q_m(\tau) = e\int_0^\tau dt \dot{n}_m(t) = e\int_0^\tau dt \left(\frac{dn_m}{dX_1}\frac{dX_1}{dt} + \frac{dn_m}{dX_2}\frac{dX_2}{dt}\right) \tag{2.7}$$

where the so called "emisivities" dn_m/dX_j, defined for each reservoir are functions of S, and consequently functions of $\vec{X}$ only. Applying Stoke's theorem to this equation using the closed curve defined in the $\vec{X}$ parameter space, the following result is found for the particle current at each cycle:

$$I_m = \frac{we}{2\pi^2}\int_A dX_1 dX_2 \sum_{\alpha\in m}\sum_\beta \mathrm{Im}\frac{\partial S^*_{\alpha\beta}}{\partial X_1}\frac{\partial S_{\alpha\beta}}{\partial X_2} \tag{2.8}$$

where the relation $I_1 = -I_2$ can be verified, implying that no charge is accumulated in the central system after the cycle. This means that Eq. (2.8) is precisely a pumped current from

one reservoir to the other. The situation is sketched in Fig. 2.7 where we represent the charge being pumped (a) during a particular cyclic driving (b).

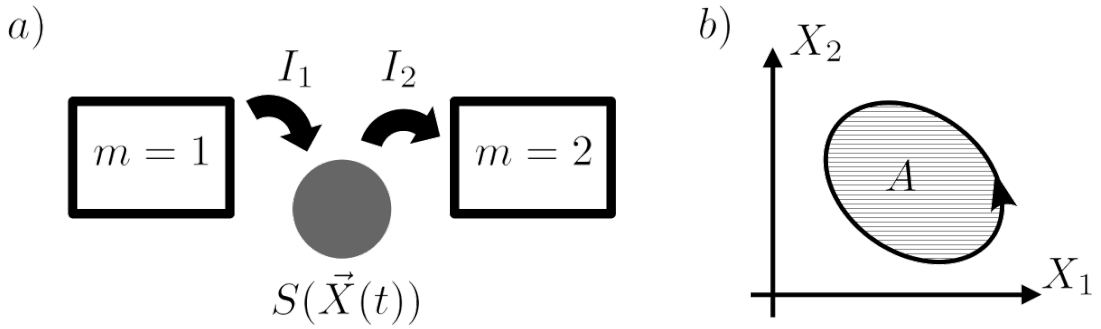

Figure 2.7: Basic sketch of an adiabatic pump. (a) A particle or heat current is extracted from reservoir $m = 1$ and deposited in the reservoir $m = 2$ at each cycle. The dynamics of the central system are ruled by a set of time-dependent parameters $\vec{X}$. (b) The parameter space. The particular driving protocol is determined by closed curve enclosing a total area A.

From Eq. (2.8) we can anticipate some of the key conditions for the adiabatic pumping to occur: at least two driving parameters must be present. And since we need a finite area A to get a nonzero result in (2.8), the drivings with harmonic dependence on time must have a phase lag, quite equivalently to what we saw already in Fig. 2.6. Like in Pothier's device, in open systems the adiabatic pump effect can be present even in the cases where the baths are held at equal temperature, or equal chemical potential. A break of time and spatial symmetry is also necessary for a finite transport during the cycle, as we will see later.

A key interest in the area of quantum pumps is the search for newer mechanisms that could lead to larger *dc* currents and better experimental setups. With this goal in mind, in this work we will show that the problem of quantum energy pumping bares a close resemblance with the problem of charge pumping. In addition, in Chapter 6 we will address the general problem of the maximization of the observed pump effect in quite realistic physical conditions. A brief overview of the vast literature on pumping of charge and heat can be found in the reviews [154, 155, 156]. One of the big motivations of the present thesis is to show how pumping affects the operation of a quantum thermal machine, and the related geometric effects naturally occurring in these systems.

2.6 Quantum thermal machines

Nothing prevent us from applying the ideas of classical thermodynamic cycles to the system sketched in Fig. 2.7. Under such perspective the central system is identified as a working substance (WS) that can operate between two or more thermal reservoirs, thus defining a quantum thermal machine. The development and implementation of thermodynamic processes in few-level quantum systems is currently a very active area of research. Thermodynamic cycles conceived for macroscopic WS, such as the Otto or Carnot cycle, has been theoretically investigated at the microscopic scale [82, 157, 83, 158, 86, 97, 159, 160, 161, 162, 10, 163, 164, 165, 166, 167, 168, 169, 170, 46, 171, 172, 173, 174, 158, 175, 176, 177, 15, 178] and realized experimentally [38, 179, 48, 39, 49, 46, 33].

Understanding how to discriminate and characterize useful work, heat, and dissipated energy in these systems is a fundamental step towards the realization of nanomachines. In the standard thermodynamic cycles, the WS operates in four steps, of which two are in contact to reservoirs at different temperatures connected one at a time, while the other two steps consist in an evolution decoupled from the reservoirs. It is however typically hard to fully isolate a quantum WS from the environment, which is required to emulate ideal classical cycles. This motivates

the study of non-equilibrium systems, where the driven WS is permanently in contact with two or more reservoirs. Unlike standard thermodynamic cycles, these microscopic machines operate away from equilibrium [180, 181], which necessarily implies entropy production and dissipation. Thermoelectric devices [30] as well as autonomous refrigerators [182, 183, 184] are seminal examples of this type of operation. In addition to its impact on emerging technologies, the study of quantum heat engines and refrigerators is also of fundamental importance to deepen our understanding of how energy flows and transforms in the quantum regime [166, 185, 186, 30, 187, 188, 189].

Turning to the system of Fig. 2.7, when the WS is connected at the same time to two or more thermal reservoirs, it is permanently thread by a heat flux $J_{\Delta T}$ if a thermal bias ΔT is imposed at the reservoirs. Hence, the very operation as a machine relies on the mechanism of heat–work conversion in order to overcome this effect as well as the dissipation generated by the driving sources. In Chapter 5 we will see that in the adiabatic regime and under a small temperature bias, the adiabatic (heat) pump J_{pump}, as described in the previous section, is the central piece for the heat–work conversion. When the pumped heat is transported in the opposite direction of the heat flux sustained by the temperature bias, we may have $J_{\Delta T} < -J_{pump}$, meaning that the machine works as a refrigerator. In this operational mode a certain amount of work must be supplied to the driving forces to keep the machine working. Surprisingly, the same mechanism can be reversed to operate the machine as a heat engine. In this case, part of the heat flux $J_{\Delta T}$ can be used to perform work against the drivings. In both cases the mere fact that we are performing a cycle at a finite time means that we will have dissipation. This additional generated heat is detrimental both to cooling and the work extraction, and must be included in the figure of merit analysis of our machines. Thus, the optimal machine, is the one leading to the best balance between the heat-work and the dissipative processes.

Chapter 3

Theoretical tools and methods

The aim of this chapter is to describe the different tools that we use to solve the non-equilibrium open systems presented in the previous chapter. We focus on the slow dynamics where the typical time scale for the driving sources is much longer than any characteristic time scale associated to the few-level quantum system coupled to the reservoirs. These conditions define the so called "adiabatic regime". Our main interest is to compute the adiabatic-response coefficients with respect to external driving forces. To this end we describe the general concepts of adiabatic linear response in Section 3.1.

In Section 3.2 we review a Hamiltonian description of heat transport developed by Luttinger [190] and Tatara [191]. This will be a very useful ingredient for the definition of the thermal geometric tensor in Chapter 5.

We can split our physical systems into two main cases, depending whether the interaction with the reservoirs can be considered strong, or not. Each case is treated in sections 3.3 and 3.4 respectively. Furthermore, among the systems with strong coupling we must take into consideration the presence of local interactions. Since our approach relies on calculations of response functions which are evaluated with respect to the system in instantaneous thermodynamic equilibrium, we review the equilibrium Green's functions approach and we discuss in detail the case of non-interacting systems in Section 3.3.1. The interacting SIAM model ($U \neq 0$ case) will be treated using a mean field approach (Section 3.3.5) and the Numerical Renormalization Group (NRG) technique, Section 3.3.6.

3.1 Adiabatic linear response

We start by considering a quantum system in thermal equilibrium described by a t-independent Hamiltonian $\hat{H}_0$. In this case, the expectation value of an observable of the system is obtained by the usual formula:

$$\left\langle \hat{\mathcal{O}} \right\rangle = \frac{1}{Z_0} \sum_n \langle \hat{n} | \, \hat{\mathcal{O}} \, | \hat{n} \rangle \, e^{-\beta E_n} = \frac{1}{Z_0} \mathrm{Tr} \left[\hat{\rho}_0 \hat{\mathcal{O}} \right] \tag{3.1}$$

where $\hat{\rho}_0 = |\hat{n}\rangle \langle \hat{n}|$ is the density operator and Z_0 the partition function defined by $Z_0 = \mathrm{Tr}\left[\hat{\rho}_0\right]$. The eigenstates of $\hat{H}_0$ are denoted by the kets $|\hat{n}\rangle$, related to the eigenvalues E_n through the relation $\hat{H}_0 |\hat{n}\rangle = E_n |\hat{n}\rangle$.

When introducing time dependence in the Hamiltonian $\hat{H}$ of the system we must consider out of equilibrium effects in the calculation of the expectation values of $\hat{\mathcal{O}}$. The aim of the linear response in the adiabatic regime is to introduce these effects in the case of slow changes in $\hat{H}(t)$. In quantum mechanics the time evolution can be formulated in three main representations [192]:

- The *Schrödinger picture*: the state of the system evolves in time $|\Psi(t)\rangle$, and the observables and other operators are essentially constant (although $\hat{H}$ can have explicit

time dependence). The evolution of the states is given by the Schrödinger equation, $i\partial_t |\Psi(t)\rangle = \hat{H}(t) |\Psi(t)\rangle$.

- The *Heisenberg picture*: in this representation the states are constant, and the time evolution is introduced through the operators using: $\mathcal{O}_H(t) = e^{iHt/\hbar}\mathcal{O}e^{-iHt/\hbar}$. We say that the operator $\mathcal{O}$ is expressed in the Heisenberg representation with respect to $\hat{H}$ (in general we will omit the subscript H). In this picture the evolution of the operators is ruled by the Heisenberg equation: $\partial_t \mathcal{O}_H(t) = (i/\hbar)\left[\mathcal{O}_H(t), \hat{H}\right]$.

- The *Interaction picture*: both the states and the operators evolves in time, is an intermediate representation between the Schrödinger and Heisenberg pictures. It is a useful representation for cases where the Hamiltonian can be split in two parts, a "simple" term $\hat{H}_0$ and a "complicated" one $\hat{V}$. When $\hat{H}$ has explicit time dependence we may write $\hat{H}(t) = \hat{H}_0 + \hat{V}(t)$, i.e. include the time dependence in the V term. The states in this picture evolves according to $|\Psi_I(t)\rangle = e^{iH_0t/\hbar}e^{-iHt/\hbar} |\Psi(0)\rangle = e^{iH_0t/\hbar} |\Psi(t)\rangle$ and the operators $\mathcal{O}_I(t) = e^{iH_0t/\hbar}\mathcal{O}e^{-iH_0t/\hbar}$.

The convenient representation for the development of the adiabatic linear response theory is the Interaction picture. As already said, we consider the temporal dependence of the system described by a Hamiltonian $H(t) = H_0 + V(t)$ where H_0 is time-independent. The evolution equation for the eigenstates of the system can be written as:

$$|n(t)\rangle = e^{-iH_0t/\hbar} |n_I(t)\rangle = e^{-iH_0t/\hbar}\hat{U}(t,t_0) |n_I(t_0)\rangle . \tag{3.2}$$

where the time evolution operator $e^{iH_0t/\hbar}e^{-iHt/\hbar} = \hat{U}(t,t_0) = T_t\left[\exp\left((-i/\hbar)\int_{t_0}^{t} dt' V(t')\right)\right]$ encodes the non-trivial evolution of the states. T_t denoting time-ordering. The time evolution operator connects the state $|\Psi_I\rangle$ at time t with the past time t_0.

We consider now a generic system as in 2.1, connected to one or more reservoirs. For simplicity we now consider that all he reservoirs have same temperature and chemical potential. The central part of the system is driven by a set of external potentials $\vec{X}(t) = [X_1(t), X_2(t), ..., X_N(t)]$ which determines the time dependence of $\mathcal{H}_S$. In this thesis, we consider Hamiltonians with the following structure

$$\hat{\mathcal{H}}_S(t) = \hat{\mathcal{H}}_S(\vec{X}(t)) = \hat{H}_{S0} - \sum_j \hat{F}_j X_j(t) \tag{3.3}$$

where $\hat{H}_{S0}$ is a t-independent term and $\hat{F}_j$ are hermitic operators representing the *generalized forces*, $\hat{F}_j = -\frac{\partial \hat{\mathcal{H}}_S(t)}{\partial X_j(t)}$. With the definition of the vector $\hat{\vec{F}} = [\hat{F}_1(t), ..., \hat{F}_N(t)]$ the previous sum can be expressed as an scalar product $\hat{\vec{F}} \cdot \dot{\vec{X}}$. At the lowest (0-th order) in the adiabatic linear-response approximation, the system is described by the *frozen* Hamiltonian $\hat{H}_t = \hat{\mathcal{H}}_S(\vec{X}(t))$ where time is taken a parameter. In this case the problem is reduced to a static system and the expectation values can be computed via the frozen density matrix $\hat{\rho}_t$ associated to $\hat{H}_t$.

Following Ref. [80], when the rate of change of the parameters $\dot{X}_j(t)$ is small we can perform an expansion on $\dot{\vec{X}}$. The dynamical perturbation to the steady state $\hat{\rho}_t$ can be estimated to $\delta\hat{\rho} \sim \tau_{\text{rel}}(\partial_{X_j}\hat{\rho}_t)\dot{X}_j$ [193, 80, 161] where τ_{rel} is the typical relaxation time of the system. More precisely, the time evolution operator at first-order expansion in $\dot{\vec{X}}$ in the interaction picture is given by

$$\hat{U}(t,t_0) = T_t\left[\exp\left\{-(i/\hbar)\int_{t_0}^{t} dt'(t-t')\hat{\vec{F}}(t')\cdot\dot{\vec{X}}(t)\right\}\right] \approx 1 - (i/\hbar)\int_{t_0}^{t} dt'(t-t')\hat{\vec{F}}(t')\cdot\dot{\vec{X}}(t). \tag{3.4}$$

where $\hat{\vec{F}}(t')$ is expressed in the Heisenberg representation with respect to $\hat{H}_t$. Eq. (3.4) can be used to evolve the states and compute the expectation value of any observable of the system, $\left\langle \hat{\mathcal{O}} \right\rangle (t) = \frac{1}{Z_0} \sum_n \langle n(t)| \hat{\mathcal{O}} |n(t)\rangle e^{-\beta E_n}$. The result of expanding the exponential to the 1st order in $\dot{\vec{X}}(t)$ in this procedure is

$$\left\langle \hat{\mathcal{O}} \right\rangle (t) = \left\langle \hat{\mathcal{O}} \right\rangle_t - i/\hbar \int_{t_0}^{t} dt'(t-t') \left\langle \left[\hat{\mathcal{O}}(t), \hat{\vec{F}}(t') \right] \right\rangle_t \cdot \dot{\vec{X}}(t) \tag{3.5}$$

where the operators $\hat{\mathcal{O}}(t)$ and $\hat{\vec{F}}(t')$ are expressed in the Heisenberg representation with respect to the frozen Hamiltonian $\hat{H}_t$. Also, the symbol $\langle ... \rangle_t$ means the expectation value computed through the frozen density matrix $\hat{\rho}_t$.

From Eq. 3.5 we define the adiabatic response functions as

$$\begin{aligned} \Lambda_t^{\hat{\mathcal{O}},\hat{F}_j} &= -i/\hbar \int_{-\infty}^{t} dt'(t-t') \left\langle \left[\hat{\mathcal{O}}(t), \hat{F}_j(t') \right] \right\rangle_t \\ \vec{\Lambda}_t^{\hat{\mathcal{O}}} &= \left[\Lambda_t^{\hat{\mathcal{O}},\hat{F}_1}, ..., \Lambda_t^{\hat{\mathcal{O}},\hat{F}_N} \right] \end{aligned} \tag{3.6}$$

where for each reference time t the forces are assumed to be acting from $t_0 = -\infty$. Eq. 3.5 is written in a simpler form:

$$\left\langle \hat{\mathcal{O}} \right\rangle (t) = \left\langle \hat{\mathcal{O}} \right\rangle_t + \vec{\Lambda}_t^{\hat{\mathcal{O}}} \cdot \dot{\vec{X}}(t) \tag{3.7}$$

.

In order to prove useful identities satisfied by the adiabatic response functions it is convenient to define the retarded adiabatic susceptibilities $\chi_t^{\hat{\mathcal{O}},\hat{F}_j}(t-t') = -(i/\hbar)\theta(t-t') \left\langle \left[\hat{\mathcal{O}}(t), \hat{F}_j(t') \right] \right\rangle_t$. In terms of the susceptibilities the adiabatic coefficients are written according to

$$\Lambda_t^{\hat{\mathcal{O}},\hat{F}_j} = -i/\hbar \int_{-\infty}^{\infty} dt'(t-t')\theta(t-t') \left\langle \left[\hat{\mathcal{O}}(t), \hat{F}_j(t') \right] \right\rangle_t = \int_{-\infty}^{\infty} d\tau \tau \chi_t^{\hat{\mathcal{O}},\hat{F}_j}(\tau) \tag{3.8}$$

where we have used the fact that the susceptibilities are evaluated with the frozen density matrix, meaning that time dependence is only through $\tau = (t-t')$.

We can Fourier-transform the previous equation:

$$\begin{aligned} \Lambda_t^{\hat{\mathcal{O}},\hat{F}_j} &= \mathrm{Re} \left[\int_{-\infty}^{\infty} d\tau \int_{-\infty}^{\infty} \frac{d\omega}{2\pi i} e^{-i\omega\tau} \partial_\omega \chi_t^{\hat{\mathcal{O}},\hat{F}_j}(\omega) \right] \\ &= \mathrm{Re} \left[-i \int_{-\infty}^{\infty} d\omega \partial_\omega \chi_t^{\hat{\mathcal{O}},\hat{F}_j}(\omega) \delta(\omega) \right] = \lim_{\omega \to 0} \frac{\mathrm{Im} \left[\chi_t^{\hat{\mathcal{O}},\hat{F}_j}(\omega) \right]}{\omega} \end{aligned} \tag{3.9}$$

where we used that the spectral function $\mathrm{Im} \left[\chi_t^{\hat{\mathcal{O}},\hat{F}_j}(\omega) \right]$ is odd in the ω variable, meaning $\mathrm{Im} \left[\chi_t^{\hat{\mathcal{O}},\hat{F}_j}(0) \right] = 0$ [194].

Based on the previous definitions, we define the susceptibilities for two arbitrary operators $\hat{\mathcal{O}}_{i,j}$ as

$$\chi_t^{\hat{\mathcal{O}}_i,\hat{\mathcal{O}}_j}(\tau) = -(i/\hbar)\theta(\tau) \left\langle \left[\hat{\mathcal{O}}_i(\tau), \hat{\mathcal{O}}_j(0) \right] \right\rangle_t . \tag{3.10}$$

and $\Lambda_t^{\hat{\mathcal{O}}_i,\hat{\mathcal{O}}_j}$ in analogy with Eq. (3.6). Eq. (3.10) is again evaluated using the equilibrium density matrix $\hat{\rho}_t$, meaning that we can deduce some properties based on microreversibility.

We verify that $\chi_t^{\hat{\mathcal{O}}_i,\hat{\mathcal{O}}_j}(-\tau) = -(i/\hbar)\theta(\tau)\left\langle\left[\hat{\mathcal{O}}_j(\tau),\hat{\mathcal{O}}_i(0)\right]\right\rangle_t$, which implies that under a time reversal transformation $\tau \to -\tau$ the adiabatic coefficient $\Lambda_t^{\hat{\mathcal{O}}_i,\hat{\mathcal{O}}_j}$ satisfies

$$\Lambda_t^{\hat{\mathcal{O}}_i,\hat{\mathcal{O}}_j} \underset{\tau\to-\tau}{\to} \mathrm{Re}\left[i\int_{-\infty}^{\infty}\frac{d\omega}{\pi}\mathrm{Im}\left[\chi_t^{\hat{\mathcal{O}},\hat{F}_j}(\omega)\right]\int_{-\infty}^{\infty}d\tau\tau\theta(-\tau)e^{-i\omega\tau}\right] = \lim_{\omega\to0}\frac{\mathrm{Im}\left[\chi_t^{\hat{\mathcal{O}},\hat{F}_j}(\omega)\right]}{\omega} = \Lambda_t^{\hat{\mathcal{O}}_j,\hat{\mathcal{O}}_i}. \tag{3.11}$$

When considering a magnetic field B, the time reversal transformation implies that one must change $B \to -B$ in the frozen Hamiltonian $\hat{H}_t$ defining $\hat{\rho}_t$. This translates into the Onsager relation:

$$\chi_t^{\hat{\mathcal{O}}_i,\hat{\mathcal{O}}_j}(B,\omega) = s_i s_j \chi_t^{\hat{\mathcal{O}}_j,\hat{\mathcal{O}}_i}(-B,\omega) \tag{3.12}$$

where the signs $s_i, s_j = \pm$ depend on the parity of the $\hat{\mathcal{O}}_j, \hat{\mathcal{O}}_i$ operators under a time reversal transformation. Applied to the adiabatic coefficients we find

$$\Lambda_t^{\hat{\mathcal{O}}_i,\hat{\mathcal{O}}_j}(B) = s_i s_j \Lambda_t^{\hat{\mathcal{O}}_j,\hat{\mathcal{O}}_i}(-B). \tag{3.13}$$

3.2 Hamiltonian description of a thermal bias: Luttinger theory

In our approach to quantum thermal machines the central system of Eq. (2.1) is driven by time-dependent external forces. The effect of the drivings on the system are captured by the response coefficients of Section 3.1. In particular, the adiabatic description of the energy dynamics requires the calculation of the current operators to evaluate the corresponding coefficients. Interestingly, we can employ a Hamiltonian representation for the temperature difference within the Kubo linear response framework, for small ΔT. Using this approach the temperature difference ΔT can be considered as a new external parameter. The interplay between the energy currents induced by the thermal bias and the time-dependent drivings becomes part of a unified object, the thermal geometric tensor, which encodes the full energy dynamics of the system in the adiabatic approximation, enabling a complete characterization of the operation of the machine.

The idea of expressing the thermal difference in a Hamiltonian language was originally introduced by Luttinger [190]. Here, we follow the revised version of Luttinger's theory presented by Tatara in Ref. [191], which we briefly review and adapt in order to deal with a Hamiltonian containing a tunneling contact between the central system and the reservoirs at which the thermal difference is applied. Luttinger's theory is formulated in the continuum starting from a Hamiltonian $\mathcal{H}_{\mathrm{E}}(t) = \int \mathrm{d}\mathbf{r} h(\mathbf{r})\psi(\mathbf{r},t)$, where $\psi(\mathbf{r},t)$ is a "gravitational" potential. Gradients of the latter induce energy flows $\mathbf{j}^E$ akin to the electrical currents induced by gradients of the electric potential. Such energy flows obey a continuity equation $\dot{h}(\mathbf{r}) = -\partial_{\mathbf{r}}\cdot\mathbf{j}^E(\mathbf{r})$ as a consequence of energy conservation, which motivates the definition

$$\mathcal{H}_{\mathrm{Lutt}}(t) = \int_{-\infty}^{t}\mathrm{d}t'\int\mathrm{d}\mathbf{r}\,\mathbf{j}^E(t')\cdot\partial_{\mathbf{r}}\psi(\mathbf{r},t), \tag{3.14}$$

with $\partial_{\mathbf{r}}\psi(\mathbf{r},t) = \partial_{\mathbf{r}}T/T$. Such formulation is consistent with the rate of change of the entropy production,

$$\dot{S} = -\int\mathrm{d}\mathbf{r}\frac{1}{T}\partial_{\mathbf{r}}\cdot\langle\mathbf{j}^E(t)\rangle = -\int\mathrm{d}\mathbf{r}\langle\mathbf{j}^E(t)\rangle\cdot\frac{\partial_{\mathbf{r}}T}{T^2}, \tag{3.15}$$

through the relation $\langle\mathcal{H}_{\mathrm{Lutt}}(t)\rangle = TS$.

Ref. [191] considers the alternative Hamiltonian

$$\mathcal{H}_{A_T}(t) = -\int d\mathbf{r}\, \mathbf{j}^E(t') \cdot \vec{A}_T(\mathbf{r}, t). \tag{3.16}$$

The Hamiltonians of Eqs. (3.14) and (3.16) coincide in the long-time average. In fact, $\int_{-\infty}^{+\infty} \mathrm{d}t\ \mathcal{H}_{\mathrm{Lutt}}(t) = \int_{-\infty}^{+\infty} \mathrm{d}t\ \mathcal{H}_{A_T}(t)$ with

$$\partial_t \vec{A}_T(\mathbf{r}, t) = \partial_{\mathbf{r}} \psi(\mathbf{r}, t) = \partial_{\mathbf{r}} T/T. \tag{3.17}$$

In this way, $\vec{A}_T(\mathbf{r}, t)$ and $\psi(\mathbf{r}, t)$ behave, respectively, in a similar way as the vector and scalar potentials of electromagnetism. The specific application of Luttinger's theory in our problem is covered in Chapter 5.

3.3 Strong-coupling treatment

When the coupling to the reservoirs cannot be assumed to be small enough to admit an expansion in the coupling constants (e.g. V_k of Eq. (2.2) and Eq. (2.5)) we must use different approaches depending on the situation. An important aspect to consider is the presence or absence of many-body interactions in the central system. In the non-interacting models the Hamiltonian can be expressed as a bilinear combination of creation and annihilation operators and the non-equilibrium problem can be exactly solved by means of Schwinger-Keldysh non-equilibrium Green's functions [195, 196, 197], as well as by scattering matrix formalism [121, 198, 199, 200]. For systems under slow evolution, we can rely on equilibrium Green's functions to evaluate the susceptibilities, as explained in the previous section. This approach will be described in Sections 3.3.1 to 3.3.3. In the forthcoming sections we will consider this approach to solve the single impurity Anderson model (SIAM) in the non-interacting ($U \neq 0$) regime. In problems with many-body interactions, the Green's function formalism has to be combined with some may-body technique. We consider a simple mean field approach to the case of the SIAM with $U \neq 0$ in Section 3.3.4. Furthermore, an exact diagonalization technique is very well suited for this problem: the Numerical Renormalization Group (NRG). We describe this method in Section 3.3.6.

3.3.1 Non-interacting systems - Equilibrium Green's functions

In this section we follow Ref. [192] to briefly review the equilibrium Green's function method. The single-particle Green's functions for a many body system are defined as

$$\begin{aligned}
G^R(\vec{r}\sigma t, \vec{r}'\sigma' t') &= -i\theta(t-t') \left\langle \left[\Psi_\sigma(\vec{r}, t), \Psi^\dagger_{\sigma'}(\vec{r}', t')\right]_{B,F} \right\rangle \\
G^A(\vec{r}\sigma t, \vec{r}'\sigma' t') &= i\theta(t'-t) \left\langle \left[\Psi_\sigma(\vec{r}, t), \Psi^\dagger_{\sigma'}(\vec{r}', t')\right]_{B,F} \right\rangle \\
G^<(\vec{r}\sigma t, \vec{r}'\sigma' t') &= -i(\pm 1) \left\langle \Psi^\dagger_\sigma(\vec{r}, t)\Psi_{\sigma'}(\vec{r}', t') \right\rangle \\
G^>(\vec{r}\sigma t, \vec{r}'\sigma' t') &= -i \left\langle \Psi_\sigma(\vec{r}, t)\Psi^\dagger_{\sigma'}(\vec{r}', t') \right\rangle
\end{aligned} \tag{3.18}$$

named respectively, the retarded (R), advanced (A), lesser ($<$) and greater ($>$) Green's function. $\Psi_\sigma(\vec{r}, t)$ are local-field operators, where σ is a labelling for the particles' degrees of freedom, like the spin. The operation $\langle A \rangle = Z^{-1}\mathrm{Tr}\,[\rho A]$ represents the statistical expectation value with respect to the equilibrium density operator $\rho = e^{-\beta H}$. Many important quantities of interest and observables can be expressed in terms of these functions. We present here the most relevant aspects of the Green's functions approach used along this thesis, including the equation of motion and the Matsubara methods. In many cases where we assume translation invariance,

we will simply drop the $\vec{r}$ reference of the field operators. Moreover, the thermal equilibrium justifies to drop the general double time dependence (t, t') in favour of a single time variable $\tau = t - t'$. Using the Fourier transform, we will mostly work in the frequency domain.
Note that in the equilibrium case, not all the four defined Green's functions are independent. From the general definitions of Eq. (3.18) we can deduce

$$\begin{aligned} G^R(\vec{r}\sigma t, \vec{r}'\sigma' t') &= \theta(t-t')\left[G^>(\vec{r}\sigma t, \vec{r}'\sigma' t') - G^<(\vec{r}\sigma t, \vec{r}'\sigma' t')\right] \\ G^A(\vec{r}\sigma t, \vec{r}'\sigma' t') &= \theta(t'-t)\left[G^<(\vec{r}\sigma t, \vec{r}'\sigma' t') - G^>(\vec{r}\sigma t, \vec{r}'\sigma' t')\right] \end{aligned} \tag{3.19}$$

which implies that any two of them suffice to compute the remaining ones.

Lehmann representation

An useful way to write the Green's functions is the Lehmann representation, which is an expansion using the system Hamiltonian eigenstate basis. Consider for example the case of fermionic operators labeled by a generic number k, $\Psi_\sigma(\vec{r}, t) \to c_k(t)$. For the diagonal part of the greater function we may write

$$\begin{aligned} G^>(k,k,t-t') = G^>(k,t-t') &= -i\left\langle c_k(t)c_k^\dagger(t')\right\rangle = -\frac{i}{Z}\sum_n \langle n|\, e^{\beta H} c_k(t) c_k^\dagger(t')\,|n\rangle \\ &= -\frac{i}{Z}\sum_{nn'} e^{-\beta E_n}\,\langle n|\, e^{iHt} c_k e^{-iHt}\,|n'\rangle\,\langle n'|\, e^{iHt'} c_k^\dagger e^{iHt'}\,|n\rangle \\ &= -\frac{i}{Z}\sum_{nn'} e^{-\beta E_n}\,\langle n|\, c_k\,|n'\rangle\,\langle n'|\, c_k^\dagger\,|n\rangle\, e^{i(E_n - E_{n'})(t-t')} \end{aligned} \tag{3.20}$$

The Fourier transform with respect to $\tau = t - t'$ results in

$$G^>(k,\omega) = -\frac{2\pi i}{Z}\sum_{nn'} e^{-\beta E_n}\,\langle n|\, c_k\,|n'\rangle\,\langle n'|\, c_k^\dagger\,|n\rangle\,\delta\left((E_n - E_{n'}) + \omega\right). \tag{3.21}$$

Analogously, the lesser and the retarded functions reads

$$G^<(k,\omega) = \frac{2\pi i}{Z}\sum_{nn'} e^{-\beta E_n}\,\langle n|\, c_k^\dagger\,|n'\rangle\,\langle n'|\, c_k\,|n\rangle\,\delta\left((E_n - E_{n'}) - \omega\right), \tag{3.22}$$

$$G^R(k,\omega) = \frac{1}{Z}\sum_{nn'} \frac{\langle n|\, c_k\,|n'\rangle\,\langle n'|\, c_k^\dagger\,|n\rangle}{\omega + (E_n - E_{n'}) + i\eta}\left(e^{-\beta E_n} + e^{-\beta E_{n'}}\right). \tag{3.23}$$

The Lehemann representation is a great tool for demonstrating formal results. For example, by means of some algebraic manipulation, Eqs. (3.21)-(3.23) can be used to prove the general relations

$$\begin{aligned} G^<(k,\omega) &= -G^>(k,\omega)e^{-\beta\omega} \\ 2\mathrm{Im}\left\{G^R(k,\omega)\right\} &= -i\left(1 + e^{-\beta\omega}\right)G^>(k,\omega). \end{aligned} \tag{3.24}$$

The spectral function

A recurrent concept within the framework of Green's functions is the spectral function $A(k, k', \omega)$ defined as

$$A(k,k',\omega) = -2\mathrm{Im}\left\{G^R(k,k',\omega)\right\}. \tag{3.25}$$

We motivate the importance of the definition through an example that will be intensively used in Chapter 4. Let's compute the occupation number for a fermionic state in thermal equilibrium:

$$\langle n_k(t)\rangle = \left\langle c_k^\dagger(t)c_k(t)\right\rangle = -iG^<(k,\tau=0) = -i\int\frac{d\omega}{2\pi}G^<(k,\omega) \tag{3.26}$$

using the second relation of Eq. (3.24) we find

$$\langle n_k \rangle = \int \frac{d\omega}{2\pi} A(k,\omega) n_F(\omega). \tag{3.27}$$

This result justifies the interpretation of the spectral function as a generalized density of states. Indeed, the diagonal part of the spectral function $A(k,k,\omega) = A(k,\omega)$ is a quantum-state resolution of an excitation of energy ω. Furthermore, the trace of the spectral function gives the density of states

$$\rho(\omega) = \sum_k A(k,\omega). \tag{3.28}$$

Expressing Eq. (3.24) in terms of the spectral function, we write the so-called fluctuation-dissipation relations for fermions:

$$\begin{aligned} iG^{>}(k,\omega) &= A(k,\omega)(1 - n_F(\omega)) \\ -iG^{<}(k,\omega) &= A(k,\omega) n_F(\omega) \end{aligned} \tag{3.29}$$

while similar results holds for bosons:

$$\begin{aligned} iG^{>}(k,\omega) &= A(k,\omega)(1 + n_B(\omega)) \\ iG^{<}(k,\omega) &= A(k,\omega) n_F(\omega) \end{aligned} \tag{3.30}$$

It also can be shown that

$$G^{R/A}(k,\omega) = \int \frac{d\omega'}{2\pi} \frac{A(k,\omega')}{\omega - \omega' \pm i\eta}. \tag{3.31}$$

Green's functions of free particles

An important case to have in mind are the free-particle results. These are both useful for reference and interpretation of more general scenarios. Let's consider the Hamiltonian for free particles with energy ε_k (we take the fermionic case):

$$H_0 = \sum_k \varepsilon_k c_k^\dagger c_k. \tag{3.32}$$

In this elementary case we can compute the time evolution of the c_k operators by direct use of the Heisenberg equation

$$\dot{c}_k(t) = -i\left[c_k(t), H_0(t)\right] = -i\left[c_k(t), \sum_{k'} \varepsilon_{k'} c_{k'}^\dagger(t) c_{k'}(t)\right] = -i\varepsilon_k c_k(t) \tag{3.33}$$

we obtain $c_k(t) = c_k(0)e^{-i\varepsilon_k t}$. With this explicit result all of the Green's functions of Eq. (3.18) can be easily computed. We focus on $G^R(k, t-t')$:

$$G^R(k,t-t') = -i\theta(t-t')\left\langle \left\{ c_k(t), c_k^\dagger(t') \right\} \right\rangle = -i\theta(t-t')e^{-i\varepsilon_k(t-t')}. \tag{3.34}$$

We transform to the frequency domain and take the imaginary part in order to compute the spectral function. Using $\tau = t - t'$

$$G^R(k,\omega) = \int_{-\infty}^{\infty} d\tau e^{i(\omega+i\eta)\tau}(-i)\theta(\tau)e^{-i\varepsilon_k\tau} = \frac{1}{\omega - \varepsilon_k + i\eta} \tag{3.35}$$

$$A(k,\omega) = -2\mathrm{Im}\left\{G^R(k,\omega)\right\} = 2\pi\delta(w - \varepsilon_k) \tag{3.36}$$

which means that excitations of energy ω are precisely the (free) particles with momentum ε_k. In more general scenarios of interacting quantum many-body states the spectral function will differ from a delta function, as the excitations of energy ω are more complicated, many body quantum states.

3.3.2 The resonant level model

A typical nanostructure that we consider in the thesis is the quantum dot (see Section 2.2). Here we study the basic properties of a single, spinless fermionic state coupled to the continuum, e.g. an electronic band. Using this model we illustrate the equation of motion theory of Green's functions. The results will be used later for a mean-field analysis of the interacting Anderson model. In fact, the Hamiltonian for this system is given by $\hat{\mathcal{H}}_{SIAM}$ of Eq. (2.2) using a single level $\hat{n}_{d,\sigma} \to \hat{d}^\dagger \hat{d}$ (omitting the label for the spin) and removing the interaction $U \to 0$:

$$H = \varepsilon_d \hat{d}^\dagger \hat{d} + \sum_k \varepsilon_k \hat{c}_k^\dagger \hat{c}_k + \sum_k V_k \left(\hat{c}_k^\dagger \hat{d} + \hat{d}^\dagger \hat{c}_k \right) \tag{3.37}$$

where the resonance is at energy ε_d and the $\hat{c}_k$ are the fermionic operators of the band, with corresponding energies ε_k. Our goal is to find the spectral function of the dot, as well as the occupation as a function of the energy.
We define a local Green's function for the dot, and a mixed Green's function composed of the dot and bath's operators

$$G_d^R(t-t') = -i\theta(t-t') \left\langle \left\{ d(t), d^\dagger(t') \right\} \right\rangle \tag{3.38}$$

$$G_{kd}^R(t-t') = -i\theta(t-t') \left\langle \left\{ c_k(t), d^\dagger(t') \right\} \right\rangle \tag{3.39}$$

Using the Heisenberg equation, we find an expression for the time evolution of the c_k operators:

$$\begin{aligned} \dot{c}_k(t) &= -i \left[c_k(t), H(t) \right] \\ &= -i\varepsilon_k c_k - i \sum_{k'} V_{k'} \left[c_k, c_{k'}^\dagger \right] d, \end{aligned} \tag{3.40}$$

and using the result of Eq. (3.40), we find a set of *equations of motion* for the Green's functions (3.39) and (3.38)

$$i\partial_t G_d^R(t-t') - \varepsilon_d G_d^R(t-t') - \sum_{k'} V_{k'} G_{kd}^R(t-t') = \delta(t-t') \tag{3.41}$$

$$i\partial_t G_{kd}^R(t-t') - \varepsilon_k G_{k'd}^R(t-t') - V_k G_d^R(t-t') = 0 \tag{3.42}$$

These set of coupled equations can be solved using a Fourier transform:

$$(\omega + i\eta) G_d^R(\omega) - \varepsilon_d G_d^R(\omega) - \sum_{k'} V_{k'} G_{k'd}^R(\omega) = 1 \tag{3.43}$$

$$(\omega + i\eta) G_{kd}^R(\omega) - \varepsilon_k G_{kd}^R(\omega) - V_k G_d^R(\omega) = 0 \tag{3.44}$$

Doing some algebra we finally find:

$$G_{kd}^R(\omega) = \frac{V_k}{(\omega - \varepsilon_k) + i\eta} G_d^R(\omega) \tag{3.45}$$

$$G_d^R(\omega) = \frac{1}{(\omega - \varepsilon_d) + i\eta - \Sigma(\omega)} \tag{3.46}$$

where we defined the *self-energy* $\Sigma(\omega) = \sum_{k'} V_{k'}^2 / (\omega - \varepsilon_k + i\eta)$. By contrasting the free-particle result of the retarded Green's function in Eq. (3.35), we see that the self-energy can be interpreted as a contribution to the particle's energy caused by the coupling to the bath. Moreover, the imaginary part of the self-energy has a broadening effect of the spectral function.
A typical approximation (that will be used again in the Anderson model) is the case of constant coupling $V(\varepsilon) = V$ and a reservoir with a constant density of states $\rho(\varepsilon) = \rho_0$ within a

bandwidth given by $-D < \varepsilon < D$. It is useful to define $\Gamma = 2\pi\rho_0 V$ for which the self-energy reduces to

$$\Sigma(\omega) \approx \frac{\Gamma}{2\pi} \ln \left| \frac{D+\omega}{D-\omega} \right| - i\frac{\Gamma}{2}. \tag{3.47}$$

The ω dependence of $\Sigma(\omega)$ is neglected and taken as a correction to the energy ε_d. With these results, the retarded Green's function of the local site, and consequently the spectral function results in

$$G_d^R(\omega) = \frac{1}{(\omega - \varepsilon_d) + i\Gamma/2} \tag{3.48}$$

$$A_d^R(\omega) = \frac{\Gamma}{(\omega - \varepsilon_d)^2 + (\Gamma/2)^2}. \tag{3.49}$$

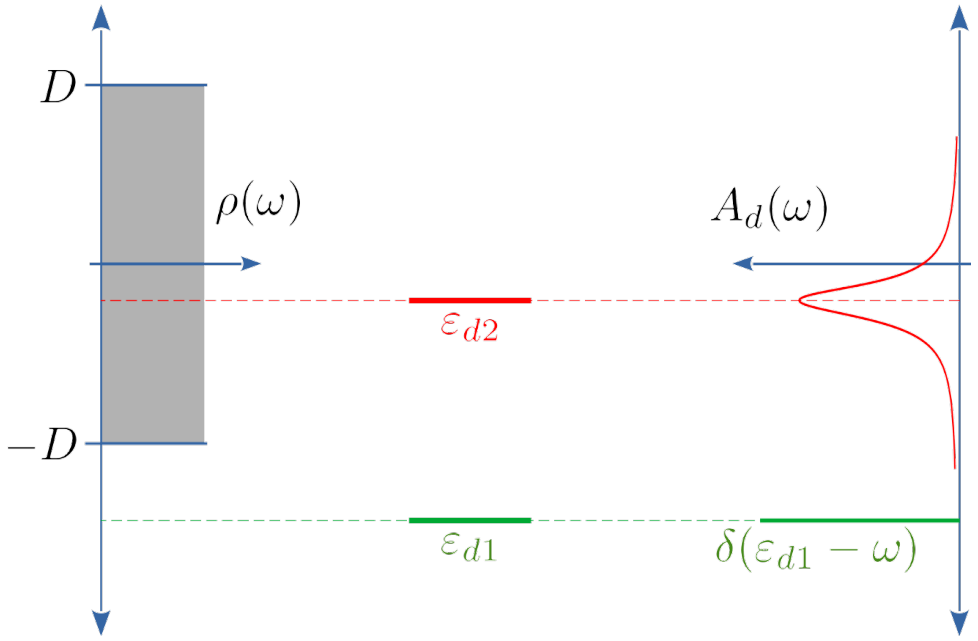

Figure 3.1: Dot with energy ε_{d1} (green) is outside the continuum bandwidth, resulting in a free-particle spectral function. The dot with energy ε_{d2} hybridizes with the bath and broadens its local spectral function.

This procedure can be generalized for the case of several resonant levels. In Fig. 3.1 we consider two resonant levels with energies ε_{d1} and ε_{d2}. In the first case (green) the resonance lies outside the limits of the conduction band and the spectral function is that of a free particle (a delta function). The second level (in red) hybridizes with the bath and the spectral function in this case takes the Lorentzian form of Eq. (3.49).

3.3.3 Imaginary time Green's Functions

The Matsubara, or imaginary-time Green's functions are a useful mathematical tool to compute finite-temperature response functions. The general idea is to merge time and temperature into a single variable, simplifying the calculations by means of a Fourier transform in this variable. They are defined in a similar way to the normal Green's functions of Eq. (3.18), but substituting the time variable by $t \to -i\tau$, where τ is real:

$$\mathcal{C}_{AB}(\tau, \tau') = -\left\langle T_\tau \left[A(\tau) B(\tau') \right] \right\rangle = -\frac{1}{Z} \mathrm{Tr} \left[e^{-\beta H} e^{\tau H} A e^{-\tau H} e^{\tau' H} B e^{-\tau' H} \right] \tag{3.50}$$

here, A and B can be many-body operators, and we assume $\tau > \tau'$ to explicitly write the rightmost equality. Since we are interested mostly in computing linear response functions, we will consider only one or two-body operators. The time ordering operator T_τ in this context is defined as

$$T_\tau \left[A(\tau)B(\tau')\right] = \theta(\tau-\tau')A(\tau)B(\tau') \pm \theta(\tau'-\tau)B(\tau')A(\tau) \tag{3.51}$$

where the $\pm$ correspond to a bosonic/fermionic case respectively. Note that Wick's theorem can be directly applied here since it is a time-ordered expression. Using the cyclic properties of the trace and the Lehmann representation of Eq. (3.50) the following important properties can be deduced:

$$\begin{aligned} -\beta < \tau - \tau' < \beta \\ \mathcal{C}_{AB}(\tau,\tau') = \mathcal{C}_{AB}(\tau-\tau') \\ \mathcal{C}_{AB}(\tau) = \pm\mathcal{C}_{AB}(\tau+\beta) \ \text{ for } \tau < 0 \end{aligned} \tag{3.52}$$

Now let us write $\mathcal{C}_{AB}(\tau)$ in terms of a Fourier series with coefficients

$$\mathcal{C}_{AB}(\tau) = \frac{1}{\beta}\sum_{n=-\infty}^{\infty} e^{-i\pi n\tau/\beta}\mathcal{C}_{AB}(n) \tag{3.53}$$

being

$$\mathcal{C}_{AB}(n) = \frac{1}{2}\int_{-\beta}^{\beta} d\tau e^{i\pi n\tau/\beta}\mathcal{C}_{AB}(\tau). \tag{3.54}$$

Furthermore, Eq. (3.54) can be simplified by making use of the last property of Eq. (3.52):

$$\begin{aligned} \mathcal{C}_{AB}(n) &= \frac{1}{2}\int_0^{\beta} d\tau e^{i\pi n\tau/\beta}\mathcal{C}_{AB}(\tau) + \frac{e^{-i\pi n\tau/\beta}}{2}\int_0^{\beta} d\tau e^{i\pi n\tau/\beta}\mathcal{C}_{AB}(\tau-\beta) \\ &= \frac{1}{2}\left(1 \pm e^{-i\pi n}\right)\int_0^{\beta} d\tau e^{i\pi n\tau/\beta}\mathcal{C}_{AB}(\tau). \end{aligned} \tag{3.55}$$

Given that $n \in Z$, the factor $1/2\left(1 \pm e^{-i\pi n}\right)$ can take only the values 0 and 1. For n even, the factor is 1 in the case of bosons ("+" sign), and 0 for fermions ("−" sign). The opposite happens when n is odd. This fact justifies the following notation for the $\mathcal{C}_{AB}(n)$ coefficients

$$\mathcal{C}_{AB}(i\omega_n) = \int_0^{\beta} d\tau e^{i\omega_n\tau}\mathcal{C}_{AB}(\tau) \tag{3.56}$$

which defines the Matsubara frequencies $\omega_n = \frac{2n\pi}{\beta}$ for bosons, and $\omega_n = \frac{2(n+1)\pi}{\beta}$ for fermions.

Matsubara function for free fermions

In order to illustrate the usefulness of the Matsubara method we compute the single particle Green's function for free fermions $\mathcal{G}_k(\tau-\tau') = \mathcal{C}_{AB}(\tau,\tau')$, considering $A(\tau) = c_k(\tau)$, $B(\tau) = c_k^\dagger(\tau)$ and the diagonal Hamiltonian of Eq. (3.32). By definition we have

$$\begin{aligned} \mathcal{G}_k(\tau-\tau') &= -\left\langle T_\tau\left[c_k(\tau)c_k^\dagger(\tau')\right]\right\rangle \\ &= \left[\theta(\tau'-\tau)n_F(\varepsilon_k) - \theta(\tau-\tau')(1-n_F(\varepsilon_k))\right]e^{-\varepsilon_k(\tau-\tau')}. \end{aligned} \tag{3.57}$$

Using Eq. (3.56) with $\omega_n = \frac{2(n+1)\pi}{\beta}$ we compute the Fourier transform of $\mathcal{G}_k(\tau-\tau')$ with respect to $\tau \equiv (\tau-\tau')$. The result is:

$$\mathcal{G}_k(i\omega_n) = \frac{1}{i\omega_n - \varepsilon_k}. \tag{3.58}$$

We see that Eq. (3.35) can be obtained through Eq. (3.58) using the replacement $i\omega_n \to \omega + i\eta$. The power of the Matsubara method relies on the fact that this property is general (see e.g. [192], Ch. 11). Using the Lehmann representation it can be shown that the retarded/advanced Green's functions and the Matsubara function are all derived from a common, analytical function $C_{AB}(z)$. As a consequence, the following analytic continuation apply:

$$G^{R/A}(\omega) = \mathcal{G}(i\omega_n \to \omega \pm i\eta). \tag{3.59}$$

In practical terms, we will use this formalism to evaluate the susceptibilities that define the adiabatic linear-response coefficients Λ_t introduced in Section 3.1. Recalling the definition of the adiabatic susceptibilities of Eq. (3.10), $\chi_t^{\hat{A},\hat{B}}(\tau) = -(i/\hbar)\theta(\tau)\left\langle\left[\hat{A}(\tau), \hat{B}(0)\right]\right\rangle_t$ we see that these are Green's functions of the form of Eq. (3.18) (before analytic continuation) with A, B two-body operators such as $\hat{n}_\sigma$. For bilinear (free) Hamiltonians, these can be expressed as products of single-particle Green's functions of the form of Eq. (3.58) by using Wick's theorem [192].

3.3.4 Interacting systems - SIAM model

The Single Impurity Anderson Model of Eq. (2.2) with local Coulomb interaction U coupled to a single conduction band is:

$$\mathcal{H}_{\text{SIAM}} = \left[\sum_\sigma \varepsilon_{d\sigma} d_\sigma^\dagger d_\sigma + U n_\uparrow n_\downarrow\right] + \sum_{k\sigma} V_k \left(d_\sigma^\dagger c_{k\sigma} + c_{k\sigma}^\dagger d_\sigma\right) + \sum_{k\sigma} \varepsilon_k c_{k\sigma}^\dagger c_{k\sigma} \tag{3.60}$$

Here the d_σ operator correspond to the impurity site and $\sigma = \{\uparrow, \downarrow\}$ the spin degree of freedom of the electrons. The index k labels the particles of the band, being $\mathcal{H}_\alpha \to \mathcal{H}_B = \sum_{k\sigma} \varepsilon_k c_{k\sigma}^\dagger c_{k\sigma}$ and $\mathcal{H}_{c,\alpha} \to \mathcal{H}_C = \sum_{k\sigma} V_k \left(d_\sigma^\dagger c_{k\sigma} + c.c.\right)$.

3.3.5 Mean field approach

A first approximation that one can do to deal with Eq. (3.60) is to replace the local interacting term by an effective (Hartree-Fock) term:

$$U n_\uparrow n_\downarrow \approx U(n_\uparrow \langle n_\downarrow\rangle + n_\downarrow \langle n_\uparrow\rangle - \langle n_\uparrow\rangle \langle n_\downarrow\rangle). \tag{3.61}$$

This approximation will destroy the many body effects (such as the Kondo resonance) but may be still good enough to describe thermodynamic quantities and static susceptibilities for a wide range of parameters, given that U is sufficiently small, as we will see in Chapter 4. The resulting Hamiltonian for the quantum dot is

$$\mathcal{H}_S = \sum_\sigma \left(\varepsilon_{d\sigma} - U \langle n_{\bar{\sigma}}\rangle\right) n_\sigma \tag{3.62}$$

where $\bar{\sigma}$ means the opposite spin to σ. We have neglected the term $U \langle n_\uparrow\rangle \langle n_\downarrow\rangle$ since it is a constant. With the definition $\tilde{\varepsilon}_{d\sigma} = \varepsilon_{d\sigma} - U \langle n_{\bar{\sigma}}\rangle$ it is clear that we have two individual resonant levels as in Eq. (3.37). The effect of the interaction in the mean field approximation for the σ state is to introduce a rigid shift in the energy, proportional to the occupation of the $\bar{\sigma}$ state. Plugging the result for the spectral function of the resonant level Eq. (3.49) into Eq. (3.27) we get:

$$\langle n_\sigma\rangle = \int \frac{d\omega}{2\pi} \frac{\Gamma}{\left(\omega - \varepsilon_{d\sigma} - U \langle n_{\bar{\sigma}}\rangle\right)^2 + (\Gamma/2)^2} n_F(\omega). \tag{3.63}$$

We finally get the mean occupation number $\langle n_\sigma\rangle$ by a self-consistent computation using Eq. (3.63) iteratively.

3.3.6 Numerical Renormalization Group

The next sections are devoted to the description of the Numerical Renormalization Group (NRG) technique that is used in Chapter 4. For this we will mainly follow the presentation of Ref. [201].

The NRG method

The NRG was introduced by Wilson [202] and it is based in the scaling and renormalization group (RG) ideas. Since it is an exact diagonalization technique, it can be used in a broad class of quantum "impurity" systems, including those containing local strong interactions like the Kondo model or the interacting Anderson model. The main restrictions are imposed on

- the conduction bands, which are assumed to be composed of non-interacting particles
- the impurity size. Due to the computational complexity, it must contain few degrees of freedom.

The main idea is to discretize the continuous conduction band hybridization function

$$\Delta(\omega) = \pi \sum_k V_k^2 \delta(\omega - \varepsilon_k) \tag{3.64}$$

using a logarithmic sampling in ω. The influence of the bath on the impurity is completely determined by $\Delta(\omega)$, then one can make modifications to $\mathcal{H}_{\text{SIAM}}$ given that $\Delta(\omega)$ is preserved. The great advantage of the logarithmic approach is that, within the finite computational resources limits, the lower energy scales are well resolved, while the higher energies (that cannot in general be disregarded) are retained. A picture of this procedure is presented in Fig. 3.3.6. The new discrete version of the problem is then mapped into a semi-infinite chain (Wilson chain) which is diagonalized iteratively. Here we describe the key aspects of the NRG procedure as presented by Bulla et al. [201], including the original results obtained by Krishna-Murthy et al. [203] for the Single Impurity Anderson Model with a constant hybridization function.

Without loss of generality, it is assumed that the bath's density of states lies on the interval $[-D, D]$. We start with a continuos representation of the conduction band and the interaction terms of Eq. (3.60):

$$\mathcal{H}_B = \sum_\sigma \int_{-D}^{D} d\varepsilon g_\sigma(\varepsilon) a^\dagger_{\varepsilon\sigma} a_{\varepsilon\sigma} \tag{3.65}$$

$$\mathcal{H}_C = \sum_\sigma \int_{-D}^{D} d\varepsilon h_\sigma(\varepsilon) \left(d^\dagger_\sigma a_{\varepsilon\sigma} + a^\dagger_{\varepsilon\sigma} d_\sigma \right) \tag{3.66}$$

where the the band operators $a^{(\dagger)}_{\varepsilon\sigma}$ are taken to fulfill the fermionic commutation relations $\left\{ a^\dagger_{\varepsilon\sigma}, a_{\varepsilon'\sigma'} \right\} = \delta(\varepsilon - \varepsilon')\delta_{\sigma\sigma'}$ and we introduce the dispersion and the hybridization functions: $g_\sigma(\varepsilon)$ and $h_\sigma(\varepsilon)$ respectively. These functions can in principle be freely chosen, but must relate to $\Delta(\omega)$ through [201, 204]

$$\Delta(\omega) = \pi \frac{d\varepsilon(\omega)}{d\omega} \left[h(\varepsilon(\omega)) \right]^2 \tag{3.67}$$

where $\varepsilon(\omega)$ is the inverse function of $g(\varepsilon)$, $g[\varepsilon(\omega)] = \omega$. The bandwidth size D is used as an energy unit of the problem, so in what follows we take $D = 1$. Eqs. (3.65) and (3.66) are an useful representation for the logarithmic discretization of the conduction band. We introduce a parameter $\Lambda > 1$ that defines a set of points in $[-1, 1]$ according to

$$\pm x_n = \pm \Lambda^{-n}, \quad n = 0, 1, 2, ... \tag{3.68}$$

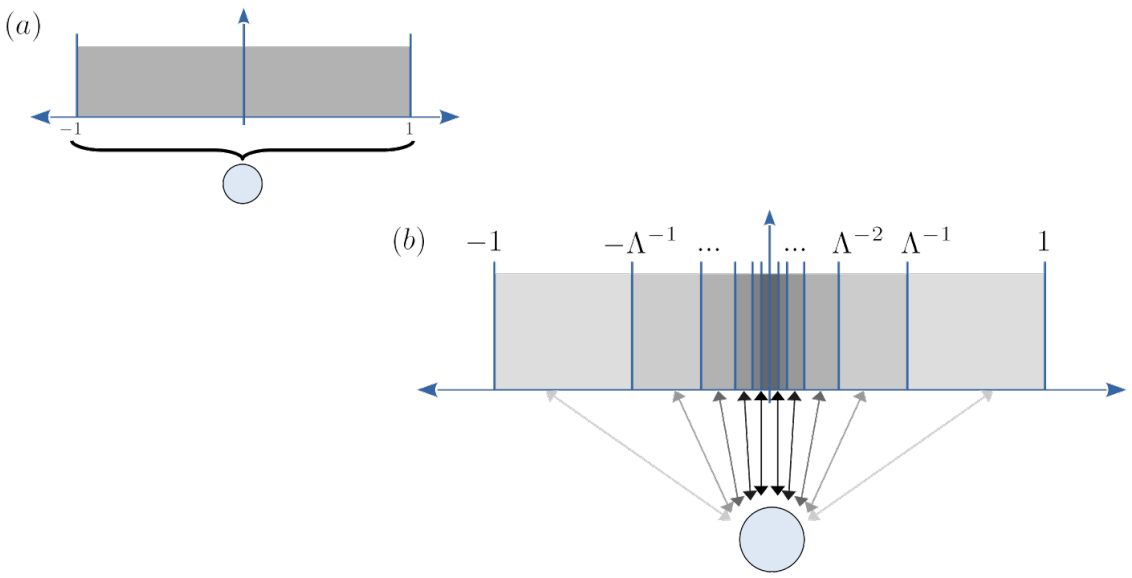

Figure 3.2: (a) Impurity fully coupled to the conduction band. (b) Logarithmic discretization

(see Fig. 3.3.6) For each interval defined by $[x_{n+1}, x_n]$ a complete set of orthonormal functions are introduced:

$$\psi^{\pm}_{np}(\varepsilon) = \begin{cases} \frac{1}{\sqrt{d_n}} e^{\pm i\omega_n p\varepsilon} & \text{for} \quad x_{n+1} < \pm\varepsilon < x_n \\ 0 & \text{otherwise} \end{cases} \tag{3.69}$$

where n labels the n-th interval and p the corresponding Fourier basis element. The lenght of each interval is given by $d_n = x_n - x_{n+1} = \Lambda^{-n}(1 - \Lambda^{-1})$ and the corresponding fundamental frequencies $\omega_n = 2\pi/d_n$.
Using the $\psi^{\pm}_{np}$ functions, an expansion of the conduction band operators of Eq. (3.65) along the logarithmic discretization is performed

$$a_{\varepsilon,\sigma} = \sum_{n,p} \left[a_{np\sigma}\psi^{+}_{np}(\varepsilon) + b_{np\sigma}\psi^{-}_{np}(\varepsilon) \right]. \tag{3.70}$$

Again, the operators $a^{(\dagger)}_{np\sigma}$ and $b^{(\dagger)}_{np\sigma}$ are required to obey the fermionic commutation relations. At this point we will consider a constant density of states in the conduction band, meaning $\Delta(\omega) = \Delta_0$ in $[-1, 1]$ and 0 otherwise. In this case, a suitable choice for the functions of Eq. (3.67) is $g(\varepsilon) = \varepsilon$ and $[h(\varepsilon)]^2 = \Delta_0/\pi$. Introducing the expansion Eq. (3.70) into the hybridization Hamiltonian term of Eq. (3.66) we get

$$\begin{aligned} \mathcal{H}_C &= \sum_{\sigma,n,p} d^{\dagger}_{\sigma} \left(\int_{x_{n+1}}^{x_n} d\varepsilon h(\varepsilon)\psi^{+}_{np}(\varepsilon)a_{np\sigma} + \int_{-x_n}^{-x_{n+1}} d\varepsilon h(\varepsilon)\psi^{-}_{np}(\varepsilon)b_{np\sigma} \right) + \text{h.c.} \\ &= \sum_{\sigma,n,p} d^{\dagger}_{\sigma} \left(\frac{\Delta_0}{\pi}\sqrt{d_n}\delta_{p,0}a_{np\sigma} + \frac{\Delta_0}{\pi}\sqrt{d_n}\delta_{p,0}b_{np\sigma} \right) + \text{h.c.} \\ &= \sum_{\sigma} d^{\dagger}_{\sigma} \sum_{n} \left(\gamma^{+}_{n}a_{n0\sigma} + \gamma^{-}_{n}b_{n0\sigma} \right) + \text{h.c.} \end{aligned} \tag{3.71}$$

with $\gamma_n^+ = \gamma_n^- = \gamma_n = \sqrt{d_n}\Delta_0/\pi$. Note that due the particular form of $h(\varepsilon)$, all the components with $p \neq 0$ were filtered. Furthermore, a particle-hole symmetric hybridization function $\Delta(\omega) = \Delta(-\omega)$ implieas that $\gamma_n^+ = \gamma_n^-$.
A similar procedure is performed for the conduction band in Eq. (3.65). In this case all the p modes appear and one must argue that retaining only the $p = 0$ states is a good approximation. In practice, for $\Lambda \leq 2$ it is safe to drop the extra terms. See Ref. [202, 201] for a discussion on this point. Dropping the $p \neq 0$ terms the resulting expression is:

$$\mathcal{H}_B = \sum_{n\sigma} \left(\xi_n^+ a_{n0\sigma}^\dagger a_{n0\sigma} + \xi_n^- b_{n0\sigma}^\dagger b_{n0\sigma} \right) \tag{3.72}$$

being $\xi_n^\pm = \pm\frac{1}{2}\Lambda^{-n}(1+\Lambda^{-1})$. Eq. (3.72) contains the first approximation of the procedure.
The next step is to obtain the semi-infinite chain representation of the problem. To this end, first we see from Eq. (3.71) that defining the (fermionic) operator

$$c_{0\sigma} = \sqrt{1/\xi_0} \sum_n \gamma_n (a_{n0\sigma} + b_{n0\sigma}) \tag{3.73}$$

leads to the impurity connecting to a single site, with a new hybridization term $\sqrt{\frac{\xi_0}{\pi}} d^\dagger c_{0\sigma}$. For the conduction band the Lanczos algorithm is used to write Eq. (3.72) in a tridiagonal form. Using

$$\mathcal{H}_B = \sum_{\sigma,n=0} \varepsilon_n c_{n\sigma}^\dagger c_{n\sigma} + t_n (c_{n\sigma}^\dagger c_{n+1\sigma} + c_{n+1\sigma}^\dagger c_{n\sigma}) \tag{3.74}$$

and the orthogonal transformation ansatz given by

$$\begin{aligned} a_{n\sigma} &= \sum_m u_{mn} c_{m\sigma} \\ b_{n\sigma} &= \sum_m v_{mn} c_{m\sigma} \end{aligned} \tag{3.75}$$

one founds the recursion relations

$$\begin{aligned} \varepsilon_n &= \sum_m \left[\xi_m^+ u_{nm}^2 + \xi_m^- v_{nm}^2 \right] \\ t_n^2 &= \sum_m \left[(\xi_m^+)^2 u_{nm}^2 + (\xi_m^-)^2 v_{nm}^2 \right] - t_{n-1} - \varepsilon_n^2 \\ u_{n+1,m} &= t_n^{-1} \left[(\xi_m^+ - \varepsilon_n) u_{nm} + t_{n-1} - u_{n-1,m} \right] \\ v_{n+1,m} &= t_n^{-1} \left[(\xi_m^- - \varepsilon_n) v_{nm} + t_{n-1} - v_{n-1,m} \right] \end{aligned} \tag{3.76}$$

which in general must be solved numerically. For the case we are analyzing here with $\Delta_\sigma(\varepsilon) = \Delta_0$ in the Anderson model, Krishna-murthy et al. found the closed expression

$$\begin{aligned} t_n &= \frac{(1+\Lambda^{-1})\Lambda^{-n/2}}{2} \frac{1-\Lambda^{-n-1}}{\sqrt{(1-\Lambda^{-2n-1})(1-\Lambda^{-2n-3})}} \\ \varepsilon_n &= 0. \end{aligned} \tag{3.77}$$

Once the ε_n and t_n coefficients are known, we finally arrive to the effective Hamiltonian in the Wilson Chain form, as depicted in Fig. 3.3.6:

$$\mathcal{H}_{\mathrm{WC}} = \mathcal{H}_S + \sqrt{\frac{\xi_0}{\pi}} \sum_\sigma \left(d_\sigma^\dagger c_{0\sigma} + d_\sigma c_{0\sigma}^\dagger \right) + \sum_n t_n (c_{n\sigma}^\dagger c_{n+1\sigma} + c_{n+1\sigma}^\dagger c_{n\sigma}) \tag{3.78}$$

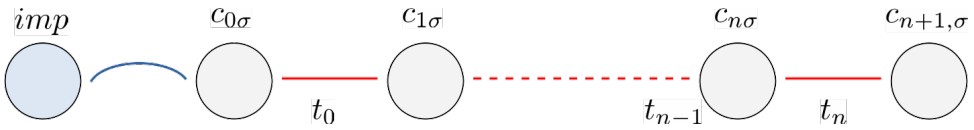

Figure 3.3: The complete mapping to the semi-infinite chain.

Numerical diagonalization

With the definition

$$H_N = \Lambda^{(N-1)/2}\left(\mathcal{H}_S + \sqrt{\frac{\xi_0}{\pi}}\sum_\sigma\left(d_\sigma^\dagger c_{0\sigma} + d_\sigma c_{0\sigma}^\dagger\right) + \sum_{\sigma,n=0}^{N-1} t_n(c_{n\sigma}^\dagger c_{n+1\sigma} + c_{n+1\sigma}^\dagger c_{n\sigma})\right) \tag{3.79}$$

the chain of Eq. (3.3.6) is obtained in the limit

$$\mathcal{H}_{WC} = \lim_{N\to\infty} \Lambda^{-(N-1)/2} H_N. \tag{3.80}$$

The relation between two successive H_N defines the iteration of the NRG

$$H_{N+1} = \sqrt{\Lambda} H_N + \Lambda^{N/2} t_N \sum_\sigma (c_{N\sigma}^\dagger c_{N+1\sigma} + c_{N+1\sigma}^\dagger c_{N\sigma}) \tag{3.81}$$

with the base case H_0 composed of the dot site, plus the interaction with the $c_{0\sigma}$ site.
The energy scale of the H_N Hamiltonian is in the order of $\Lambda^{-(N-1)/2}$, meaning it captures the physics at temperatures around $k_B T \approx \Lambda^{-(N-1)/2} D$. The reason to include the $\Lambda^{(N-1)/2}$ factor in the definition of H_N is to rescale the numbers to $\mathcal{O}(1)$ values. This ensures the numerical stability of the iteration.
At this point Eq. (3.81) can be interpreted as a renormalizarion group transformation of the form $H_{N+1} = R[H_N]$. Since in the NRG procedure we lack a specific set of parameters to relate the transformation trough R, the RG flow is directly characterized by the energies $E_{i,N}$ of the H_N Hamiltonian. Plotting $E_{i,N}$ against N reveals the different regimes of the Anderson model, and the convergence of the method. In Fig. 3.3.6 we reproduce Fig. 4 of Ref. [201].

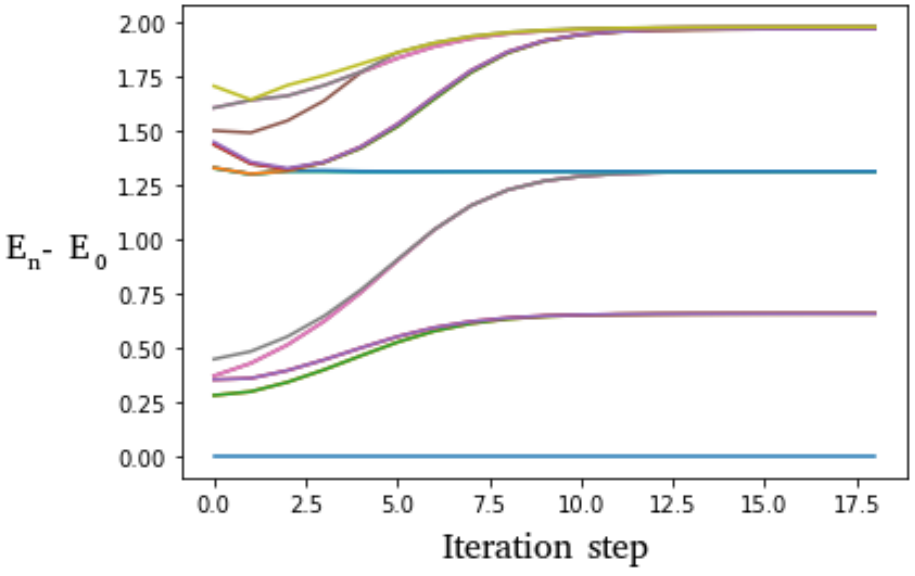

Figure 3.4: Convergence of the method - NRG flow

In practice, the algorithm in the N-th iteration consist on the following steps:

- Find a basis $|m\rangle_N$ where H_N is diagonal, $H_N \to H_N^d$
- Sort the basis with respect to the eigenenergies of H_N in ascending order and truncate the elements to a limiting size N_s
- Find the matrix representation of the $c_{N\sigma}$ and $c_{N\sigma}^\dagger$ operators in the $|m\rangle_N$ basis
- Add site: construct H_{N+1} using H_N^d and the $c_{N\sigma}$ matrices

Note that adding a site to the Hamiltonian implies to expand the basis by a factor of 4 (to account for the $\{|0\rangle_{N+1}, |\uparrow\rangle_{N+1}, |\downarrow\rangle_{N+1}, |\uparrow\downarrow\rangle\}_{N+1}$ states of the new site) meaning that after a few steps we reach the truncation size N_s (usually taken in the order of 1000 for the SIAM). An important detail in the NRG scheme is that truncation is an *ad hoc* step motivated by technical limitations and could introduce undesirable effects. For each particular application one must check the accuracy of the method and adjust the relevant parameters Λ and N_s.
We end this Section referring to the supplemental material, where an actual (minimal) working implementation of the NRG iteration applied to the SIAM model can be found.

Computation of physical quantities

At each iteration step N we end with a basis set $|m\rangle_N$ associated to an energy scale in the order of $k_B T_N \approx \frac{1}{2}(1+\Lambda^{-1})\Lambda^{-(N-1)/2} D$, as well as the energy spectrum. By keeping track the representation of an $\mathcal{O}$ operator in the $|m\rangle_N$ basis, we can compute the expectation value $\langle\mathcal{O}\rangle$ at any NRG iteration using

$$\langle\mathcal{O}\rangle_N = \frac{1}{Z}\sum_m e^{-\beta E_m}{}_N \langle m|\,\mathcal{O}\,|m\rangle_N . \tag{3.82}$$

where $\beta = 1/(k_B T_N)$.

In contrast to the thermal expectation values of operators Eq. (3.82) that are T-dependent, dynamic quantities such as the spectral function Eq. (3.25) or the susceptibilities of Eq. (3.10) have an additional dependence on energy. For this reason they are more difficult to compute and are, in general, obtained with less precision.

In what follows we sketch the computation of the spectral function and the adiabatic charge susceptibility $\chi^{\sigma\sigma'}(T,t) = -i\theta(t)\langle[n_\sigma(t), n_{\sigma'}(0)]\rangle$ of the quantum dot for the Anderson model, which are two important functions that we use intensively in Chapter 4. We omit the N subscript, understanding that the following expressions are computed at a fixed NRG iteration step at temperature T_N. The spectral function in the time domain is

$$A(T,t) = -2\mathrm{Im}\left\{G^R(T,t)\right\}. \tag{3.83}$$

where $G^R(T,t) = -i\theta(t)\left\langle\left\{d(t), d^\dagger(0)\right\}\right\rangle$. We can write $G^R(T,t)$ in the Lehmann decomposition as

$$G^R(T,t) = -i\theta(t)\sum_{m,n}\frac{e^{-\beta E_n} + e^{-\beta E_m}}{Z(\beta)}\langle n|\,d(t)\,|m\rangle\langle m|\,d^\dagger(0)\,|n\rangle \tag{3.84}$$

Here $Z(\beta) = \sum_n e^{-\beta E_n}$ is the partition function and $|n\rangle$ ($|m\rangle$) are the eigenstates corresponding to energies $E_{n(m)}$ of H_N. Using $d(t) = e^{iHt}d(0)e^{-iHt}$ and plugging the previous decomposition into Eq. (3.83), we find, after a Fourier transform:

$$A(T,w) = \sum_{m,n}\frac{e^{-\beta E_n} + e^{-\beta E_m}}{Z(\beta)}\left|\langle m|\,d^\dagger(0)\,|n\rangle\right|^2\delta\left(\omega - (E_m - E_n)\right) \tag{3.85}$$

which again involves the representation of the $d^\dagger$ operator in the $|n\rangle$ basis. An extra step in the numerical computation is to provide a broadening of the δ functions to recover a continuous

spectrum. This is usually performed using log-Gaussian functions of the same total weight, but alternative approaches had been considered in the literature [205, 206].

We now focus on the susceptibilities $\chi^{\sigma\sigma'}(T,t)$, which are the key ingredient for the calculation of the adiabatic response functions as introduced in Eq. (3.8). In the Lehmann representation we find

$$\chi^{\sigma\sigma'}(T,t) = i\theta(t)\sum_{n,m}\frac{e^{\beta E_n}-e^{\beta E_m}}{Z(\beta)}\langle n|\, n_\sigma(0)\,|m\rangle\,\langle m|\, n_{\sigma'}(0)\,|n\rangle\, e^{i(E_n-E_m)t} \tag{3.86}$$

After Fourier transform we get:

$$\begin{aligned}\chi^{\sigma\sigma'}(T,\omega) = i\sum_{n,m}\frac{e^{\beta E_n}-e^{\beta E_m}}{Z(\beta)}\langle n|\, n_\sigma(0)\,|m\rangle\,\langle m|\, n_{\sigma'}(0)\,|n\rangle\,\times \\ \times\left[\frac{i}{\omega-(E_n-E_m)}+\pi\delta(\omega-(E_n-E_m))\right].\end{aligned} \tag{3.87}$$

Now, using Eq. (3.9) we find the following expression for the adiabatic charge coefficient $\Lambda_t^{n_\sigma,n_{\sigma'}}$

$$\Lambda_t^{n_\sigma,n_{\sigma'}} = \lim_{\omega\to 0}\frac{\pi}{\omega}\sum_{n,m}\frac{e^{\beta E_n}-e^{\beta E_m}}{Z(\beta)}\langle n|\, n_\sigma(0)\,|m\rangle\,\langle m|\, n_{\sigma'}(0)\,|n\rangle\,\delta(\omega-(E_n-E_m)) \tag{3.88}$$

that can be computed at every iteration of the NRG procedure.

3.4 Weak-coupling treatment

3.4.1 Quantum Master Equations

When the system-bath coupling is weak, we can rely on a simple approach based on master equations for the reduced density matrix of the central system. This is the case with the qubit systems described in Section 2.3.

Here we follow Bhandari et al. [103] to illustrate the derivation of the QME formalism for the case of a central quantum system slowly driven by external parameters $\vec{X}$. We will, however, specialize from the beginning to our case of interest and omit much of the discussion in favour of a short exposition. In particular, we will consider the case where the system is coupled to baths of bosonic excitations. The resulting equations will be valid up to first order in the small velocities $\dot{\vec{X}}$ and the coupling constants $V_{k\alpha}$.

We start by considering the central Hamiltonian $\mathcal{H}_S(\vec{X}(t))$ and an unitary matrix $U(\vec{X}(t))$ that diagonalizes $\mathcal{H}_s$ at time t,

$$\tilde{\mathcal{H}}_S(\vec{X}) = U(\vec{X})\mathcal{H}_S(\vec{X})U^\dagger(\vec{X}) = \sum_\ell \varepsilon_\ell(\vec{X})|\ell(\vec{X})\rangle\langle\ell(\vec{X})| \tag{3.89}$$

where the relation $\tilde{\mathcal{H}}_S(\vec{X})\,|\ell(\vec{X})\rangle = \varepsilon_\ell(\vec{X})\,|\ell(\vec{X})\rangle$ defines the instantaneous eigenstates $|\ell(\vec{X})\rangle$ of the Hamiltonian. From now on we omit the explicit dependence on t, remembering that it comes through the $\vec{X}$ parameters. Written in the basis of these eigenstates we define the density matrix

$$\hat{\rho}_{\ell j}(\vec{X}) = |\ell(\vec{X})\rangle\langle j(\vec{X})| \tag{3.90}$$

and we write the contact Hamiltonians in the same basis:

$$\tilde{\mathcal{H}}_{c,\alpha}(\vec{X}) = \sum_{k_\alpha}\sum_{\ell j} V_{k_\alpha}\lambda_{\alpha,\ell j}(\vec{X})\left[\hat{b}^\dagger_{k_\alpha}\hat{\rho}_{\ell j}+\hat{\rho}_{\ell j}\hat{b}_{k_\alpha}\right] \tag{3.91}$$

where the $\lambda_{\alpha,\ell j}$ coefficients are the contact matrix of Eq. (2.5) rotated to the diagonal basis of $\mathcal{H}_S$:

$$\lambda_{\alpha,\ell j} = \left[U(\vec{X})\sigma_\alpha U^\dagger(\vec{X})\right]_{\ell j} \tag{3.92}$$

Derivation of the master equation

Let $\hat{\rho}_0$ be the state of the global system at time t_0. We call $\hat{\rho}^{\rm tot}(t)$ the state evolved in time through the full Hamiltonian $\mathcal{H}$:

$$\hat{\rho}^{\rm tot}(t) = \mathcal{U}(t,t_0)\hat{\rho}_0\mathcal{U}^\dagger(t,t_0) \tag{3.93}$$

with $\mathcal{U}(t,t_0) = \hat{T}\left\{\exp\left[-\frac{i}{\hbar}\int_{t_0}^{t} dt'\mathcal{H}(t')\right]\right\}$ being the time evolution operator. Any observable $\mathcal{O}$ acting on the subspace of the central system S can be decomposed as

$$\mathcal{O}(t) = \sum_{\ell j} O_{\ell j}(t)\hat{\rho}_{\ell j}(t) \tag{3.94}$$

where $O_{\ell j} = \langle \ell | \mathcal{O}(t) | j \rangle$ are the elements of $\mathcal{O}(t)$ in the $|\ell(\vec{X})\rangle$ basis. The expectation value of this operator at time t is computed as

$$\langle \mathcal{O}(t) \rangle = {\rm Tr}\left[\hat{\rho}^{\rm tot}(t)\mathcal{O}(t)\right] = {\rm Tr}\left[\hat{\rho}^{\rm tot}(t)\sum_{\ell j} O_{\ell j}(t)\hat{\rho}_{\ell j}(t)\right] = \sum_{\ell j} O_{\ell j}(t)\rho_{\ell j}(t) \tag{3.95}$$

with $\hat{\rho}^{\rm tot}(t)$ the state of the full system and the density matrix $\rho_{\ell j}$ is defined according to $\rho_{\ell j}(t) = {\rm Tr}\left[\hat{\rho}^{\rm tot}(t)\hat{\rho}_{\ell j}(t)\right]$. Note that $O_{\ell j}(t)$ is easy to compute since the basis $|\ell(\vec{X})\rangle$ is assumed to be known. For calculating $\rho_{\ell j}(t)$ we need the master equation.

Using Eq. (3.93) for the evolved state, the density matrix elements are computed using

$$\rho_{\ell j}(t) = {\rm Tr}\left[\hat{\rho}^{\rm tot}(t)\hat{\rho}_{\ell j}(t)\right] = {\rm Tr}\left[\hat{\rho}_0\mathcal{U}^\dagger(t,t_0)\hat{\rho}_{\ell j}\mathcal{U}(t,t_0)\right] = {\rm Tr}\left[\hat{\rho}_0\hat{\rho}^{\mathcal{H}}_{\ell j}(t)\right] \tag{3.96}$$

where the $\mathcal{H}$ superscript indicates that the operator is written in the Heisenberg representation. It is useful to define the following mixed Green's functions,

$$\begin{aligned} G^{<}_{\ell j,k_\alpha}(t,t') &= -i\left\langle \hat{b}^{\dagger\mathcal{H}}_{k_\alpha}(t')\hat{\rho}^{\mathcal{H}}_{\ell j}(t)\right\rangle \\ G^{<}_{k_\alpha,\ell j}(t,t') &= -i\left\langle \hat{\rho}^{\mathcal{H}}_{j\ell}(t')\hat{b}^{\mathcal{H}}_{k_\alpha}(t)\right\rangle \end{aligned} \tag{3.97}$$

Applying ${\rm Tr}\left[\rho_0\ \cdot\right]$ on both sides of the Heisenberg equation and using (3.97) we arrive to a first equation for $\rho_{\ell j}$

$$\begin{aligned} \frac{d\rho_{\ell j}}{dt} = \frac{i}{\hbar}[\varepsilon_\ell(t) - \varepsilon_j(t)]\rho_{\ell j}(t) + \frac{1}{\hbar}\sum_{k_\alpha,\alpha} V_{k_\alpha} \times \\ \left[\sum_m \lambda_{\alpha,m\ell}(t)\left(G^{<}_{mj,k_\alpha}(t,t) + G^{<}_{k_\alpha,jm}(t,t)\right) - \sum_n \lambda_{\alpha,jn}(t)\left(G^{<}_{\ell n,k_\alpha}(t,t) + G^{<}_{k_\alpha,n\ell}(t,t)\right)\right] \end{aligned} \tag{3.98}$$

A final expression for the master equation requires the evaluation of the Green's functions of Eq. (3.97) up to linear order in the coupling constants V_{k_α} (meaning second order in Eq. (3.98)) and up to linear order in the velocities of the driving parameters $\dot{\vec{X}}$. This can be achieved by using a Dyson equation and perturbation theory at the lowest order in $V_{k\alpha}$ in combination with Langreth theorem in a non-equilibrium approach, plus an expansion using the adiabatic approximation. Here we simply state the result of [103] for the corresponding matrix elements, $\rho_{\ell j}(t)$:

$$\frac{d\rho_{\ell j}(t)}{dt} = \frac{i\epsilon_{\ell j}(t)}{h}\rho_{\ell j} + \sum_{m,n,\alpha}\left[M^{jn}_{m\ell,\alpha}\rho_{mn} + M^{\ell n}_{jm,\alpha}\rho_{nm} - M^{mn}_{jm,\alpha}\rho_{\ell n} - M^{mn}_{m\ell,\alpha}\rho_{nj}\right] \tag{3.99}$$

where we have introduced a shorthand notation for $\varepsilon_\ell(t) - \varepsilon_j(t) = \epsilon_{ij}(t)$ for the instantaneous energy differences. The transition rates $M^{ju}_{m\ell,\alpha}(t)$ for the problems coupled to bosonic baths are given by

$$M^{ju}_{ml,\alpha}(t) = \frac{\lambda_{\alpha,ml}(t)\lambda_{\alpha,ju}(t)}{h}\left[n_\alpha(\epsilon_{ju})\Gamma_\alpha(\epsilon_{ju}) + (1+n_\alpha(\epsilon_{uj}))\Gamma(\epsilon_{uj})\right], \tag{3.100}$$

being $n_\alpha(\varepsilon) = 1/\left(e^{\varepsilon/(k_B T_\alpha)} - 1\right)$ the Bose-Einstein distribution function corresponding to the temperature of the α-reservoir and $\Gamma_\alpha(\varepsilon)$ the α-bath spectral function. In our problems we consider Ohmic baths of the form $\Gamma_\alpha(\varepsilon > 0) = \gamma_\alpha \varepsilon e^{-\varepsilon/\varepsilon_C}$ with a cutoff frequency ε_C, and $\Gamma_\alpha(\varepsilon \leq 0) = 0$. The value of γ_α depends on the coupling strength as $|V_{k_\alpha}|^2$. This quantity defines the relaxation time $\tau_{\rm rel}$ between the central system and the reservoirs, $\tau_{\rm rel} \propto \gamma_\alpha^{-1}\varepsilon$.

By defining the vector $\mathbf{p}(t) = (\rho_{11}, .., \rho_{1n}, \rho_{21}, ..., \rho_{2n}, ..., \rho_{n1}, ..., \rho_{nn})^T$ Eq. (3.99) can be written in a compact form:

$$\frac{d\mathbf{p}(t)}{dt} = \mathbf{M}(t)\mathbf{p}(t). \tag{3.101}$$

We can make explicit the different contributions to $\mathbf{p}(t)$ in the adiabatic approximation by splitting it into a *frozen* plus an *adiabatic* contribution,

$$\mathbf{p}(t) = \mathbf{p}^f(t) + \mathbf{p}^a(t), \tag{3.102}$$

where the first term corresponds to the description with the Hamiltonian frozen at a given time, for which the parameters take values $\vec{X}$, while the second one corresponds to the correction $\propto d_t\vec{X}$. The frozen contribution $\mathbf{p}^f$ is calculated as a function of the time-dependent parameters $\vec{X}$ only (frozen time), and satisfies the stationary (static) limit $\frac{d\mathbf{p}^f(t)}{dt} = 0$. Hence, it can be calculated from

$$0 = \mathbf{M}(\vec{X}) \cdot \mathbf{p}^f(\vec{X}), \tag{3.103}$$

with the normalization condition $\sum_{j=1}\rho^f_{jj} = 1$. On the other hand, the adiabatic component satisfies

$$\frac{\partial \mathbf{p}^f}{\partial t} = \sum_\ell \frac{\partial \mathbf{p}^f(\vec{X})}{\partial X_\ell}\dot{X}_\ell(t) = \mathbf{M}(\vec{X}) \cdot \mathbf{p}^{\mathbf{a}}(t), \tag{3.104}$$

with the normalization condition $\sum_{j=1}\rho^a_{jj} = 0$. An important detail for the calculation of the partial derivatives appearing in the left side of Eq. (3.104) is to take into account the effects of the basis dependence in $\vec{X}$. A practical way to perform the derivative is by expressing ρ^f in the laboratory (fixed) basis first, and then rotate back to the instantaneous diagonal basis.

We can modify $\mathbf{M}$ to include the normalization condition for $\mathbf{p}^a$ in a single equation [207, 55]. Naming $\tilde{\mathbf{M}}$ the resulting matrix, we can finally invert Eq. (3.104) to obtain the closed expression

$$\mathbf{p}^a(t) = \sum_n \tilde{\mathbf{M}}^{-1}(\vec{X}) \cdot \frac{\partial \mathbf{p}^f}{\partial X_n}\dot{X}_n(t). \tag{3.105}$$

Chapter 4

Quantum dot under adiabatic magnetoelectric driving

This chapter is based on the paper *Phys. Rev. B 99, 115424: "Work exchange, geometric magnetization, and fluctuation-dissipation relations in a quantum dot under adiabatic magnetoelectric driving"*.

4.1 Introduction

In the present chapter we study the adiabatic dynamics of the charge, spin and energy of a quantum dot (QD) with a Coulomb interaction under two-parameter driving, associated to time-dependent gate voltage and magnetic field. The quantum dot is coupled to a single reservoir at temperature $T = 0$. This problem corresponds to the RC quantum circuit described in Section 2.4, where the capacitive element is precisely the dot.

When the *ac* driving potential is applied to the QD, a net amount of energy is dissipated in the form of heat. Several recent works indicate that for adiabatic driving and the reservoir is at temperature $T = 0$, such heat generation follows an instantaneous Joule law (IJL) with the universal resistance $R_0 = h/2e^2$ per conducting channel. This result holds for a non-interacting QD [143, 144, 145] as well as for a quantum dot with Coulomb interactions [149] and extends to more complex configurations containing normal and superconducting leads [208]. In the case of QD with many-body interactions and single-parameter driving, the proof of the universal IJL relies on an identity known as the Korringa-Shiba relation [209], derived for Fermi liquids. After Ref. [143], several studies also focused on the distribution of the heat production along the different pieces of the device and the role of the energy reactance [210, 211, 144, 145, 212, 213, 214].

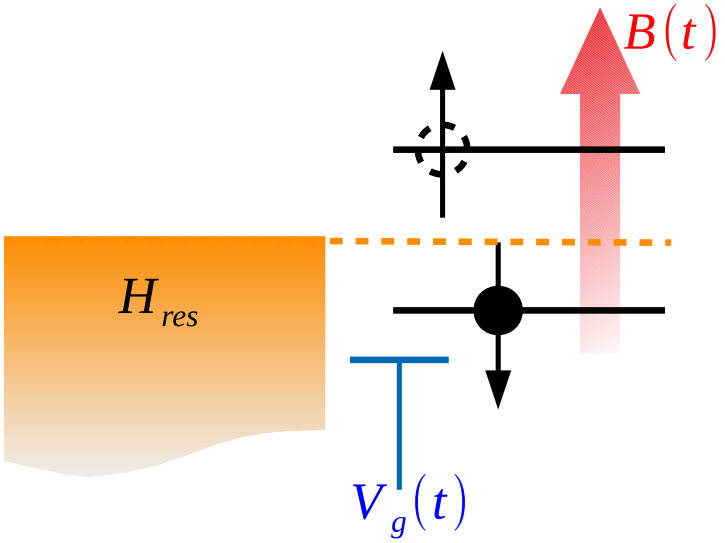

Figure 4.1: Sketch of the setup. A quantum dot connected to a single electronic reservoir at $T = 0$ is driven by means of a gate voltage $V_g(t)$ and a magnetic field $B(t)$. We model the device by an Anderson Hamiltonian with a single level and Coulomb interaction U.

So far, all studies of the RC quantum circuit focused on driving protocols with a single time-dependent parameter, corresponding to an *ac* gate voltage at the quantum dot. Adiabatically driven systems with several time-dependent parameters enable more interesting effects. The most well known example is the quantum pumping of charge between two electron reservoirs in electron systems locally modulated by two time-dependent parameters. As we described in Section 2.5, the net transfer of charge in this case can be characterized by a geometric quantity akin to the Berry phase [54, 52]. Other geometrical aspects of adiabatically driven systems, like geometric magnetism [69] adiabatic perturbation theory in closed systems [215], the thermodynamic metric in qubit systems [81] and rectification [216] have been recently analyzed. Topological properties of the energy conversion have been so far considered only beyond the adiabatic regime [217]. In the present chapter we study the RC circuit under two-parameter driving. In addition to the usual *ac* driving at the gate voltage, we include the effect of an *ac* magnetic field. A sketch of the setup is presented in Fig. 4.1. We solve this problem with the

adiabatic approach introduced in Section 3.1 (see Ref. [80]), which treats the non-equilibrium dynamics by expanding the evolution operator in powers of the velocities of the time-dependent parameters. The coefficients of such expansion depend on frozen equilibrium susceptibilities. In our case, the latter can be numerically exactly evaluated by recourse to numerical renormalization group (NRG) introduced in Section 3.3.6 [218, 219] as in Ref. [149]. Alike to the case of single-parameter driving, the only dissipative element is the contact resistance. Hence, dissipation of energy follows an IJL with the universal resistance R_0 per spin channel. We show that this fact, when analyzed from the perspective of a fluctuation-dissipation relation, implies a series of relations between the static and dynamical charge and spin susceptibilities, which constitute generalizations of the so called Korringa-Shiba law. We show that these relations are valid for both the interacting and non-interacting cases. The interesting feature that the two-parameter driving brings about is the non-equilibrium accumulation of a polarized charge in the QD. The latter can be characterized by a geometric quantity, akin to the pumped charge in quantum pumps in the sense of Section 2.5 [54, 52]. We show that many-body interactions are crucial for this effect to be realized in the present system. In fact the non-interacting limit effectively decouples into two single-parameter driven problems (one for each spin orientation).

The chapter is organized as follows. We introduce the model in Section 4.2. The theoretical approach is presented in Section 4.3 and the results are presented in Section 4.4.

4.2 Model

We consider the Anderson impurity model as described in Section 2.2.1. The driving is encoded in the parameters $X_\sigma(t) = \varepsilon_{0\sigma} + eV_g(t) + s_\sigma \mu_B B(t)$, being $s_\sigma = \pm 1$ for $\sigma = \{\uparrow, \downarrow\}$. We work in the symmetric condition where $\varepsilon_{0\sigma} = -1/2U$. The Hamiltonian for the QD in this case reads

$$\mathcal{H}_S = \sum_\sigma V_\sigma(t)\hat{n}_\sigma + U(\hat{n}_\uparrow - 1/2)(\hat{n}_\downarrow - 1/2), \tag{4.1}$$

with $V_\sigma(t) = eV_g(t) + s_\sigma \mu_B B(t)$. The latter includes the effect of the time-dependent gate voltage $V_g(t)$, which shifts the energy levels of the quantum dot as a function of time, and a time-dependent magnetic $B(t)$, which introduces a time-dependent Zeeman splitting for the two spin orientations within the quantum dot. The constants e and μ_B are, respectively, the electron charge and the Bohr magneton. The Coulomb repulsion is denoted by U and $\hat{n}_\sigma$ the dot number operator for electrons with spin σ. For this work we consider the QD coupled to a single fermionic bath, obtaining a complete Hamiltonian in the form of Eq. (2.1):

$$\mathcal{H} = \mathcal{H}_S(t) + \sum_k \epsilon_k c^\dagger_{k\sigma} c_{k\sigma} + V \sum_k \left(d^\dagger_\sigma c_{k\sigma} + c^\dagger_{k\sigma} d_\sigma \right) \tag{4.2}$$

4.3 Adiabatic response

As we mentioned in Section 3.1, the adiabatic regime refers to changes in the time-dependent parameters within a time scale which is much larger than the typical life-time of the electrons in the quantum dot. In the non-interacting case, the latter is determined by the coupling V and the density of states of the reservoir. In systems with many-body interactions, this quantity can be renormalized in a non-trivial way. Here we characterize the adiabatic dynamics as the linear-response regime in the "velocities" $\dot{V}_\sigma(t)$, following the steps of Section 3.1.

4.3.1 Dynamics of charge, spin and work

Applying the adiabatic linear response theory to the instantaneous occupation $n_\sigma(t) = \langle \hat{n}_\sigma \rangle(t)$ operators with the dot Hamiltonian $\mathcal{H}_S$ of Eq. (4.1) we define the coefficients [80, 149]

$$\begin{aligned} \Lambda^{\sigma\sigma'}(t) &= -(i/\hbar)\int_{-\infty}^{\infty} dt' \Theta(t-t') \left\langle \left[\hat{n}_\sigma(t), \hat{n}_{\sigma'}(t')\right] \right\rangle \\ &= -(i/\hbar)\int_{-\infty}^{\infty} d\tau \Theta(\tau) \left\langle [\hat{n}_\sigma(\tau), \hat{n}_{\sigma'}(0)] \right\rangle \end{aligned} \tag{4.3}$$

And so we have that the mean occupancy of the dot with electrons with spin σ at time t, noted as $n_\sigma(t) = \langle \hat{n}_\sigma \rangle(t)$, is

$$n_\sigma(t) = n_{f\sigma}(t) + \sum_{\sigma'} \Lambda^{\sigma\sigma'}(t)\dot{V}_{\sigma'}(t) \tag{4.4}$$

where $n_{f\sigma}(t) = \langle \hat{n}_\sigma \rangle_t$ is the *frozen* occupancy of the dot, i.e. the occupancy evaluated with the equilibrium density matrix, corresponding to the Hamiltonian $\mathcal{H}_{f,t} = \mathcal{H}(t)$ frozen at the time t.

The adiabatic Onsager coefficients $\Lambda^{\sigma\sigma'}(t)$ in this problem can be computed from Eq. (3.9)

$$\Lambda^{\sigma\sigma'}(t) = -\lim_{\omega\to 0} \frac{\mathrm{Im}\left\{\chi_t^{\sigma\sigma'}(\omega)\right\}}{\omega}. \tag{4.5}$$

Here $\chi_t^{\sigma\sigma'}(\omega)$ is the Fourier transform of the susceptibility defined in Eq. (3.10), $\chi_t^{\sigma\sigma'}(t-t') = -(i/\hbar)\Theta(t-t')\langle [n_\sigma(t), n_{\sigma'}(t')]\rangle_t$, evaluated with the equilibrium frozen density matrix.

The local charge and magnetic moment at the QD are given by

$$\begin{aligned} en(t) &= e\sum_\sigma n_\sigma(t), \\ m(t) &= n_\uparrow(t) - n_\downarrow(t). \end{aligned} \tag{4.6}$$

Consequently, we can define the susceptibilities $\chi_t^c(t-t') = -(i/\hbar)\theta(t-t')\langle [n(t), n(t')]\rangle$, $\chi_t^m(t-t') = -(i/\hbar)\theta(t-t')\langle [m(t), m(t')]\rangle$, and $\chi_t^{cm}(t-t') = \chi_t^{mc}(t-t') = -(i/\hbar)\theta(t-t')\langle [n(t), m(t')]\rangle$. From these susceptibilities, we can define the transport coefficients in a similar way as in Eq. (4.5). These coefficients can be collected into a dynamical Onsager matrix

$$\vec{\Lambda}_C(t) = \begin{pmatrix} \Lambda_c(t) & \Lambda_{cm}(t) \\ \Lambda_{mc}(t) & \Lambda_m(t) \end{pmatrix}. \tag{4.7}$$

The latter coefficients are related to the previously defined ones through

$$\begin{aligned} \Lambda_c(t) &= \Lambda^{\uparrow\uparrow}(t) + \Lambda^{\downarrow\uparrow}(t) + \Lambda^{\uparrow\downarrow}(t) + \Lambda^{\downarrow\downarrow}(t), \\ \Lambda_{cm}(t) = \Lambda_{mc}(t) &= \Lambda^{\uparrow\uparrow}(t) - \Lambda^{\downarrow\downarrow}(t), \\ \Lambda_m(t) &= \Lambda^{\uparrow\uparrow}(t) - \Lambda^{\downarrow\uparrow}(t) - \Lambda^{\uparrow\downarrow}(t) + \Lambda^{\downarrow\downarrow}(t). \end{aligned} \tag{4.8}$$

The current between the QD and the reservoir can be calculated from

$$I_\sigma(t) = e\dot{n}_\sigma(t), \tag{4.9}$$

and reads

$$I_\sigma(t) = e\frac{dn_{f\sigma}(t)}{dt} + e\frac{d\left[\sum_{\sigma'}\Lambda^{\sigma\sigma'}(t)\dot{V}_{\sigma'}(t)\right]}{dt}. \tag{4.10}$$

The *ac* power associated to the driving is $P(t) = \langle \partial\mathcal{H}/\partial t\rangle$. For the Hamiltonian (4.2) it can be expressed as $P(t) = \sum_\sigma P_\sigma(t)$, with

$$P_\sigma(t) = n_\sigma(t)\dot{V}_\sigma(t). \tag{4.11}$$

The instantaneous occupancies $n_\sigma(t)$ play the role of conjugated forces to the driving potentials $V_\sigma(t)$. In fact, notice that the latter satisfy $n_\sigma(t) = \langle \partial H/\partial V_\sigma \rangle$. From Eq. (4.11) we see that, in the present problem, the power is determined by the dynamics of the charge with σ polarization. In the adiabatic framework, Eq. (4.4) leads to

$$P_\sigma(t) = n_{f\sigma}(t)\dot{V}_\sigma(t) + \sum_{\sigma'} \Lambda^{\sigma\sigma'}(t)\dot{V}_{\sigma'}(t)\dot{V}_\sigma(t). \tag{4.12}$$

4.3.2 Onsager and symmetry relations

Since the susceptibilities entering the adiabatic dynamics are evaluated with the frozen Hamiltonian $H_{f,t}$ corresponding to the equilibrium condition at time t, they obey micro-reversibility, [220] which leads to the Onsager relation 3.13

$$\Lambda^{\sigma\sigma'}(V, B) = \Lambda^{\sigma'\sigma}(V, -B). \tag{4.13}$$

The Hamiltonian defined by Eq. (4.1) is invariant under the transformation $\{\downarrow, \uparrow\} \to \{\uparrow, \downarrow\}$. This leads to the additional relation satisfied by the Onsager coefficients

$$\Lambda^{\sigma\sigma'}(V, B) = \Lambda^{\bar{\sigma}\bar{\sigma}'}(V, B), \tag{4.14}$$

where $\bar{\downarrow} = \uparrow$ and viceversa. Also notice that the term $\langle [\hat{n}_\sigma(t), \hat{n}_{\bar{\sigma}}(t')] \rangle$ is zero in the non-interacting limit, hence the cross susceptibilities vanish for $\sigma \neq \sigma'$ in that case.

Combining the last property with the relation Eq. (4.13), we find that the crossed coefficient satisfies

$$\Lambda^{\sigma\bar{\sigma}}(V, B) = \Lambda^{\bar{\sigma}\sigma}(V, B). \tag{4.15}$$

Notice that this relation implies that the matrix $\underline{\Lambda}(t)$ is purely symmetric, i.e. $\underline{\Lambda}(t) \equiv \underline{\Lambda}^S(t)$.

4.3.3 Geometric contribution to the occupancies

Let us focus on a cyclic driving protocol, where both driving fields depend on time with the same period $\tau = \Omega/2\pi$, $V_g(t+\tau) = V_g(t)$, $B(t+\tau) = B(t)$, hence $V_\sigma(t+\tau) = V_\sigma(t)$. Within the adiabatic linear-response description, we see from the second term of Eq. (4.4) that the occupancy of the quantum dot has a non-equilibrium contribution, $n_{\sigma,\mathrm{non-eq}} = \sum_{\sigma'} \Lambda^{\sigma\sigma'}(t)\dot{V}_{\sigma'}(t)$. We define the vectors $\mathbf{V}(t) = (V_\uparrow(t), V_\downarrow(t))$ and $\mathbf{n}(t) = (n_\uparrow(t), n_\downarrow(t))$ and we introduce the definition of the matrix $\underline{\Lambda}(t)$, with matrix elements $\Lambda^{\sigma\sigma'}(t)$. Using these definitions we can write

$$\mathbf{n}_{\mathrm{non-eq}}(t) = \underline{\Lambda}(\mathbf{V}) \cdot \dot{\mathbf{V}}(t). \tag{4.16}$$

In this expression we have introduced a notation that highlights the fact that the time-dependence of $\underline{\Lambda}(t) \equiv \underline{\Lambda}(\mathbf{V})$ is because of the time-dependent parameters $V_\sigma(t)$.

Although the previous result is presented here in the case of $N = 2$ external parameters, it is clear that Eq. (4.16) can be written for larger N. For a system with several parameters, this non-equilibrium term has a geometric character when averaged over one period,

$$\overline{\mathbf{n}}_{\mathrm{non-eq}} = \frac{1}{\tau}\int_0^\tau dt \underline{\Lambda}(\mathbf{V}) \cdot \dot{\mathbf{V}}(t) = \oint_{\mathcal{C}} \underline{\Lambda}(\mathbf{V}) \cdot d\mathbf{V}. \tag{4.17}$$

The geometric nature of this component becomes explicit in the last equality, where we see that this quantity depends only on the protocol defined in the parameter space V. In the present problem, this implies a finite non-equilibrium accumulation of charge and a finite magnetization induced at the quantum dot, akin to the pumped charge in quantum pumps [54, 52] driven by two or more parameters as seen in Section 2.5.

4.3.4 Power, dissipation and work exchange

We now turn to analyze the expected mechanisms in the dynamics of the energy. As in the case of the charge, the power developed by the driving sources contains an equilibrium and a non-equilibrium component. The latter is associated to dissipation of energy and heat production.

We can easily see that the first term $\propto \dot{V}_\sigma(t)$ in Eq. (4.12) is a conservative contribution, in the sense that it has a zero mean when averaged over one period. Explicitly,

$$P_{\rm cons}(t) = \sum_\sigma P_{\sigma,{\rm cons}}(t) = \sum_\sigma n_{f\sigma}(t)\dot{V}_\sigma(t) = \mathbf{n}_f(t)\cdot\dot{\mathbf{V}}(t) \tag{4.18}$$

To see this, we note that we can relate $\mathbf{n}_f(t)$ to the mean value of the frozen Hamiltonian $H_f(\mathbf{V}) = \langle \mathcal{H}_{f,t}\rangle$ through $\mathbf{n}_f(t) \equiv \mathbf{n}_f(\mathbf{V}) = \partial_{\mathbf{V}} H_f(\mathbf{V})$. As in (4.16) we have made explicit the time dependence of $\mathbf{n}_f(t)$ through the V_σ parameters. Then, we can express the average over one period of the conservative component of the power as follows,

$$\overline{P_{\rm cons}} = \frac{1}{\tau}\int_0^\tau dt\; \mathbf{n}_f(t)\cdot\dot{\mathbf{V}}(t) = \oint_{\mathcal{C}} \partial_{\mathbf{V}} H_f(\mathbf{V})\cdot d\mathbf{V} = 0, \tag{4.19}$$

where $\oint_{\mathcal{C}}$ denotes the integral over a closed contour in the parameter space $\mathbf{V}$. Therefore $\mathbf{n}_f(t)$ is the conservative term of the force.

The second term of Eq. (4.12) contributes to the non-conservative component of the power. Using our previous vector notation we define

$$P_{\rm non-cons}(t) = \dot{\mathbf{V}}^T(t)\cdot\underline{\Lambda}(t)\cdot\dot{\mathbf{V}}(t), \tag{4.20}$$

where the superscript T stands for transposing the vector. In general we can decompose the matrix $\underline{\Lambda}(t) = \underline{\Lambda}^S(t) + \underline{\Lambda}^A(t)$ into symmetric $\underline{\Lambda}^S(t)$ and antisymmetric $\underline{\Lambda}^A(t)$ parts, and from Eq. (4.20) we see that only the symmetric component develops power (we already know that $\underline{\Lambda}(t) = \underline{\Lambda}^S(t)$ in this problem). Later we will discuss this decomposition with more detail in Section 5.3.

In the adiabatic regime, we expect that the evolution satisfies the second principle of thermodynamics instantaneously, the matrix $\Lambda^S(t)$ should be positive definite, implying that its eigenvalues are $\lambda_m(t) \geq 0$. The instantaneously dissipated heat equals the total non-conservative power and reads

$$P_{\rm non-cons}(t) = \sum_m \lambda_m(t)\tilde{\dot{\mathbf{V}}}(t)^2, \tag{4.21}$$

where we have defined $\tilde{\dot{\mathbf{V}}}(t) = \mathbf{U}\dot{\mathbf{V}}(t)$, being $\mathbf{U}$ the unitary transformation that diagonalizes $\underline{\Lambda}^S(t)$. In a system with several driving parameters, it is possible to have exchange of work between the different induced forces, in addition to dissipation of energy. In fact, the non-conservative power developed by each force can be expressed as

$$\begin{aligned} P_{{\rm non-cons},\sigma}(t) &= \sum_{\sigma'} \Lambda^{\sigma,\sigma'}\dot{V}_\sigma(t)\dot{V}_{\sigma'}(t), \\ &= P_{{\rm diss},\sigma}(t) + s_\sigma P_{\rm exch}(t), \end{aligned} \tag{4.22}$$

with $s_\sigma = \pm$. Hence, while it is satisfied

$$\sum_\sigma P_{{\rm non-cons},\sigma}(t) = \sum_\sigma P_{{\rm diss},\sigma}(t), \tag{4.23}$$

there is a finite amount of power $P_{\rm exch}(t)$, which can be exchanged between the two forces, associated to the charges with different spin orientations. Interestingly, this exchange may take

place instantaneously, and also have a net finite average over a period,

$$\overline{P}_{\rm exch} = \frac{1}{\tau}\int_0^\tau P_{\rm exch}(t). \tag{4.24}$$

4.3.5 Fluctuation-dissipation relations at $T = 0$

Fluctuation-dissipation relations are usually explained by the energy balance [221]. In the present problem, the only dissipation mechanism is due to the electron flow in the lead. Notice that in a system with electron-electron interactions like the one considered here, extra dissipation mechanisms might take place. However, the present model is known to be a Fermi liquid and such effects like inelastic-scattering are irrelevant within the low-energy regime, dominating the adiabatic dynamics [209, 136, 149].

From the previous description, we can show that the instantaneous dissipated power follows a Joule law per spin channel characterized by a universal resistance $R_0 = h/(2e^2)$. We define

$$P_{{\rm Joule},\sigma}(t) = R_0\left[I_\sigma(t)\right]^2 = R_0\left[e\frac{dn_\sigma(t)}{dt}\right]^2. \tag{4.25}$$

If we keep only terms up to second order in $\dot{V}_\sigma(t)$ in Eq. (4.25), we get $P_{{\rm Joule},\sigma}(t) = R_0\left[e\frac{dn_{f\sigma}(t)}{dt}\right]^2$. From Eq. (4.4), we see that this is directly related to the fluctuation of the frozen occupation, $\delta n_{f\sigma}(t)$, under a small variation of the gates taking place in a small time interval δt, $\delta V_\sigma(t) = V_\sigma(t+\delta t) - V_\sigma(t)$. Hence,

$$\frac{dn_{f\sigma}(t)}{dt} = \lim_{\delta t\to 0}\sum_\sigma \frac{\delta n_{f\sigma}(t)}{\delta V_{\sigma'}(t)}\frac{\delta V_{\sigma'}(t)}{\delta t}. \tag{4.26}$$

Introducing the definition of the static frozen susceptibility,

$$\chi_t^{\sigma\sigma'}(0) = \frac{\delta n_{f\sigma}(t)}{\delta V_{\sigma'}(t)}, \tag{4.27}$$

Eq. (4.26) can be expressed as follows

$$\frac{dn_{f\sigma}(t)}{dt} = \sum_\sigma \chi_t^{\sigma\sigma'}(0)\dot{V}_{\sigma'}(t). \tag{4.28}$$

Using Eqs. (4.22) and (4.23) and collecting the coefficients proportional to the different combinations of $\dot{V}_\sigma(t)\dot{V}_{\sigma'}(t)$, we find that $P_{{\rm diss},\sigma}(t) = P_{{\rm Joule},\sigma}(t)$ within the adiabatic approximation, if the following identities are satisfied

$$\begin{aligned}
\frac{h}{2}\left\{\left[\chi_t^{\sigma\sigma}(0)\right]^2 + \left[\chi_t^{\overline{\sigma}\sigma}(0)\right]^2\right\} &= \Lambda^{\sigma\sigma}(t), \\
h\left[\chi_t^{\uparrow\uparrow}(0)\chi_t^{\uparrow\downarrow}(0) + \chi_t^{\downarrow\downarrow}(0)\chi_t^{\downarrow\uparrow}(0)\right] &= \Lambda^{\uparrow\downarrow}(t) + \Lambda^{\downarrow\uparrow}(t).
\end{aligned} \tag{4.29}$$

The first of these identities has been discussed in Refs. [143, 144, 145] for a non-interacting quantum dot, in which case, $\chi_t^{\overline{\sigma}\sigma}(0) = \Lambda^{\overline{\sigma}\sigma}(t) = 0$. In the interacting case, this identity was originally derived by Shiba on the basis of Fermi liquid theory in Ref. [209], for a system without magnetic field. This was later generalized in Ref. [136] for a system with magnetic field. The second identity is identically zero in the non-interacting case and, to the best of our knowledge, it has not been previously discussed in the literature. It is highly non-trivial and are a consequence of the fact that in the present model the spin fluctuations do not induce extra mechanisms of dissipation to the Joule law expressed by Eq. (4.25).

4.3.6 Generalized Korringa-Shiba relations

These relations are basically combinations of the relations expressed by Eq. (4.29). In fact, substituting the fluctuation-dissipation relations presented in Eq. (4.29) into the definitions of Eq. (4.7), the following relations can be proved

$$\Lambda_c(t) = \frac{h}{2}\left[\left(\chi_t^{\downarrow\downarrow}(0)+\chi_t^{\downarrow\uparrow}(0)\right)^2+\left(\chi_t^{\uparrow\downarrow}(0)+\chi_t^{\uparrow\uparrow}(0)\right)^2\right], \tag{4.30}$$

$$\Lambda_m(t) = \frac{h}{2}\left[\left(\chi_t^{\downarrow\downarrow}(0)-\chi_t^{\downarrow\uparrow}(0)\right)^2+\left(-\chi_t^{\uparrow\downarrow}(0)+\chi_t^{\uparrow\uparrow}(0)\right)^2\right], \tag{4.31}$$

$$\Lambda_{cm}(t) = \frac{h}{2}\left[\left(\chi_t^{\uparrow\uparrow}(0)\right)^2-\left(\chi_t^{\downarrow\downarrow}(0)\right)^2+\left(\chi_t^{\downarrow\uparrow}(0)-\chi_t^{\uparrow\downarrow}(0)\right)\times\left(\chi_t^{\downarrow\uparrow}(0)+\chi_t^{\uparrow\downarrow}(0)\right)\right]. \tag{4.32}$$

Notice that Eq. (4.30) is the Korringa-Shiba (KS) law presented in Refs. [209, 136]. Here, we show that the assumption of a dissipation mechanism in the form of the universal IJL in the driving problem with two parameters leads to the additional relations expressed in Eqs. (4.31) and (4.32).

4.4 Results

4.4.1 Verifying the KS relations

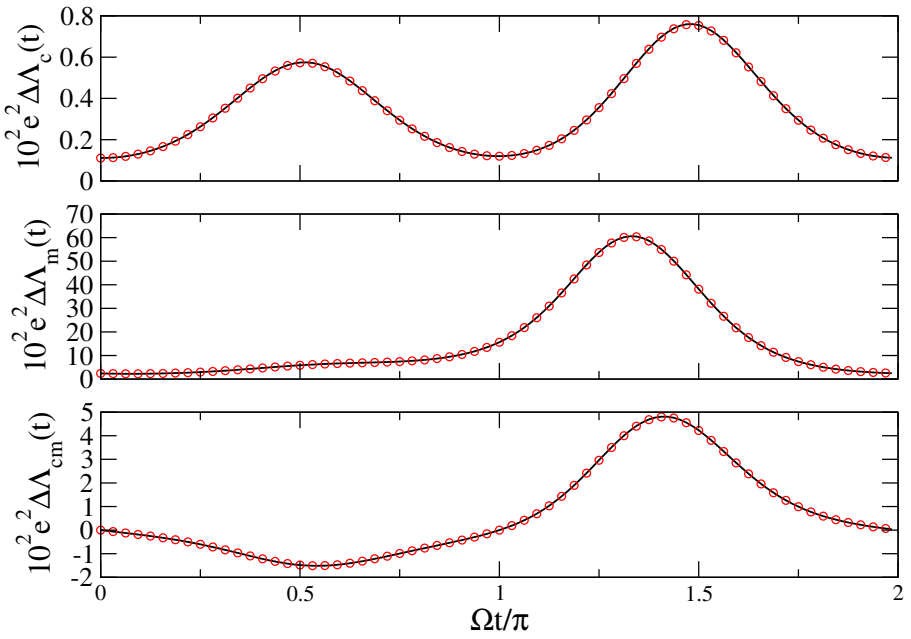

Figure 4.2: Generalized KS relations computed by NRG for $U = 0.03$ and $\Delta = 0.0008$. The driving protocol is $V(t) = V_0\sin(\Omega t)$, $B(t) = B_0\sin(\Omega t+\pi/4)+0.0005$, with $V_0 = 0.006$, and $B_0 = 0.0003$. Energies are expressed in units of the bandwidth of the reservoir. Top panel: Eq. (4.30), middle panel: Eq. (4.31), bottom panel: Eq. (4.32). Solid lines correspond to the direct calculation of the Onsager coefficients $\underline{\Lambda}_C$ and symbols to the evaluations from the frozen occupancies.

The fluctuation dissipation relations, or, equivalently, the generalized KS relations introduced in the previous section have a very important outcome. Namely, the dynamics of the

driven quantum dot in contact to the reservoir at $T = 0$ can be fully described by the knowledge of the frozen QD occupancy per spin $n_{f,\sigma}(t)$. In fact, given these occupancies, the static susceptibilities can be evaluated from Eq. (4.27). Then, the fluctuation-dissipation or KS relations lead to $\underline{\Lambda}(t)$ or $\underline{\Lambda}_C(t)$. These coefficients enable the full characterization of the charge, spin and energy dynamics. Therefore, we start by verifying the fulfilment of the KS relations.

In the non-interacting case with $U = 0$, all local properties of the QD are characterized by the instantaneous spin-resolved local density of states. Applying the result of Eq. (3.49) using $\Gamma = 2\Delta$ we have:

$$\rho_\sigma(\varepsilon, V_\sigma) = \frac{2\Delta}{(\varepsilon - V_\sigma(t))^2 + \Delta^2}, \tag{4.33}$$

where Δ depends on the hybridization between the QD and the reservoir, assuming for the latter a constant density of states. The frozen occupancy, the static susceptibility and the adiabatic Onsager coefficients can be easily calculated. The results are [144, 145, 149]

$$\begin{aligned} n_{f,\sigma}(t) &= \int \frac{d\varepsilon}{2\pi} n_F(\varepsilon)\rho_\sigma(\varepsilon, V_\sigma(t)), \\ \chi_t^{\sigma\sigma'}(0) &= \delta_{\sigma,\sigma'}\rho_\sigma(\mu), \qquad \Lambda^{\sigma\sigma'}(t) = \delta_{\sigma,\sigma'}\left[\rho_\sigma(\mu)\right]^2, \end{aligned} \tag{4.34}$$

where $n_F(\varepsilon) = \Theta(\mu - \varepsilon)$ is the Fermi-Dirac distribution function at $T = 0$ and μ is the chemical potential of the reservoir. From the previous expressions, we can readily verify that the KS relations are explicitly satisfied.

For the interacting case, we rely on numerical results obtained by the Numerical Renormalization Group (NRG) described in Section 3.3.6 [218, 219]. Results are shown in Figs. 4.2, where we see an excellent agreement between the direct calculations of the Onsager coefficients $\Lambda_c(t)$, $\Lambda_m(t)$, $\Lambda_{cm}(t)$, and the calculation of these coefficients from the evaluation of the static susceptibilities $\chi_t^{\sigma\sigma'}(0)$ and the identities of Eqs. (4.30), (4.31), and (4.32).

4.4.2 Instantaneous occupancy

The dynamics of the occupancy in the present system can be qualitatively understood in terms of a mean-field picture, where the Coulomb interaction term is replaced by $U[(n_{f,\downarrow} - 1/2)\hat{n}_\uparrow + (n_{f,\uparrow} - 1/2)\hat{n}_\downarrow]$. As we saw in Section 3.3.5, this leads to a local spin-resolved density of states obeying Eq. (4.33) upon the replacement $V_\sigma \to \tilde{V}_\sigma(t) = eV(t) + s_\sigma\mu_B B(t) + U(n_{f,\bar{\sigma}} - 1/2)$, with the self-consistent relation

$$n_{f,\sigma}^{MF}(t) = \int \frac{d\varepsilon}{2\pi} f(\varepsilon)\rho_\sigma(\varepsilon, \tilde{V}_\sigma). \tag{4.35}$$

It is important to notice that this quantity effectively depends on two parameters entering the definition of $\tilde{V}_\sigma$: V_σ and $V_{\bar{\sigma}}$. This is in contrast to the non-interacting case given by Eq. (4.34), which depends only on V_σ.

A sketch of the evolution is indicated in Fig. 4.3, where the levels corresponding to the up and down occupancies are represented in red and blue, respectively. For fixed B, assuming a configuration where the dot is initially singly occupied as in the left panel of the figure, there is an energy gap between the occupied state with a given spin orientation (down spin in this configuration) and the state with the opposite spin orientation. Such energy gap depends, not only on the magnitude of the Zeeman splitting (equal to $2\mu_B B$), but also on the Coulomb energy (equal to $Un_{f,\bar{\sigma}}$, in the mean-field description). The effect of changing the gate voltage is to move these two levels upwards or downwards rigidly in energy, until a change in the occupation takes place. The sketch shown in the right panel of Fig. 4.3 corresponds to a protocol where $V_g(t)$ decreases, lowering the energy of the levels and enabling the doubly occupancy. Changing in time the magnetic field implies a change in time of the Zeeman splitting.

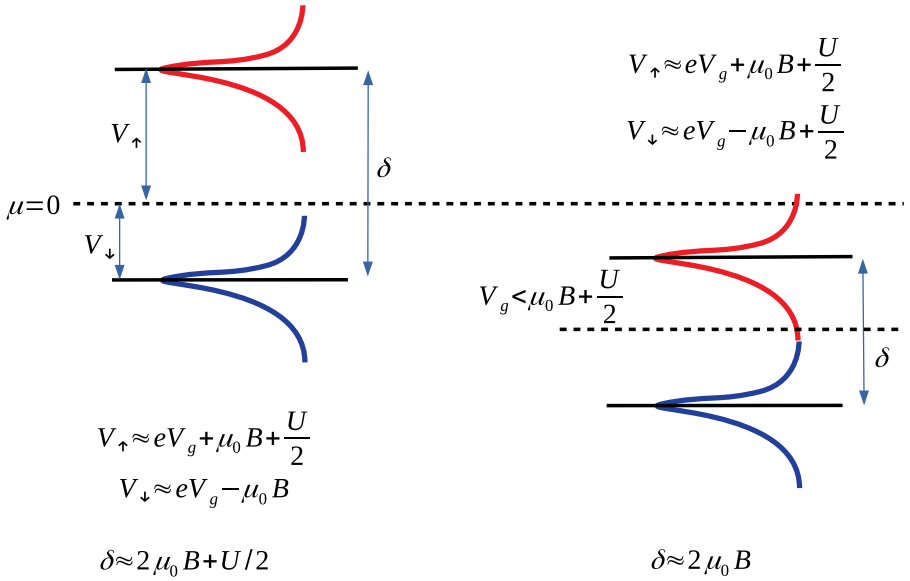

Figure 4.3: Sketch of the evolution of the occupancy of the QD. The energy of the singly and doubly occupied states have an energy gap δ which depends on the Coulomb interaction and on the magnetic field.

Results for the occupancy with down spin orientation, $n_{f,\downarrow}$ as function of the frozen parameters $V_g(t)$ and $B(t)$ are shown in Fig. 4.4, where the results obtained within the mean field description are compared with the ones calculated numerically with the NRG method of Refs. [218, 219], considering a reservoir with a constant density of states and a bandwidth D Notice that the occupancy with the opposite spin orientation is given by $n_{f,\uparrow}(V_g, B) = n_{f,\downarrow}(V_g, -B)$. We see that the mean-field approximation is in very good qualitative agreement with the exact numerical calculation, which means that the exact results may be interpreted in terms of simple pictures of two moving levels as the ones sketched in Fig. 4.3.

The up and down frozen occupancies along the green curve in the previous figure are presented in Fig. 4.5. Here, we also notice the good agreement between the NRG and mean-field description. This is because for the parameters chosen, the amplitude of the Zeeman splitting $2\mu B$ is larger than the Kondo energy $k_B T_K = \sqrt{V^2 \pi U/2D^2}\exp\left(-\pi^2 V^2 U/8D\right)$ [219, 218]. Under these conditions, the Kondo effect is not robust, and the physics is dominated by Coulomb blockade in combination with the magnetic field, as described by the sketch of Fig. 4.3. This regime can be properly described by a simple mean-field approximation.

We can appreciate an interesting mechanism, which takes place just at the moment where the occupancy change takes place (see arrows in the figure). This consists in a counter fluctuation in one of the occupancies when the other one changes from a filled to an empty configuration. This effect is a consequence of the shift in energy $U n_{f,\bar{\sigma}}(t)$ experienced by the electrons with spin σ, as $n_{f,\bar{\sigma}}(t)$ changes, which induces a concomitant change in $n_{f,\sigma}(t)$. A similar effect was found for driving only in $V_g(t)$ and constant magnetic field (see Ref [149]).

4.4.3 Instantaneous Joule law and work exchange

The fact that the KS relations are satisfied implies that the rate at which the total energy is dissipated follows an IJL with the universal resistance R_0. This is, precisely, expressed in Eq. (4.25). This does not necessarily mean that the total power developed in each spin channel follows the Joule law (4.25). However, it can be directly verified from Eq. (4.33) and (4.34) that each spin component of the non-conservative power is purely dissipative, and follows the

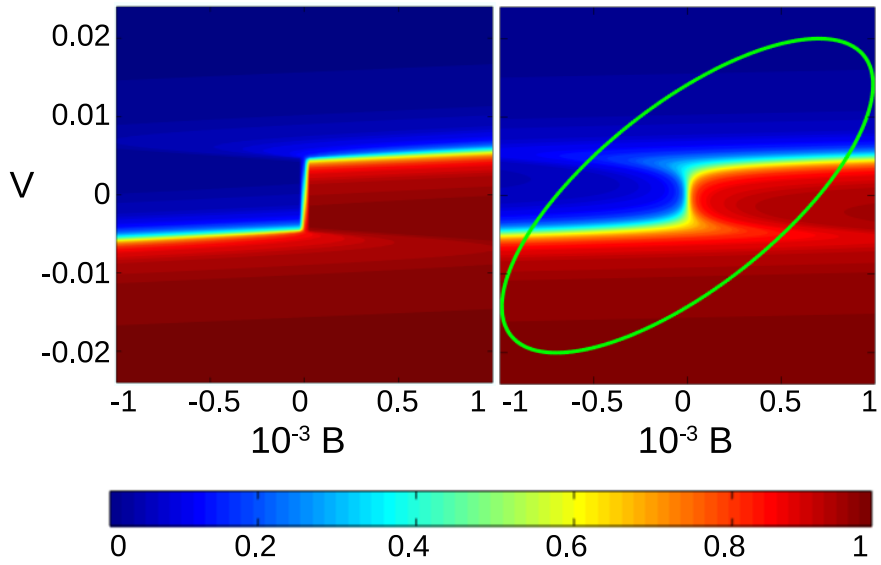

Figure 4.4: Occupancy map of $n_{f,\downarrow}$ in the mean field approximation for $U = 0.01$ and $\Delta = 0.0008$. The green elipse indicates the driving protocol $V(t) = V_0 \sin(\Omega t)$, $B(t) = B_0 \sin(\Omega t + \pi/4) + 0.0005$, with $V_0 = 0.02$, and $B_0 = 0.001$. Left and right panels correspond to results computed with mean-field and NRG, respectively. Energies are expressed in units of the bandwidth D of the reservoir.

instantaneous Joule law per spin channel in the non-interacting limit ($U = 0$):

$$P_{\mathrm{non-cons},\sigma}(t) = P_{\mathrm{diss},\sigma}(t) = P_{\mathrm{Joule},\sigma}(t), \qquad U = 0. \tag{4.36}$$

For the interacting system ($U \neq 0$) the fulfilment of the KS relations discussed previously, indicate that the dissipative component of the non-conservative power per spin channel follows a IJL, as expressed in Eq. (4.25). However, in the interacting case, the non-conservative components may contain an extra term, denoted by $P_{\mathrm{exch}}(t)$ in Eq. (4.22). Fig. 4.6 shows the behavior of the spin-resolved non-conservative power $P_{\mathrm{non-cons},\sigma}(t)$ in the interacting system with two-parameter driving. In the upper panel of the figure, this power is shown, along with the dissipative component $P_{\mathrm{Joule},\sigma}(t)$ for the two spin orientations. We can see that, although $P_{\mathrm{non-cons},\sigma}(t)$ differs from $P_{\mathrm{Joule},\sigma}(t)$, the corresponding difference is, precisely, the exchanged power between the two spin orientations $P_{\mathrm{exch}}(t)$, which is shown in the middle panel. The lower panel of the Fig. displays the total non-conservative power, where we see that it is fully dissipative and coincides with $\sum_\sigma P_{\mathrm{Joule},\sigma}(t)$. Interestingly, we can see in Fig. 4.6 that $P_{\mathrm{exch}}(t)$ has a non-vanishing mean value when integrated over a period, as indicated in Eq. (4.24).

We now turn to analyze the structure of the matrix $\underline{\Lambda}(\mathbf{V})$ for the interacting QD. As discussed in relation to Eq. (4.21), all the eigenvalues of this matrix are positive in the dissipative system and we can directly verify this property. Fig. 4.7 shows the minimum eigenvalue $\underline{\Lambda}(\mathbf{V})$.

It is interesting to notice that the largest values of the minimal eigenvalue correspond to parameters favoring the charge fluctuation of the QD. Notice that the highest values are concentrated on values of $V_g(t)$ for which the two many-body levels of the quantum dot, which separated in the energy δ indicated in Fig. 4.3, become aligned with the Fermi energy of the reservoir. For those parameters, the change in the occupation for small changes in $V_\sigma(t)$, thus the charge current $I_\sigma(t)$ achieves high values. Hence, the dissipation following the Joule law is also large.

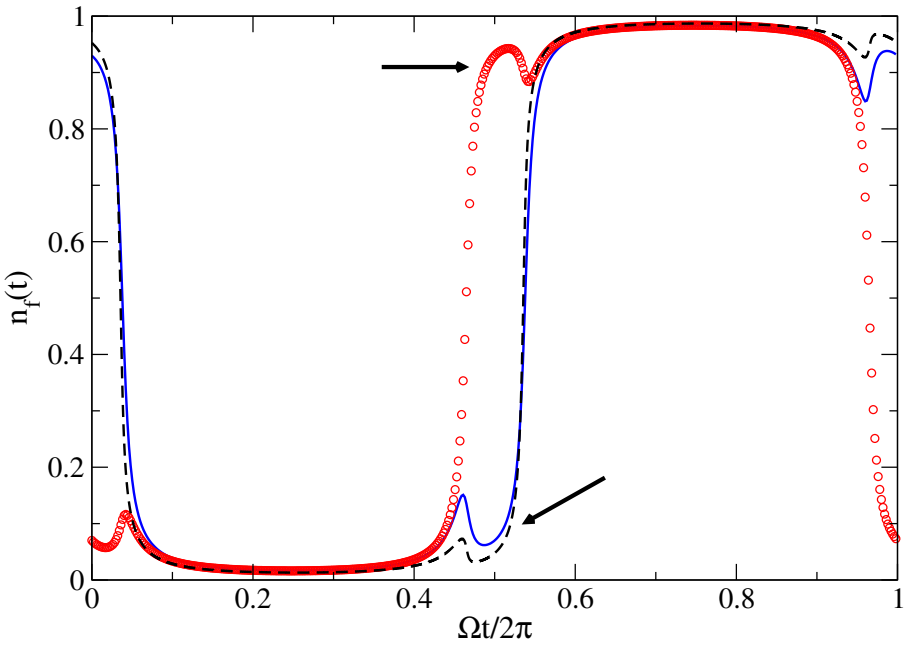

Figure 4.5: Frozen occupation along the curve of Figure 4.4. Solid line (blue): $n_{f\downarrow}(t)$ computed by NRG. Dashed line (black): $n_{f\downarrow}(t)$ computed in mean field approximation for parameters along the green curve of Fig. 4. Circles (red): $n_{f\uparrow}(t)$ computed by NRG.

4.4.4 Non-equilibrium polarized charge population

In contrast to the case where the QD is driven by a single parameter, it is possible in the present case to induce a net non-equilibrium polarized charge in the quantum dot. Akin to the pumped charge between two reservoirs in quantum dots driven by two parameters, this quantity has a geometric character, as expressed by Eq. (4.17). Importantly, for the dynamics to depend actually on two parameters, it is necessary to have a many-body interaction in the quantum dot. In fact, notice that in the non-interacting case, Eq. (4.33) and (4.34) make it explicit that the dynamics of $n_{f,\sigma}(t)$ depends only on the single parameter $V_\sigma(t)$ and it is completely independent from $V_{\overline{\sigma}}(t)$. Instead, in the interacting case, even at the simple mean-field level it can be seen that the evolution of the occupation $n_{f,\sigma}(t)$ depends on the two parameters $V_\sigma(t)$ and $V_{\overline{\sigma}}(t)$ [see Eq. (4.35)]. Results for the net charge accumulation with each spin orientation, calculated with NRG, are shown in Fig. 4.8. It is important to notice, that such a non-equilibrium charge accumulation takes place against the condition imposed by the chemical potential of the reservoir. As stressed before, this quantity has a geometric nature, similar to the pumped charge in two-parameter two-terminal driven systems. [54, 52] This also bears resemblance to the geometric magnetism discussed in Ref. [69] and it is interesting at this point to discuss similarities and differences between that work and the present contribution. Both works have a common point of view in the general approach, in the sense that in both cases, the adiabatic dynamics is addressed as a linear-response treatment in the velocities $\dot{\mathbf{V}}$. In Ref. [69] the name "geometric magnetism" is used to characterize the antisymmetric component of Onsager matrix $\underline{\Lambda}$. This is because the resulting induced force in that case has the formal structure of a Lorentz force, like the one experienced by a charged particle in a magnetic field. In such adiabatic dynamics the field is not a real, but a ficticios one. In the system we analyze here, the adiabatic dynamics has a purely symmetric $\underline{\Lambda}$. Since the induced force is associated to a real spin polarization in the quantum dot, we have real magnetism in the present problem. In both cases, the induced net forces can be expressed in terms of a geometric quantity, like the contour integral of Eq. (4.17). The latter is conceptually similar to the pumped charge considered in Refs. [54, 52]. Importantly, the dynamics ruled by an antisymmetric Onsager

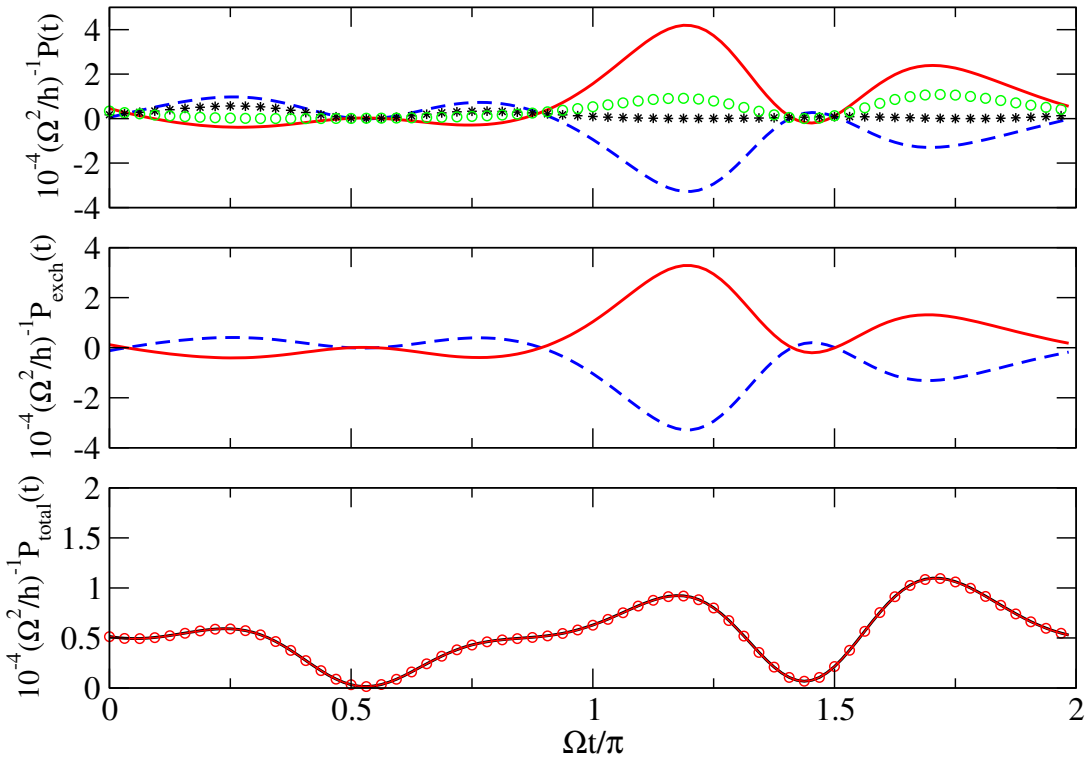

Figure 4.6: Computed powers with NRG. $U = 0.03$ and $\Delta = 0.0008$, under the driving protocol $V_g(t) = V_0 \sin(\Omega t)$, $B(t) = B_0 \sin(\Omega t + \pi/4) + 0.0005)$ with $V_0 = 0.006$ and $B_0 = 0.0003$. Energies are expressed in units of the bandwidth of the reservoir. Top panel: plots in solid red, dashed blue, green circles and black stars correspond, respectively, to $P_\uparrow(t)$, $P_\downarrow(t)$, $P_{\text{Joule},\uparrow}(t)$, $P_{\text{Joule},\downarrow}(t)$. Middle panel: Plots in solid line red and dashed blue correspond to $P_\uparrow(t) - P_{Joule,\uparrow}(t)$ and $P_\downarrow(t) - P_{Joule,\downarrow}(t)$, respectively. Bottom panel: the total power $P_\uparrow(t) + P_\downarrow(t)$ is plotted in solid black and coincides with the total total Joule dissipation. $P_{\text{Joule},\uparrow}(t) + P_{\text{Joule},\downarrow}(t)$, which is plotted in red circles.

matrix is non-dissipative, while the one ruled by a symmetric $\underline{\Lambda}$ is dissipative.

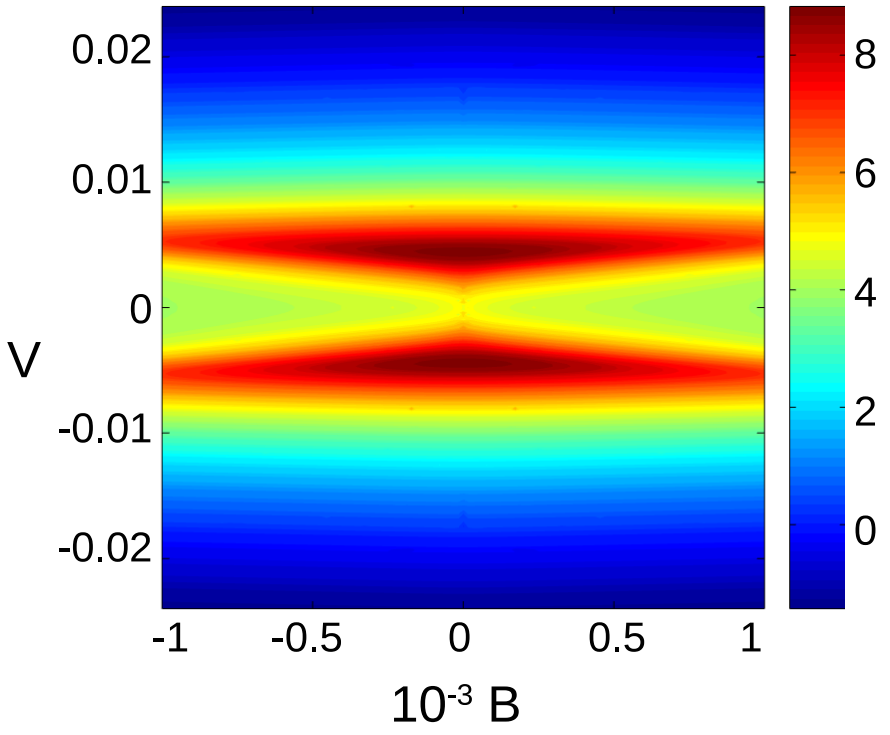

Figure 4.7: Minimal eigenvalue (in log scale) of the matrix $\underline{\Lambda}(\mathbf{V})$ for $U = 0.01$ and $\Delta = 0.0008$. Energies are expressed in units of the bandwidth of the reservoir.

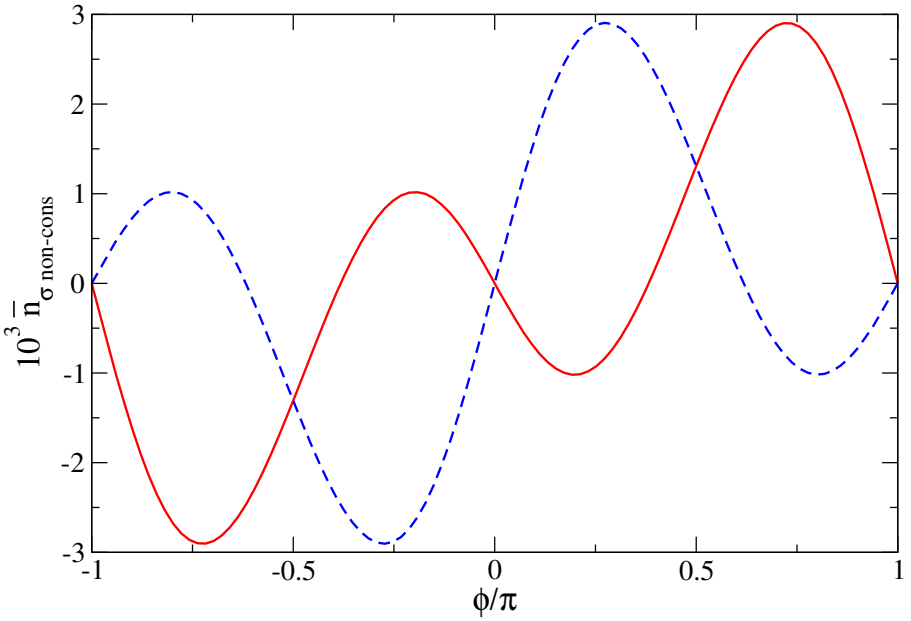

Figure 4.8: Mean charge accumulation for each spin orientation for $U = 0.03$ and $\Delta = 0.0008$, computed with NRG, as a function of the phase difference ϕ of the driving protocol $V_g(t) = V_0 \sin(\Omega t)$, $B(t) = B_0 \sin(\Omega t + \phi) + 0.0005)$, for $V_0 = 0.006$ and $B_0 = 0.0003$. Dashed line (blue): $\sigma = \downarrow$. Solid line (red): $\sigma = \uparrow$.

Chapter 5

Geometric properties of adiabatic quantum thermal machines

This chapter is based on the paper *Phys. Rev. B.102 155407: "Geometric properties of adiabatic quantum thermal machines"*.

5.1 Introduction

In the present chapter we will consider adiabatically driven thermal machines as presented in Section 2.6. They perform cycles in contact to several reservoirs. Their cycle is controlled by time-periodic changes of a set of parameters which are slow compared to the typical time scales associated with the (quantum) working substance (see for example Refs. [193, 98]). The modulation can be associated with parameters of the baths (temperature, chemical potential, ...) or the working medium (external fields, coupling coefficients, ...), see Fig. 5.1. We will refer to these quantum machines as *geometric thermal machines*. In this regime and for small amplitude of the thermal bias, the operation has a purely geometric description. At the heart of this description is the *thermal geometric tensor*, to be introduced in Section 5.3. We will see that within the adiabatic linear response regime, the process of heat-work conversion is related to the antisymmetric component of the thermal geometric tensor, while the dissipation and entropy production are related to the symmetric component of the same tensor. Importantly, the antisymmetric component has the structure of a Berry curvature, which depends only on the geometry of the cycle in parameter space, and can be straightforwardly expressed in terms of a line integral in this space. This representation is very useful for identifying optimal protocols of heat-work conversion. Furthermore, the symmetric component has a geometric interpretation in terms of thermodynamic length and can also be represented as a line integral for cyclic protocols, which is useful in the design of efficient protocols. Our approach does not only allow one to describe a whole class of quantum machines in a unifying picture. It also has practical implications such as improved ways to optimize their performance, as we will see later in Chapter 6. These results apply universally to any periodically and adiabatically driven quantum system in contact with various reservoirs, irrespective of the statistics obeyed by the particles, the strength of the coupling between the system and the reservoir, or the presence of many-body interactions.

The chapter is organized as follows. In Section 5.2 we introduce the model of an adiabatic thermal machine, some basic definitions and signs conventions. We perform an analysis of the thermodynamic behaviour of the machines and introduce the linear-response formalism to treat *ac* adiabatic and thermal driving. Section 5.3 is devoted to the formal definition of the thermal geometric tensor. The principal results of this chapter is presented in Section 5.4 and shows how the performance characteristics of the engine (efficiency, output power, etc.) are of geometric origin. The central results of this approach are captured by Eqs. (5.28), (5.29) and (5.30), which show that the pumped heat, the concomitant heat-work conversion and the dissipated power have a geometric interpretation. In the same section we will also analyze several classes of adiabatic machines depending on the various adiabatic drivings. Following this general formulation, Section. 5.5 focuses on a specific example of a thermal machine, which is particularly relevant for experimental implementation. We consider a driven quantum dot coupled to two electron reservoirs. Appendices A and B at the end of the Thesis contain further details on some derivation of the main results and explicit calculations for the example presented in the main text.

5.2 Model of a geometric thermal machine

A sketch of the geometric thermal machine that we analyze throughout this chapter is shown in Fig. 5.1. It consists of a central region containing the working substance, constituted by a few-level quantum system, coupled to two thermal baths, as described in Section 2.6. The quantum system is periodically driven by a set of N slowly-varying parameters $\vec{X}(t)$. The baths are macroscopic reservoirs of bosonic excitations or fermionic particles. The macroscopic variables characterizing the thermal environment such as the bath temperatures can also slowly vary in time. We parametrize the bath temperatures as $T_\alpha(t) = T + \delta T_\alpha(t)$ (with $\alpha = h, c$ referring to

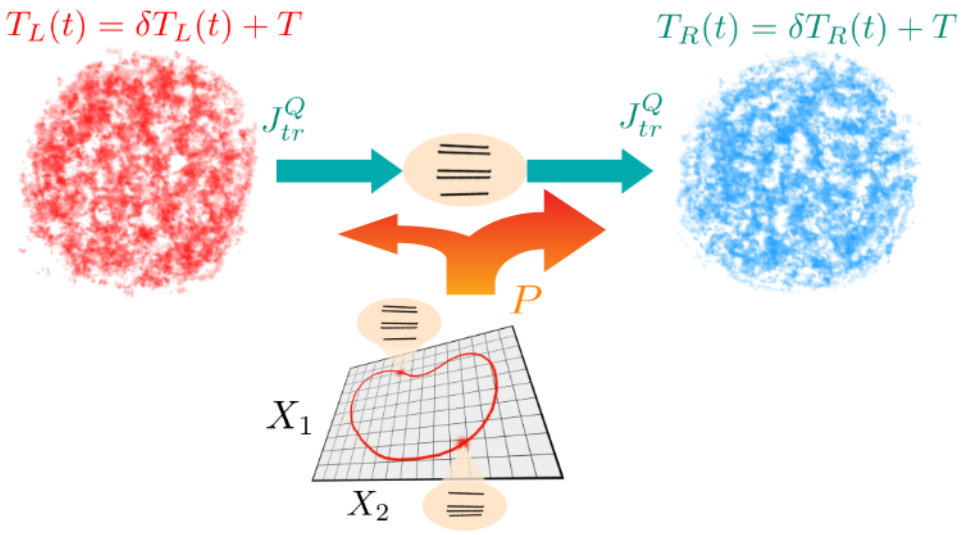

Figure 5.1: Geometrical thermal machine setup. A central, parametrically driven quantum system described by the Hamiltonian $\mathcal{H}_\mathcal{S}$ is coupled to macroscopic reservoirs. A cycle of the machine is completely characterized by a closed path in the parameter space $\mathbf{X}$. After a complete cycle the averaged power P is dissipated as heat in the reservoirs. The net transported energy $J^Q_{\rm tr}$ flows from one reservoir to the other.

N	Number of slowly varying coupling parameters
N + 1	Number of slowly varying coupling parameters including thermal bias
$\vec{v}$	Arrows denote N-dimensional vectors
$\mathbf{v}$	Bold fonts denote $(N+1)$-dimensional vectors
$\ell\,,\ell'$	Labels of elements of N-dimensional vectors or matrices
$\mu\,,\nu$	Labels of elements of $(N+1)$-dimensional vectors or matrices
$\underline{\underline{\mathbf{M}}}$	$(N+1)\times(N+1)$ matrix

Table 5.1: Notation used in the text

the hot and cold reservoirs) and define $\Delta T(t) = \delta T_h(t) - \delta T_c(t)$. A (possible) time dependence in the bath temperatures is only included in $\delta T_\alpha(t)$.

Let us start with the simple observation that the thermal bias, without the action of the *ac* driving, induces a net heat flow from the hot to the cold reservoir. On the other hand, it is useful to consider an analogy with the operation of classical machines and notice that the modulation of the parameters $\vec{X}(t)$ is introduced by some mechanism, which is akin to a weight moving a wheel in the classical case. By the combined effects of thermal bias and *ac* driving forces, it is possible to realize *heat-work conversion*, which constitutes the key for the operation of the device as a thermal machine. Two main operational modes are possible:

(i) In the heat engine mode, part of the heat flowing in the direction of the thermal bias is transformed into work performed against the mechanisms ruling the dynamics of $\vec{X}(t)$.

(ii) In the refrigerator mode, part of the work induced by the action of the *ac* parameters can be used to extract heat from the cold reservoir, against the action of the thermal bias. In the latter case, the thermal bias plays the role of the weight.

In the operation of the thermal machines, these processes come along with dissipation of energy leading to entropy production. The efficiency of the thermal machine relies on the appropriate balance between the heat-work conversion mechanism and dissipation.

5.2.1 Heat, work, and operational modes

As we are interested in the dynamics for slow driving and small temperature biases, it is convenient to define the $N+1$-dimensional vector of "velocities",

$$\dot{\mathbf{X}}(t) = \left\{ \dot{\vec{X}}(t), \Delta T(t)/T \right\} \tag{5.1}$$

These two types of vector notation (arrow and bold character) appear in several places throughout the chapter. For later reference, the Table 5.1 summarizes the different symbols used in the text.

A temperature bias as well as time-dependent system and bath parameters generally induce net heat transport between the reservoirs. At the same time, any driving mechanism generates heat that is dissipated into the reservoirs. Hence, the total heat current entering a given reservoir has a component resulting from the net transport between the two reservoirs and a component originated in the dissipation because of the action of the driving forces. The net heat current J^Q_α, averaged over one cycle of period $\tau = 2\pi/\Omega$, satisfies [222],

$$J^Q_h + J^Q_c = P, \tag{5.2}$$

where $P > 0$ is the total dissipative power generated by the driving forces, also averaged over one period. Identifying the component due to transport and that due to dissipation in J^Q_α is a non trivial task in general. The transport component satisfies

$$J^Q_{\mathrm{tr},c} = -J^Q_{\mathrm{tr},h} \equiv J^Q_{\mathrm{tr}}, \tag{5.3}$$

and we notice that only the total dissipative heat contributes to Eq. (5.2). In the next section, we exactly calculate J^Q_α to linear order in $\dot{\mathbf{X}}(t)$ and we show that it satisfies Eq. (5.3). Hence, we identify it with the leading term of the transport current.

The net heat transported per cycle between the two reservoirs is

$$Q_{\mathrm{tr}} = \frac{2\pi}{\Omega} J^Q_{\mathrm{tr}}. \tag{5.4}$$

This component is defined such that $Q_{\mathrm{tr}} > 0$ when heat flows in the direction of the thermal bias (hot to cold). We also define the net work W performed by the *ac* forces during one cycle. We take $W < 0$ when the *ac* forces exert work on the system. The balance between Q_{tr} and W is the key to the performance of the thermal machine, which may operate as a heat engine by transforming heat into work against the time-dependent driving or as a refrigerator, by using the work performed by the *ac* driving to pump heat from the cold to the hot reservoir. In the absence of heat-work conversion, one finds that $Q_{\mathrm{tr}} \geq 0$ and $W \leq 0$. In the heat-engine mode, the heat–work conversion mechanism operates against the *ac* forces and consequently $W > 0$. In the refrigerator mode, the heat–work conversion mechanism operates by using part of the work done by the *ac* forces to pump heat against the thermal bias, so that $Q_{\mathrm{tr}} < 0$.

5.2.2 Adiabatic linear response

To analyze the performance of the adiabatic thermal machines, we need to compute the currents. This can be done by conventional many-body techniques, such as the non-equilibrium Green's function formalism, scattering matrix theory (for systems without many-body interactions), or master equations (for weak coupling between system and reservoirs). Although we use these techniques to solve specific examples, we employ the Hamiltonian representation for the temperature difference of Section 3.2 and a Kubo linear response framework for small ΔT to derive general results. This enables us to analyze the energy dynamics induced by the thermal driving on the same footing with that induced by the time-dependent driving. Here we follow the

Luttinger's approach [190] to thermal transport, which introduces a "gravitational" potential whose gradients induce energy flows akin to the electrical currents induced by gradients of the electrochemical potential. Details of this approach were given in Section 3.2.

We then introduce the Hamiltonian $\mathcal{H}$ governing the system of Fig. 5.1, which is a realization of the prototypical Hamiltonian described in Section 2.1, with the addition of the Luttinger terms

$$\mathcal{H}(t) = \mathcal{H}_S(t) + \mathcal{H}_{\rm baths} + \mathcal{H}_c + \mathcal{H}_{\rm th}(t). \tag{5.5}$$

The first term $\mathcal{H}_S(t)$ is the Hamiltonian of the quantum system. It depends on time through the N slowly and periodically varying parameters (driving potentials) $\vec{X}(t) = \{X_\ell(t)\}$ with $\ell = 1, \ldots, N$, so that $\mathcal{H}_S(t) \equiv \mathcal{H}_S[\vec{X}(t)]$. The second term describes the two reservoirs, in this case $\mathcal{H}_{\rm baths} = \mathcal{H}_h + \mathcal{H}_c$. When considering a bath of fermionic particles, they are held at the same chemical potential $\mu_h = \mu_c = \mu$ and should be described by the grand-canonical Hamiltonian, $\mathcal{H}_\alpha \to \mathcal{H}_\alpha - \mu\mathcal{N}_\alpha$, where $\mathcal{N}_\alpha$ denotes the number of particles in reservoir α. The coupling between system and reservoirs, such as tunneling of particles and/or the exchange of energy between system and reservoirs, is captured by $\mathcal{H}_c = \mathcal{H}_{c,h} + \mathcal{H}_{c,c}$. Its form depends on the specific implementation. A particular example will be given in Section 5.5, and later in Chapter 6.

The last term in Eq. (5.5) accounts for the fact that the two reservoirs are held at different temperatures and derives from the Luttinger formulation of thermal transport. Adapting the definition of Eq. (3.16) to the present case, we define

$$\mathcal{H}_{\rm th}(t) = -\sum_{\alpha=h,c} \mathcal{J}^E_\alpha(t)\xi_\alpha(t), \tag{5.6}$$

where $\xi_\alpha(t)$ plays the same role as the thermal vector potential and the operator representing the energy flux entering reservoir α is given by

$$\mathcal{J}^E_\alpha = \dot{\mathcal{H}}_\alpha = -i\left[\mathcal{H}_\alpha, \mathcal{H}\right]/\hbar. \tag{5.7}$$

Recall that $\mathcal{H}_\alpha$ is the Hamiltonian of reservoir α. When the chemical potential is the same for all reservoirs, time averaging the mean value of this operator over one period $\tau = 2\pi/\Omega$ directly gives the heat current,

$$J^Q_\alpha = \frac{\Omega}{2\pi}\int_0^{2\pi/\Omega} {\rm d}t \langle \mathcal{J}^E_\alpha(t)\rangle. \tag{5.8}$$

The relation between the Luttinger field and the temperature bias, the counterpart of Eq. (3.17), reads

$$\dot{\xi}_\alpha(t) = \delta T_\alpha(t)/T. \tag{5.9}$$

Our quantum machine operates in a regime in which both the driving parameters $\vec{X}(t)$ and the temperature bias δT_α (with the associated parameter $\xi_\alpha(t)$) vary in time. Adiabatic driving implies that the driving frequency Ω is small compared to any characteristic frequency of the system's degrees of freedom as well as the relevant relaxation times associated with the coupling to the reservoirs. We can then regard the velocities at which the parameters are changed and the temperature bias as sufficiently small so that the currents can be computed using the linear response of Section 3.1 [80] for $\dot{\mathbf{X}}$. This procedure is similar to the one of Ref. [223] for closed driven systems. Recalling Eq. (3.5) for the adiabatic time evolution of any observable $\mathcal{O}$, in this case we find the Kubo-like formula

$$\langle \mathcal{O}\rangle(t) = \langle \mathcal{O}\rangle_t + \sum_{\ell=1}^{N} \Lambda_t^{\mathcal{O},\mathcal{F}_\ell}\dot{X}_\ell(t) + \sum_{\alpha=L,R} \Lambda_t^{\mathcal{O},\mathcal{J}^{\mathcal{E}}_\alpha}\dot{\xi}_\alpha(t). \tag{5.10}$$

As in Eq. (3.5), the left-hand side denotes an average with respect to the nonequilibrium density matrix, while $\langle \mathcal{O}\rangle_t$ is an average with respect to the equilibrium density matrix of the frozen

Hamiltonian $\mathcal{H}_t = \mathcal{H}_S(t) + \mathcal{H}_{\text{baths}} + \mathcal{H}_c$, $\rho_t = \sum_m p_m |m\rangle\langle m|$, where $p_m = e^{-\beta\varepsilon_m}/Z_t$, $\beta = 1/k_B T$, and $\mathcal{H}_t|m\rangle = \varepsilon_m|m\rangle$. Notice that the instantaneous eigenvectors $|m\rangle$ and eigenenergies ε_m depend on the time t. Recall also the definition of the $\mathcal{F}_\ell$ operators

$$\mathcal{F}_\ell = -\frac{\partial \mathcal{H}}{\partial X_\ell}, \quad \text{with } \ell = 1, \ldots, N \tag{5.11}$$

which has the interpretation of a force induced by the driving. Refer back to Section 3.1 for a more detailed discussion of these objects.

Within this framework, we can evaluate the adiabatic evolution of any observable. We are particularly interested in the energy current flowing into the coldest reservoir and the induced forces. Similar to the definition in Eq. (5.1), we find it convenient to define the $N+1$-dimensional force vector

$$\boldsymbol{\mathcal{F}} = (\vec{\mathcal{F}}, \mathcal{J}_R^E). \tag{5.12}$$

Using this notation, the adiabatic dynamics for the forces and the energy current into the coldest reservoir can be written in the form of Eq. (3.7)

$$\langle \boldsymbol{\mathcal{F}} \rangle(t) = \langle \boldsymbol{\mathcal{F}} \rangle_t + \underline{\underline{\boldsymbol{\Lambda}}}(\vec{X}) \cdot \dot{\mathbf{X}}. \tag{5.13}$$

In Eq. (5.13), we introduce the response matrix $\underline{\underline{\boldsymbol{\Lambda}}}(\mathbf{X})$ with elements defined as

$$\Lambda_{\mu,\nu}(\vec{X}) = \begin{cases} \Lambda_t^{\mathcal{F}_\mu, \mathcal{F}_\nu} & \mu \leq N \\ \sum_{\alpha=L,R} \Lambda_t^{\mathcal{J}_\alpha^E, \mathcal{F}_\nu} & \mu = N+1. \end{cases} \tag{5.14}$$

Some important features of the adiabatic susceptibilities are derived in Appendix A. The physical response depends on the two Luttinger parameters $\xi_h(t)$ and $\xi_c(t)$ only through the temperature bias $\dot{X}_{N+1}(t) = \Delta T(t)/T$, as can be seen using Eqs. (A.7) and (A.8). Also, note that in deriving the linear response expression for the current, one should neglect the term $\mathcal{H}_t^{\text{th}}$, which would lead to a "diamagnetic" component of the heat current [191]. The notation in Eq. (5.14) highlights the fact that the $\Lambda_{\mu,\nu}(\vec{X})$ depend on time only through the parameters $\vec{X}$.

As the coefficients of Eq. (5.14) are evaluated with respect to the frozen equilibrium density matrix, they obey the Onsager relations of Eq. (3.13) [80, 194]

$$\Lambda_{\mu,\nu}(\vec{X}, \vec{B}) = s_\mu s_\nu \Lambda_{\nu,\mu}(\vec{X}, -\vec{B}), \tag{5.15}$$

where $s_\nu = \pm$ for operators $\mathcal{F}_\nu$ which are even/odd under time reversal. In view of its relevance for time-reversal symmetry, we made a possible dependence on an applied magnetic field $\vec{B}$ explicit here, but will suppress it in the following unless necessary.

5.2.3 Adiabatic forces, currents, and entropy production over a cycle

In the geometric description of the adiabatic thermal machines, the central role is played by integrals of the forces in Eq. (5.13) over a period, rather than by the instantaneous quantities. First consider the energy current $\langle \mathcal{J}_c^E \rangle(t)$ which leads to a description of the heat fluxes introduced in Eq. (5.3) within the adiabatic linear response formalism.

The average of the instantaneous heat current over one period, $\langle \mathcal{J}_c^E \rangle(t)$, defines the transported heat flux within the adiabatic linear response formalism. In fact, evaluating this current with the adiabatic expansion of Eq. (5.10) and using the identities of Eqs. (A.7) and (A.8) we can see that the average over one period is identical in magnitude and opposite in signs at the two reservoirs. Hence, we eliminate the label α and write

$$J_{\text{tr}}^Q = \frac{\Omega}{2\pi} \int_0^{2\pi/\Omega} \mathrm{d}t \sum_{\nu=1}^{N+1} \Lambda_{N+1,\nu}(\vec{X}) \dot{X}_\nu(t). \tag{5.16}$$

The term corresponding to the sum $\nu = 1, \ldots, N$ is the pumping contribution to the heat current. The last term of Eq. (5.16), corresponding to $\nu = N+1$, is the heat current flowing in response to a finite temperature bias across the device (i.e. the thermal conductivity).

Note the strong similartity with the definition of the emissivities, Eq. (2.8). For a single driving parameter and $\Delta T = 0$, it is straightforward to show that the pumped heat current vanishes. At least two parameters are necessary for pumping. This was originally noticed in the framework of scattering matrix theory for driven electron systems [54, 52]. Moreover, a spatially symmetric system has $\Lambda_t^{\mathcal{J}_L^E,\mathcal{F}_\ell} = -\Lambda_t^{\mathcal{J}_R^E,\mathcal{F}_\ell}$, so that these quantities should be zero in view of Eq. (A.8). Hence, breaking of spatial symmetry is another necessary condition for a non-vanishing pumping contribution to the heat current [199, 222].

The net generated power has components associated to the time-dependent driving forces as well as to the thermal bias,

$$\begin{aligned} P = \frac{\Omega}{2\pi}\int_0^{2\pi/\Omega} \mathrm{d}t \left\langle \frac{\partial \mathcal{H}}{\partial t} \right\rangle &= \frac{\Omega}{2\pi}\int_0^{2\pi/\Omega} \mathrm{d}t \left(\sum_{\ell=1}^{N} \langle \mathcal{F}_\ell \rangle \dot{X}_\ell(t) + \sum_{\alpha,\beta=L,R} \langle \mathcal{J}_\alpha^E \rangle(t) \dot{\xi}_\alpha(t) \right) \\ &= \frac{\Omega}{2\pi}\int_0^{2\pi/\Omega} \mathrm{d}t \;\; \dot{\mathbf{X}} \cdot \underline{\underline{\mathbf{\Lambda}}}(\vec{X}) \cdot \dot{\mathbf{X}}. \end{aligned} \tag{5.17}$$

The response matrix on the right-hand side of Eq. (5.17) was introduced through the definition of forces and the energy current in Eq. (5.13). While Eq. (5.16) for the fluxes are linear in $\dot{\mathbf{X}}$, Eq. (5.17) is bilinear in these parameters. This reflects the fact that the dissipated heat, defined in Eq. (5.2) is at least second order in these quantities – equivalent to being $\mathcal{O}(\Omega^2)$ [199, 222]. The cross terms proportional to the thermal bias and *ac* driving usually have opposite signs and cancel one another when evaluating the total power. This happens, in particular, in the absence of a magnetic field with driving forces symmetric under time reversal, as a consequence of the Onsager relations (5.15).

From Eq. (5.2) for the total dissipated heat flux we have the following expression for the entropy production rate

$$T\dot{S} = J_L^Q + J_R^Q = P. \tag{5.18}$$

Substituting Eq. (5.17) we get

$$\dot{S} = \frac{\Omega}{2\pi T}\int_0^{2\pi/\Omega} \mathrm{d}t \;\; \dot{\mathbf{X}}(t) \cdot \underline{\underline{\mathbf{\Lambda}}}(\vec{X}) \cdot \dot{\mathbf{X}}(t). \tag{5.19}$$

We present an alternative derivation for the above expression in Appendix B.

The forces $\langle \mathcal{F}_\ell \rangle(t)$ enter the work performed by the thermal machine, as will be discussed in more detail in Section 5.4 below. We also find it useful to introduce average of the force over one period,

$$F_\ell = \frac{\Omega}{2\pi}\int_0^{2\pi/\Omega} \mathrm{d}t \langle \mathcal{F}_\ell \rangle(t) = F_{\ell,\mathrm{BO}} + F_{\ell,\mathrm{ar}}, \quad \ell, = 1, \ldots, N. \tag{5.20}$$

The first term of Eq. (5.20) corresponds to the instantaneous *equilibrium* (Born-Oppenheimer) description given by the first term of Eq. (5.13), while the second term is the first order *adiabatic reaction force* defined in Ref. [59].

5.3 Thermal geometric tensor

It is instructive to decompose the tensor $\Lambda_{\mu,\nu}(\vec{X})$ into its symmetric and antisymmetric parts,

$$\Lambda_{\mu,\nu}^{S,A} = \frac{1}{2}\left(\Lambda_{\mu,\nu} \pm \Lambda_{\nu,\mu}\right). \tag{5.21}$$

Eq. (5.19) for the entropy production implies that the symmetric component $\Lambda^S_{\mu,\nu}$ controls dissipation. Since the rate of entropy production $\dot{S}$ is non-negative, the symmetric part $\Lambda^S_{\mu,\nu}$ can be viewed as a metric tensor on the space of thermodynamic states [83, 82, 81]. Then, geodesics with respect to this metric correspond to adiabatic trajectories which minimize dissipation [83, 82, 81]. This contribution to $\Lambda_{\mu,\nu}(\vec{X})$ has also been referred to as geometric friction [68, 83, 69].

Lehmann representation for the thermoadiabatic tensor

The Fourier transform of the adiabatic susceptibilities entering in Eq. (5.14) are given by Eq. (3.9), we see that the elements of this tensor can be expressed as

$$\Lambda_{\mu,\nu}(\vec{X}) = -(i/\hbar)\partial_\omega \chi_t^{\mathcal{F}_\mu,\mathcal{F}_\nu}(\omega)|_{\omega=0} = \lim_{\omega\to 0} \frac{\mathrm{Im}\left[\chi_t^{\mathcal{F}_\mu,\mathcal{F}_\nu}(\omega)\right]}{\omega}, \tag{5.22}$$

being $\chi_t^{\mathcal{F}_\mu,\mathcal{F}_\nu}(\omega)$ the Fourier transform of the susceptibility defined by Eq. (3.10), $\chi_t^{\mathcal{F}_\mu,\mathcal{F}_\nu}(t-t') = -(i/\hbar)\theta(t-t')\langle[\mathcal{F}_\mu(t),\mathcal{F}_\nu(t')]\rangle_t$. Using the notation $\mathcal{F}_\mu = -\partial_\mu \mathcal{H}_t$ and expressing the susceptibility in the Lehmann representation we have

$$\chi_t^{\mathcal{F}_\mu,\mathcal{F}_\nu}(\omega) = \hbar \sum_{n,m} p_m \left(\varepsilon_m - \varepsilon_n\right)^2 \left[\frac{\langle\partial_\mu m|n\rangle\langle n|\partial_\nu m\rangle}{\omega - (\varepsilon_m - \varepsilon_n) + i\eta} - \frac{\langle\partial_\nu m|n\rangle\langle n|\partial_\mu m\rangle}{\omega - (\varepsilon_n - \varepsilon_m) + i\eta}\right], \tag{5.23}$$

with $\eta = 0^+$. Here, $|n\rangle$ and ε_n denote the instantaneous eigenstates and eigenenergies of $\mathcal{H}_t$ and p_m is the corresponding thermal weight. We have used the following identities, calculated from $\mathcal{H}_t|n\rangle = \varepsilon_n|n\rangle$ and $\langle n|\partial_\mu\left(\mathcal{H}_t|m\rangle\right)$:

$$\begin{aligned}
\langle n|\partial_\mu \mathcal{H}_t|m\rangle &= \left(\varepsilon_m - \varepsilon_n\right)\langle n|\partial_\mu m\rangle + \delta_{n,m}\partial_\mu\varepsilon_m, \\
\langle m|\partial_\mu \mathcal{H}_t|n\rangle &= \left(\varepsilon_m - \varepsilon_n\right)\langle \partial_\mu m|n\rangle + \delta_{n,m}\partial_\mu\varepsilon_m.
\end{aligned} \tag{5.24}$$

Calculating the derivative as indicated in Eq. (5.22), we have $\Lambda_{\mu,\nu}(\vec{X}) = \Lambda^A_{\mu,\nu}(\vec{X}) + \Lambda^S_{\mu,\nu}(\vec{X})$. The result for the symmetric component is

$$\begin{aligned}
\Lambda^S_{\mu,\nu}(\vec{X}) = \quad & \hbar\pi \lim_{\omega\to 0} \sum_{n,m} p_m \frac{\left(\varepsilon_n - \varepsilon_m\right)^2}{\omega} \mathrm{Re}[\langle\partial_\mu m|n\rangle\langle n|\partial_\nu m\rangle] \\
& \times \left[\delta(\omega - (\varepsilon_m - \varepsilon_n)) - \delta(\omega - (\varepsilon_n - \varepsilon_m))\right].
\end{aligned} \tag{5.25}$$

Similarly, the antisymmetric component can be expressed as

$$\Lambda^A_{\mu,\nu}(\vec{X}) = 2\hbar \sum_m p_m \,\mathrm{Im}\left[\langle\partial_\mu m|\partial_\nu m\rangle\right]. \tag{5.26}$$

In the limit of zero temperature, the sum over m is dominated by the ground state and $\Lambda^A_{\mu,\nu}(\vec{X})$ reduces to its Berry curvature. For $\Delta T = 0$, this component can be viewed as a velocity-dependent force, akin to a Lorentz force, which does not contribute to the net entropy production. This contribution has been referred to as geometric magnetism [68, 58, 61, 62, 63].

5.3.1 Definition of the thermal geometric tensor

It is interesting to compare $\Lambda_{\mu,\nu}$ to the quantum geometric tensor for the instantaneous ground state $|\psi\rangle$ of a closed system as a function of parameters X_ℓ [215, 224],

$$g_{\ell,\ell'} = \langle\partial_\ell\psi\,|\partial_{\ell'}\psi\rangle - \langle\,\partial_\ell\psi|\,\psi\rangle\,\langle\psi\,|\partial_{\ell'}\psi\,\rangle\,. \tag{5.27}$$

Analogous to $\Lambda_{\mu,\nu}$, the symmetric part of $g_{\ell,\ell'}$ defines a metric on the manifold of ground states and the antisymmetric part equals the Berry curvature. The crucial difference between the

two tensors is that the quantum geometric tensor is defined for a discrete spectrum, while $\Lambda_{\mu,\nu}$ assumes a continuous spectrum. This does not lead to essential differences for the antisymmetric components of the tensors which are non-dissipative. In contrast, the symmetric part of $\Lambda_{\mu,\nu}$ controls dissipation and therefore vanishes for a discrete (or gapped) spectrum. We can therefore view $\Lambda_{\mu,\nu}$ as the analog of the quantum geometric tensor for systems with continuous spectra. In view of this analogy, we refer to $\Lambda_{\mu,\nu}$ as the *thermal geometric tensor*.

In time reversal symmetric systems subject to driving parameters $\vec{X}$ which also respect time reversal symmetry, different parts of the thermal geometric tensor are either purely symmetric or antisymmetric. The Onsager relations (5.15) imply that $\Lambda_{\ell,\ell'} = \Lambda_{\ell',\ell}$ $(\ell, \ell' = 1, \ldots, N)$ is purely symmetric (corresponding to geometric friction without geometric magnetism). In contrast, $\Lambda_{N+1,\ell} = -\Lambda_{\ell,N+1}$ (corresponding to geometric magnetism without geometric friction). In systems which break time reversal symmetry, both the symmetric and the antisymmetric components of the thermal geometric tensor are generally nonzero.

5.4 Thermal machines and geometry

The above analysis implies that there are several purely geometric quantities which enter into the operation of adiabatic quantum thermal machines. We will show in the following that in a very concrete sense, it is the geometric aspects (in the sense of Berry) which are responsible for the heat-work conversion underlying thermal machines. We will see that the Carnot limit of the efficiency can be reached by means of purely geometric effects.

An essential quantity is the total heat transported between the leads per cycle, $Q_{\rm tr}$ defined in Eq. (5.4). In a heat engine, this heat is in part converted into useful work while in a refrigerator, this heat is extracted from the colder reservoir. The transported heat takes the form

$$Q_{\rm tr} = \oint \sum_{\ell=1}^{N} \Lambda_{N+1,\ell} \mathrm{d}X_\ell + \oint \mathrm{d}t \Lambda_{N+1,N+1} \frac{\Delta T}{T}. \tag{5.28}$$

The first term on the right hand side is geometric, depending only on the path, and has a simple physical interpretation. It is just the heat which is pumped between the reservoirs due to the periodic variation of the parameters $\vec{X}$,

$$Q_{\rm tr,ac} = \oint \sum_{\ell=1}^{N} \Lambda_{N+1,\ell} \mathrm{d}X_\ell. \tag{5.29}$$

The second term describes the heat current driven by the applied temperature bias as a result of the heat conductance $\Lambda_{N+1,N+1}$ of the system. Notice that the two terms typically have a different dependence on the period $\tau = 2\pi/\Omega$. Due to its geometric nature, the first term is independent of the period. In contrast, the second term is in general proportional to the period.

The pumped heat per cycle is essential for the operation of adiabatic quantum thermal machines. To see this, we compute the work $W = -\oint \mathrm{d}\vec{X} \cdot \vec{F}$ per period performed on the system during one cycle of the *ac* sources. The forces, as described by Eq. (5.13), have an instantaneous and a linear-response component. The instantaneous contribution depends only on the parameters $\vec{X}$ and is evaluated in the absence of the temperature bias. This *equilibrium* contribution to the force is necessarily conservative (in the mechanical sense) and thus gives a vanishing contribution to the work performed over a cycle. Thus, only the linear-response component contributes to the work per cycle,

$$W = -\left(\oint \mathrm{d}t \sum_{\ell,\ell'=1}^{N} \dot{X}_\ell \Lambda_{\ell,\ell'} \dot{X}_{\ell'} + \oint \sum_{\ell=1}^{N} \mathrm{d}X_\ell \Lambda_{\ell,N+1} \frac{\Delta T}{T} \right). \tag{5.30}$$

First consider the second term on the right hand side. For constant $\Delta T/T$, this term is again a purely geometric line integral over a closed contour. Unlike the contribution of the instantaneous component, this term is in general nonconservative and gives a finite contribution when integrated over a closed cycle. The reason is that this term originates from the *nonequilibrium* contribution to the force which is generated by the temperature bias. Along with Eq. (5.29) for the pumped heat, this geometric term is the essence of *heat-work* conversion and hence crucial for the operation of the thermal machine. In contrast, the first term in Eq. (5.30) describes frictional losses. Unlike the second term, which can take either sign, this term is always positive. It then becomes evident that heat-work conversion is rooted in the geometric terms in Eqs. (5.28) (in the sense of Berry) and (5.30), and it is the nongeometric terms (in the sense of Berry) that are responsible for losses. We will see this again below when we discuss the efficiencies of quantum thermal machines.

As a result of the Onsager relations (5.15), the geometric contributions to the transported heat and the work are very closely related. If the system is time reversal invariant (which also requires that the parameters $\vec{X}$ couple to time-reversal-even operators), the Onsager relations imply that $\Lambda_{N+1,\ell} = -\Lambda_{\ell,N+1}$ and the prefactor of $\Delta T/T$ in Eq. (5.30) just equals minus the pumped heat between the reservoirs. In that case, Eq. (5.30) is written as

$$W = Q_{\mathrm{tr,ac}}\frac{\Delta T}{T} - \oint \mathrm{d}t \sum_{\ell,\ell'=1}^{N} \dot{X}_\ell \Lambda_{\ell,\ell'} \dot{X}_{\ell'}. \tag{5.31}$$

We can then understand the operation of a heat engine as follows. During one cycle of the machine, the cyclic variation of the parameters pumps heat from the high-temperature to the low-temperature reservoir. The corresponding change in free energy is converted into work. A positive balance (i.e. $W > 0$) of the two terms contributing to Eq. (5.31) can be used to work against a load. Here, the load corresponds to an external agent which couples to the dynamics of the parameters $\vec{X}$. This is analogous to the operation principle of inverted quantum pumps as adiabatic quantum motors [225, 226, 227, 228, 229]. Similarly, in a refrigerator we have $Q_{\mathrm{tr,ac}} < 0$ and work $W = Q_{\mathrm{tr,ac}}\Delta T/T$ must be supplied by the *ac* sources to overcome the thermal bias and to pump heat from the low-temperature to the high-temperature reservoir. Both terms are negative since one has to overcome the frictional losses in addition to pumping heat from the cold to the hot reservoir. It is important to notice that the two terms in Eq. (5.30) are typically of different orders in the period $2\pi/\Omega$. While the first, nongeometric contribution is inversely proportional to the period, the second, geometric contribution is independent of it. Thus, one can often neglect the nongeometric term when considering the limit of small frequency Ω.

It is also interesting to discuss this heat-work conversion in the context of the entropy production rate defined in Eq. (5.18). With the definitions of this section, we can write

$$T\dot{S} = \frac{\Omega}{2\pi}\left(-W + Q_{\mathrm{tr}}\frac{\Delta T}{T}\right) = \frac{\Omega}{2\pi}\left(\oint \mathrm{d}t \sum_{\ell,\ell'=1}^{N} \dot{X}_\ell \Lambda_{\ell,\ell'} \dot{X}_{\ell'} + \oint \sum_{\ell=1}^{N} \mathrm{d}X_\ell \Lambda_{\ell,N+1}\frac{\Delta T}{T}\right). \tag{5.32}$$

The first term corresponds to the total power generated by the *ac* sources, while the second term corresponds to the power invested to transport the heat Q_{tr} per cycle in the presence of the thermal bias ΔT. Due to the heat-work conversion, the geometric component of W exactly cancels the component $Q_{\mathrm{tr,ac}}$ of Q_{tr} in the dissipated power (still assuming time-reversal invariance). Entropy production is then associated with the nongeometric contributions to heat and work. As we will show below, under certain circumstances the first term in Eq. (5.30) can also be viewed as a geometric quantity even though it cannot be immediately rewritten as a line integral.

We close this section by a few additional remarks. The operation of a heat engine or refrigerator requires that a net amount of heat $Q_{\mathrm{tr,ac}}$ is pumped between the reservoirs during

a cycle, requiring that the force is nonconservative. Above, we have focused on the case that $\Delta T/T$ is constant over the cycle. In principle, the conditions for the operation of adiabatic quantum thermal machines can be less stringent if one allows $\Delta T/T$ to vary along the cycle, for instance by coupling the system to different reservoirs at different stages.

In the absence of time reversal symmetry, the Onsager relations connect the response functions $\Lambda_{\mu,\nu}$ at different magnetic fields. In this case, there is no general relation between $\Lambda_{N+1,\ell}$ and $\Lambda_{\ell,N+1}$ for a fixed magnetic field, and in addition to the antisymmetric contribution $\Lambda^A_{N+1,\ell} = -\Lambda^A_{\ell,N+1}$, there could also be a symmetric contribution, $\Lambda^S_{N+1,\ell} = \Lambda^S_{\ell,N+1}$. Unlike $\Lambda^A_{\mu,\nu}$, the symmetric $\Lambda^S_{\mu,\nu}$ is associated with entropy production and dissipation according to Eq. (5.17). Even if both the dissipative and the nondissipative contributions to the pumped heat flow from the hot to the cold reservoir, the work performed on a load would involve the difference between the antisymmetric and the symmetric contribution.

The time average of the forces $\vec{F}$ as defined in Eq. (5.20) also has contributions which are purely geometric. From Eq. (5.13), the first-order adiabatic reaction component can be readily rewritten as

$$F_{\ell,\mathrm{ar}} = \frac{\Omega}{2\pi}\left\{\oint \sum_{\ell'=1}^{N} \Lambda_{\ell,\ell'}\mathrm{d}X_{\ell'} + \oint \mathrm{d}t\Lambda_{\ell,N+1}\frac{\Delta T}{T}\right\} \tag{5.33}$$

Here, the first term on the right hand side is a line integral which is purely geometric in that it depends only on the path.

Finally, we remark that under certain conditions, the dissipated component of W, corresponding to the first term of Eq. (5.30), can also be formally represented in terms of a line integral over a closed path in parameter space. This is not as straightforward as for Eqs. (5.33), (5.28), and (5.30) since the power is bilinear in $\dot{\mathbf{X}}$. It is, however, possible when there exists a well-defined mapping between $\dot{\mathbf{X}}$ and $\mathbf{X}$ as the latter varies along the closed path γ. In particular, such a mapping exists for the case of periodic driving. For a smooth path γ, one can write the relations $\dot{X}_\mu = \Omega g_\mu(\vec{X})|_\gamma$ for all μ, where the functions $g_\mu(\vec{X})|_\gamma$ are defined by eliminating the parametrization in t between $X_\mu(t)$ and $\dot{X}_\mu(t)$. Then, we can write the dissipated power as a line integral by using this relation to eliminate one of the factors of $\dot{X}_\mu$ in Eq. (5.17) via these relations. Note that the resulting line integral has a prefactor of Ω, making it explicit that the dissipated power is inversely proportional to the period of the driving, as already mentioned above.

The line integrals controlling the operation of adiabatic thermal quantum machines are reminiscent of line integrals over Berry connections. This motivates us to introduce the vector fields

$$\vec{A}^{A/S}_\mu = \left(\Lambda^{A/S}_{\mu,1}(\vec{X}),\ldots,\Lambda^{A/S}_{\mu,N}(\vec{X})\right) \tag{5.34}$$

with $\mu = 1,\ldots,N+1$ for the rows of the thermal geometric tensor. Similarly, we introduce

$$\vec{L} = \sum_\ell \left(\tilde{\Lambda}^S_{\ell,1}(\vec{X}),\ldots,\tilde{\Lambda}^S_{\ell,N}(\vec{X})\right), \tag{5.35}$$

where $\tilde{\Lambda}^S_{\mu,\nu}(\vec{X}) = g_\mu(X_\mu)\Lambda^S_{\mu,\nu}(\vec{X})$. These vector fields control the pumped heat and the work performed on the system as well as the dissipated power. Thus, they are useful to illustrate the operation of the specific thermal machine which we discuss in Section 5.5. In terms of these vector potentials Eqs. (5.29) and (5.30) read, respectively,

$$Q_{\mathrm{tr,ac}} = \oint \vec{A}_{N+1}(\vec{X})\cdot d\vec{X}, \tag{5.36}$$

with $\vec{A}_\mu(\vec{X}) = \vec{A}^A_\mu(\vec{X}) + \vec{A}^S_\mu(\vec{X})$ and

$$W = \oint \left[\frac{\Delta T}{T}\left(\vec{A}^A_{N+1}(\vec{X}) - \vec{A}^S_{N+1}(\vec{X})\right) - \vec{L}(\vec{X})\right]\cdot d\vec{X}. \tag{5.37}$$

In the latter equation, the term $\vec{A}^S_{N+1}(\vec{X})$ does not contribute for many systems. In particular, this is the case in the presence of time-reversal symmetry (including driving parameters $\vec{X}$ coupling to time-reversal-even operators). In such cases, we can write $W = (\Delta T/T)Q_{\mathrm{tr,ac}} - \oint \vec{L}(\vec{X})$.

5.4.1 Efficiencies

Heat engine

In a heat engine, heat transported from the high to the low temperature reservoir is partially converted into useful work. We can then define an efficiency for the heat engine as

$$\eta^{(\mathrm{he})} = \frac{W}{Q_{\mathrm{tr}}}. \tag{5.38}$$

This expression can be readily analyzed for a time-reversal-invariant system with constant $\Delta T/T$. In the limit of adiabatic operation of the heat engine, $\Omega \to 0$, we can neglect the frictional losses to leading order and only the second term on the right hand side of Eq. (5.30) contributes to the work performed against the load, $W \simeq Q_{\mathrm{tr,ac}}\Delta T/T$. If the heat transfer across the system is dominated by the geometric contribution, one finds $Q_{\mathrm{tr}} \simeq Q_{\mathrm{tr,ac}}$, and hence that the efficiency approaches $\eta^{(he)} \simeq \Delta T/T$. Remarkably, this is just the Carnot efficiency. We thus find that a purely geometric quantum thermal machine reaches the optimal efficiency, and it is the nongeometric contributions to W and Q_{tr} (in the sense of Berry) which are responsible for deviations from the Carnot efficiency. Indeed, a finite heat conductance diminishes the efficiency of the heat engine, as do frictional losses described by the first term on the right hand side of Eq. (5.30). Note that the contribution of the heat conductance to the transferred heat is proportional to the period of the cycle. This implies that this term is less detrimental to the efficiency as the frequency at which the machine operates increases. Conversely, by increasing the frequency, the effect of the frictional losses becomes larger.

While the overall efficiency is fundamentally limited to the Carnot limit, there is no fundamental limit to reducing the detrimental effects of the nongeometric contributions. While the frictional forces become arbitrarily small as one approaches the truly adiabatic limit, the limit of a negligible heat conductance $\Lambda_{N+1,N+1} \simeq 0$ can be realized in a topological quantum pump. In such pumps, the ground state is separated from the excited states by a gap. Consequently, the symmetric contributions to $\Lambda_{\mu,\nu}$ –including the heat conductance– are strongly suppressed.

Refrigerator

A refrigerator uses work W performed on the system to remove heat from a cold to a hot reservoir. Thus, we can define a corresponding efficiency or coefficient of performance (COP) as

$$\eta^{(\mathrm{fr})} = \frac{-Q_{\mathrm{tr}}}{-W}. \tag{5.39}$$

Again focusing on a time reversal invariant system with constant $\Delta T/T$, this efficiency approaches the Carnot limit $\eta^{fr} = T/\Delta T$ for zero heat conductance. The efficiency is reduced by a finite heat conductance since, for a refrigerator, its contribution to the numerator has the opposite sign compared to the pumped heat.

Heat pump

Of course, the device can also be used as an adiabatic heat pump in the absence of a thermal bias $\Delta T/T$. Heat is transported from left to right or vice versa due to the variation of $\vec{X}$.

According to Eq. (5.30), we need to exert work $-W$ associated with dissipation, even if there is no temperature bias. We can then define a corresponding efficiency of heat pumping through

$$\eta^{(\mathrm{pump})} = \frac{|Q_{\mathrm{tr,ac}}|}{-W}. \tag{5.40}$$

The denominator in this expression is proportional to Ω, so that the efficiency of the heat pump grows as it becomes more adiabatic.

5.5 Driven quantum dot: a strong coupling example

We now illustrate the general formalism introduced in the previous sections with an example. The configuration consists of a central *quantum dot* driven by a time-dependent magnetic

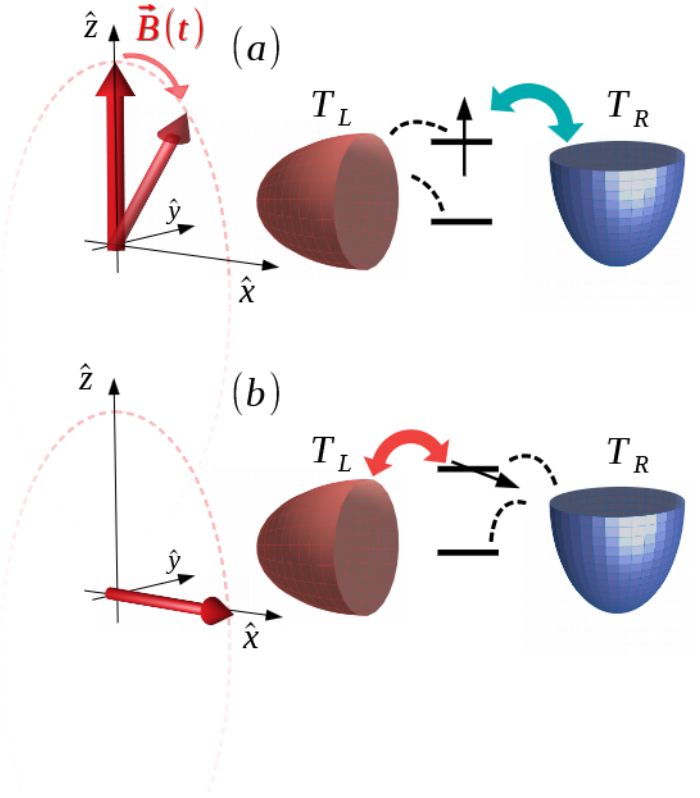

Figure 5.2: Illustration of the quantum dot driven by a magnetic field and connected to electron reservoirs with different polarizations, represented by different orientations of the paraboloids. The hybridization strength is modified according to the magnetic field's pointing direction. In (a) the electron hopping between the quantum dot and the right (z-polarized) reservoir is favored, as is denoted by the thick arrow. In (b) the pointing direction of the magnetic field has changed to x and now the quantum dot is stronger coupled to the left reservoir.

field and coupled to electron reservoirs with different polarizations. For the quantum dot the Hamiltonian $\mathcal{H}_S$ reads

$$\mathcal{H}_S(t) = \Psi_d^\dagger \left[V_g \, \hat{\sigma}_0 - \vec{B}(t) \cdot \hat{\vec{\sigma}} \right] \Psi_d, \tag{5.41}$$

where $\Psi_d^\dagger = (d_\uparrow^\dagger, d_\downarrow^\dagger)$ is a spinor representing the spin degrees of freedom of the electron in the quantum dot, while $d_\sigma^\dagger$ and d_σ are respectively the creation and annihilation fermionic operators for these particles. The quantum dot contains two levels as a consequence of the Zeeman splitting introduced by the magnetic field. $\hat{\vec{\sigma}} = (\hat{\sigma}_x, \hat{\sigma}_y, \hat{\sigma}_z)$ is composed of the 2×2 Pauli matrices and

$\hat{\sigma}_0$ is the identity, while $\vec{B}(t) = (B_x(t), B_y(t), B_z(t))$ is the external time-periodic magnetic field and V_g is a gate voltage, which rigidly shifts the energies of the two levels.

The reservoirs are represented by systems of non-interacting fermions. The electrons in the α reservoir are spin-polarized along the magnetization $\vec{m}_\alpha$. The Hamiltonian $\mathcal{H}_\alpha$ which describes the reservoir reads

$$\mathcal{H}_\alpha = \sum_{k\alpha} \Psi^\dagger_{k\alpha} \left[\varepsilon_{k\alpha} - \vec{m}_\alpha \cdot \hat{\vec{\sigma}}\right] \Psi_{k\alpha}, \quad \alpha = h, c, \tag{5.42}$$

where $\Psi^\dagger_{k\alpha} = \left(c^\dagger_{k\alpha,\uparrow}, c^\dagger_{k\alpha,\downarrow}\right)$ are spinors composed by the fermionic creation/annihilation operators $c^\dagger_{k\alpha,\sigma}$ and $c_{k\alpha,\sigma}$. We assume that both reservoirs have chemical potential $\mu_h = \mu_c = 0$.

The coupling between the quantum dot and the reservoirs is represented by

$$\mathcal{H}_{c,\alpha} = \sum_{k\alpha,\sigma=\uparrow,\downarrow} V_{k\alpha,\sigma} \left(c^\dagger_{k\alpha,\sigma} d_\sigma + d^\dagger_\sigma c_{k\alpha,\sigma}\right). \tag{5.43}$$

In order to solve the problem, it is convenient to change the basis of $\mathcal{H}_\alpha$ to the one where the quantization axis for the spin coincides with the direction of $\vec{m}_\alpha$. This is accomplished by a transformation $\left(c^\dagger_{k\alpha,\uparrow}, c^\dagger_{k\alpha,\downarrow}\right) = \hat{U}^\alpha \left(c^\dagger_{k\alpha,+}, c^\dagger_{k\alpha,-}\right)$. In the new basis the Hamiltonians for the reservoirs and the couplings read

$$\mathcal{H}_\alpha = \sum_{k\alpha,s=\pm} c^\dagger_{k\alpha,s} \varepsilon_{k\alpha,s} c_{k\alpha,s}, \quad \alpha = h, c, \tag{5.44}$$

and

$$\mathcal{H}_{c,\alpha} = \sum_{k\alpha,s=\pm,\sigma=\uparrow,\downarrow} v_{k_\alpha s,\sigma} \left(c^\dagger_{k\alpha,s} d_\sigma + H.c.\right), \tag{5.45}$$

with $v_{k_\alpha s,\sigma} = U^\alpha_{s,\sigma} V_{k\alpha,\sigma}$.

As discussed in Section 5.2.3, in order to have a non-vanishing pumping component we need to break spatial symmetry. We achieve this by considering different polarizations in the reservoirs. For concreteness, we consider the *hot* reservoir polarized along the positive x, and the *cold* one polarized along the positive z direction. An illustration of the whole setup is sketched in Fig. 5.2. Electrons with spins $z,\uparrow$ $(x,\uparrow)$ will mostly tunnel between the quantum dot and the R (L) reservoir. Therefore, when the magnetic field polarizes the quantum dot along the positive x direction, the tunneling of the electrons between the quantum dot and the h reservoir is optimal, while the tunnel between the dot and the c reservoir is optimal when the electron in the dot is polarized along the positive z direction.

In addition, the quantum dot has a gate voltage, which moves its energy levels upwards or downwards in energy, thus tuning different parts of the spectrum of the quantum dot into the relevant transport window ($\sim k_B T$) around the chemical potential of the reservoirs. This ingredient can be used to improve the performance, as we will discuss in Section 5.5.

The heat-engine operational mode in the present case could be practically realized by implementing the time-dependent magnetic field by means of a rotating classical magnetic moment. The dynamics of the latter realizes the load of the heat engine. In such a case, a pumped heat $Q_{\mathrm{tr,ac}}$ flowing in the direction of the heat current induced by the thermal bias, will generate a torque and exert work on the magnetic moment, akin to the spin torque induced by an electrical bias [230, 231, 232, 226].

We will analyze in detail protocols with two time-dependent parameters of the form $\vec{B}(t) = (B_x(t), 0, B_z(t))$, without focusing on the detailed mechanism generating the magnetic field.

$$\begin{aligned} B_x(t) &= B_{x,0} + B_{x,1}\cos(\Omega t + \phi), \\ B_z(t) &= B_{z,0} + B_{z,1}\cos(\Omega t). \end{aligned} \tag{5.46}$$

These two components of $\vec{B}(t)$ are identified with the time-dependent parameters of Eq. (6.1) as follows

$$\vec{X}(t) = (X_1(t), X_2(t)) \equiv (B_z(t), B_x(t))\,. \tag{5.47}$$

In addition, we will consider a constant difference of temperature ΔT, which defines $\dot{X}_3 = \Delta T/T$. We will show results for the heat pump and refrigerator modes.

Green's function approach

We can solve the problem exactly for arbitrary strength of the coupling between the quantum dot and the reservoirs by recourse to Green's functions. We will use the equilibrium finite-temperature formalism (see Section 3.3.3) to evaluate the frozen susceptibilities and compute the response functions from Eq. (5.14). This problem could be also exactly solved by recourse to the non-equilibrium Schwinger - Keldysh formalism in the Floquet representation and afterwards consider the expansion in small $\hbar\Omega$ and ΔT as in Refs. [80, 222] arriving at the same results as the ones we present here. We briefly summarize the results below and show some details on the calculations in Appendix C,

$$\begin{aligned} \Lambda^A_{3,\ell}(\vec{B}) &= -\frac{1}{h}\int d\varepsilon \frac{dn_F(\varepsilon)}{d\varepsilon}\varepsilon \mathrm{Tr}\left[\hat{\Gamma}_c\hat{\rho}(\varepsilon)\hat{\sigma}_\ell\hat{\rho}(\varepsilon)\right],\ \ell = 1,2 \\ \Lambda^S_{\ell,\ell'}(\vec{B}) &= -\frac{1}{h}\int d\varepsilon \frac{dn_F(\varepsilon)}{d\varepsilon} \mathrm{Tr}\left[\hat{\sigma}_\ell\hat{\rho}(\varepsilon)\hat{\sigma}_{\ell'}\hat{\rho}(\varepsilon)\right],\ \ell,\ell' = 1,2 \\ \Lambda^S_{3,3}(\vec{B}) &= -\frac{1}{h}\int d\varepsilon \frac{dn_F(\varepsilon)}{d\varepsilon}\varepsilon^2 \mathrm{Tr}\left[\hat{\Gamma}_c\hat{G}_t(\varepsilon)\hat{\Gamma}_h\hat{G}^\dagger_t(\varepsilon)\right], \end{aligned} \tag{5.48}$$

where $n_F(\varepsilon)$ is the Fermi-Dirac distribution function. We have also introduced the hybridization matrix $\hat{\Gamma}_\alpha$, with elements

$$(\hat{\Gamma}_\alpha)_{\sigma,\sigma'} = 2\pi \sum_{k\alpha,s=\pm} U^\alpha_{\sigma,s}U^\alpha_{\sigma',s}|V_{k\alpha}|^2\delta(\varepsilon - \varepsilon_{k\alpha,s}). \tag{5.49}$$

We consider the h (c) reservoirs fully polarized with spins along the positive x (z) directions and a constant density of states. Thus, $\Gamma_\alpha \simeq \sum_{k\alpha}|V_{k\alpha}|^2\delta(\varepsilon - \varepsilon_{k\alpha,+})$ and $\hat{\Gamma}_\alpha \simeq \Gamma_\alpha\hat{\tau}_\alpha$, with

$$\hat{\tau}_h \equiv \frac{1}{2}\left(\hat{\sigma}_x + \hat{\sigma}_0\right), \quad \hat{\tau}_c \equiv \frac{1}{2}\left(\hat{\sigma}_z + \hat{\sigma}_0\right). \tag{5.50}$$

The local density of states is described by the matrix

$$\hat{\rho}(\varepsilon) = -2\mathrm{Im}[\hat{G}_t(\vec{B},\varepsilon)] = \hat{G}_t(\vec{B},\varepsilon)\hat{\Gamma}\left[\hat{G}_t(\vec{B},\varepsilon)\right]^\dagger, \tag{5.51}$$

which depends on the frozen Green's function

$$\hat{G}_t(\vec{B},\varepsilon) = \left(\varepsilon - \vec{B}(t)\cdot\hat{\vec{\sigma}} + i\hat{\Gamma}/2\right)^{-1}, \tag{5.52}$$

with $\hat{\Gamma} = \hat{\Gamma}_h + \hat{\Gamma}_c$.

In Eqs. (5.48) we have highlighted the symmetric or antisymmetric nature of the components in each case. The fact that the components $\Lambda_{3,\ell}(\vec{B})$ are purely antisymmetric while $\Lambda_{\ell,\ell'}(\vec{B})$

are purely symmetric is a consequence of Onsager relations in combination with symmetry properties of the setup. These properties can be directly verified from the explicit calculations of Appendix C. The last component $\Lambda^S_{3,3}(\vec{B})$ is proportional to the thermal conductance. By using the fact that we can define a relation of the form $\dot{B}_\ell = g_\ell(\vec{B})\Omega$ for the protocol of Eq. (5.47), we can express the total work in terms of purely geometric quantities by appliying the results for the vector potentials, Eqs. (5.34) and (5.35). In the present case, they read

$$\begin{aligned}
\vec{A}^A_3(\vec{B}) &= \left(\Lambda^A_{3,1}(\vec{B}), \Lambda^A_{3,2}(\vec{B})\right), \\
\vec{A}^S_\ell(\vec{B}) &= \left(\Lambda^S_{\ell,1}(\vec{B}), \Lambda^S_{\ell,2}(\vec{B})\right), \quad \ell = 1, 2, \\
\tilde{\vec{A}}(\vec{B}) &= \Omega \sum_{\ell=1}^{2} g_\ell(\vec{B}) \left(\Lambda^S_{\ell,1}(\vec{B}), \Lambda^S_{\ell,2}(\vec{B})\right),
\end{aligned} \tag{5.53}$$

We have highlighted the antisymmetric and symmetric character in each case. Notice that, according to the analysis of Sections 5.2.3 and 5.3, the symmetric component contributes purely to dissipation of energy and entropy production, while the antisymmetric one is related to useful work.

Results

In Figure 5.3 we present the pumped heat $Q_{\mathrm{tr,ac}}(\phi)$ and the work developed by the *ac* sources W for $\Delta T = 0$, as function of the driving phase difference ϕ between the two *ac* components of the magnetic field.

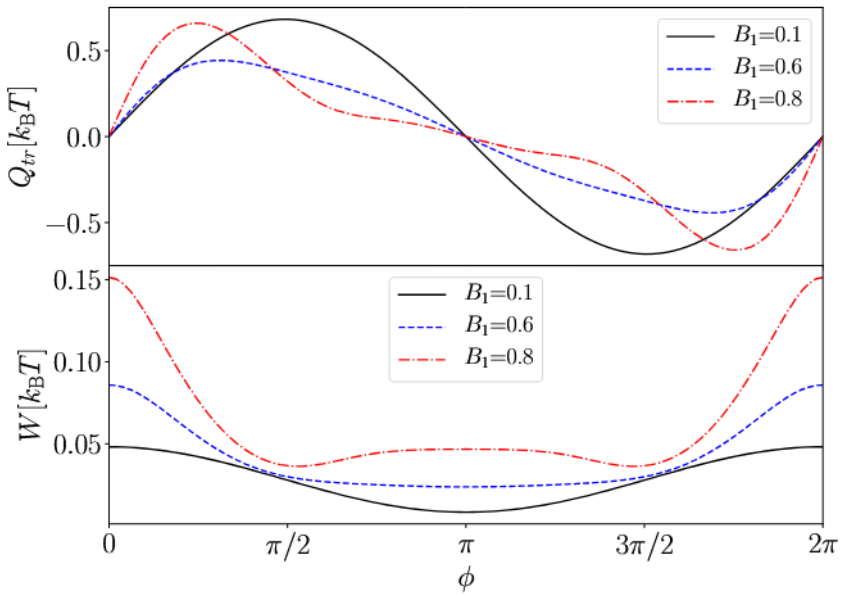

Figure 5.3: Pumped heat $Q_{\mathrm{tr,ac}} = Q_{\mathrm{tr}}$ (upper panel) and work done by the *ac* sources W (lower panel) for $\Delta T = 0$ as functions of the phase difference in the protocol defined by $B_x(t) = B_{x,0} + B_{x,1}\cos(\Omega t + \phi)$, $B_z(t) = B_{z,0} + B_{z,1}\cos(\Omega t)$ with $B_{x,0} = B_{z,0} = 0.4k_BT$ and $B_{x,1} = B_{z,1} = B_1 k_B T$. $\Gamma_h = \Gamma_c = 0.4k_BT$ and $\hbar\Omega = k_BT/800$. The plot with $B_1 = 0.1$ is multiplied by a factor 20 in order to be shown in the same scale.

We see that for small enough amplitudes of the driving ($B_{x,1}$ and $B_{z,1}$) the integrals in Eqs. (5.37) and (5.36) are proportional to the area, in the parameter space, enclosed by the closed contour defining the protocol. Indeed, using the Green's theorem, these integrals can be

written as a surface integral of the derivatives of $\vec{A}_3^A$ with respect to $\vec{B}$. When $B_{x,1}$ and $B_{z,1}$ are small, such derivatives do not depend on $\vec{B}$ and can be factorized outside the integral. For this reason, the pumped heat $Q_{\rm tr,ac}$ behaves as $\propto \sin(\phi)$ and the generated work as $\propto \cos(\phi)$ plus a constant. For larger values of the driving amplitude the pumped heat departs from this behaviour. However, $Q_{\rm tr,ac}(\phi)$ vanishes for $\phi = 0, \pi$ for any value of $B_{x,1} = B_{z,1}$.

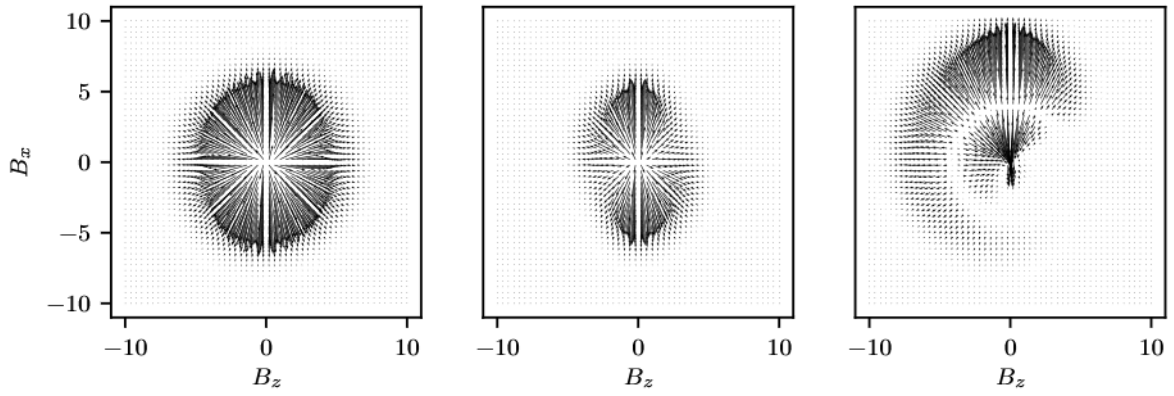

Figure 5.4: Vector fields $\vec{A}_3^A(\vec{B})$ for a driving protocol with $\vec{B}(t) = (B_x(t), 0, B_z(t))$, corresponding to a quantum dot coupled to reservoirs with different polarizations. c (h) reservoirs is polarized along positive z (x) direction. Left panel corresponds to $\Gamma_h = \Gamma_c$ and $V_g = 0$, middle correspond to $\Gamma_c = 0.1\Gamma_h$ and $V_g = 0$, while right panel corresponds to $\Gamma_c = 0.1\Gamma_h$ and $V_g = 2\Gamma_c$. The temperature of the reservoirs is $k_B T = 0.5\Gamma_c$.

We now focus on the properties in the operation of the quantum-dot machine. To this end, we further analyze the structure of the vector potentials $\vec{A}_\mu^{S/A}(\vec{B})$ and $\vec{L}^{S/A}(\vec{B})$ in Eq. (5.53) with the tensor $\Lambda_{\mu,\nu}(\vec{B})$ of Eq. (5.48). The vector map for $\vec{A}_3^A(\vec{B})$ in the parameter space for a given temperature T is shown in Fig. 5.4. This representation is useful to visualize the symmetries of the setup and to select the driving protocol that maximizes the contour integral $\oint \vec{A}_3^A(\vec{B}) \cdot d\vec{B}$. In the left panel the quantum dot is contacted with the same strength to both reservoirs ($\Gamma_h = \Gamma_c$), h being polarized along positive x and c along positive z direction, as indicated in the sketch of Fig. 5.2. In the middle panel, the contact is stronger to h than to c ($\Gamma_c = 0.1\Gamma_h$). Consequently, we can visualize a higher intensity of the field $\vec{A}_3^A$ along the B_x than along the B_z direction. Both left and middle plots have $V_g = 0$, in which case the Hamiltonian of Eq. (5.41) is symmetric under the simultaneous transformations $\Psi_d^\dagger \to \Psi_d$ and $\vec{B} \to -\vec{B}$. The first one is a particle-hole transformation, under which the heat current changes the sign. Consequently, the field maps of Fig. 5.4 present the symmetry $\vec{A}_3^A(\vec{B}) = -\vec{A}_3^A(-\vec{B})$. In the right panel, we can visualize that the breaking of the particle-hole symmetry by a gate voltage introduces a strong asymmetry in the vector field.

With the picture of Fig. 5.4 in mind, we can readily design a closed trajectory that optimizes pumping. The latter corresponds to a path that goes parallel to the vector field within the region where its intensity is high, and closes antiparallel to the vector field in a very low-intensity region. An example of such a trajectory is shown in Fig. 5.5. The corresponding vectors $\vec{L}^S(\vec{B})$ along the trajectory are also shown in cyan. Trajectories leading to high efficiencies of the machine would have as small dissipation as possible, in addition to high values of heat pumping. While the optimization of the pumping can be easily achieved by recourse to the vector field representation $\vec{A}_3^A(\vec{B})$, it is not easy to optimize a trajectory to decrease the integral over $\vec{L}^S(\vec{B})$. However, we know that this quantity can be reduced by decreasing the pumping frequency Ω.

Given a positive thermal bias ΔT, i.e. for $T_c < T_h$, we focus on the protocol of Fig. 5.5, for which we found a parameter set which removes heat from the cold reservoir (c). In Fig. 5.6 we

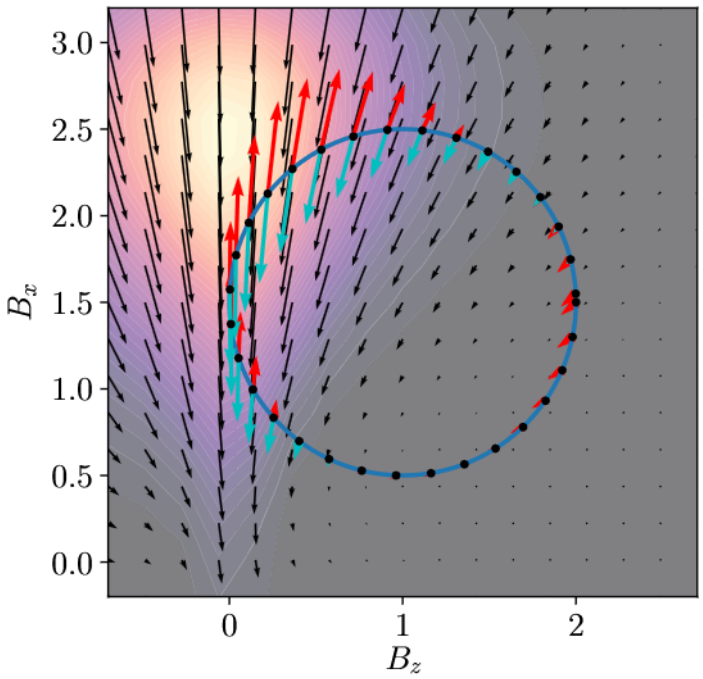

Figure 5.5: Vector fields $\vec{A}_3^A(\vec{B})$ (cyan) and $\vec{L}^S(\vec{B})$ (red) over a closed path (solid blue curve) for the configuration shown in the lower panel of Fig. 5.4 ($\Gamma_R = 0.1\Gamma_L$). The driving protocol defining the path is $B_x(t) = B_{x,0} + B_{x,1}\cos(\Omega t + \phi)$, $B_z(t) = B_{z,0} + B_{z,1}\cos(\Omega t)$ with $B_{x,0} = 1.5\Gamma_c$, $B_{z,0} = \Gamma_c$, $B_{x,1} = B_{z,1} = \Gamma_c$, $\phi = \pi/2$. The black arrows represent $\vec{A}_3(\vec{B})$ outside the defined protocol.

illustrate the performance (COP) of the driven quantum dot operating in refrigeration mode. We plot the COP $\eta^{(\mathrm{fr})}$ as a black dashed curve, defined in Eq. (5.39), and the normalized COP $\eta^{(\mathrm{fr})}/\eta_{\mathrm{C}}^{(\mathrm{fr})}$ (red curve) as functions of ΔT, where $\eta_C^{(\mathrm{fr})} = T/\Delta T$ is the Carnot COP. Starting from $\Delta T = 0$, the plot shows that $\eta^{(\mathrm{fr})}$ monotonously decreases with ΔT. This behaviour can be understood by recalling that the refrigeration mode results from a competition between the heat induced by the temperature difference and the pumped heat against the thermal bias. In fact, Q_{tr} is made up of two components: i) the component $Q_{\Delta T} = 2\pi J^Q_{\mathrm{tr},\Delta T}/\Omega$, which is the heat current flowing from the hot to the cold reservoir during one period, therefore entering the reservoir c ($Q_{\Delta T} > 0$). This component increases linearly with ΔT; ii) $Q_{\mathrm{tr,ac}}$, which is the pumped heat current extracted from the cold reservoir c ($Q_{\mathrm{tr,ac}} < 0$), which is independent of ΔT. Therefore Q_{tr} remains negative as long as $Q_{\Delta T}$ is not large enough to compensate $Q_{\mathrm{tr,ac}}$. In that condition the thermal machine is no longer a refrigerator (a further increase of ΔT leads to a sign reversal of the heat current).

On the other hand, the ratio $\eta^{(\mathrm{fr})}/\eta_{\mathrm{C}}^{(\mathrm{fr})}$ (red curve) is bell-shaped, since this ratio becomes $\propto \Delta T$. In the inset of Fig. 5.6 we plot the normalized COP as a function of the inverse of the driving frequency Ω. Since $Q_{\Delta T} \propto \Omega^{-1}$, increasing the frequency – within the adiabatic regime – favors the pumping component Q_{ac} relative to $Q_{\Delta T}$. Notice, however, that by increasing the frequency the dissipative component represented by $\tilde{\vec{A}}$ in Eq. (5.37) becomes more detrimental to the efficiency. There is, thus, a compromise between the two effects and an optimal frequency of operation. In the present case, we achieve values as large as 14 % η_C^{fr}. The key to obtain high efficiency values is the selection of an appropriate pumping protocol, taking for example advantage of the extra features introduced by the existence of the gate voltage V_g.

We close this section by analyzing the geometric component of the first-order adiabatic reaction force defined in Eq. (5.33). In the present problem, the latter coincides with the

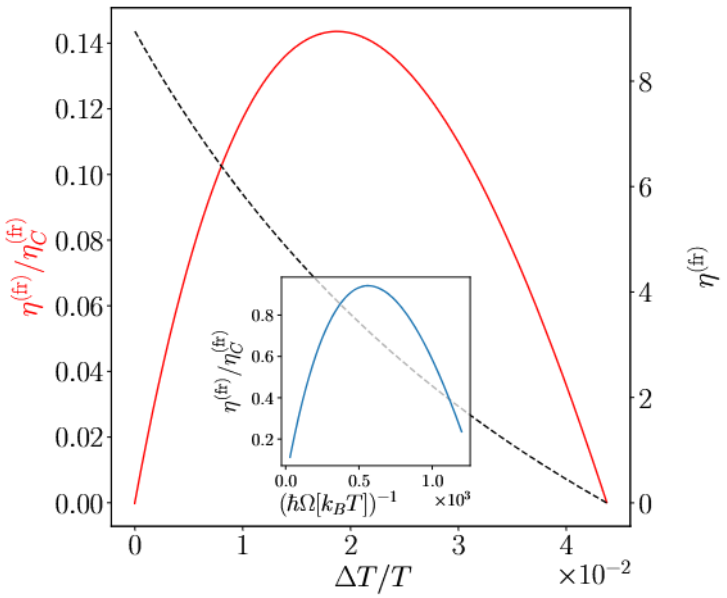

Figure 5.6: Coefficient of performance for refrigeration (absolute in dashed black and normalized to the Carnot value in red) versus ΔT for the protocol of Fig. 5.5 for $\hbar\Omega = \Gamma_R/200$ Inset: Normalized coefficient of performance for refrigeration as a function of $\hbar\Omega$ for $\Delta T = T/150$.

magnetic moment of the quantum dot. For $\Delta T = 0$, the magnetic moment of the quantum dot is given by

$$\begin{aligned} m_\ell &= \frac{\Omega}{2\pi}\int_0^{2\pi/\Omega} dt\langle\Psi_d^\dagger\hat{\sigma}_\ell\Psi_d\rangle(t) = m_\ell^{\mathrm{BO}} + m_\ell^{\mathrm{geo}}, \\ m_\ell^{\mathrm{geo}} &= \frac{\Omega}{2\pi}\oint \vec{A}_\ell^S(\vec{B})\cdot d\vec{B}, \end{aligned} \tag{5.54}$$

with $\hat{\sigma}_{x,y}$ for $\ell \equiv 1, 2$, respectively. Here, m_ℓ^{BO} is the average over one period of the the instantaneous magnetization corresponding to the equilibrium frozen Hamiltonian, while m_ℓ^{geo} is the geometric component, corresponding to the first-order adiabatic reaction force of Eq. (5.33). The vectors $\vec{A}_\ell^S(\vec{B})$ are calculated from Eq. (5.48) as defined in Eq. (5.53). Interestingly, the symmetric component of the thermal geometric tensor, which defines the dissipation, is directly related in the present problem to a local physical quantity, which is the quantum dot geometric magnetization [67]. The latter is experimentally accessible. In fact, notice that the component m_ℓ^{BO} does not explicitly depend on the driving frequency, while the second term has an explicit linear dependence on Ω. Therefore, in a concrete experimental measurement of the quantum dot magnetization, both components should be distinguishable from one another.

The associated vector fields $\vec{A}_\ell^S(\vec{B})$ are shown in Fig. 5.7 for configurations with stronger coupling to the h (x-polarized) reservoir than to the c (z-polarized) one and a finite gate voltage V_g, with the same values of the parameters as in the right panel of Fig. 5.4. In this representation, we can visualize higher intensity of the fields along $B_x, B_z > 0$ relative to $B_x, B_z < 0$, as a consequence of the polarization of the reservoirs along the positive x and z-axis. The amplitudes of $\vec{A}_1^S(\vec{B})$, shown in the left panel, are larger than those of $\vec{A}_2^S(\vec{B})$, shown in the right panel, due to the larger coupling to the reservoir polarized along x. The result of calculating the integrals over closed trajectories with different phase lags ϕ between the components B_x and B_z is shown in Fig. 5.8. As in the case of the pumped heat, both components of the magnetization vanish at $\phi = 0, \pi$.

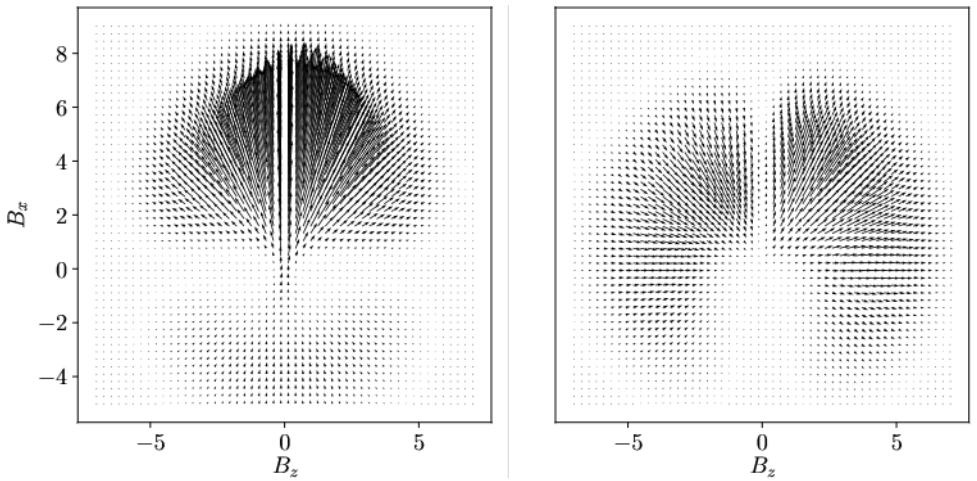

Figure 5.7: Vector fields $\vec{A}_1^S(\vec{B})$ (left) and $\vec{A}_2^S(\vec{B})$ (right) following Eqs. (5.53) and (5.48), for the parameters of the right panel of Fig. 5.4.

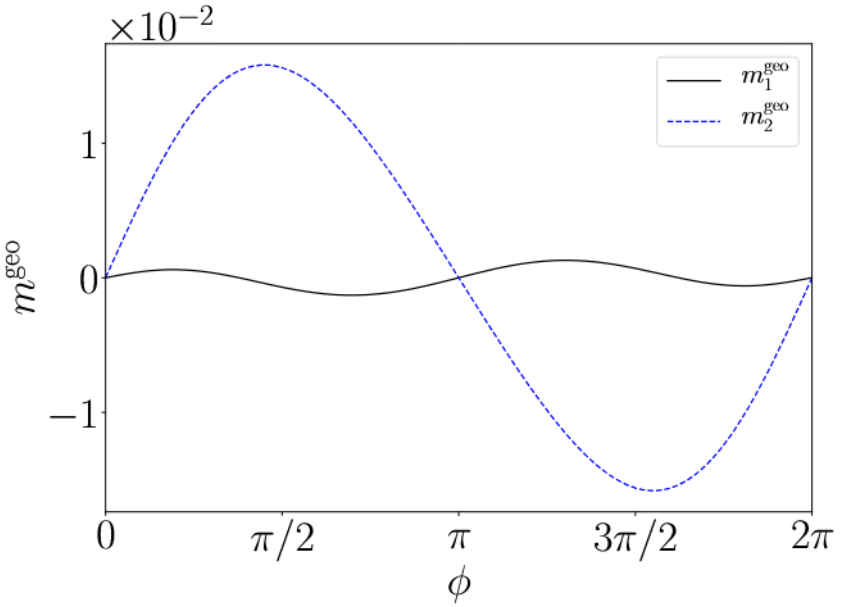

Figure 5.8: Components of the geometric magnetization $m_{1,2}^{\text{geo}}$, defined in Eq. (5.54) as functions of the phase-lag ϕ corresponding to paths of the form $B_x(t) = B_{x,0} + B_{x,1}\cos(\Omega t + \phi)$, $B_z(t) = B_{z,0} + B_{z,1}\cos(\Omega t)$ with $B_{x,0} = 1.5\Gamma_R$, $B_{z,0} = \Gamma_R$, $B_{x,1} = B_{z,1} = \Gamma_R$, on the vector fields of Fig. 5.7.

Chapter 6

Geometric optimization of Nonequilibrium Adiabatic Thermal Machines and Implementation in a Qubit System

This chapter is based on the paper *PRX Quantum 3, 010326: "Geometric Optimization of Nonequilibrium Adiabatic Thermal Machines and Implementation in a Qubit System"*.

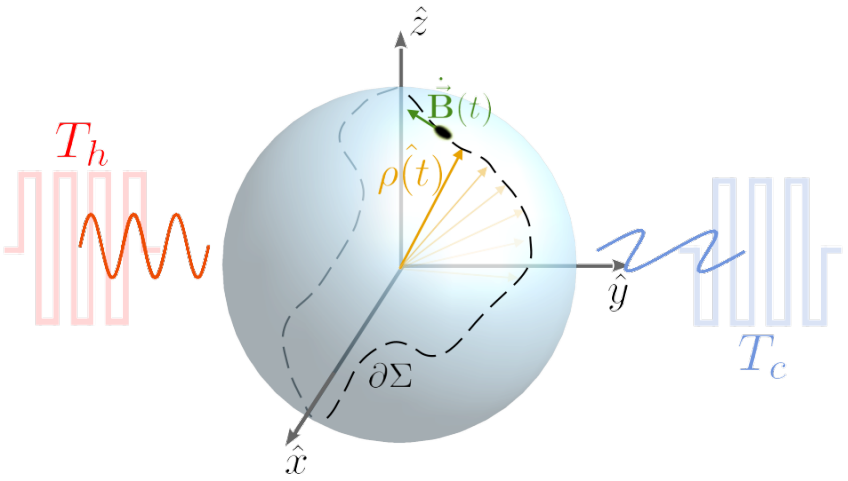

Figure 6.1: Schematic configuration of the setup. A working substance WS is in contact with two reservoirs at different temperatures, T_c and T_h. The state $\hat{\rho}$ of the system changes at slow but finite speed along a closed path defined by the Hamiltonian $\mathcal{H}(\vec{B}(t))$ in a quasistatic process.

6.1 Introduction

The aim of the present chapter is to optimize the performance of thermal machines with cycles in permanent contact to two or more reservoirs at different temperatures using the geometric approach developed in Chapter 5 (and in particular Section 5.4). To this end we combine the geometrical description of the two competing mechanisms of the non-equilibrium thermal machine (namely heat-work conversion and dissipation) in order to find optimal protocols for maximizing power generation of the heat-engine operation and the efficiency of the refrigerator mode. We show that the problem of finding such optimal protocols reduces to an *isoperimetric problem* [233] (also studied as *Cheeger Problem* [234, 235]), that is the task of finding the shape which maximizes the ratio between area and length. This is one of the oldest geometric problems in history, and was solved already by the ancient Greeks in the standard 2-dimensional Euclidean plane [236]. Nevertheless, when the underlying area density or length metrics are nontrivial [237, 238, 239, 240], no general solution is known.
We illustrate these ideas in a prominent quantum system playing the role of the working substance (WS): a qubit driven by two parameters slowly changing in time and asymmetrically coupled to two thermal reservoirs at different temperature (see Fig. 6.1). We show analytically that the limiting value for the area in the parameter space is given by the celebrated Landauer bound [241, 242], which has been the motivation of many studies including several experiments (see e.g. [243, 244]). We also find that, operating as a heat engine, the qubit thermal machine offers a very good ratio between generated power and efficiency in a wide range of parameters.

The chapter is structured as follows. In Section 6.2, we introduce the set-up and define the relevant thermodynamic quantities to characterize the cycle. In Section 6.3, we describe the underlying geometry of the system. In Section 6.4 we describe the heat engine and refrigeration modes of the machine, and perform the optimization with respect to the driving time. In Section 6.5, we develop the full optimization of the machine. We then compute in detail all the relevant quantities in a model of one of the most paradigmatic and simplest quantum engines, namely a driven qubit system (see Refs. [174, 97, 161]).

6.2 The setup and its thermodynamics

We focus on the usual configuration where the WS operates in contact to two reservoirs at different temperatures $T_{\rm h}$ (hot) and $T_{\rm c}$ (cold), with $T_{\rm h} = T + \Delta T$ and $T_{\rm c} \equiv T$. A particular

example, which will be studied in detail in forthcoming sections is sketched in Fig. 6.1. The full system is described once more by the Hamiltonian 2.1

$$\mathcal{H}(t) = \mathcal{H}_{\rm WS}(t) + \sum_{\alpha={\rm c,h}} (\mathcal{H}_\alpha + \mathcal{H}_{{\rm cont},\alpha}) \tag{6.1}$$

where we renamed $\mathcal{H}_S(t) \equiv \mathcal{H}_{\rm WS}(\vec{B}(t))$ in this context to emphasize the fact that the central system acts as the working substance, with $\vec{B}(t) = (B_1(t), \ldots, B_N(t))\,,\ j = 1, N$ being the control parameters. We are from the beginning interested in cycles, so we consider time-dependent protocols satisfying $\vec{B}(t+\tau) = \vec{B}(t)$, being τ the period of the cycle. The reservoirs are represented by the Hamiltonian

$$\mathcal{H}_\alpha = \sum_k \varepsilon_{k\alpha} b^\dagger_{k\alpha} b_{k\alpha}, \quad \alpha = {\rm c, h}, \tag{6.2}$$

with $b_{k\alpha}$ and $b^\dagger_{k\alpha}$ being the annihilation and creation operators of a bosonic excitation. The coupling is represented by

$$\mathcal{H}_{{\rm cont},\alpha} = \sum_k V_{k\alpha} \hat{\pi}_\alpha \Big(b_{k\alpha} + b^\dagger_{k\alpha} \Big), \tag{6.3}$$

where $\hat{\pi}_\alpha$ is a matrix with the dimension of the Hilbert space of the WS.

The crucial concepts that characterize the operation of the thermal machine are the work performed and the net heat exchanged between the two reservoirs during the cycle. The operation of the driven quantum system as a thermal machine in the presence of a temperature bias relies on the mechanism of heat–work conversion. Following the ideas of the previous chapters, in the present case we make the two main assumptions:

(i) slow driving [193], characterized by a small rate of change of the driving parameters with time, $d_t\vec{B}$ (short for $\frac{d}{dt}\vec{B}$). In most of the cases, such time scale is determined by the relaxation time $\tau_{\rm rel}$ of the WS with the reservoirs.

(ii) a small temperature bias ΔT between the two reservoirs.

This enables us to work in the linear-response regime with respect to $d_t\vec{B}$ and ΔT, specifically in the adiabatic linear response theory of Section 3.1 [80] using the framework developed in Chapter 5, which is useful when $\tau \gg \tau_{\rm rel}$. We also consider small temperature bias, such that $\Delta T/T \ll 1$. Recalling Eq. (5.13), this description leads to a linear relation between the relevant energy fluxes operating the cycle and the components of the vector $d_t\mathbf{X} = (d_t\vec{B}, \Delta T/T)$. The relevant quantities are the net *output work* and *transferred heat* between the hot and cold reservoirs. They are, respectively, defined as the average over one period of the power developed by the driving sources, and the energy flux into the α-reservoir,

$$W = -\int_0^\tau dt\, \langle \frac{\partial \mathcal{H}_{\rm WS}}{\partial \vec{B}} \rangle \cdot d_t\vec{B}, \tag{6.4}$$

$$Q_\alpha = -\frac{i}{\hbar}\int_0^\tau dt\, \langle [\mathcal{H}_\alpha, \mathcal{H}] \rangle\,, \tag{6.5}$$

where $\langle O \rangle = {\rm Tr}\,[\rho O]$, being ρ the global state of system and baths (which in general will be correlated due to the contacts). The corresponding expectations values were evaluated in linear response with respect to $d_t\mathbf{X}$ in Chapter 5, and we can apply the results directly from Eq. (5.28) and Eq. (5.30) in the present context as

$$W = \frac{\Delta T}{T}\int_0^\tau dt\ \vec{\Lambda}\cdot d_t\vec{B} - \int_0^\tau dt\ d_t\vec{B}\cdot\underline{\Lambda}\cdot d_t\vec{B}\ , \tag{6.6}$$

$$Q = \int_0^\tau dt\ \vec{\Lambda}\cdot d_t\vec{B} + \frac{\Delta T}{T}\int_0^\tau\ dt\ \kappa\ . \tag{6.7}$$

(remembering that $Q_{\rm c} = -Q_{\rm h} \equiv Q$). We have renamed the different components of the thermal tensor Eq. (5.14) for the sake of clarity in the discussion that follows.

The coefficients associated to the mechanism of *heat–work* conversion are denoted by $\vec{\Lambda}(\vec{B})$ and corresponds to the elements $\Lambda_{N+1,\ell},\ \ 0 \leq \ell \leq N$ of Eq. (5.14).

The matrix $\underline{\Lambda}$ is an alias for the coefficients $\Lambda_{\ell,\ell'},\ \ 0 \leq \ell, \ell' \leq N$, and defines the finite-time dissipation developed by the time-dependent controls.

Finally we rename $\kappa = \Lambda_{N+1,N+1}$, the heat transport as a response to the temperature bias. We stress that $\{\vec{\Lambda}, \underline{\Lambda}, \kappa\}$ are all local functions of $\vec{B}$, while they also depend on the coupling parameters, the density of states of the thermal baths and T.

Notice that the fundamental component for the thermal machine to operate is the heat–work conversion term $\int_0^\tau dt\ \vec{\Lambda}\cdot d_t\vec{B}$. In fact, without this component, the only surviving processes are the dissipation of the energy supplied by the driving forces and the trivial conduction of heat as a response to the thermal bias.

It is important to notice that the second terms of Eqs. (6.6) and (6.7) have a defined sign. In our convention, $\underline{\Lambda}$ is positive definite since it is directly related to the entropy production rate, which means that it is detrimental for the work output. Similarly, κ can be seen to be positive, as a consequence of the fact that this component of the transferred heat describes the flux from the hottest to the coldest reservoir. These are direct consequences of the second law of thermodynamics. Instead, the line integral $\int_0^\tau dt\ \vec{\Lambda}\cdot d_t\vec{B}$ may have any sign, depending on the driving protocol and it is enough to time-reverse the function $\vec{B}(t)$ to flip the sign. As mentioned before, this term describes the *heat–work* conversion process and its sign defines the type of operation of the machine. In fact, when it is negative, the contribution of the first term of Eq. (6.7) may overcome the heat flowing into the coldest reservoir and enable the operation of the machine as a *refrigerator*. This has an associated cost, described by the first term of Eq. (6.6), which must be developed by the driving sources. In the opposite situation where $\int_0^\tau dt\ \vec{\Lambda}\cdot d_t\vec{B} \geq 0$, the first term of Eq. (6.6) may overcome the second one, enabling the mechanism of work output. This has an associated extra heat transfer from the hot to the cold reservoirs, which is accounted for the first term of Eq. (6.7). This operation corresponds to a *heat engine*.

6.3 Geometry of the problem

We now elaborate on the interpretation of the different terms in Eqs. (6.6) and (6.7) presented in the previous Section, which allows for the optimization of the thermodynamic protocols in terms of clear geometrical quantities.

First, we factorize the total duration τ in the expressions Eqs. (6.6) and (6.7), such to decouple the time-rescaling from the geometrical contribution to the different quantities. Indeed by considering an adimensional time unit θ such that

$$\vec{B}(t) = \vec{B}(\theta\tau)\ , \quad \theta \in [0,1]\ , \tag{6.8}$$

we can define, identifying from now on the adimensional time derivative $\dot{\vec{B}} \equiv \partial\vec{B}/\partial\theta = \tau d_t \vec{B}$,

$$A = \int_0^1 d\theta\ \vec{\Lambda}\cdot\dot{\vec{B}}\ , \tag{6.9}$$

$$L^2 = \int_0^1 d\theta\ \dot{\vec{B}}\cdot\underline{\Lambda}\cdot\dot{\vec{B}}\ , \tag{6.10}$$

$$\langle\kappa\rangle = \int_0^1 d\theta\ \kappa\ . \tag{6.11}$$

Accordingly, Eqs. (6.6) and (6.7) can be expressed as follows,

$$W = \frac{\Delta T}{T}A - \frac{L^2}{\tau} \tag{6.12}$$

$$Q = A + \frac{\Delta T}{T}\tau\langle\kappa\rangle. \tag{6.13}$$

The names A and L^2 are related the geometrical meaning of the quantities above, as we discuss below. The representation of Eq. (6.9) highlights the fact that A corresponds to a Berry-type phase in the parameter space as discussed in Chapter 5. Notice, that, in order to have a non-vanishing value of A, at least two time-dependent parameters are necessary. This is basically the same argument widely discussed in the literature of adiabatic charge pumping [52, 54, 198, 197]. In addition, it is necessary to break some symmetries in the system to have a finite value of this closed integral.

Given that $\vec{B}(\theta)$ represents a closed trajectory in space, we can use Stokes' theorem –in a three-dimensional space or its corresponding generalization in higher dimensions– to re-express the line-integral defining A

$$A = \int_{\partial\Sigma}\vec{\Lambda}\cdot d\vec{B} = \int_{\Sigma}(\vec{\nabla}_B\wedge\vec{\Lambda})\cdot d\vec{\Sigma}\ , \tag{6.14}$$

where Σ is a surface in the $\vec{B}$ space, with boundary $\partial\Sigma$ coinciding with the control trajectory. In the case of having 4 or more parameters, Eq. (6.14) should be replaced by the Generalized Stokes' Theorem applied to differential forms in the appropriate dimension [1]. In this representation, A is the flux of the vector $\vec{\nabla}_B\wedge\vec{\Lambda}$ through the area enclosed by the control trajectory, and can be also interpreted as the integral over this area weighted by the Berry curvature [51]. We can therefore *think of A as the area of the surface defined by the control trajectory* (with local weight depending on the Berry curvature). Note that this geometrical translation clarifies as well that A depends *only* on the geometry of the trajectory $\vec{B}(\theta)$: that is, not only A is independent of τ, but it is also invariant under any reparametrization $\theta'(\theta)$ which might change the local speed and time spent on different points of the trajectory.

Concerning L^2, *it can be interpreted as a length squared of the control trajectory* $\vec{B}(\theta)$, as it is clear from (6.10) that it represents the integral of a quadratic form that defines a metric in the $\vec{B}$ space. At the same time, given the presence of two time derivatives, L^2 can depend in general on reparametrizations $\theta'(\theta)$. However, L^2 represents losses due to dissipation in the driving – see Eq. (6.6) – and we are therefore interested in its minimum value, which can be obtained through a Cauchy-Schwarz inequality

$$L^2 \geq \left(\int_0^1 d\theta\ \sqrt{\dot{\vec{B}}\cdot\underline{\Lambda}\cdot\dot{\vec{B}}}\right)^2 = \left(\int_{\partial\Sigma}\sqrt{d\vec{B}\cdot\underline{\Lambda}\cdot d\vec{B}}\right)^2 \equiv \mathcal{L}^2\ . \tag{6.15}$$

[1] Identifying $\vec{\Lambda}\cdot d\vec{B}$ with a 1-form ω over $\mathbf{R}^n$, we can express Eq. (6.14) as $A = \int_{\partial\Sigma}\omega = \int_\Sigma d\omega$, where $d\omega$ is the exterior derivative of ω.

The lower bound $\mathcal{L}$ is fully geometric (it depends solely on $\partial\Sigma$) and it is always achievable by choosing the time-parametrization θ' such that $\dot{\vec{B}} \cdot \underline{\Lambda} \cdot \dot{\vec{B}}$ is constant. $\mathcal{L}$ is a natural extension of the standard thermodynamic length [71, 72, 73, 74, 75, 89, 90, 91, 83, 78, 95, 81] to non-equilibrium set-ups where the WS is simultaneously interacting with several baths.

Finally, it is apparent that $\langle\kappa\rangle$ Eq.(6.11) represents the simple average of a scalar number (the heat conductance) along the trajectory. In general it clearly also depends on reparametrizations of the adimensional time $\theta'(\theta)$, as the average can be arbitrarily close to the maximum value $\kappa_{\max}$ of the trajectoy, in case θ' is such to spend almost all the time close to $\kappa_{\max}$. Similarly $\langle\kappa\rangle$ can be arbitrarily close to the minimum value along the trajectory $\kappa_{\min}$.

6.4 Performance of the machine and time-optimization

In this section we discuss the different operation modes of the thermal machine, and introduce the relevant figures of merit for its characterization.

6.4.1 Heat engine

The system described in the previous sections can be used to extract work from two reservoirs with a temperature bias. This is the *engine* operating mode of the system. We write the power of the heat engine and its efficiency as

$$P = \frac{W}{\tau} = \frac{\Delta T}{T}\frac{A(1-\frac{\tau_D}{\tau})}{\tau} , \tag{6.16}$$

$$\eta = \frac{W}{Q} = \eta_C \frac{1-\frac{\tau_D}{\tau}}{1+\frac{\tau}{\tau_k}} , \tag{6.17}$$

where we substituted Eqs. (6.6)-(6.7) and we defined the dissipation and heat leak timescales

$$\tau_D = \frac{T}{\Delta T}\frac{L^2}{A} , \quad \tau_\kappa = \frac{T}{\Delta T}\frac{A}{\langle\kappa\rangle} . \tag{6.18}$$

In the previous expressions $\eta_C = \Delta T/T$ is the Carnot efficiency. Given the expressions above, we can optimize the duration of the cycles in order to maximize the power or the efficiency, obtaining correspondingly

$$\tau_P = 2\tau_D, \quad \tau_\eta = \tau_D + \sqrt{\tau_D(\tau_D+\tau_\kappa)} . \tag{6.19}$$

We see that the duration for maximum efficiency is always larger than the duration for maximum power. The corresponding maximum power and efficiency at maximum power are

$$P_{\max} = \frac{1}{4}\frac{(\Delta T)^2}{T^2}\frac{A^2}{L^2} , \quad \eta_{P_{\max}} = \frac{\eta_C}{2}\frac{x-1}{x+1} \tag{6.20}$$

while the maximum efficiency and power at maximum efficiency

$$\eta_{\max} = \eta_C\left(1-\frac{2}{\sqrt{x}+1}\right) , \quad P_{\eta_{\max}} = \frac{(\Delta T)^2}{T^2}\langle\kappa\rangle\frac{(\sqrt{x}-1)^2}{\sqrt{x}} , \tag{6.21}$$

with

$$x = 1 + \frac{A^2}{L^2\langle\kappa\rangle}. \tag{6.22}$$

See Fig. 6.2 for a summary and visual explanation of these results.

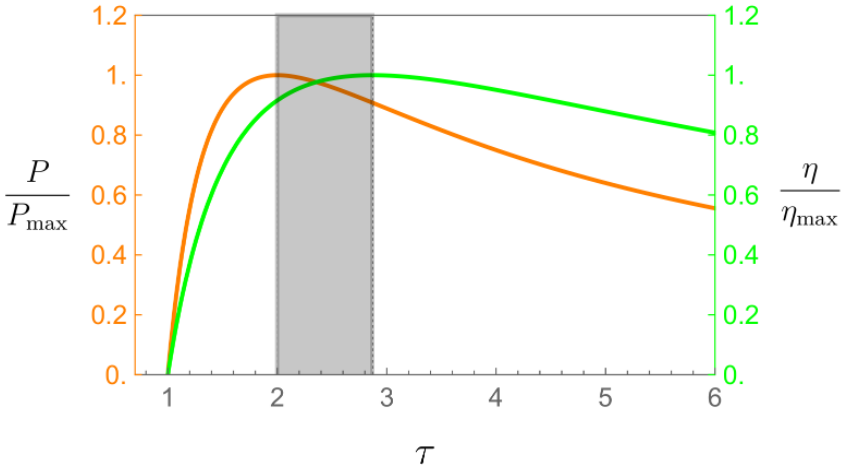

Figure 6.2: *Engine mode: Power and efficiency vs. cycle duration.*
The optimal operating region is the gray interval between the two dashed lines: indeed for any point outside the region, there is a point inside with both larger efficiency and larger power.
In the limit of big heat leaks $\langle\kappa\rangle$ the corresponding heat leaks timescale τ_κ (6.18) is small, and the difference between τ_P and τ_η (6.19) shrinks. That is, when the heat leak is the dominant loss, power and efficiency maximization tend to coincide, as one could expect (this can be verified by direct inspection of (6.16) and (6.17)); the corresponding maximum efficiency is also small in this limit.
In the opposite limit of no leaks $\langle\kappa\rangle \to 0$, τ_κ tends to infinite, and we recover the standard scenario in which power is maximized for a finite time, while the efficiency is maximum for $\tau \to \infty$, where it tends to the Carnot efficiency, as the dominant loss is due to finite-time dissipation. For finite values of $\langle\kappa\rangle$, the scenario is intermediate. In the plot $\tau_D = 1$ and $\tau_\kappa = 2.5$.

6.4.2 Refrigerator

In the *heat pump* or *refrigerating* mode, external work is supplied to the system to extract heat from the cold bath and transfer it to the hot one. Therefore we define the cooling power P' and the coefficient of performance (COP) η'

$$P' = \frac{-Q}{\tau} = A\frac{1-\frac{\tau}{|\tau_k|}}{\tau}\,, \tag{6.23}$$

$$\eta' = \frac{Q}{W} = \eta'_C\frac{1-\frac{\tau}{|\tau_k|}}{1+\frac{|\tau_D|}{\tau}}\,, \tag{6.24}$$

where $\eta'_C = T/\Delta T$ is the Carnot COP. The difference with the engine operating mode is that in this case both Q and W are negative (heat is transferred against the thermal bias and work is performed *on* the system). We have therefore $A < 0$ which implies $\tau_\kappa < 0$ and $\tau_D < 0$ are formally negative as well (which is the reason of the absolute values in the equations). By direct inspection of (6.23) we see that the maximum power of such mode is unbounded, as in the limit $\tau \to 0$ the power tends to infinity. The slow-driving approximation $\tau_{\rm rel}/\tau \ll 1$ prevents us from analyzing the limit of arbitrary small τ and a reliable analysis of the cooling power requires a description beyond linear response [245, 246]. Thus, we focus only on maximizing the efficiency of this operation, for which we get

$$\tau_{\eta'} = \tau_\eta = \sqrt{\tau_D(\tau_D+\tau_\kappa)} - |\tau_D|\,, \tag{6.25}$$

$$\eta'_{\max} = \frac{T}{\Delta T}\left(1 - \frac{2}{\sqrt{x}+1}\right) , \tag{6.26}$$

$$P'_{\eta'_{\max}} = \frac{\Delta T}{T}\langle\kappa\rangle\sqrt{x} , \tag{6.27}$$

with x defined as in Eq. (6.22).

6.5 Full optimization and the isoperimetric problem

In the previous section we showed how to choose the optimal duration for cycles of two kinds of thermal machines, and we derived formal expressions for the resulting powers and efficiencies. The resulting figures of merit still depend on the particular trajectory chosen for the cycle. Finding the fully-optimal solution is nontrivial, but we show in the following how the geometrical picture of the thermodynamics introduced in Sections 6.3 and 6.4, helps in finding the most advantageous control trajectories to be exerted on the machine.

An interesting question in the present problem is whether we can find a protocol that maximizes the output power of the system. We have shown in Section 6.3 that, given a parametrization $\vec{B}(\theta\tau)$ defined over $\partial\Sigma$ in the parameter space, we can compute the duration τ that upper bounds the power for that protocol. The result is expressed in Eq. (6.20). Besides, we know from the definition in Eq. (6.14) that the value of A^2 does not depend on reparametrizations θ', while the value of L^2 can be lower-bounded by $\mathcal{L}^2$ according to Eq. (6.15). With all these considerations, we find that the maximum power developed by a protocol moving along a curve $\partial\Sigma$ is expressed by

$$P_{\max}(\partial\Sigma) = \frac{1}{4}\frac{(\Delta T)^2}{T^2}\frac{A^2}{\mathcal{L}^2}. \tag{6.28}$$

Eq. (6.28) tells us that the problem of finding the maximum output power of the system is equivalent to the problem of maximizing the term $A^2/\mathcal{L}^2$ over the set of all closed curves $\partial\Sigma$ in the parameter space (known as isoperimetric or Cheeger problem [233, 234, 235]). The optimization of this geometrical quantity is not a simple task in general, since one must choose a test curve $\partial\Sigma$ that maximizes A^2, while keeping $\mathcal{L}^2$ small, being those quantities nontrivial functions of $\partial\Sigma$ when the corresponding metrics are not flat [237, 238, 239, 240].

For what concerns the efficiencies, $\eta_{\max}$, $\eta'_{\max}$, $\eta_{P_{\max}}$ are all increasing functions of the same parameter $A^2/(L^2\langle\kappa\rangle)$. Like in Eq. (6.15) the denominator can be lower bounded with a Cauchy-Schwarz inequality

$$L^2\langle\kappa\rangle = \left(\int_0^1 d\theta\ \dot{\vec{B}}\cdot\underline{\Lambda}\cdot\dot{\vec{B}}\right)\left(\int_0^1 d\theta\ \kappa\right) \geq \left(\int_0^1 d\theta\ \sqrt{\kappa}\sqrt{\dot{\vec{B}}\cdot\underline{\Lambda}\cdot\dot{\vec{B}}}\right)^2 . \tag{6.29}$$

In complete analogy to Eq. (6.15), the bound can be always saturated, by choosing a reparametrization $\theta'(\theta)$ such that $\dot{\vec{B}}\cdot\underline{\Lambda}\cdot\dot{\vec{B}}/\kappa$ is constant in time, and can be interpreted again as a length defined by an underlying metric

$$\left(\int_{\partial\Sigma}\sqrt{d\vec{B}\cdot\underline{\Lambda_\kappa}\cdot d\vec{B}}\right)^2 \equiv \mathcal{L}_\kappa^2 , \qquad \underline{\Lambda_\kappa} = \underline{\Lambda}\kappa . \tag{6.30}$$

The length $\mathcal{L}_\kappa$ is fully geometric, i.e. it depends only on the set of points defined by the trajectory $\partial\Sigma$, and the maximization of $\eta_{\max}$, $\eta'_{\max}$, $\eta_{P_{\max}}$ is also mapped to an isoperimetric problem

$$\max\frac{A^2}{L^2\langle\kappa\rangle} = \max_{\partial\Sigma}\frac{A^2}{\mathcal{L}_\kappa^2} . \tag{6.31}$$

The geometric expressions (6.28) and (6.31), which map the thermodynamic optimization to an isoperimetric (Cheeger) problem, are the main results of this paper.

6.6 A qubit thermal machine

We will exemplify these results for the specific case of a driven qubit, in which case, the Hamiltonian for the working substance entering Eq. (6.1) is $\mathcal{H}_{\rm WS}(t) = \mathcal{H}_{\rm qb}(t)$, where

$$\mathcal{H}_{\rm qb}(t) = \vec{B}(t) \cdot \hat{\vec{\sigma}} \tag{6.32}$$

with $\hat{\vec{\sigma}} = (\hat{\sigma}_z, \hat{\sigma}_x)$ being the Pauli matrices and $\vec{B}(t) \equiv (B_z(t), B_x(t))$, being periodic with period τ.

As already highlighted in Section 6.2, a key ingredient to have the heat–work mechanism in the linear response regime, is some protocol leading to $A \neq 0$. We recall that this quantity represents also the net pumped heat as a consequence of the time-dependent driving. In linear response, A depends on response functions that are evaluated with the two reservoirs at the same temperature T (see [80, 161] and Appendix D). When the two reservoirs are equally coupled, any protocol implemented via changing $\vec{B}$ generates the same energy flow between them and the qubit. This prevents a net energy transfer between the reservoirs and $A = 0$. Therefore, it is necessary to introduce some asymmetry in the coupling between the qubit and the reservoirs in order to have $A \neq 0$. For this reason, we consider the Hamiltonian describing the coupling to the reservoirs introduced in Eq. (6.3) with $\hat{\pi}_{\rm h} \equiv \hat{\sigma}_x$, $\hat{\pi}_{\rm c} = \hat{\sigma}_z$, which breaks the c $\leftrightarrow$ h symmetry in the absence of a temperature bias. Any other combination of Pauli matrices with $\hat{\sigma}_{\rm h} \neq \hat{\sigma}_{\rm c}$ would lead to similar results. As mentioned before, the other crucial ingredient is a protocol depending on at least two parameters, which is necessary to define a non-trivial surface Σ. In our case, we consider just two parameters: $B_z(t)$ and $B_x(t)$.

We solve the problem in the limit of weak coupling between the WS and the reservoirs by deriving the adiabatic master equation by means of the non-equilibrium Green's function formalism at second order of perturbation theory in V_α as explained in Section 3.4 [103]. Details are shown in Appendices D and D.1. In the specific calculations discussed below, we considered the simplest case, where the two reservoirs have the same spectral density, $\Gamma_{\rm c}(\epsilon) = \Gamma_{\rm h}(\epsilon) = \Gamma(\epsilon) = \bar{\Gamma}\epsilon e^{-\epsilon/\epsilon_C}$ for $\epsilon \geq 0$.

6.6.1 Adiabatic linear-response coefficients

The adiabatic linear response matrix $\underline{\Lambda}$ is originally expressed as a function of the coordinates (B_z, B_x). This matrix is positive defined and symmetric. When diagonalized it is found that the eigenvectors, $|r\rangle = (\sin(\phi), \cos(\phi))^T$, $|\phi\rangle = (\cos(\phi), -\sin(\phi))^T$ correspond to radial and tangential directions and thus $\underline{\Lambda}$ can be expressed as follows,

$$\underline{\Lambda} = \lambda_r |r\rangle\langle r| + \lambda_\phi |\phi\rangle\langle\phi|, \tag{6.33}$$

with $\lambda_r, \lambda_\phi \geq 0$. This suggests that it is natural to implement the following change of coordinates: $B_z = B_r \cos\phi$, $B_x = B_r \sin\phi$. We get

$$\dot{\vec{B}} \cdot \underline{\Lambda} \cdot \dot{\vec{B}} \equiv \lambda_r \dot{B}_r^2 + \lambda_\phi B_r^2 \dot{\phi}^2 \equiv \lambda_r |\dot{\vec{B}}_r|^2 + \lambda_\phi |\dot{\vec{B}}_\phi|^2. \tag{6.34}$$

The analytical expression for the radial component reads,

$$\lambda_r(\vec{B}) = \frac{\hbar\beta \sinh(\beta B_r)}{\Gamma(2B_r)\cosh^3(\beta B_r)} \tag{6.35}$$

and for the tangential one is

$$\lambda_\phi(\vec{B}) = \frac{\hbar\Gamma(2B_r)}{4B_r^3}, \tag{6.36}$$

being $\beta = 1/k_B T$. The first component is associated to changes in the energy gap between the two states of the qubit, while the second one leaves the spectrum unchanged but introduces a rotation of the eigenstate basis.

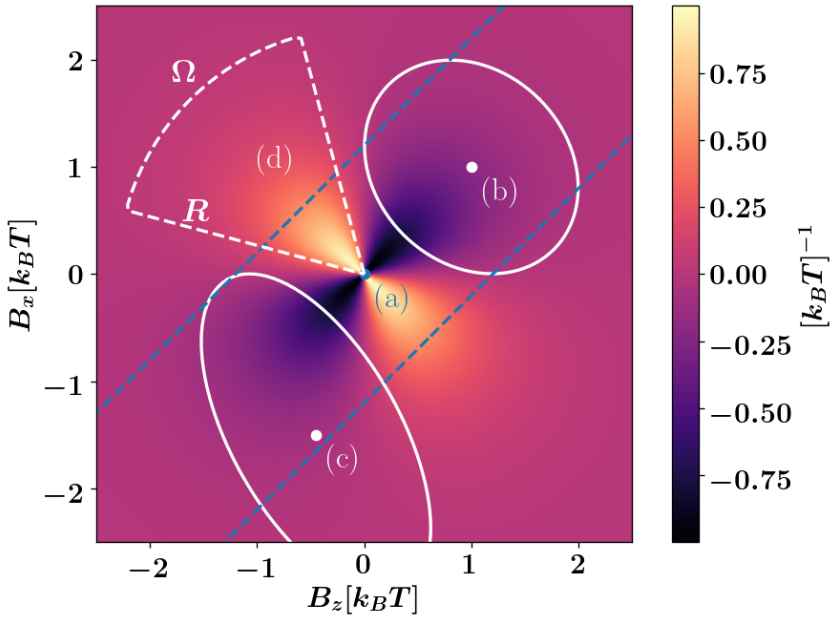

Figure 6.3: The Berry-type curvature $\left[\vec{\nabla}_B \wedge \vec{\Lambda}(B)\right]_y$. The integration of this quantity over the area enclosed by the control trajectory defines the A as in Eq. (6.14). Parameters are $\epsilon_C = 120 k_B T$ and $\bar{\Gamma} = 0.2$. Curves (a), (b) and (c) are heuristically searched protocols of elliptic shape, centered in $(0,0)$, $(1,1)$ and $(-1.5,-0.45)$ respectively, that maximize the value $A^2/\mathcal{L}^2$ (see Sec. 6.6.3). Curve (d) is a protocol with the shape of a circular sector centered at $(0,0)$, with radius R and spanning an angle Ω symmetrically with respect to the quadrant's bisector.

Regarding the other coefficients, the components of the vector $\vec{\Lambda}(\vec{B}) = (\Lambda_z, \Lambda_x) = \Lambda_r \langle r| + \Lambda_\phi \langle \phi|$ read

$$\Lambda_r(\vec{B}) = \frac{\beta B_r \sin^2(\phi)}{\cosh^2(\beta B_r)}, \quad \Lambda_\phi(\vec{B}) = 0\,, \tag{6.37}$$

while the parametric thermal conductance is

$$\kappa(\vec{B}) = \frac{\beta B_r^2 \sin^2(2\phi)\Gamma(2B_r)}{\sinh(2\beta B_r)\hbar}. \tag{6.38}$$

6.6.2 Geometrical quantities and bound for the heat–work conversion

Given the above coefficients we can now calculate all the relevant geometrical quantities for the characterization of the machine, namely, A, L and $\langle\kappa\rangle$ defined respectively in Eqs. (6.9), (6.10) and (6.11).

As already mentioned when the representation of Eq. (6.14) was introduced, the net pumped heat quantified by A is simply the value of the Berry curvature integrated over the area of the (B_z, B_x) plane enclosed by a particular protocol. The Berry curvature as a function of (B_z, B_x) is shown in Fig. 6.3. Because of the nature of the setup, this quantity changes sign at $B_x = 0$ and $B_z = 0$. Therefore, protocols with constant B_r lead to $A = 0$. For any protocol, the sign can be simply switched by changing the circulation of the boundary curve, hence switching the operation from heat engine to refrigerator or viceversa.

It is also easy to visualize in Fig. (6.3), that protocols enclosing a large portion of the dark blue or bright yellow areas lead to a large value of $|A|$. Focusing on simple curves that do not cross themselves we consider a circular-sector trajectory like the curve (d) depicted in Fig. (6.3), characterized by a radius R and an aperture angle Ω symmetric with respect to the

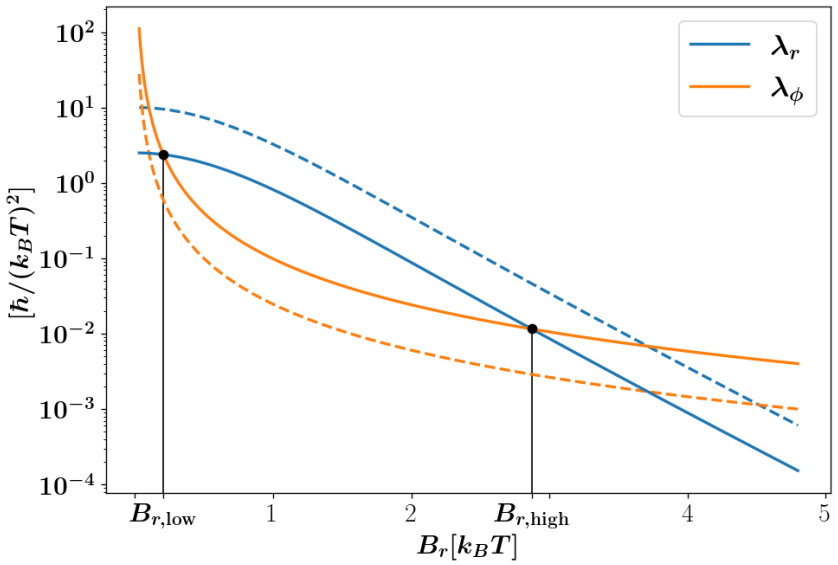

Figure 6.4: Positive eigenvalues of $\underline{\Lambda}$ -see Eq. (6.33)- as a function of $|\vec{B}| = B_r$. Parameters are $\epsilon_C = 120 k_B T$ and $\bar{\Gamma} = 0.2$ (solid lines), $\bar{\Gamma} = 0.05$ (dashed lines). Note for $\bar{\Gamma} = 0.2$ (solid lines) that most of the relevant region of Fig. 6.3 lies inside the interval $(B_{r,\text{low}}, B_{r,\text{high}})$ where the radial dissipation is about one order of magnitude bigger than the polar dissipation.

the quadrant's bisector. It is clear from the figure that the protocol leading to the maximum achievable value of $|A|$ in the present setup corresponds to a trajectory fully enclosing a quadrant. Such a trajectory is, for instance, the special case of the circular-sector trajectory with $\Omega = \pi/2$ that: i) starts at the origin and goes to infinity along the B_x axis, ii) rotates $\pi/2$ counterclockwise and aligns in the B_z axis, iii) returns to the origin along the B_z axis.

This limiting protocol corresponds to a quasistatic Carnot cycle and the resulting value of A is

$$A_{\text{lim}} = \int_{\text{quadrant}} (\vec{\nabla}_B \wedge \vec{\Lambda}) \cdot d\hat{y} = \pm k_B T \log(2), \tag{6.39}$$

where the signs are determined by the enclosed quadrant and the circulation considered. Notice that, according to Eq. (6.7), this corresponds to the extreme values for the energy that could be transported between the two reservoirs at the same temperature T through the qubit, and coincides with the famous bound obtained by Landauer's argument [241] according to which the change of Shannon entropy in the process of erasing the information encoded in a bit is $\pm \log(2)$. In the present case, it is associated to the transfer of the same amount of entropy between the reservoirs (a similar result was found quantum dots [25]). At finite ΔT, according to Eq. (6.6) this quantity also sets the maximum value of the work that can be extracted in the heat-engine operational mode (for $A_{\text{lim}} > 0$) in the limit of vanishing dissipation. This result is, respectively,

$$W_{\text{lim}} = k_B (T_{\text{h}} - T_{\text{c}}) \log(2) = A_{\text{lim}}\, \eta_C. \tag{6.40}$$

We now turn to analyze L^2, which assesses the dissipated energy for a particular protocol. This quantity is determined by $\underline{\Lambda}$ given by Eq. (6.10). For the qubit, this matrix can be decomposed in two contributions, as expressed in Eq. (6.33) which are associated to the dissipation of energy originated in the radial and polar changes of $\vec{B}$.

We see from the analytical expressions of Eqs. (6.35) and (6.36) that $\underline{\Lambda}$ is symmetric along the polar axis, i.e. it only depends on B_r. This is illustrated in the left panel of Fig. D.1 in Appendix D.1. In Fig. 6.4 we show the dependence of the coefficients λ_r and λ_ϕ on B_r for two different values of the $\bar{\Gamma}$ parameter. For some values of $\bar{\Gamma}$ we find an interval $(B_{r,\text{low}}, B_{r,\text{high}})$ for which the dissipation is mainly due to changes in the energy spectrum induced by finite

$\dot{B}_r$. The specific values $B_{r,\text{low}}$, $B_{r,\text{high}}$ depend on the working temperature and the coupling constant $\bar{\Gamma}$ between the qubit and the reservoirs. More details on the $\underline{\Lambda}$ submatrix and the dissipation structure of the qubit can be found in Appendix D.1.

The final value of L^2 for a protocol $\vec{B}(\theta\tau)$ defined over $\partial\Sigma$ in the parameter space still depends on the chosen parametrization θ. Out of all the possible parametrizations, Eq. (6.15) tells us that there exists a particular one for which $L^2 = \mathcal{L}^2$. Furthermore, this corresponds to the lower bound for L^2 and, importantly, it is a function of $\partial\Sigma$ only (it is geometrical).

In addition, for a given θ associated to $\partial\Sigma$, we are able to obtain the optimal parametrization $\bar{\theta}(\theta)$ that saturates the bound, and defines the less dissipative protocol $\vec{B}(\bar{\theta}\tau)$ around $\partial\Sigma$ in time τ. The new value of the velocity at a given time can be computed using (6.15), demanding that $\dot{\vec{B}}(\theta\tau)\cdot\underline{\Lambda}(\vec{B})\cdot\dot{\vec{B}}(\theta\tau)$ is constant at each point. The result is

$$\frac{\partial\vec{B}(\bar{\theta}\tau)}{\partial\bar{\theta}} = \dot{\vec{B}}(\theta\tau)\sqrt{\frac{\mathcal{L}^2}{\dot{\vec{B}}(\theta\tau)\cdot\underline{\Lambda}(\vec{B})\cdot\dot{\vec{B}}(\theta\tau)}} \tag{6.41}$$

where the dot in $\dot{\vec{B}}$ is the derivative with respect to the original parametrization θ. This driving ensures constant entropy production along the cycle.

6.6.3 Maximum power

Although a global maximum for $P_{\max}(\partial\Sigma)$ in Eq. (6.28) is hard to find, it is still possible to design simple trajectories with useful output power and reasonable efficiency. We perform a numerical search of $\max_{\partial\Sigma} A^2/\mathcal{L}^2$ using a gradient descent method, restricted to the space of elliptic trajectories centered at a given point $\vec{B}$. The trajectories (a), (b) and (c) shown in Fig. 6.3 are examples of the resulting curves. We choose this type of curves because elliptical trajectories are easy to implement experimentally, and flexible enough to perform an extensive optimal search. The advantage of the elliptical protocols is not obvious, taking into account that Fig. 6.3 suggests that the circular-sector protocols are better than the ellipses for maximising A. However, this is not the case for $A^2/\mathcal{L}^2$: we show in Section 6.6.5 that suitable chosen ellipses can clearly outperform circular-sector protocols in terms of power output.

Focusing on the elliptic protocols, we see that the highest values of power are achieved for test curves that avoid the region of small $|\vec{B}|$, where the dissipation coefficient λ_ϕ diverges. The curve (a) centered at $(0,0)$ is an interesting example. It maximizes A^2 by enclosing the two lobes in the first and third quadrant of Fig. 6.3, and closes the curve near infinity in order to avoid the central region of high dissipation.

In Fig. 6.5 we depict the value of $\max_{\partial\Sigma} A^2/\mathcal{L}^2$ found by the mentioned heuristic method, as a function of the (fixed) central point of the ellipse. We distinguish two different regimes leading to the optimal power, as a consequence of the crossover between the two mechanisms of dissipation discussed in the context of Fig. 6.4. For small B_r, where the less dissipative protocol is radial, the optimal trajectories are like the case (a) in Fig. 6.3, while in the opposite limit where B_r is large, the optimal protocols are like the ones indicated with (b) and (c) in that Fig.

6.6.4 Maximum efficiency

Following the same philosophy of the analysis of L^2 presented in Fig. 6.4, we plot in Fig. 6.6 the maximum eigenvalue of $\underline{\Lambda}_\kappa$ (defined in Eq. (6.30)) in order to visualize the value of the thermal losses when the system evolves in the direction of maximum dissipation. Note that since $\kappa(\vec{B})$ is a scalar, hence, an equivalent decomposition to Eq. (6.33) can be done for Λ_κ^2 as follows:

$$\underline{\Lambda_k} = \lambda_{kr}|r\rangle\langle r| + \lambda_{k\phi}|\phi\rangle\langle\phi|. \tag{6.42}$$

Furthermore the analysis presented for L^2 in Section 6.6.2, and particularly the results shown in Fig. 6.4 and Appendix D.1 still hold for the eigenvalues and eigenvectors of $\underline{\Lambda}_\kappa$.

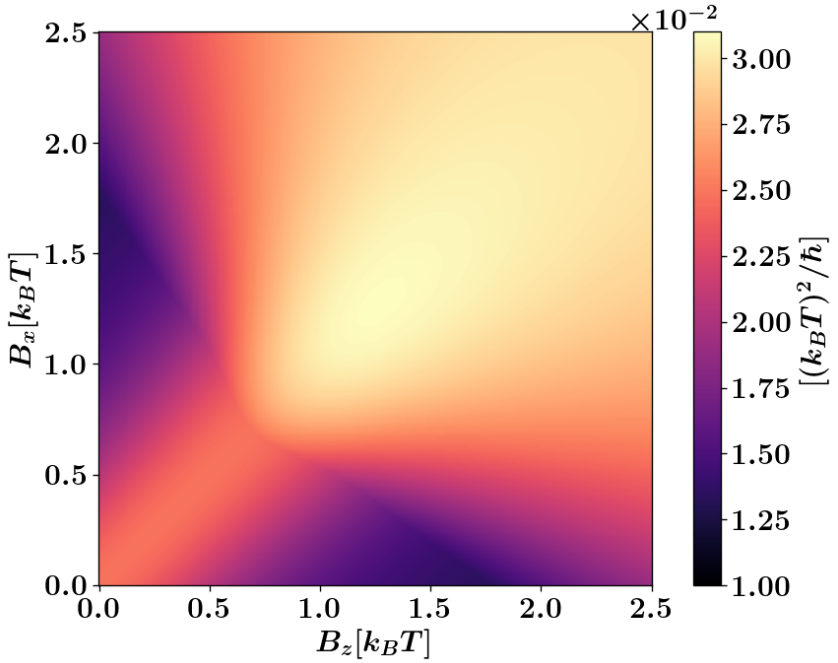

Figure 6.5: max $A^2/\mathcal{L}^2$ as a function of $\vec{B}$, for an heuristic optimization of elliptic trajectories centered at $\vec{B}$. Parameters are $\epsilon_C = 120 k_B T$ and $\bar{\Gamma} = 0.2$. Only positive values of B_x and B_z are shown, since this quantity is symmetric with respect to $B_x = 0$ and $B_z = 0$.

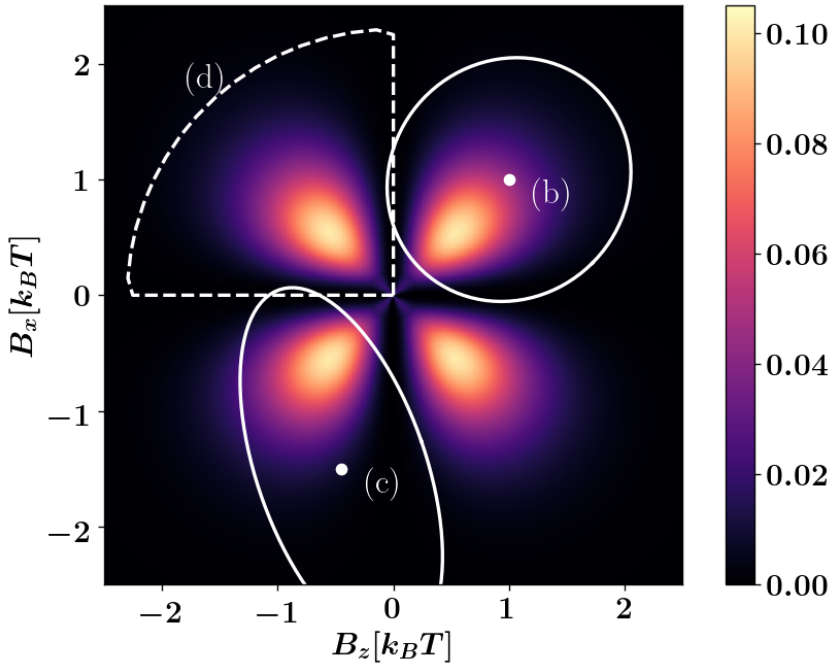

Figure 6.6: Maximum eigenvalue of $\underline{\Lambda}_\kappa$, indicating the losses due to the combined effect of dissipation and thermal conduction. Parameters are $\epsilon_C = 120 k_B T$ and $\bar{\Gamma} = 0.2$. Curves (b) and (c) are heuristically searched protocols of elliptic shape, centered at $(1, 1)$ and $(-1.5, -0.45)$ respectively, that maximize the value $A^2/\mathcal{L}^2_\kappa$. Curve (d) (circular sector) is a quarter of circumference centered at $(0, 0)$, joined by two radial lines of length R along the axis.

In the case of the efficiency, an optimal solution is trivially found by looking at Fig. 6.6 and considering again the circular-sector curve (d) with $\Omega = \pi/2$. From (6.38) we see that along the B_x and B_z axis we have $\kappa = 0$, because in those regions the system is coupled to only one of the reservoirs. It is clear from Eq. (6.30) that for the limiting circular-sector protocol with $R \to \infty$, enclosing the full quadrant and leading to Eq. (6.39) we have $\langle\kappa\rangle = 0$, which implies $x = \infty$ in Eq. (6.21), hence $\eta_{\max} = \eta_C$. In fact, as already mentioned, this protocol is an equilibrium Carnot cycle for the qubit, where the changes along the axis are the isothermal compression and expansion. More details of the efficiency of this protocol can be found in Section 6.6.5.

In addition to this particular solution of special interest, we illustrate the usefulness of the method in a more generic way. The strong equivalence between the geometrical quantities $A^2/\mathcal{L}^2$ and $A^2/\mathcal{L}_\kappa^2$ allows us to replicate the analysis done in the previous subsection in a straightforward manner. Once again, for a given a trajectory the value of A^2 is computed from Eq. (6.14) while the lower bound for $L^2\langle\kappa\rangle$ and the corresponding optimal parametrization is given by (6.30) in complete analogy with Eqs. (6.15) and (6.41) from the maximum power analysis.

We perform the numerical search of $\max_{\partial\Sigma}\{A^2/\mathcal{L}_\kappa^2\}(\vec{B})$ again for the special case of closed elliptic curves centered at a given point $\vec{B}$. The computed result is presented in Fig. 6.7. In Fig. 6.6 we also show some of these trajectories, centered at the points $\vec{B} = \{(1,1), (-1.5, -0.45)\}$. Note that, while some differences can be spotted between these trajectories and the ones shown in Fig. 6.3, the qualitative intuition is that efficient protocols are the ones with big A^2.

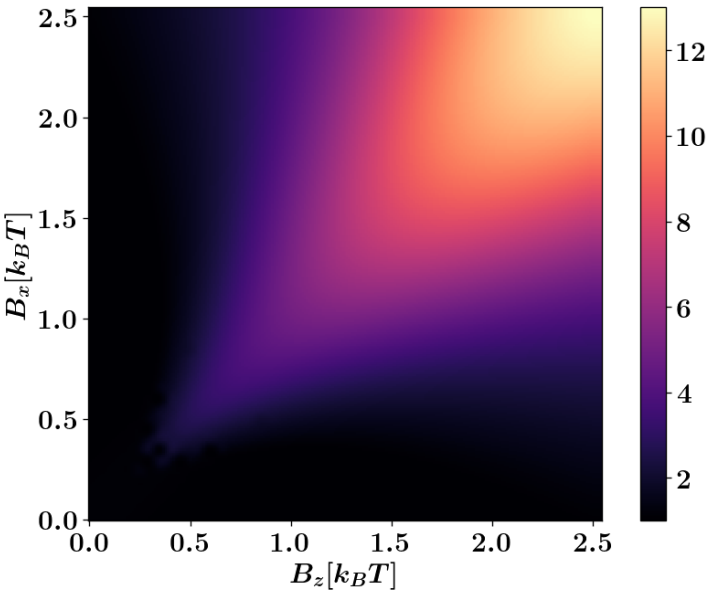

Figure 6.7: Maximum $A^2/\mathcal{L}_\kappa^2$ as a function of $\vec{B}$ for a heuristic optimization of elliptic trajectories centered at $\vec{B}$. Parameters are $\epsilon_C = 120k_BT$ and $\bar{\Gamma} = 0.2$.

6.6.5 More discussion on the circular sector

Here we present a more detailed study on the power and the efficiency of the circular sector defined in Section 6.6.2. In Fig. 6.8 we compute the geometrical value $A^2/\mathcal{L}^2$ as a function of the two parameters R and Ω that define the curves of this class.

We see from Fig. 6.8 that for big enough R the value of $A^2/\mathcal{L}^2$ depends only on Ω. This fact can be understood by looking at the left panel of Fig. D.1: for $B_r > B_{r,\text{high}}$ we have $\underline{\Lambda} \approx 0$, which implies that the dissipation outside the solid circle is negligible, and only the radial sections contained in the solid circle contributes significantly to L^2. Furthermore, since $\underline{\Lambda}$ has rotational symmetry, the value of L^2 is independent of the direction of the radial parts. These

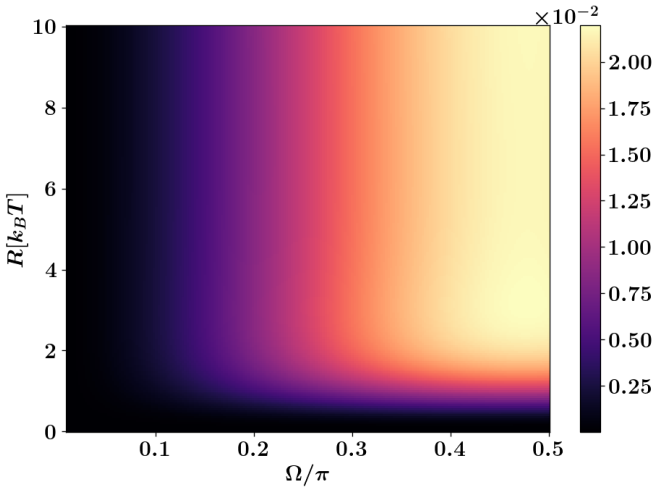

Figure 6.8: Geometrical values $A^2/\mathcal{L}^2$ for the circular-sector protocols. We found a saturation value equal to $0.022(k_BT)^2/\hbar$ which corresponds to the trajectory defined by $\Omega = \pi/2$ and $R \to \infty$.

two observations leads us to the conclusion that $\mathcal{L}^2$ has a saturation value in the circular sectors with $R >> B_{r,\text{high}}$. Finally, the dependence on Ω is explained by looking at Fig. 6.3, where it is clear that $A = A(\Omega)$ for $R >> B_{r,\text{high}}$ as well, and the maximum occurs at $\Omega = \pi/2$. The saturation value of $A^2/\mathcal{L}^2$ for the circular sector is found to be $\max_{\text{circ-sec}} \frac{A^2}{\mathcal{L}^2} = 0.022(k_BT)^2/\hbar$, which comparing to Fig. 6.5 is around 30% smaller than the ellipses case.

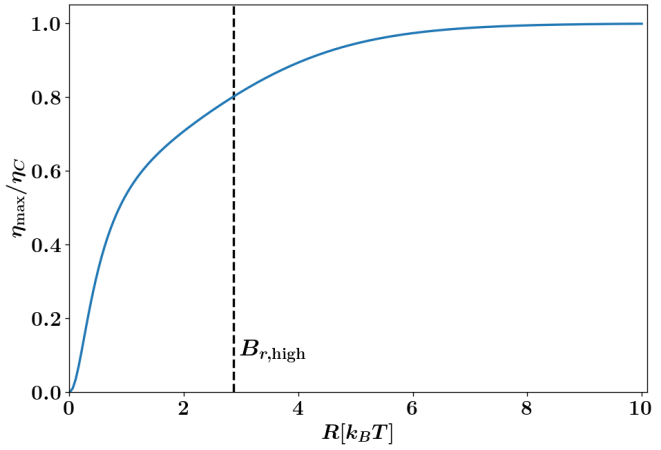

Figure 6.9: Computed efficiency for the circular sector with $\Omega = \pi/2$ as a function of the R parameter. At $R \to \infty$ we recover Carnot efficiency for the optimal parametrization.

In Fig. 6.9 we show the computed maximum efficiency η_{max} in Eq. (6.21) of the circular-sector protocol with $\Omega = \pi/2$ as a function of R.

Recall from discussion in Section 6.6.4 that the limiting case of the circular sectors with the mentioned Ω and $R \to \infty$ defines a Carnot cycle when optimized for maximum efficiency. This fact is clearly seen in Fig. 6.9 as the saturation value of η_{max}/η_C goes to 1 as $R >> B_{r,\text{high}}$.

6.6.6 The impact of optimizing the driving speed

The aim of this section is to gather further insight on the effect of selecting the optimal protocol, regarding the trajectory $\partial\Sigma$ and the optimal speed for the circulation on the resulting power and efficiency of a heat engine.

We consider an elliptical protocol for which we can define a "trivial" circulation with constant angular velocity. For the case of the power, we compare the results of such trivial circulation with the one corresponding to the optimal velocity as defined in Eq. (6.41). For the case of the efficiency we compare the trivial circulation with with the one corresponding to the optimal velocity, as defined in Eq. (6.41) with the replacements $\mathcal{L} \to \mathcal{L}_\kappa$ and $\underline{\Lambda} \to \underline{\Lambda}_\kappa$.

For sake of concreteness we focus on $\partial\Sigma$ given by the protocol (b) of Fig. 6.3. Results are shown in Fig. 6.10, where we show the power and efficiency of the machine as a function of the cycle total duration. Plots in solid and dashed lines correspond, respectively, to the protocols with constant angular velocity and optimal velocity. We note from this figure that the optimized parametrization is around two times bigger in power, and around four times more efficient, with respect to the trivial parametrization of the ellipse circulated at a constant angular velocity. Dashed lines in Fig. 6.10 are akin to those of Fig. 6.2 where power values are normalized to $P_{\max}$ and efficiencies to $\eta_{\max}$, and summarizes the performance of the machine.

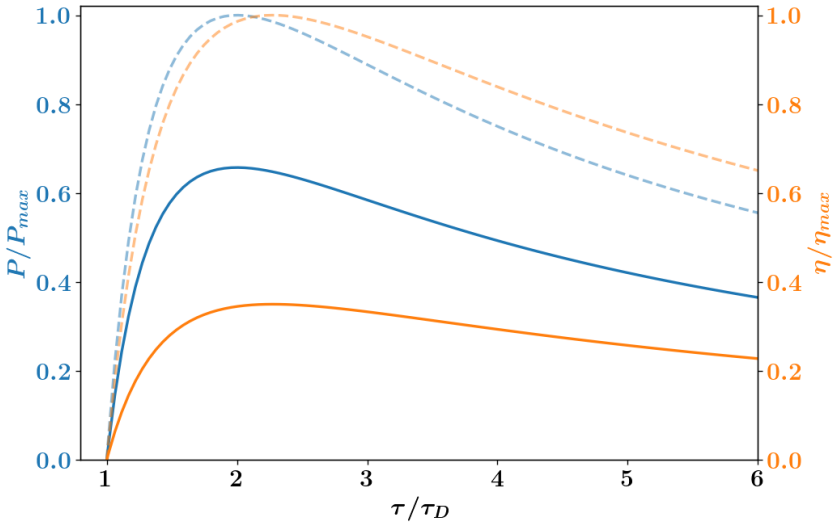

Figure 6.10: Power (blue) and efficiency (orange) for curve (b) of Fig. 6.6 as a function of the cycle duration τ. Solid lines: circulating around the curve at constant angular velocity. Dashed lines: Using the optimal velocities given by Eqs. (6.15) (for power) and (6.30) (for efficiency).

6.6.7 Estimates for the performance

To finalize the analysis of the qubit heat engine, it is interesting to analyze concrete values characterizing its performance. As before, we focus on the protocol (b) of Fig. 6.3, for which we have

$$A^2 = 0.233 k_B^2 T^2 \quad \mathcal{L}^2 = 7.71\hbar. \tag{6.43}$$

For these values, we find using Eq. (6.20):

$$P_{\max} = \left(1.364 \times 10^{-2} \frac{pW}{K^2}\right) (\Delta T)^2,$$

which for a working temperature of $T = 100mK$ and a temperature bias corresponding to $\Delta T = 0.05T$, as in previous Figures, gives $P_{\max} = 0.341aW$ with efficiency $\eta_{P_{max}} = 0.23\eta_C$. The total time τ_P for maximum power output per cycle is computed through Eq. (6.19):

$$\tau_P = 2\tau_D = 48.8ns$$

which corresponds to an operation frequency in the order of $0.1GHz$.

It is interesting to compare the value obtained for the maximum power in the protocol under consideration with the power associated to the limiting value for the work given by Eq. (6.39). Such limiting power can be obtained by replacing τ_P of Eq. (6.18) in Eq. (6.12), where we see that at finite time the net work done by the machine operating at maximum power is $W_{P_{\max}} = A\ \eta_C/2$. Taking into account that for the heat engine $A \leq \log(2) k_B T$ – see Eq. (6.39)– we conclude that the bound for the maximum operating power in a cycle of duration τ_P is $P_{\lim} = \log(2)\ k_B T\ \eta_C/(2\tau_P)$. For the case of the protocol (b), given the values of Eq. (6.43), we get $P_{\max} = 0.7 P_{\lim}$.

In a similar way using Eq. (6.21), the optimized parametrization that maximizes the efficiency of the cycle give us the value $\eta_{\max} = 0.34\eta_C$.

Specific values for the maximum efficiency of the machine operating under other protocols can be obtained by substituting in Eq. (6.22) the values shown in Fig.6.7. This calculation shows that this machine can achieve a performance as high as $\eta_{\max} > 0.55\eta_C$. These results are very encouraging regarding the possibility of the experimental implementation of this system.

Chapter 7

Summary and conclusions

In the present thesis we have investigated the adiabatic dynamics of a wide family of few-level quantum devices in contact to thermal reservoirs. We have applied some of the general results to particular examples, in an effort to give concrete use of the developed theory and aiming for the future experimental verification of the theoretical work.

In Chapter 4 we have investigated the adiabatic dynamics of a QD with many-body interactions connected to a single reservoir at $T = 0$ and under the effect of two-parameter driving with a gate voltage and a magnetic field. This induces time-dependent flow of charge, spin and energy through the contact between the QD and the reservoir. Under these conditions, the net dynamics is fully dissipative[247]. We have verified that energy is instantaneously dissipated in the form of a Joule law with a universal resistance R_0. This was previously discussed in the framework of non-interacting, [143, 144, 145], as well as interacting systems under single-parameter driving[149].

We also have derived fluctuation-dissipation relations within the framework of adiabatic linear response theory, which constitute generalizations of the so-called Korringa-Shiba law, previously derived for Fermi liquids[209, 69]. We showed that in the presence of many-body interactions, other interesting effects take place as a consequence of the two-parameter driving. These are the net work exchange between forces as well as the non-equilibrium polarized charge population with geometric nature, akin to quantum pumps[54, 52]. These features are amenable to be explored experimentally in quantum capacitors like those studied in Refs. [124, 125, 126, 127]. In fact, these systems are constructed in the quantum Hall regime, under the effect of a strong magnetic field. By introducing a time-dependent component in this magnetic field, along with the variation of the gate voltage would lead to a scenario like the one studied in the present work. At finite T, the effects we have studied could be relevant in the implementation of driving protocols for thermal machines, [185, 248, 66, 249, 228, 250, 251] as well as in the discussion of shortcuts to adiabaticity[252, 253, 254].

In Chapter 5 we have presented a general description of the geometrical properties of quantum thermal machines under the effect of adiabatic periodic driving and a small thermal bias due to the contact to reservoirs at different temperatures. The cyclic time-dependence is introduced via classical variables, varying slowly in time, that enter the quantum Hamiltonian of the system. We show that the operation of the thermal machine, consisting of a few-level quantum system, is fully characterized by the thermal tensor $\Lambda_{\mu,\nu}$ defined in Section 5.3.

The formal derivation of this tensor is obtained by means of the adiabatic linear response theory complemented by Luttinger's representation of the thermal bias. The symmetric component of $\Lambda_{\mu,\nu}$ characterizes the total rate of entropy production, thus controlling the dissipation of all the sources involved in the operation of the machine. When the system is driven by two or more periodically-varying parameters, it is possible to obtain pumping of heat between reservoirs, even in the absence of a temperature bias. The heat pumped, the work performed on the system, and the dissipated power can be described by means of vector fields defined through the

thermal tensor. In particular, the pumped heat by the driving and the work performed can be expressed in a purely geometric form as line integrals of those vector fields over the closed paths which represent the driving cycles in the parameter space. In the presence of a thermal bias, these two quantities allow the characterization of a thermal machine which realizes heat-work conversion.

We have illustrated these ideas using a paradigmatic quantum system coupled to two thermal reservoirs: a quantum dot coupled to electronic reservoirs and driven by an harmonically time-dependent and rotating magnetic field. We solve the problem exactly for arbitrary coupling by recourse to linear response and Green's function formalisms. We have calculated the vector fields responsible for the geometric characterization of the systems as thermal machines. We have computed the heat pumped and the work as functions of the phase lag between the two driving parameters. The efficiency of the thermal machines has been analyzed in terms of the temperature difference between reservoirs, the average temperature, and the frequency of the driving parameters.

Finally, in Chapter 6 we have applied the geometrical approach of Chapter 5 to describe the two competing mechanisms of a non-equilibrium adiabatic thermal machine: the dissipation of energy and the heat–work conversion. While the first mechanism is described in terms of a length, the second one can be represented by and area in the parameter space. We then showed that the problem of finding optimal protocols reduces to an isoperimetric problem, which consists in finding the optimal ratio between area and length in a space with non-trivial metrics.

We applied this description to a thermal machine which consists of a single qubit asymmetrically coupled to two bosonic reservoirs at small different temperatures and driven by a cyclic protocol controlled by two parameters that vary slowly in time. We solved this problem in the limit of weak coupling between the qubit and the reservoirs. We analytically show the limiting value of the pumped heat between reservoirs is given by Landauer bound in an ideal Carnot cycle. We analyzed in this problem the type of cycles leading to optimal performance of the machine. Interestingly, the qubit machine has a very good ratio between performance and power within a wide set of parameters.

Possible directions for further exploration

In terms of the physical systems explored in the thesis, a natural extension for the quantum dot studied in Chapter 4 is to include a second reservoir to find the geometric properties of the particle transport. At $T = 0$ the Korringa-Shiba relations derived in this work can be applied directly to simplify the heavy computations of the response functions in the interacting case. Interpreted as a thermal machine, the energy transport properties of the interacting quantum dot can also be studied using the framework developed in Chapters 5 and 6.

According to our analysis in Section 6.6.7 for the qubit machine, efficiencies larger than 0.55 of the Carnot cycle can be achieved and values of the corresponding output power of 0.7 of the limiting power, corresponding to the work done in an ideal Carnot cycle divided by the duration of the cycle at which the maximum power is achieved. These estimates are very encouraging for the experimental implementation of this machine. In this sense, a very promising platform is a superconducting qubit coupled to resonators, in which there are several configurations under study for some years now [255, 256, 257, 258, 259, 260]. Other possible platforms are those in which the Otto cycle has been already implemented, like AMO systems [46, 179, 45], as well as spin systems in NMR setups [33]. Quantum dots, where electron pumping has been observed [35, 104] are also candidates for implementing the heat engine and refrigerator operations as well as nanomechanical systems [44, 261]. This geometrical optimization can be also very naturally extended to analyze other systems like motors operating under slow driving and a bias voltage [225, 226, 228, 64].

In the present work we have focused on the linear-response regime, where the geometric

description becomes explicit. The weak-coupling calculations of the heat and work presented in Section 6.6 and Appendix D can be extended to analyze the operation beyond this regime for specific thermal machines in future works. Finally, the analysis performed for the qubit machine can easily be extended to include more complex architectures (such as two or more interacting qubits) allowing the design of optimal heat engines and refrigerators with concrete experimental realizations such as those of Ref. [260, 114].

Appendix A

Identities satisfied by the adiabatic susceptibilities

In order to prove the identities used to write Eq. (5.14), satisfied by the adiabatic susceptibilities for the thermal driving corresponding to the *frozen* Hamiltonian $\mathcal{H}_t$, we proceed by writing the following equation satisfied by the current operators,

$$\mathcal{J}_L^E(t) + \mathcal{J}_R^E(t) = \dot{\mathcal{H}}_S(t), \tag{A.1}$$

where $\dot{\mathcal{H}}_S$ encloses all the terms of $\mathcal{H}_t$ corresponding to the central system and contacts between system and reservoirs. All the operators are expressed in Heisenberg representation with respect to $\mathcal{H}_t$

$$\sum_{\alpha,\beta=L,R} \Lambda_t^{\mathcal{J}_\alpha^E,\mathcal{J}_\beta^E} = \Lambda_t^{\dot{\mathcal{H}}_S,\dot{\mathcal{H}}_S} = 0. \tag{A.2}$$

In order to prove that the right-hand side (rhs) of this equation is zero we start from the definition of the adiabatic susceptibility as expressed in the form of Eq. (3.9),

$$\Lambda_t^{\dot{\mathcal{H}}_S,\dot{\mathcal{H}}_S} = -i \lim_{\omega\to 0} \partial_\omega \chi_t^{\dot{S},\dot{S}}(\omega) = \lim_{\omega\to 0} \frac{\mathrm{Im}[\chi_t^{\dot{S},\dot{S}}(\omega)]}{\omega}, \tag{A.3}$$

being $\chi_t^{\dot{S},\dot{S}}(\omega)$ the Fourier transform of the susceptibility defined in Eq. (3.10), $\chi_t^{\dot{S},\dot{S}}(t-t') = -i/\hbar\theta(t-t')\langle\left[\dot{\mathcal{H}}_S(t),\dot{\mathcal{H}}_S(t')\right]\rangle_t$. Since all the mean values correspond to the equilibrium frozen Hamiltonian $\mathcal{H}_t$, we have $\chi_t^{\dot{S},\dot{S}}(t-t') = \partial_t\partial_{t'}\chi_t^{S,S}(t-t')$, being $\chi_t^{S,S}(t-t') = -(i/\hbar)\theta(t-t')\langle[\mathcal{H}_S(t),\mathcal{H}_S(t')]\rangle_t$. Hence,

$$\chi_t^{\dot{S},\dot{S}}(\omega) = -\omega^2\chi_t^{S,S}(\omega). \tag{A.4}$$

For a system with a bounded spectrum, $\Lambda_t^{\dot{\mathcal{H}}_S,\dot{\mathcal{H}}_S} = 0$ when the limit $\omega \to 0$ is evaluated in Eq. (A.3). In fact, introducing the Lehmann representation in $\chi_t^{S,S}(\omega)$ and using (A.4) and (A.3) we get

$$\begin{aligned}\Lambda_t^{\dot{\mathcal{H}}_S,\dot{\mathcal{H}}_S} = \pi \lim_{\omega\to 0} \omega^2 \sum_{n,m} p_m |\langle m|H_S|n\rangle|^2 \\ \times \left[\delta(\omega - (\varepsilon_m - \varepsilon_n)) - \delta(\omega - (\varepsilon_n - \varepsilon_m))\right]\end{aligned} \tag{A.5}$$

with $\mathcal{H}_t|m\rangle = \varepsilon_m|m\rangle$. In the latter equation $|\langle m|H_S|n\rangle|^2$ is finite for a system with a bounded spectrum, while $\sum_{n,m}\left[\delta(\omega - (\varepsilon_m - \varepsilon_n)) - \delta(\omega - (\varepsilon_n - \varepsilon_m))\right]$ is the density of states for the excitations of the full system. Typically, the latter function is gapped or has a power-law behavior $\sim |\omega|^\gamma$ with $\gamma > 0$, which proves the rhs of Eq. (A.2).

Using Eq. (A.2), we get the identities of Eq. (A.7). A similar argument can be elaborated for the identities related to the response functions combining energy currents and ac-driving forces. In that case, we can prove

$$\begin{aligned}\sum_{\alpha=L,R}\Lambda_t^{\mathcal{J}_\alpha^E,\mathcal{F}_l}&=\Lambda_t^{\dot{\mathcal{H}}_S,\mathcal{F}_l}=0,\\ \sum_{\alpha=L,R}\Lambda_t^{\mathcal{F}_l,\mathcal{J}_\alpha^E}&=\Lambda_t^{\mathcal{F}_l,\dot{\mathcal{H}}_S}=0,\end{aligned}\tag{A.6}$$

following similar reasoning as with Eq. (A.2).

Summarizing, the adiabatic response functions in which the energy current enters are

$$\begin{aligned}\Lambda_t^{\mathcal{J}_\alpha^E,\mathcal{J}_\alpha^E}&=\Lambda_t^{\mathcal{J}_{\bar\alpha}^E,\mathcal{J}_{\bar\alpha}^E}\\ \Lambda_t^{\mathcal{J}_\alpha^E,\mathcal{J}_\alpha^E}&=-\Lambda_t^{\mathcal{J}_\alpha^E,\mathcal{J}_{\bar\alpha}^E},\qquad(\text{A.7})\\ \Lambda_t^{\mathcal{F}_l,\mathcal{J}_\alpha^E}&=-\Lambda_t^{\mathcal{F}_l,\mathcal{J}_{\bar\alpha}^E},\\ \Lambda_t^{\mathcal{J}_\alpha^E,\mathcal{F}_l}&=-\Lambda_t^{\mathcal{J}_{\bar\alpha}^E,\mathcal{F}_l},\qquad(\text{A.8})\end{aligned}$$

up to some function that vanishes when averaging over one period. In the above equations $\bar\alpha$ denotes the reservoir opposite to α.

Appendix B

Entropy production rate

In what follows, we present a microscopic derivation of the expression for the entropy production rate associated to the combined effect of the time-dependent and thermal driving in the adiabatic regime.

ac driving

We start by analyzing the effect of the time-dependent driving. To this end, we can proceed along the lines of Refs. [84, 144] and start from the definition of von Neumann entropy

$$S(t) = -k_B \mathrm{Tr}\left[\rho(t) \ln \rho(t)\right]. \tag{B.1}$$

We also introduce the following auxiliary function,

$$S[\mathcal{H}_t] = k_B \mathrm{Tr}\left[\rho(t)\left(\beta \mathcal{H}_t + \ln Z_t\right)\right], \tag{B.2}$$

with $Z_t = \mathrm{Tr}\left[e^{-\beta \mathcal{H}_t}\right]$. Under a small change in the parameter space, $\mathbf{X}(t) \to \mathbf{X}(t+\delta t)$, the Hamiltonian evolves to

$$\mathcal{H}_{t+\delta t} = \mathcal{H}_t + \frac{\partial \mathcal{H}(t)}{\partial \mathbf{X}} \cdot \dot{\mathbf{X}}(t)\delta t = \mathcal{H}_t - \boldsymbol{\mathcal{F}} \cdot \dot{\mathbf{X}}(t)\delta t. \tag{B.3}$$

Consequently,

$$S[\mathcal{H}_{t+\delta t}] = k_B \mathrm{Tr}\left[\rho(t+\delta t)\left(\beta \mathcal{H}_{t+\delta t} + \ln Z_{t+\delta t}\right)\right]. \tag{B.4}$$

The change in the latter function is $\delta S[\mathcal{H}] = S[\mathcal{H}_{t+\delta t}] - S[\mathcal{H}_t]$, which keeping terms up to first order in δt explicitly reads

$$\begin{aligned} \delta S[\mathcal{H}] = {} & k_B \beta \left\{\mathrm{Tr}\left[\rho(t+\delta t)\mathcal{H}_t\right] - \mathrm{Tr}\left[\rho(t)\mathcal{H}_t\right]\right\} + \\ & k_B \ln Z_{t+\delta t} - k_B \ln Z_t - k_B \beta \mathrm{Tr}\left[\rho(t)\boldsymbol{\mathcal{F}}\right] \cdot \dot{\mathbf{X}}(t)\delta t. \end{aligned} \tag{B.5}$$

In the last Eq. we have used $\mathrm{Tr}\left[\rho(t+\delta t)\right] = \mathrm{Tr}\left[\rho(t)\right] = 1$. We can identify the first term with a change in the internal energy,

$$U = \mathrm{Tr}\left[\rho(t)\mathcal{H}_t\right], \tag{B.6}$$

i. e. $\delta U = \mathrm{Tr}\left[\rho(t+\delta t)\mathcal{H}_t\right] - \mathrm{Tr}\left[\rho(t)\mathcal{H}_t\right]$, as well as the change in the internal free energy,

$$F = -k_B T \ln Z_t. \tag{B.7}$$

The other terms are related to the work developed in the change of the time-dependent parameters [262],

$$\delta W = -\mathrm{Tr}\left[\rho(t)\boldsymbol{\mathcal{F}}\right] \cdot \dot{\mathbf{X}}(t)\delta t. \tag{B.8}$$

Therefore, Eq. (B.6) can be expressed as follows

$$T\delta S[\mathcal{H}] = \delta U - \delta F + \delta W. \tag{B.9}$$

Following Ref. [84, 263, 264, 265], we define the non-equilibrium entropy production as the following difference

$$\delta S^{\text{neq}} = \delta S - \delta S[\mathcal{H}], \tag{B.10}$$

and we evaluate it for a protocol $\delta\mathcal{C}$ in the parameter space starting in $\mathbf{X}(t_0)$ and ending in $\mathbf{X}(\tau)$, which consists in a sequence of the previous small changes. Using Eq. (B.1) and (B.6), and introducing the definition of the relative entropy $S\left[\rho(t)||\rho_t\right] = S(t) + k_B \text{Tr}\left[\rho(t)\ln\rho_t\right]$, the non-equilibrium entropy change can be written as in Ref. [84]

$$\begin{aligned} \delta S^{\text{neq}} &= S\left[\rho(\tau)||\rho_\tau\right] - S\left[\rho(t_0)||\rho_{t_0}\right] \\ &\quad + k_B\beta \int_{\delta\mathcal{C}} \text{d}t \text{Tr}\left[\rho(t)\boldsymbol{\mathcal{F}}\right] \cdot \dot{\mathbf{X}}(t). \end{aligned} \tag{B.11}$$

Appendix C

Driven quantum dot - calculation of the thermal geometric tensor

We need to calculate the following coefficients

$$\begin{aligned}\Lambda_{\mu,\nu}(t) &= \frac{1}{\hbar}\int_{-\infty}^{-\infty} dt'(t-t')\chi_{\mu,\nu}(t-t') \\ &= -\lim_{\omega\to 0}\frac{\mathrm{Im}\left[\chi_{\mu,\nu}(\omega)\right]}{\hbar\omega}, \quad \mu,\nu=1,2,3 \end{aligned} \tag{C.1}$$

with

$$\chi_{\mu,\nu}(t-t') = -i\theta(t-t')\langle\left[\mathcal{F}_\mu(t),\mathcal{F}_\nu(t')\right]\rangle, \tag{C.2}$$

being $\mathcal{F}_{1,2} = \Psi_d^\dagger\ \hat{\sigma}_{x,z}\Psi_d$, and $\mathcal{F}_3 = \mathcal{J}_{Q,R} = -i\sum_{k_R,s,\sigma}\varepsilon_{k_R,s}v_{k_R,s,\sigma}c_{k_R,s}^\dagger d_\sigma + H.c.$. We can calculate (C.1) following standard procedures based on the formalism of imaginary-time Green's functions. We can define $\hat{\mathcal{G}}(\tau) = -\langle T_\tau\left[\Psi_d(\tau)\Psi_d^\dagger(0)\right]\rangle$ and $\hat{\mathcal{G}}_{k_R,d}(\tau) = -\langle T_\tau\left[\Psi_{k_R}(\tau)\Psi_d^\dagger(0)\right]\rangle$, where T_τ denotes ordering along the imaginary axis. In terms of this, it is possible to write

$$\begin{aligned}\chi_{\ell,\ell'}(iq_n) &= \frac{1}{\beta}\sum_{ik_n}\mathrm{Tr}\left[\hat{\sigma}_\ell\hat{\mathcal{G}}(ik_n+iq_n)\hat{\sigma}_{\ell'}\hat{\mathcal{G}}(ik_n)\right], \\ \chi_{3,\ell}(iq_n) &= \frac{1}{\beta}\sum_{ik_n}\sum_{k_R}\mathrm{Tr}\Big\{\hat{\varepsilon}_{k_R}\hat{v}_R\Big[i\hat{\mathcal{G}}(ik_n+iq_n)\hat{\sigma}_\ell \\ &\quad \times\hat{\mathcal{G}}_{d,k_R}(ik_n) - i\hat{\mathcal{G}}_{k_R,d}(ik_n)\hat{\sigma}_\ell\hat{\mathcal{G}}(ik_n-iq_n)\Big]\Big\} \\ &= -\chi_{\ell,3}(iq_n), \qquad \ell,\ell'=1,2, \\ \chi_{3,3}(iq_n) &= -\frac{1}{\beta}\sum_{ik_n}\sum_{k_R,k_L'} \\ &\quad \mathrm{Tr}\Big\{\hat{\varepsilon}_{k_R}\hat{v}_R\hat{\mathcal{G}}_{k_R,d}(ik_n+iq_n)\hat{\varepsilon}_{k_R'}\hat{v}_L\hat{\mathcal{G}}_{k_L',d}(ik_n) \\ &\quad +\hat{\mathcal{G}}_{d,k_R}(ik_n+iq_n)\hat{\varepsilon}_{k_R}\hat{v}_R\hat{\mathcal{G}}_{d,k_L'}(ik_n)\hat{\varepsilon}_{k_L'}\hat{v}_L\Big\}\end{aligned} \tag{C.3}$$

with $\varepsilon_{k_\alpha,s,s'} = \varepsilon_{k_\alpha,s}\delta_{s,s'}$, $\alpha = L,R$, $q_n = 2\pi n/\beta$ and $k_n = (2n+1)\pi/\beta$.

It is convenient to introduce the spectral representation

$$\begin{aligned}\hat{\mathcal{G}}(ik_n) &= \int\frac{d\varepsilon}{2\pi}\frac{\hat{\rho}_t(\varepsilon)}{ik_n-\varepsilon}, \\ \hat{\mathcal{G}}_{k_\alpha,d}(ik_n) &= \int\frac{d\varepsilon}{2\pi}\frac{\hat{\rho}_{k_\alpha,d}(\varepsilon)}{ik_n-\varepsilon}\end{aligned} \tag{C.4}$$

with

$$\hat{\rho}_t(\varepsilon) = -2\mathrm{Im}\left[\hat{G}_t(\varepsilon)\right] = \hat{G}_t(\varepsilon)\hat{\Gamma}\left[\hat{G}_t(\varepsilon)\right]^\dagger, \tag{C.5}$$

$$\hat{\rho}_{k_\alpha,d}(\varepsilon) = \hat{\rho}^0_{k_\alpha}(\varepsilon)\hat{v}_\alpha\hat{\rho}_t(\varepsilon) + \hat{\rho}^0_{k_\alpha}(\varepsilon)\hat{v}_\alpha\hat{\rho}_t(\varepsilon), \tag{C.6}$$

where $\rho^0_{k_\alpha,s,s'}(\varepsilon) = 2\pi\delta_{s,s'}\delta(\varepsilon - \varepsilon_{k_\alpha,s})$ and $G^0_{k_\alpha,s,s'}(\varepsilon) = \delta_{s,s'}\left(\varepsilon + i\eta - \varepsilon_{k_\alpha,s}\right)^{-1}$. The retarded frozen Green's function of the quantum dot in contact to the reservoirs is given in Eq. (5.52), while $\hat{\Gamma} = -2\mathrm{Im}\left[\hat{G}_t(\varepsilon)^{-1}\right] = \sum_\alpha \hat{\Gamma}_\alpha$ is the hybridization matrix accounting for the contact between the quantum dot and the reservoirs, being $\hat{\Gamma}_\alpha = \sum_{k_\alpha} \hat{v}_{k_\alpha}\hat{\rho}^0_{k_\alpha}\hat{v}_{k_\alpha}$.

Using Eq. (C.4) into Eq. (C.3), after some algebra and performing the analytic continuation to the real axis we get

$$\begin{aligned}
\Lambda_{\ell,\ell'}(t) &= -\frac{1}{h}\int d\varepsilon \frac{df(\varepsilon)}{d\varepsilon}\mathrm{Tr}\left[\hat{\sigma}_\ell\hat{\rho}_t(\varepsilon)\hat{\sigma}_{\ell'}\hat{\rho}_t(\varepsilon)\right],\ \ell,\ell' = 1,2 \\
\Lambda_{3,\ell}(t) &= -\frac{1}{h}\int d\varepsilon\ \varepsilon\frac{df(\varepsilon)}{d\varepsilon}\mathrm{Tr}\left[\hat{\Gamma}_R\hat{\rho}_t(\varepsilon)\hat{\sigma}_\ell\hat{\rho}_t(\varepsilon)\right], \\
&= -\Lambda_{\ell,3}(t) \qquad \ell = 1,2, \\
\Lambda_{3,3}(t) &= -\frac{1}{h}\int d\varepsilon\ \varepsilon^2\frac{df(\varepsilon)}{d\varepsilon}\mathrm{Tr}\left[\hat{\Gamma}_R\hat{G}_t(\varepsilon)\hat{\Gamma}_L\hat{G}^\dagger_t(\varepsilon)\right],
\end{aligned} \tag{C.7}$$

Appendix D

Calculation of the adiabatic coefficients for the Master equation approach

In what follows we calculate all the linear response coefficients entering Eqs. (6.6) and (6.7) in the weak-coupling limit between the qubit and the reservoir, following Ref. [103]. We rely on the adiabatic quantum-master equation approach under small temperature bias ΔT to evaluate the coefficients $\Lambda_{\mu,\nu}$, which enable the calculation of the net transferred heat and work defined in Eqs. (6.6) and (6.7).

We can now use the described approach in 3.4 to obtain explicit expressions for the linear-response coefficients entering in the thermal geometric tensor $\Lambda_{\mu,\nu}$. To this end we calculate the power developed by the ac-driving sources as follows,

$$P_{ac}(t) = \mathrm{Tr}\left[\dot{\mathcal{H}}_{\mathrm{qb}}(t)\rho(t)\right], \tag{D.1}$$

being

$$\dot{\mathcal{H}}_{\mathrm{qb}}(t) = \sum_{\ell} \frac{\partial \mathcal{H}_{\mathrm{qb}}(t)}{\partial B_\ell}\dot{B}_\ell(t). \tag{D.2}$$

We now write

$$W = -\int_0^\tau dt P_{ac}(t), \tag{D.3}$$

and replace Eq. (3.102) into Eq. (D.1), to finally use the solutions for $\mathbf{p}^f$ and $\mathbf{p}^a$ obtained in the previous subsection. The resulting expression can be directly compared to the formal relation in Eq. (6.6) for W, where the matrix elements of the thermal geometric tensor are multiplied by different powers of $\dot{B}_k$.

In order to discriminate the contribution of the developed power $\propto \Delta T$, and recalling that we are considering small temperature differences, we introduce the following extra expansion in frozen component: $\rho^f = \rho^f_T + \delta_T\rho^f\Delta T$. Therefore,

$$\Lambda_{\ell,3}(\vec{B}) = -\mathrm{Tr}\left[\frac{\partial \mathcal{H}_{\mathrm{qb}}}{\partial B_\ell}\delta_T\rho^f,\right]. \tag{D.4}$$

while

$$\Lambda_{\ell,n}(\vec{B}) = [\underline{\Lambda}]_{\ell,n}(\vec{B}) = \mathrm{Tr}\left[\frac{\partial \mathcal{H}_{\mathrm{qb}}}{\partial B_\ell}\left(\tilde{\mathbf{M}}_T^{-1}(\vec{B})\frac{\partial \mathbf{p^f}_T}{\partial B_n}\right)\right], \tag{D.5}$$

where we highlight with the sub-index T that the quantities are calculated with the reservoirs at the same temperature T and the quantity between parentheses is to be understood as a $2x2$ matrix. Notice that the contribution of Eq. (D.1) evaluated with ρ^f_T corresponds to an

equilibrium quantity. It represents the power developed by the conservative ac forces, and it, thus, leads to a vanishing value when averaged over the cycle.

In the same formalism used to derive the reduced density matrix, the heat current entering the reservoir α, calculated at the second order of perturbation theory in the coupling to the reservoirs and within the adiabatic regime, reads [55, 103],

$$J_\alpha(t) = \sum_{m,n,u} \epsilon_{un}(t) \mathrm{Re}\left[M^{nu}_{mn,\alpha}(t)\rho_{un}(t)\right]. \tag{D.6}$$

We can follow the same logic as before to calculate this current at the first order in ΔT and $\dot{\vec{B}}$. The first one is "thermal" component associated to the the frozen components evaluated with a thermal bias ΔT, while the second one is the heat current "pumped" by the ac driving without temperature bias.

The linear-response net transported heat between the two reservoirs is

$$Q = \int_0^\tau dt J_\mathrm{c}(t) = -\int_0^\tau dt J_\mathrm{h}(t). \tag{D.7}$$

We follow the convention of Ref. [161] and consistently with the definition (6.7), we focus on the current entering the cold reservoir to define the net transported heat. Associating each term of Eq. (6.7) with those arising from Eq. (D.6) upon substituting ρ by its expansion in ΔT and $\dot{\vec{B}}$, we identify the linear coefficients,

$$\Lambda_{3,\ell}(\vec{B}) = \vec{\Lambda}_\ell(\vec{B}) = \sum_{m,n,u} \epsilon_{un} \mathrm{Re}\left[M^{nu}_{mn,\mathrm{c},T}\left(\tilde{\mathbf{M}}_T^{-1}\frac{\partial \mathbf{p}^\mathbf{f}}{\partial B_\ell}\right)_{un}\right] \tag{D.8}$$

and

$$\Lambda_{3,3}(\vec{B}) = \frac{\kappa(\vec{B})}{T} = \sum_{m,n,u} \epsilon_{um} \mathrm{Re}\left[M^{nu}_{mn,\mathrm{c},T}\delta_T\rho^f\right]_{un} \tag{D.9}$$

These coefficients satisfy the following Onsager equations [80, 161],

$$\Lambda_{3,\ell} = -\Lambda_{\ell,3}, \quad \Lambda_{1,2} = \Lambda_{2,1}. \tag{D.10}$$

D.1 Explicit expressions for $\underline{\Lambda}(\vec{B})$, $\vec{\Lambda}(\vec{B})$ and $\kappa(\vec{B})$ in the case of equal baths coupling

Assuming equal spectral density in the L and R baths, i.e.

$$\begin{aligned} \Gamma_L(\epsilon) &= \bar{\Gamma}_L \epsilon e^{-\epsilon/\epsilon_C} = \Gamma(\epsilon) \\ \Gamma_R(\epsilon) &= \bar{\Gamma}_R \epsilon e^{-\epsilon/\epsilon_C} = \Gamma(\epsilon) \end{aligned} \tag{D.11}$$

with $\bar{\Gamma}_L = \bar{\Gamma}_R$ constants, we get explicit expressions for the complete geometric tensor. Using $(B_x, B_z) = B_r(\sin\phi, \cos\phi)$ and $\beta = 1/(k_B T)$ we arrive to the following results.

D.1.1 Explicit expression for $\underline{\Lambda}$

The Hamiltonian for the qubit can be expressed, after an appropriate unitary transformation U, in the instantaneous diagonal basis $|j\rangle, j = 1, 2$ as follows:

$$\mathcal{H}_\mathrm{qb}(t) = E_1(t)|1\rangle\langle 1| + E_2(t)|2\rangle\langle 2|, \tag{D.12}$$

where $E_{1,2}(t) = \mp B_r(t)$ are the eigenvalues of the Hamiltonian of Eq. (6.32).

Using Eq. (D.12) and the expression for the reduced density matrix in the same basis, we can write for the terms with partial derivatives in Eq. (D.5):

$$\frac{\partial \mathcal{H}_{\rm qb}}{\partial B_\ell} = \sum_j \partial_\ell E_j(\vec{B})|j\rangle\langle j| + E_j(\vec{B})(|\partial_\ell j\rangle\langle j| + |j\rangle\langle \partial_\ell j|) \tag{D.13}$$

$$\frac{\partial \mathbf{p}^{\mathbf{f}}{}_T}{\partial B_n} = \sum_{ij} \partial_\ell p^f_{T,ij}(\vec{B})|i\rangle\langle j| + p^f_{T,ij}(\vec{B})(|\partial_\ell i\rangle\langle j| + |i\rangle\langle \partial_\ell j|) \tag{D.14}$$

with the notation $\frac{\partial}{\partial B_\ell} = \partial_\ell$. We note that the term $E_j(\vec{B})$ depends only on the absolute value of the magnetic field B_r. In addition, the density matrix $\mathbf{p}^f_T(\vec{B})$ is a function of the energy spectrum, since it is computed in thermal equilibrium considering both baths at equal temperature T, and thus depends only on B_r as well.

On the other hand, the operators $|\partial_\ell i\rangle\langle j|$ and $|i\rangle\langle \partial_\ell j|$ are nonzero only for variations in the polar coordinate ϕ because the eigenvectors $|i\rangle$ are associated to the unitary transformation that makes $\mathcal{H}_{\rm qb}$ diagonal, and do not change when $\vec{B}$ stays in the same direction.

These facts allows us to separate the linear response coefficient $\underline{\Lambda}$ into a radial contribution λ_r (changes in the energy spectrum) and a polar contribution λ_ϕ (basis rotation). Inserting the solution to (3.103) and (3.105) into Eq. (D.5) we get:

$$\langle r|\underline{\Lambda}|r\rangle = \lambda_r(\vec{B}) = \frac{\hbar\beta \sinh(\beta B_r)}{\Gamma(2B_r)\cosh^3(\beta B_r)} \tag{D.15}$$

$$\langle \phi|\underline{\Lambda}|\phi\rangle = \lambda_\phi(\vec{B}) = \frac{\hbar\Gamma(2B_r)}{4B_r^3} \tag{D.16}$$

Eq. (D.5) finally reads:

$$\underline{\Lambda} = \lambda_r|r\rangle\langle r| + \lambda_\phi|\phi\rangle\langle\phi|. \tag{D.17}$$

We now turn to analyze L^2, which quantifies the dissipated energy for a particular protocol, determined by $\underline{\Lambda}$ through Eq. (6.11). In the upper panel of Fig. D.1 we show the maximum eigenvalue, $\max[\lambda_r, \lambda_\phi]$ as a function of (B_z, B_x). This plot reflects the behavior resulting from the analytical expressions of Eqs. (D.15) and (D.16). At every point, and depending on the values of $\bar{\Gamma}$ and T, this maximum eigenvalue corresponds to a pure polar or pure radial displacement of $\vec{B}$. Within the small circle plotted in dashed lines and outside the one in solid lines, the highest eigenvalue is λ_ϕ, while within the two circles, λ_r is the largest one. This means that for small $B_r < B_{r,\rm low}$ as well as for large $B_r > B_{r,\rm high}$, protocols leading to the smallest dissipation are those associated to changes in B_r, while for $B_{r,\rm low} < B_r < B_{r,\rm high}$, protocols associated to rotations are the least dissipative ones. The specific values $B_{r,\rm low}$, $B_{r,\rm high}$ depend on the temperature and the coupling between the qubit and the reservoirs, as shown in Fig. 6.4 for two values of Γ.

The precise shape of the interval $B_{r,\rm low}$, $B_{r,\rm high}$ is shown in the lower panel of Fig. D.1 and depends only on $\bar{\Gamma}$, while the final value has a linear dependence on k_BT. We see that for $\bar{\Gamma} \gtrapprox 0.6$ the rotational dissipation dominates for all values of $|\vec{B}|$.

D.1.2 Explicit expression for $\vec{\Lambda}$ and κ

Again, plugging the expressions describing $\mathbf{p}(t)$ given by Eqs. (3.103) and (3.105) into Eq. (D.8) we get for the qubit:

$$\vec{\Lambda}_1(\vec{B}) = -\beta B_r \sin^3(\phi)\mathrm{sech}^2(\beta B_r) \tag{D.18}$$

$$\vec{\Lambda}_2(\vec{B}) = -\beta B_r \sin^2(\phi)\cos(\phi)\mathrm{sech}^2(\beta B_r). \tag{D.19}$$

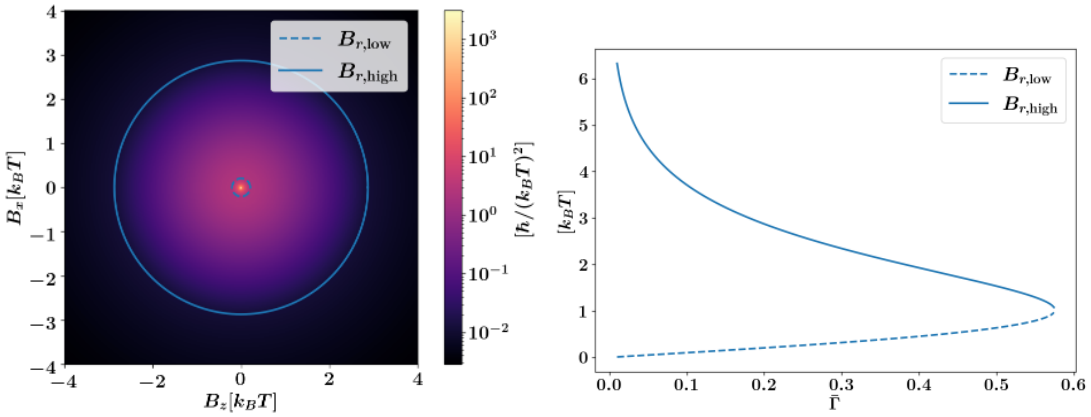

Figure D.1: Left panel: Maximum eigenvalue $\max[\lambda_r, \lambda_\phi]$, which ultimately defines the maximum possible dissipation at a given point $\vec{B}$. Right panel: $B_{r,\mathrm{low}}$ (dash line) and $B_{r,\mathrm{high}}$ (solid line) as function of $\bar{\Gamma}$. The values B_r for which $\lambda_r = \lambda_\phi$ are determined by $\bar{\Gamma}$ only and scales linearly with k_BT.

And lastly, using Eq. (D.9), the thermal conductance is explicitly written as:

$$\kappa(\vec{B}) = \frac{4B_r^2 \sin^2(\phi)\cos^2(\phi)\Gamma(2B_r)\mathrm{csch}\left(\frac{2B_r}{Tk_B}\right)}{\hbar k_B T}. \tag{D.20}$$

Bibliography

[1] H. E. D. Scovil and E. O. Schulz-DuBois. "Three-Level Masers as Heat Engines". In: *Physical Review Letters* 2.6 (Mar. 15, 1959), pp. 262–263. ISSN: 0031-9007. DOI: 10.1103/PhysRevLett.2.262. URL: https://link.aps.org/doi/10.1103/PhysRevLett.2.262 (visited on 08/17/2021).

[2] J. E. Geusic, E. O. Schulz-DuBios, and H. E. D. Scovil. "Quantum Equivalent of the Carnot Cycle". In: *Physical Review* 156.2 (Apr. 10, 1967), pp. 343–351. ISSN: 0031-899X. DOI: 10.1103/PhysRev.156.343. URL: https://link.aps.org/doi/10.1103/PhysRev.156.343 (visited on 08/17/2021).

[3] Eitan Geva and Ronnie Kosloff. "On the classical limit of quantum thermodynamics in finite time". In: *The Journal of Chemical Physics* 97.6 (Sept. 15, 1992), pp. 4398–4412. ISSN: 0021-9606, 1089-7690. DOI: 10.1063/1.463909. URL: http://aip.scitation.org/doi/10.1063/1.463909 (visited on 08/17/2021).

[4] A. E. Allahverdyan and Th. M. Nieuwenhuizen. "Extraction of Work from a Single Thermal Bath in the Quantum Regime". In: *Physical Review Letters* 85.9 (Aug. 28, 2000), pp. 1799–1802. ISSN: 0031-9007, 1079-7114. DOI: 10.1103/PhysRevLett.85.1799. URL: https://link.aps.org/doi/10.1103/PhysRevLett.85.1799 (visited on 08/17/2021).

[5] Peter Hänggi and Fabio Marchesoni. "Artificial Brownian motors: Controlling transport on the nanoscale". In: *Reviews of Modern Physics* 81.1 (Mar. 30, 2009), pp. 387–442. ISSN: 0034-6861, 1539-0756. DOI: 10.1103/RevModPhys.81.387. URL: https://link.aps.org/doi/10.1103/RevModPhys.81.387 (visited on 08/17/2021).

[6] Jochen Gemmer, M. Michel, and Günter Mahler. *Quantum Thermodynamics*. Vol. 784. Lecture Notes in Physics. Berlin, Heidelberg: Springer Berlin Heidelberg, 2010. ISBN: 978-3-540-70509-3 978-3-540-70510-9. DOI: 10.1007/978-3-540-70510-9. URL: http://link.springer.com/10.1007/978-3-540-70510-9 (visited on 08/17/2021).

[7] Michał Horodecki and Jonathan Oppenheim. "Fundamental limitations for quantum and nanoscale thermodynamics". In: *Nature Communications* 4.1 (Oct. 2013), p. 2059. ISSN: 2041-1723. DOI: 10.1038/ncomms3059. URL: http://www.nature.com/articles/ncomms3059 (visited on 08/17/2021).

[8] Felix Binder et al., eds. *Thermodynamics in the Quantum Regime: Fundamental Aspects and New Directions*. Vol. 195. Fundamental Theories of Physics. Cham: Springer International Publishing, 2018. ISBN: 978-3-319-99045-3 978-3-319-99046-0. DOI: 10.1007/978-3-319-99046-0. URL: http://link.springer.com/10.1007/978-3-319-99046-0 (visited on 08/17/2021).

[9] R Alicki. "The quantum open system as a model of the heat engine". In: *Journal of Physics A: Mathematical and General* 12.5 (May 1979), pp. L103–L107. ISSN: 0305-4470, 1361-6447. DOI: 10.1088/0305-4470/12/5/007. URL: https://iopscience.iop.org/article/10.1088/0305-4470/12/5/007 (visited on 08/17/2021).

[10] Eitan Geva and Ronnie Kosloff. "A quantum-mechanical heat engine operating in finite time. A model consisting of spin-1/2 systems as the working fluid". In: *The Journal of Chemical Physics* 96.4 (Feb. 15, 1992), pp. 3054–3067. ISSN: 0021-9606, 1089-7690. DOI: 10.1063/1.461951. URL: http://aip.scitation.org/doi/10.1063/1.461951 (visited on 08/17/2021).

[11] Noah Linden, Sandu Popescu, and Paul Skrzypczyk. "How Small Can Thermal Machines Be? The Smallest Possible Refrigerator". In: *Physical Review Letters* 105.13 (Sept. 21, 2010), p. 130401. ISSN: 0031-9007, 1079-7114. DOI: 10.1103/PhysRevLett.105.130401. URL: https://link.aps.org/doi/10.1103/PhysRevLett.105.130401 (visited on 08/17/2021).

[12] Michael Wiedmann, Jürgen T. Stockburger, and Joachim Ankerhold. "Out-of-equilibrium operation of a quantum heat engine: The cost of thermal coupling control". In: *New Journal of Physics* 22.3 (Mar. 6, 2020), p. 033007. ISSN: 1367-2630. DOI: 10.1088/1367-2630/ab725a. arXiv: 1903.11368. URL: http://arxiv.org/abs/1903.11368 (visited on 08/27/2021).

[13] Roie Dann and Ronnie Kosloff. "Quantum Signatures in the Quantum Carnot Cycle". In: *New Journal of Physics* 22.1 (Jan. 30, 2020), p. 013055. ISSN: 1367-2630. DOI: 10.1088/1367-2630/ab6876. arXiv: 1906.06946. URL: http://arxiv.org/abs/1906.06946 (visited on 08/27/2021).

[14] Tamiro Villazon, Anatoli Polkovnikov, and Anushya Chandran. "Swift heat transfer by fast-forward driving in open quantum systems". In: *Physical Review A* 100.1 (July 24, 2019), p. 012126. ISSN: 2469-9926, 2469-9934. DOI: 10.1103/PhysRevA.100.012126. URL: https://link.aps.org/doi/10.1103/PhysRevA.100.012126 (visited on 08/17/2021).

[15] A. Tobalina, I. Lizuain, and J. G. Muga. "Vanishing efficiency of a speeded-up ion-in-Paul-trap Otto engine". In: *EPL (Europhysics Letters)* 127.2 (Aug. 28, 2019), p. 20005. ISSN: 1286-4854. DOI: 10.1209/0295-5075/127/20005. URL: https://iopscience.iop.org/article/10.1209/0295-5075/127/20005 (visited on 08/17/2021).

[16] Ken Funo et al. "Speeding up a quantum refrigerator via counterdiabatic driving". In: *Physical Review B* 100.3 (July 8, 2019), p. 035407. ISSN: 2469-9950, 2469-9969. DOI: 10.1103/PhysRevB.100.035407. URL: https://link.aps.org/doi/10.1103/PhysRevB.100.035407 (visited on 08/17/2021).

[17] P A Erdman et al. "Maximum power and corresponding efficiency for two-level heat engines and refrigerators: optimality of fast cycles". In: *New Journal of Physics* 21.10 (Oct. 29, 2019), p. 103049. ISSN: 1367-2630. DOI: 10.1088/1367-2630/ab4dca. URL: https://iopscience.iop.org/article/10.1088/1367-2630/ab4dca (visited on 08/17/2021).

[18] Robert Biele et al. "Controlling heat and particle currents in nanodevices by quantum observation". In: *npj Quantum Materials* 2.1 (Dec. 2017), p. 38. ISSN: 2397-4648. DOI: 10.1038/s41535-017-0043-6. URL: http://www.nature.com/articles/s41535-017-0043-6 (visited on 08/17/2021).

[19] Cyril Elouard et al. "Extracting Work from Quantum Measurement in Maxwell's Demon Engines". In: *Physical Review Letters* 118.26 (June 29, 2017), p. 260603. ISSN: 0031-9007, 1079-7114. DOI: 10.1103/PhysRevLett.118.260603. URL: http://link.aps.org/doi/10.1103/PhysRevLett.118.260603 (visited on 08/17/2021).

[20] Cyril Elouard and Andrew N. Jordan. "Efficient Quantum Measurement Engines". In: *Physical Review Letters* 120.26 (June 27, 2018), p. 260601. ISSN: 0031-9007, 1079-7114. DOI: 10.1103/PhysRevLett.120.260601. URL: https://link.aps.org/doi/10.1103/PhysRevLett.120.260601 (visited on 08/17/2021).

[21] Lorenzo Buffoni et al. "Quantum Measurement Cooling". In: *Physical Review Letters* 122.7 (Feb. 21, 2019), p. 070603. ISSN: 0031-9007, 1079-7114. DOI: 10.1103/PhysRevLett.122.070603. URL: https://link.aps.org/doi/10.1103/PhysRevLett.122.070603 (visited on 08/17/2021).

[22] J. P. Pekola and F. W. J. Hekking. "Normal-Metal-Superconductor Tunnel Junction as a Brownian Refrigerator". In: *Physical Review Letters* 98.21 (May 25, 2007), p. 210604. ISSN: 0031-9007, 1079-7114. DOI: 10.1103/PhysRevLett.98.210604. URL: https://link.aps.org/doi/10.1103/PhysRevLett.98.210604 (visited on 08/17/2021).

[23] Padraig Murphy, Subroto Mukerjee, and Joel Moore. "Optimal thermoelectric figure of merit of a molecular junction". In: *Physical Review B* 78.16 (Oct. 28, 2008), p. 161406. ISSN: 1098-0121, 1550-235X. DOI: 10.1103/PhysRevB.78.161406. URL: https://link.aps.org/doi/10.1103/PhysRevB.78.161406 (visited on 08/17/2021).

[24] M. Esposito, K. Lindenberg, and C. Van den Broeck. "Thermoelectric efficiency at maximum power in a quantum dot". In: *EPL (Europhysics Letters)* 85.6 (Mar. 2009), p. 60010. ISSN: 0295-5075, 1286-4854. DOI: 10.1209/0295-5075/85/60010. URL: https://iopscience.iop.org/article/10.1209/0295-5075/85/60010 (visited on 08/17/2021).

[25] Stefan Juergens et al. "Thermoelectric performance of a driven double quantum dot". In: *Physical Review B* 87.24 (June 19, 2013), p. 245423. ISSN: 1098-0121, 1550-235X. DOI: 10.1103/PhysRevB.87.245423. URL: https://link.aps.org/doi/10.1103/PhysRevB.87.245423 (visited on 08/27/2021).

[26] D. Gelbwaser-Klimovsky, R. Alicki, and G. Kurizki. "Minimal universal quantum heat machine". In: *Physical Review E* 87.1 (Jan. 25, 2013), p. 012140. ISSN: 1539-3755, 1550-2376. DOI: 10.1103/PhysRevE.87.012140. URL: https://link.aps.org/doi/10.1103/PhysRevE.87.012140 (visited on 08/27/2021).

[27] Björn Sothmann, Rafael Sánchez, and Andrew N Jordan. "Thermoelectric energy harvesting with quantum dots". In: *Nanotechnology* 26.3 (Jan. 21, 2015), p. 032001. ISSN: 0957-4484, 1361-6528. DOI: 10.1088/0957-4484/26/3/032001. URL: https://iopscience.iop.org/article/10.1088/0957-4484/26/3/032001 (visited on 08/17/2021).

[28] Ronnie Kosloff and Amikam Levy. "Quantum Heat Engines and Refrigerators: Continuous Devices". In: *Annual Review of Physical Chemistry* 65.1 (Apr. 2014), pp. 365–393. ISSN: 0066-426X, 1545-1593. DOI: 10.1146/annurev-physchem-040513-103724. URL: http://www.annualreviews.org/doi/10.1146/annurev-physchem-040513-103724 (visited on 08/17/2021).

[29] Patrick P. Hofer et al. "Autonomous quantum refrigerator in a circuit QED architecture based on a Josephson junction". In: *Physical Review B* 94.23 (Dec. 16, 2016), p. 235420. ISSN: 2469-9950, 2469-9969. DOI: 10.1103/PhysRevB.94.235420. URL: https://link.aps.org/doi/10.1103/PhysRevB.94.235420 (visited on 08/17/2021).

[30] Giuliano Benenti et al. "Fundamental aspects of steady-state conversion of heat to work at the nanoscale". In: *Physics Reports* 694 (June 2017), pp. 1–124. ISSN: 03701573. DOI: 10.1016/j.physrep.2017.05.008. URL: https://linkinghub.elsevier.com/retrieve/pii/S0370157317301540 (visited on 08/17/2021).

[31] Claudio Chamon et al. "Heat Pumping in Nanomechanical Systems". In: *Physical Review Letters* 106.13 (Apr. 1, 2011), p. 135504. ISSN: 0031-9007, 1079-7114. DOI: 10.1103/PhysRevLett.106.135504. URL: https://link.aps.org/doi/10.1103/PhysRevLett.106.135504 (visited on 08/17/2021).

[32] Liliana Arrachea et al. "Microscopic model of a phononic refrigerator". In: *Physical Review B* 86.12 (Sept. 17, 2012), p. 125424. ISSN: 1098-0121, 1550-235X. DOI: 10.1103/PhysRevB.86.125424. URL: https://link.aps.org/doi/10.1103/PhysRevB.86.125424 (visited on 08/17/2021).

[33] John P. S. Peterson et al. "Experimental Characterization of a Spin Quantum Heat Engine". In: *Physical Review Letters* 123.24 (Dec. 9, 2019), p. 240601. ISSN: 0031-9007, 1079-7114. DOI: 10.1103/PhysRevLett.123.240601. URL: https://link.aps.org/doi/10.1103/PhysRevLett.123.240601 (visited on 08/17/2021).

[34] B. Roche et al. "A two-atom electron pump". In: *Nature Communications* 4.1 (June 2013), p. 1581. ISSN: 2041-1723. DOI: 10.1038/ncomms2544. URL: http://www.nature.com/articles/ncomms2544 (visited on 08/17/2021).

[35] H Pothier et al. "Single-Electron Pump Based on Charging Effects". In: *Europhysics Letters (EPL)* 17.3 (Jan. 14, 1992), pp. 249–254. ISSN: 0295-5075, 1286-4854. DOI: 10.1209/0295-5075/17/3/011. URL: https://iopscience.iop.org/article/10.1209/0295-5075/17/3/011 (visited on 08/17/2021).

[36] Michele Campisi, Jukka Pekola, and Rosario Fazio. "Nonequilibrium fluctuations in quantum heat engines: theory, example, and possible solid state experiments". In: *New Journal of Physics* 17.3 (Mar. 20, 2015), p. 035012. ISSN: 1367-2630. DOI: 10.1088/1367-2630/17/3/035012. URL: https://iopscience.iop.org/article/10.1088/1367-2630/17/3/035012 (visited on 08/17/2021).

[37] Holger Thierschmann et al. "Three-terminal energy harvester with coupled quantum dots". In: *Nature Nanotechnology* 10.10 (Oct. 2015), pp. 854–858. ISSN: 1748-3387, 1748-3395. DOI: 10.1038/nnano.2015.176. URL: http://www.nature.com/articles/nnano.2015.176 (visited on 08/17/2021).

[38] J.P. Pekola and I.M. Khaymovich. "Thermodynamics in Single-Electron Circuits and Superconducting Qubits". In: *Annual Review of Condensed Matter Physics* 10.1 (Mar. 10, 2019), pp. 193–212. ISSN: 1947-5454, 1947-5462. DOI: 10.1146/annurev-conmatphys-033117-054120. URL: https://www.annualreviews.org/doi/10.1146/annurev-conmatphys-033117-054120 (visited on 08/17/2021).

[39] Alberto Ronzani et al. "Tunable photonic heat transport in a quantum heat valve". In: *Nature Physics* 14.10 (Oct. 2018), pp. 991–995. ISSN: 1745-2473, 1745-2481. DOI: 10.1038/s41567-018-0199-4. URL: http://www.nature.com/articles/s41567-018-0199-4 (visited on 08/17/2021).

[40] Andreas Dechant, Nikolai Kiesel, and Eric Lutz. "All-Optical Nanomechanical Heat Engine". In: *Physical Review Letters* 114.18 (May 6, 2015), p. 183602. ISSN: 0031-9007, 1079-7114. DOI: 10.1103/PhysRevLett.114.183602. URL: https://link.aps.org/doi/10.1103/PhysRevLett.114.183602 (visited on 08/17/2021).

[41] A. D. O'Connell et al. "Quantum ground state and single-phonon control of a mechanical resonator". In: *Nature* 464.7289 (Apr. 2010), pp. 697–703. ISSN: 0028-0836, 1476-4687. DOI: 10.1038/nature08967. URL: http://www.nature.com/articles/nature08967 (visited on 08/17/2021).

[42] Liliana Arrachea, Niels Bode, and Felix von Oppen. "Vibrational cooling and thermoelectric response of nanoelectromechanical systems". In: *Physical Review B* 90.12 (Sept. 30, 2014), p. 125450. ISSN: 1098-0121, 1550-235X. DOI: 10.1103/PhysRevB.90.125450. URL: https://link.aps.org/doi/10.1103/PhysRevB.90.125450 (visited on 08/17/2021).

[43] P. Stadler, W. Belzig, and G. Rastelli. "Ground-State Cooling of a Mechanical Oscillator by Interference in Andreev Reflection". In: *Physical Review Letters* 117.19 (Nov. 2, 2016), p. 197202. ISSN: 0031-9007, 1079-7114. DOI: 10.1103/PhysRevLett.117.197202. URL: https://link.aps.org/doi/10.1103/PhysRevLett.117.197202 (visited on 08/17/2021).

[44] C. Urgell et al. "Cooling and self-oscillation in a nanotube electromechanical resonator". In: *Nature Physics* 16.1 (Jan. 2020), pp. 32–37. ISSN: 1745-2473, 1745-2481. DOI: 10.1038/s41567-019-0682-6. URL: http://www.nature.com/articles/s41567-019-0682-6 (visited on 08/17/2021).

[45] J.-P. Brantut et al. "A Thermoelectric Heat Engine with Ultracold Atoms". In: *Science* 342.6159 (Nov. 8, 2013), pp. 713–715. ISSN: 0036-8075, 1095-9203. DOI: 10.1126/science.1242308. URL: https://www.sciencemag.org/lookup/doi/10.1126/science.1242308 (visited on 08/17/2021).

[46] O. Abah et al. "Single-Ion Heat Engine at Maximum Power". In: *Physical Review Letters* 109.20 (Nov. 14, 2012), p. 203006. ISSN: 0031-9007, 1079-7114. DOI: 10.1103/PhysRevLett.109.203006. URL: https://link.aps.org/doi/10.1103/PhysRevLett.109.203006 (visited on 08/17/2021).

[47] Shujin Deng et al. "Superadiabatic quantum friction suppression in finite-time thermodynamics". In: *Science Advances* 4.4 (Apr. 2018), eaar5909. ISSN: 2375-2548. DOI: 10.1126/sciadv.aar5909. URL: https://advances.sciencemag.org/lookup/doi/10.1126/sciadv.aar5909 (visited on 08/17/2021).

[48] J. Rossnagel et al. "A single-atom heat engine". In: *Science* 352.6283 (Apr. 15, 2016), pp. 325–329. ISSN: 0036-8075, 1095-9203. DOI: 10.1126/science.aad6320. URL: https://www.sciencemag.org/lookup/doi/10.1126/science.aad6320 (visited on 08/17/2021).

[49] Rogério J. de Assis et al. "Efficiency of a Quantum Otto Heat Engine Operating under a Reservoir at Effective Negative Temperatures". In: *Physical Review Letters* 122.24 (June 19, 2019), p. 240602. ISSN: 0031-9007, 1079-7114. DOI: 10.1103/PhysRevLett.122.240602. URL: https://link.aps.org/doi/10.1103/PhysRevLett.122.240602 (visited on 08/18/2021).

[50] Y. Aharonov and D. Bohm. "Significance of Electromagnetic Potentials in the Quantum Theory". In: *Physical Review* 115.3 (Aug. 1, 1959), pp. 485–491. ISSN: 0031-899X. DOI: 10.1103/PhysRev.115.485. URL: https://link.aps.org/doi/10.1103/PhysRev.115.485 (visited on 08/17/2021).

[51] Michael V. Berry. "Quantal phase factors accompanying adiabatic changes". In: *Proceedings of the Royal Society of London. A. Mathematical and Physical Sciences* 392.1802 (Mar. 8, 1984), pp. 45–57. ISSN: 0080-4630. DOI: 10.1098/rspa.1984.0023. URL: https://royalsocietypublishing.org/doi/10.1098/rspa.1984.0023 (visited on 02/11/2022).

[52] P. W. Brouwer. "Scattering approach to parametric pumping". In: *Physical Review B* 58.16 (Oct. 15, 1998), R10135–R10138. ISSN: 0163-1829, 1095-3795. DOI: 10.1103/PhysRevB.58.R10135. URL: https://link.aps.org/doi/10.1103/PhysRevB.58.R10135 (visited on 08/17/2021).

[53] T. A. Shutenko, I. L. Aleiner, and B. L. Altshuler. "Mesoscopic fluctuations of adiabatic charge pumping in quantum dots". In: *Physical Review B* 61.15 (Apr. 15, 2000), pp. 10366–10375. ISSN: 0163-1829, 1095-3795. DOI: 10.1103/PhysRevB.61.10366. URL: https://link.aps.org/doi/10.1103/PhysRevB.61.10366 (visited on 08/17/2021).

[54] J. E. Avron et al. "Optimal Quantum Pumps". In: *Physical Review Letters* 87.23 (Nov. 13, 2001), p. 236601. ISSN: 0031-9007, 1079-7114. DOI: 10.1103/PhysRevLett.87.236601. URL: https://link.aps.org/doi/10.1103/PhysRevLett.87.236601 (visited on 08/17/2021).

[55] Hernán L. Calvo et al. "Interaction-induced charge and spin pumping through a quantum dot at finite bias". In: *Physical Review B* 86.24 (Dec. 12, 2012), p. 245308. ISSN: 1098-0121, 1550-235X. DOI: 10.1103/PhysRevB.86.245308. URL: https://link.aps.org/doi/10.1103/PhysRevB.86.245308 (visited on 08/17/2021).

[56] Masahiro Hasegawa and Takeo Kato. "Temperature-Driven and Electrochemical-Potential-Driven Adiabatic Pumping via a Quantum Dot". In: *Journal of the Physical Society of Japan* 86.2 (Feb. 15, 2017), p. 024710. ISSN: 0031-9015, 1347-4073. DOI: 10.7566/JPSJ.86.024710. URL: https://journals.jps.jp/doi/10.7566/JPSJ.86.024710 (visited on 08/17/2021).

[57] Masahiro Hasegawa and Takeo Kato. "Effect of Interaction on Reservoir-Parameter-Driven Adiabatic Charge Pumping via a Single-Level Quantum Dot System". In: *Journal of the Physical Society of Japan* 87.4 (Apr. 15, 2018), p. 044709. ISSN: 0031-9015, 1347-4073. DOI: 10.7566/JPSJ.87.044709. URL: https://journals.jps.jp/doi/10.7566/JPSJ.87.044709 (visited on 08/17/2021).

[58] Jie Ren, Peter Hänggi, and Baowen Li. "Berry-Phase-Induced Heat Pumping and Its Impact on the Fluctuation Theorem". In: *Physical Review Letters* 104.17 (Apr. 27, 2010), p. 170601. ISSN: 0031-9007, 1079-7114. DOI: 10.1103/PhysRevLett.104.170601. URL: https://link.aps.org/doi/10.1103/PhysRevLett.104.170601 (visited on 08/17/2021).

[59] M V Berry and P Shukla. "High-order classical adiabatic reaction forces: slow manifold for a spin model". In: *Journal of Physics A: Mathematical and Theoretical* 43.4 (Jan. 29, 2010), p. 045102. ISSN: 1751-8113, 1751-8121. DOI: 10.1088/1751-8113/43/4/045102. URL: https://iopscience.iop.org/article/10.1088/1751-8113/43/4/045102 (visited on 08/17/2021).

[60] Michele Campisi, Peter Talkner, and Peter Hänggi. "Fluctuation Theorem for Arbitrary Open Quantum Systems". In: *Physical Review Letters* 102.21 (May 26, 2009), p. 210401. ISSN: 0031-9007, 1079-7114. DOI: 10.1103/PhysRevLett.102.210401. URL: https://link.aps.org/doi/10.1103/PhysRevLett.102.210401 (visited on 08/17/2021).

[61] Niels Bode et al. "Scattering Theory of Current-Induced Forces in Mesoscopic Systems". In: *Physical Review Letters* 107.3 (July 11, 2011), p. 036804. ISSN: 0031-9007, 1079-7114. DOI: 10.1103/PhysRevLett.107.036804. URL: https://link.aps.org/doi/10.1103/PhysRevLett.107.036804 (visited on 08/17/2021).

[62] Niels Bode et al. "Current-induced forces in mesoscopic systems: A scattering-matrix approach". In: *Beilstein Journal of Nanotechnology* 3 (Feb. 20, 2012), pp. 144–162. ISSN: 2190-4286. DOI: 10.3762/bjnano.3.15. URL: https://www.beilstein-journals.org/bjnano/articles/3/15 (visited on 08/17/2021).

[63] Mark Thomas et al. "Scattering theory of adiabatic reaction forces due to out-of-equilibrium quantum environments". In: *Physical Review B* 86.19 (Nov. 19, 2012), p. 195419. ISSN: 1098-0121, 1550-235X. DOI: 10.1103/PhysRevB.86.195419. URL: https://link.aps.org/doi/10.1103/PhysRevB.86.195419 (visited on 02/11/2022).

[64] Lucas J. Fernández-Alcázar, Raúl A. Bustos-Marún, and Horacio M. Pastawski. "Decoherence in current induced forces: Application to adiabatic quantum motors". In: *Physical Review B* 92.7 (Aug. 5, 2015), p. 075406. ISSN: 1098-0121, 1550-235X. DOI: 10.1103/PhysRevB.92.075406. URL: https://link.aps.org/doi/10.1103/PhysRevB.92.075406 (visited on 08/17/2021).

[65] Hernán L. Calvo, Federico D. Ribetto, and Raúl A. Bustos-Marún. "Real-time diagrammatic approach to current-induced forces: Application to quantum-dot based nanomotors". In: *Physical Review B* 96.16 (Oct. 23, 2017), p. 165309. ISSN: 2469-9950, 2469-9969. DOI: 10.1103/PhysRevB.96.165309. URL: https://link.aps.org/doi/10.1103/PhysRevB.96.165309 (visited on 08/17/2021).

[66] Lucas J. Fernández-Alcázar, Horacio M. Pastawski, and Raúl A. Bustos-Marún. "Nonequilibrium current-induced forces caused by quantum localization: Anderson adiabatic quantum motors". In: *Physical Review B* 99.4 (Jan. 2, 2019), p. 045403. ISSN: 2469-9950, 2469-9969. DOI: 10.1103/PhysRevB.99.045403. URL: https://link.aps.org/doi/10.1103/PhysRevB.99.045403 (visited on 08/17/2021).

[67] Pablo Terrén Alonso, Javier Romero, and Liliana Arrachea. "Work exchange, geometric magnetization, and fluctuation-dissipation relations in a quantum dot under adiabatic magnetoelectric driving". In: *Physical Review B* 99.11 (Mar. 18, 2019), p. 115424. ISSN: 2469-9950, 2469-9969. DOI: 10.1103/PhysRevB.99.115424. URL: https://link.aps.org/doi/10.1103/PhysRevB.99.115424 (visited on 08/17/2021).

[68] Michael Victor Berry and J. M. Robbins. "Chaotic classical and half-classical adiabatic reactions: geometric magnetism and deterministic friction". In: *Proceedings of the Royal Society of London. Series A: Mathematical and Physical Sciences* 442.1916 (Sept. 8, 1993), pp. 659–672. ISSN: 0962-8444, 2053-9177. DOI: 10.1098/rspa.1993.0127. URL: https://royalsocietypublishing.org/doi/10.1098/rspa.1993.0127 (visited on 08/17/2021).

[69] Michele Campisi, Sergey Denisov, and Peter Hänggi. "Geometric magnetism in open quantum systems". In: *Physical Review A* 86.3 (Sept. 17, 2012), p. 032114. ISSN: 1050-2947, 1094-1622. DOI: 10.1103/PhysRevA.86.032114. URL: https://link.aps.org/doi/10.1103/PhysRevA.86.032114 (visited on 08/17/2021).

[70] Juzar Thingna et al. "Geometric quantum pumping in the presence of dissipation". In: *Physical Review B* 90.9 (Sept. 24, 2014), p. 094517. ISSN: 1098-0121, 1550-235X. DOI: 10.1103/PhysRevB.90.094517. URL: https://link.aps.org/doi/10.1103/PhysRevB.90.094517 (visited on 08/17/2021).

[71] F. Weinhold. "Metric geometry of equilibrium thermodynamics". In: *The Journal of Chemical Physics* 63.6 (Sept. 15, 1975), pp. 2479–2483. ISSN: 0021-9606, 1089-7690. DOI: 10.1063/1.431689. URL: http://aip.scitation.org/doi/10.1063/1.431689 (visited on 08/27/2021).

[72] Peter Salamon et al. "The significance of Weinhold's length". In: *The Journal of Chemical Physics* 73.2 (July 15, 1980), pp. 1001–1002. ISSN: 0021-9606, 1089-7690. DOI: 10.1063/1.440217. URL: http://aip.scitation.org/doi/10.1063/1.440217 (visited on 08/27/2021).

[73] Peter Salamon and R. Stephen Berry. "Thermodynamic Length and Dissipated Availability". In: *Physical Review Letters* 51.13 (Sept. 26, 1983), pp. 1127–1130. ISSN: 0031-9007. DOI: 10.1103/PhysRevLett.51.1127. URL: https://link.aps.org/doi/10.1103/PhysRevLett.51.1127 (visited on 08/26/2021).

[74] J. Nulton et al. "Quasistatic processes as step equilibrations". In: *The Journal of Chemical Physics* 83.1 (July 1985), pp. 334–338. ISSN: 0021-9606, 1089-7690. DOI: 10.1063/1.449774. URL: http://aip.scitation.org/doi/10.1063/1.449774 (visited on 08/27/2021).

[75] F. Schlögl. "Thermodynamic metric and stochastic measures". In: *Zeitschrift für Physik B Condensed Matter* 59.4 (Dec. 1985), pp. 449–454. ISSN: 0722-3277, 1434-6036. DOI: 10.1007/BF01328857. URL: http://link.springer.com/10.1007/BF01328857 (visited on 08/27/2021).

[76] Dénes Petz and Gabor Toth. "The Bogoliubov inner product in quantum statistics: Dedicated to J. Merza on his 60th birthday". In: *Letters in Mathematical Physics* 27.3 (Mar. 1993), pp. 205–216. ISSN: 0377-9017, 1573-0530. DOI: 10.1007/BF00739578. URL: http://link.springer.com/10.1007/BF00739578 (visited on 09/29/2022).

[77] Sebastian Deffner and Eric Lutz. "Generalized Clausius Inequality for Nonequilibrium Quantum Processes". In: *Physical Review Letters* 105.17 (Oct. 19, 2010), p. 170402. ISSN: 0031-9007, 1079-7114. DOI: 10.1103/PhysRevLett.105.170402. URL: https://link.aps.org/doi/10.1103/PhysRevLett.105.170402 (visited on 09/29/2022).

[78] Sebastian Deffner and Eric Lutz. "Thermodynamic length for far-from-equilibrium quantum systems". In: *Physical Review E* 87.2 (Feb. 28, 2013), p. 022143. ISSN: 1539-3755, 1550-2376. DOI: 10.1103/PhysRevE.87.022143. URL: https://link.aps.org/doi/10.1103/PhysRevE.87.022143 (visited on 08/27/2021).

[79] Roger Balian. "The Entropy-Based Quantum Metric". In: *Entropy* 16.7 (July 15, 2014), pp. 3878–3888. ISSN: 1099-4300. DOI: 10.3390/e16073878. URL: http://www.mdpi.com/1099-4300/16/7/3878 (visited on 09/29/2022).

[80] María Florencia Ludovico et al. "Adiabatic response and quantum thermoelectrics for ac-driven quantum systems". In: *Physical Review B* 93.7 (Feb. 18, 2016), p. 075136. ISSN: 2469-9950, 2469-9969. DOI: 10.1103/PhysRevB.93.075136. URL: https://link.aps.org/doi/10.1103/PhysRevB.93.075136 (visited on 08/17/2021).

[81] Matteo Scandi and Martí Perarnau-Llobet. "Thermodynamic length in open quantum systems". In: *Quantum* 3 (Oct. 24, 2019), p. 197. ISSN: 2521-327X. DOI: 10.22331/q-2019-10-24-197. URL: https://quantum-journal.org/papers/q-2019-10-24-197/ (visited on 08/17/2021).

[82] A. T. Rezakhani et al. "Quantum Adiabatic Brachistochrone". In: *Physical Review Letters* 103.8 (Aug. 21, 2009), p. 080502. ISSN: 0031-9007, 1079-7114. DOI: 10.1103/PhysRevLett.103.080502. URL: https://link.aps.org/doi/10.1103/PhysRevLett.103.080502 (visited on 08/17/2021).

[83] David A. Sivak and Gavin E. Crooks. "Thermodynamic Metrics and Optimal Paths". In: *Physical Review Letters* 108.19 (May 8, 2012), p. 190602. ISSN: 0031-9007, 1079-7114. DOI: 10.1103/PhysRevLett.108.190602. URL: https://link.aps.org/doi/10.1103/PhysRevLett.108.190602 (visited on 08/17/2021).

[84] Sebastian Deffner and Eric Lutz. "Nonequilibrium Entropy Production for Open Quantum Systems". In: *Physical Review Letters* 107.14 (Sept. 30, 2011), p. 140404. ISSN: 0031-9007, 1079-7114. DOI: 10.1103/PhysRevLett.107.140404. URL: https://link.aps.org/doi/10.1103/PhysRevLett.107.140404 (visited on 08/17/2021).

[85] Harry J. D. Miller et al. "Work Fluctuations in Slow Processes: Quantum Signatures and Optimal Control". In: *Physical Review Letters* 123.23 (Dec. 4, 2019), p. 230603. ISSN: 0031-9007, 1079-7114. DOI: 10.1103/PhysRevLett.123.230603. URL: https://link.aps.org/doi/10.1103/PhysRevLett.123.230603 (visited on 08/17/2021).

[86] Paolo Abiuso and Martí Perarnau-Llobet. "Optimal Cycles for Low-Dissipation Heat Engines". In: *Physical Review Letters* 124.11 (Mar. 19, 2020), p. 110606. ISSN: 0031-9007, 1079-7114. DOI: 10.1103/PhysRevLett.124.110606. URL: https://link.aps.org/doi/10.1103/PhysRevLett.124.110606 (visited on 02/11/2022).

[87] Yuki Hino and Hisao Hayakawa. "Geometrical formulation of adiabatic pumping as a heat engine". In: *Physical Review Research* 3.1 (Feb. 26, 2021), p. 013187. ISSN: 2643-1564. DOI: 10.1103/PhysRevResearch.3.013187. URL: https://link.aps.org/doi/10.1103/PhysRevResearch.3.013187 (visited on 02/16/2022).

[88] Yuki Izumida. "Hierarchical Onsager symmetries in adiabatically driven linear irreversible heat engines". In: *Physical Review E* 103.5 (May 14, 2021), p. L050101. ISSN: 2470-0045, 2470-0053. DOI: 10.1103/PhysRevE.103.L050101. URL: https://link.aps.org/doi/10.1103/PhysRevE.103.L050101 (visited on 02/16/2022).

[89] Bjarne Andresen. "Finite-time thermodynamics and thermodynamic length". In: *Revue Générale de Thermique* 35.418 (Nov. 1996), pp. 647–650. ISSN: 00353159. DOI: 10.1016/S0035-3159(96)80060-2. URL: https://linkinghub.elsevier.com/retrieve/pii/S0035315996800602 (visited on 08/27/2021).

[90] L. Diósi et al. "Thermodynamic length, time, speed, and optimum path to minimize entropy production". In: *The Journal of Chemical Physics* 105.24 (Dec. 22, 1996), pp. 11220–11225. ISSN: 0021-9606, 1089-7690. DOI: 10.1063/1.472897. URL: http://aip.scitation.org/doi/10.1063/1.472897 (visited on 08/27/2021).

[91] Gavin E. Crooks. "Measuring Thermodynamic Length". In: *Physical Review Letters* 99.10 (Sept. 7, 2007), p. 100602. ISSN: 0031-9007, 1079-7114. DOI: 10.1103/PhysRevLett.99.100602. URL: https://link.aps.org/doi/10.1103/PhysRevLett.99.100602 (visited on 08/27/2021).

[92] Tan Van Vu and Yoshihiko Hasegawa. "Geometrical Bounds of the Irreversibility in Markovian Systems". In: *Physical Review Letters* 126.1 (Jan. 4, 2021), p. 010601. ISSN: 0031-9007, 1079-7114. DOI: 10.1103/PhysRevLett.126.010601. URL: https://link.aps.org/doi/10.1103/PhysRevLett.126.010601 (visited on 02/16/2022).

[93] Patrick R. Zulkowski et al. "Geometry of thermodynamic control". In: *Physical Review E* 86.4 (Oct. 26, 2012), p. 041148. ISSN: 1539-3755, 1550-2376. DOI: 10.1103/PhysRevE.86.041148. URL: https://link.aps.org/doi/10.1103/PhysRevE.86.041148 (visited on 02/16/2022).

[94] Patrick R. Zulkowski, David A. Sivak, and Michael R. DeWeese. "Optimal Control of Transitions between Nonequilibrium Steady States". In: *PLoS ONE* 8.12 (Dec. 26, 2013). Ed. by Gerardo Adesso, e82754. ISSN: 1932-6203. DOI: 10.1371/journal.pone.0082754. URL: https://dx.plos.org/10.1371/journal.pone.0082754 (visited on 02/16/2022).

[95] Marcus V. S. Bonança and Sebastian Deffner. "Optimal driving of isothermal processes close to equilibrium". In: *The Journal of Chemical Physics* 140.24 (June 28, 2014), p. 244119. ISSN: 0021-9606, 1089-7690. DOI: 10.1063/1.4885277. URL: http://aip.scitation.org/doi/10.1063/1.4885277 (visited on 08/27/2021).

[96] Patrick R. Zulkowski and Michael R. DeWeese. "Optimal protocols for slowly driven quantum systems". In: *Physical Review E* 92.3 (Sept. 2015). Number of pages: 6 Publisher: American Physical Society, p. 032113. DOI: 10.1103/PhysRevE.92.032113. URL: https://link.aps.org/doi/10.1103/PhysRevE.92.032113.

[97] Paolo Abiuso et al. "Geometric Optimisation of Quantum Thermodynamic Processes". In: *Entropy* 22.10 (Sept. 24, 2020), p. 1076. ISSN: 1099-4300. DOI: 10.3390/e22101076. URL: https://www.mdpi.com/1099-4300/22/10/1076 (visited on 02/16/2022).

[98] Kay Brandner and Keiji Saito. "Thermodynamic Geometry of Microscopic Heat Engines". In: *Physical Review Letters* 124.4 (Jan. 29, 2020), p. 040602. ISSN: 0031-9007, 1079-7114. DOI: 10.1103/PhysRevLett.124.040602. URL: https://link.aps.org/doi/10.1103/PhysRevLett.124.040602 (visited on 08/18/2021).

[99] Harry J. D. Miller and Mohammad Mehboudi. "Geometry of Work Fluctuations versus Efficiency in Microscopic Thermal Machines". In: *Physical Review Letters* 125.26 (Dec. 22, 2020), p. 260602. ISSN: 0031-9007, 1079-7114. DOI: 10.1103/PhysRevLett.125.260602. URL: https://link.aps.org/doi/10.1103/PhysRevLett.125.260602 (visited on 02/16/2022).

[100] Harry J. D. Miller et al. "Thermodynamic Uncertainty Relation in Slowly Driven Quantum Heat Engines". In: *Physical Review Letters* 126.21 (May 27, 2021), p. 210603. ISSN: 0031-9007, 1079-7114. DOI: 10.1103/PhysRevLett.126.210603. URL: https://link.aps.org/doi/10.1103/PhysRevLett.126.210603 (visited on 02/16/2022).

[101] Adam G. Frim and Michael R. DeWeese. "Optimal finite-time Brownian Carnot engine". In: *arXiv:2107.05673 [cond-mat]* (July 12, 2021). arXiv: 2107.05673. URL: http://arxiv.org/abs/2107.05673 (visited on 02/16/2022).

[102] Zi Wang et al. "Geometric heat pump: Controlling thermal transport with time-dependent modulations". In: *Frontiers of Physics* 17.1 (Feb. 2022), p. 13201. ISSN: 2095-0462, 2095-0470. DOI: 10.1007/s11467-021-1095-4. URL: https://link.springer.com/10.1007/s11467-021-1095-4 (visited on 09/24/2021).

[103] Bibek Bhandari et al. "From nonequilibrium Green's functions to quantum master equations for the density matrix and out-of-time-order correlators: Steady-state and adiabatic dynamics". In: *Physical Review B* 104.3 (July 20, 2021), p. 035425. ISSN: 2469-9950, 2469-9969. DOI: 10.1103/PhysRevB.104.035425. URL: https://link.aps.org/doi/10.1103/PhysRevB.104.035425 (visited on 02/17/2022).

[104] M. Switkes et al. "An Adiabatic Quantum Electron Pump". In: *Science* 283.5409 (Mar. 19, 1999), pp. 1905–1908. ISSN: 0036-8075, 1095-9203. DOI: 10.1126/science.283.5409.1905. URL: https://www.science.org/doi/10.1126/science.283.5409.1905 (visited on 03/14/2022).

[105] L. I. Glazman and M. É. Raĭkh. "Resonant Kondo transparency of a barrier with quasilocal impurity states". In: *Soviet Journal of Experimental and Theoretical Physics Letters* 47 (Apr. 1, 1988). ADS Bibcode: 1988JETPL..47..452G, p. 452. ISSN: 0021-3640. URL: https://ui.adsabs.harvard.edu/abs/1988JETPL..47..452G (visited on 10/06/2022).

[106] Tai Kai Ng and Patrick A. Lee. "On-Site Coulomb Repulsion and Resonant Tunneling". In: *Physical Review Letters* 61.15 (Oct. 10, 1988), pp. 1768–1771. ISSN: 0031-9007. DOI: 10.1103/PhysRevLett.61.1768. URL: https://link.aps.org/doi/10.1103/PhysRevLett.61.1768 (visited on 10/06/2022).

[107] D. Goldhaber-Gordon et al. "Kondo effect in a single-electron transistor". In: *Nature* 391.6663 (Jan. 1998), pp. 156–159. ISSN: 0028-0836, 1476-4687. DOI: 10.1038/34373. URL: http://www.nature.com/articles/34373 (visited on 10/06/2022).

[108] Anasua Chatterjee et al. "Semiconductor qubits in practice". In: *Nature Reviews Physics* 3.3 (Mar. 2021), pp. 157–177. ISSN: 2522-5820. DOI: 10.1038/s42254-021-00283-9. URL: http://www.nature.com/articles/s42254-021-00283-9 (visited on 07/28/2022).

[109] John Clarke and Frank K. Wilhelm. "Superconducting quantum bits". In: *Nature* 453.7198 (June 2008), pp. 1031–1042. ISSN: 0028-0836, 1476-4687. DOI: 10.1038/nature07128. URL: http://www.nature.com/articles/nature07128 (visited on 02/14/2023).

[110] Ashley Montanaro. "Quantum algorithms: an overview". In: *npj Quantum Information* 2.1 (Jan. 12, 2016), p. 15023. ISSN: 2056-6387. DOI: 10.1038/npjqi.2015.23. URL: https://www.nature.com/articles/npjqi201523 (visited on 02/14/2023).

[111] G Wendin. "Quantum information processing with superconducting circuits: a review". In: *Reports on Progress in Physics* 80.10 (Oct. 1, 2017), p. 106001. ISSN: 0034-4885, 1361-6633. DOI: 10.1088/1361-6633/aa7e1a. URL: https://iopscience.iop.org/article/10.1088/1361-6633/aa7e1a (visited on 02/14/2023).

[112] Jukka P. Pekola and Bayan Karimi. "*Colloquium* : Quantum heat transport in condensed matter systems". In: *Reviews of Modern Physics* 93.4 (Oct. 5, 2021), p. 041001. ISSN: 0034-6861, 1539-0756. DOI: 10.1103/RevModPhys.93.041001. URL: https://link.aps.org/doi/10.1103/RevModPhys.93.041001 (visited on 03/05/2023).

[113] Liliana Arrachea. "Energy dynamics, heat production and heat–work conversion with qubits: toward the development of quantum machines". In: *Reports on Progress in Physics* 86.3 (Mar. 1, 2023), p. 036501. ISSN: 0034-4885, 1361-6633. DOI: 10.1088/1361-6633/acb06b. URL: https://iopscience.iop.org/article/10.1088/1361-6633/acb06b (visited on 03/05/2023).

[114] Andrew Guthrie et al. "Cooper-Pair Box Coupled to Two Resonators: An Architecture for a Quantum Refrigerator". In: *Physical Review Applied* 17.6 (June 10, 2022), p. 064022. ISSN: 2331-7019. DOI: 10.1103/PhysRevApplied.17.064022. URL: https://link.aps.org/doi/10.1103/PhysRevApplied.17.064022 (visited on 02/14/2023).

[115] Morten Kjaergaard et al. "Superconducting Qubits: Current State of Play". In: *Annual Review of Condensed Matter Physics* 11.1 (Mar. 10, 2020), pp. 369–395. ISSN: 1947-5454, 1947-5462. DOI: 10.1146/annurev-conmatphys-031119-050605. URL: https://www.annualreviews.org/doi/10.1146/annurev-conmatphys-031119-050605 (visited on 02/14/2023).

[116] Y. Nakamura, Yu. A. Pashkin, and J. S. Tsai. "Coherent control of macroscopic quantum states in a single-Cooper-pair box". In: *Nature* 398.6730 (Apr. 1999), pp. 786–788. ISSN: 0028-0836, 1476-4687. DOI: 10.1038/19718. URL: https://www.nature.com/articles/19718 (visited on 02/14/2023).

[117] J. E. Mooij et al. "Josephson Persistent-Current Qubit". In: *Science* 285.5430 (Aug. 13, 1999), pp. 1036–1039. ISSN: 0036-8075, 1095-9203. DOI: 10.1126/science.285.5430.1036. URL: https://www.science.org/doi/10.1126/science.285.5430.1036 (visited on 02/14/2023).

[118] T. P. Orlando et al. "Superconducting persistent-current qubit". In: *Physical Review B* 60.22 (Dec. 1, 1999), pp. 15398–15413. ISSN: 0163-1829, 1095-3795. DOI: 10.1103/PhysRevB.60.15398. URL: https://link.aps.org/doi/10.1103/PhysRevB.60.15398 (visited on 02/14/2023).

[119] Heinz-Peter Breuer and Francesco Petruccione. *The Theory of Open Quantum Systems*. Oxford University Press, Jan. 25, 2007. ISBN: 978-0-19-921390-0. DOI: 10.1093/acprof:oso/9780199213900.001.0001. URL: https://oxford.universitypressscholarship.com/view/10.1093/acprof:oso/9780199213900.001.0001/acprof-9780199213900 (visited on 07/28/2022).

[120] Marco Cattaneo et al. "Local versus global master equation with common and separate baths: superiority of the global approach in partial secular approximation". In: *New Journal of Physics* 21.11 (Nov. 1, 2019), p. 113045. ISSN: 1367-2630. DOI: 10.1088/1367-2630/ab54ac. URL: https://iopscience.iop.org/article/10.1088/1367-2630/ab54ac (visited on 08/03/2022).

[121] M. Büttiker, A. Prêtre, and H. Thomas. "Dynamic conductance and the scattering matrix of small conductors". In: *Physical Review Letters* 70.26 (June 28, 1993), pp. 4114–4117. ISSN: 0031-9007. DOI: 10.1103/PhysRevLett.70.4114. URL: https://link.aps.org/doi/10.1103/PhysRevLett.70.4114 (visited on 08/18/2021).

[122] M. Büttiker, H. Thomas, and A. Prêtre. "Mesoscopic capacitors". In: *Physics Letters A* 180.4 (Sept. 1993), pp. 364–369. ISSN: 03759601. DOI: 10.1016/0375-9601(93)91193-9. URL: https://linkinghub.elsevier.com/retrieve/pii/0375960193911939 (visited on 10/01/2022).

[123] A. Prêtre, H. Thomas, and M. Büttiker. "Dynamic admittance of mesoscopic conductors: Discrete-potential model". In: *Physical Review B* 54.11 (Sept. 15, 1996), pp. 8130–8143. ISSN: 0163-1829, 1095-3795. DOI: 10.1103/PhysRevB.54.8130. URL: https://link.aps.org/doi/10.1103/PhysRevB.54.8130 (visited on 08/18/2021).

[124] Julien Gabelli et al. "Violation of Kirchhoff's Laws for a Coherent RC Circuit". In: *Science* 313.5786 (July 28, 2006), pp. 499–502. ISSN: 0036-8075, 1095-9203. DOI: 10.1126/science.1126940. arXiv: cond-mat/0610572. URL: http://arxiv.org/abs/cond-mat/0610572 (visited on 08/18/2021).

[125] Gwendal Fève et al. "An On-Demand Coherent Single Electron Source". In: *Science* 316.5828 (May 25, 2007), pp. 1169–1172. ISSN: 0036-8075, 1095-9203. DOI: 10.1126/science.1141243. arXiv: 0705.4394. URL: http://arxiv.org/abs/0705.4394 (visited on 08/18/2021).

[126] J Gabelli et al. "A coherent *RC* circuit". In: *Reports on Progress in Physics* 75.12 (Dec. 1, 2012), p. 126504. ISSN: 0034-4885, 1361-6633. DOI: 10.1088/0034-4885/75/12/126504. URL: https://iopscience.iop.org/article/10.1088/0034-4885/75/12/126504 (visited on 08/18/2021).

[127] F. D. Parmentier et al. "Current noise spectrum of a single-particle emitter: Theory and experiment". In: *Physical Review B* 85.16 (Apr. 23, 2012), p. 165438. ISSN: 1098-0121, 1550-235X. DOI: 10.1103/PhysRevB.85.165438. URL: https://link.aps.org/doi/10.1103/PhysRevB.85.165438 (visited on 08/18/2021).

[128] Zohar Ringel, Y. Imry, and O. Entin-Wohlman. "Delayed currents and interaction effects in mesoscopic capacitors". In: *Physical Review B* 78.16 (Oct. 6, 2008), p. 165304. ISSN: 1098-0121, 1550-235X. DOI: 10.1103/PhysRevB.78.165304. URL: https://link.aps.org/doi/10.1103/PhysRevB.78.165304 (visited on 08/18/2021).

[129] Christophe Mora and Karyn Le Hur. "Universal resistances of the quantum resistance–capacitance circuit". In: *Nature Physics* 6.9 (Sept. 2010), pp. 697–701. ISSN: 1745-2473, 1745-2481. DOI: 10.1038/nphys1690. URL: http://www.nature.com/articles/nphys1690 (visited on 08/18/2021).

[130] Yuji Hamamoto et al. "Dynamic response of a mesoscopic capacitor in the presence of strong electron interactions". In: *Physical Review B* 81.15 (Apr. 22, 2010), p. 153305. ISSN: 1098-0121, 1550-235X. DOI: 10.1103/PhysRevB.81.153305. URL: https://link.aps.org/doi/10.1103/PhysRevB.81.153305 (visited on 08/18/2021).

[131] Minchul Lee et al. "Effect of many-body correlations on mesoscopic charge relaxation". In: *Physical Review B* 83.20 (May 12, 2011), p. 201304. ISSN: 1098-0121, 1550-235X. DOI: 10.1103/PhysRevB.83.201304. URL: https://link.aps.org/doi/10.1103/PhysRevB.83.201304 (visited on 08/18/2021).

[132] Michele Filippone and Christophe Mora. "Fermi liquid approach to the quantum R C circuit: Renormalization group analysis of the Anderson and Coulomb blockade models". In: *Physical Review B* 86.12 (Sept. 12, 2012), p. 125311. ISSN: 1098-0121, 1550-235X. DOI: 10.1103/PhysRevB.86.125311. URL: https://link.aps.org/doi/10.1103/PhysRevB.86.125311 (visited on 08/27/2021).

[133] Guillem Rosselló, Rosa López, and Jong Soo Lim. "Time-dependent heat flow in interacting quantum conductors". In: *Physical Review B* 92.11 (Sept. 4, 2015), p. 115402. ISSN: 1098-0121, 1550-235X. DOI: 10.1103/PhysRevB.92.115402. URL: https://link.aps.org/doi/10.1103/PhysRevB.92.115402 (visited on 08/27/2021).

[134] Prasenjit Dutt et al. "Strongly correlated dynamics in multichannel quantum RC circuits". In: *Physical Review B* 87.15 (Apr. 18, 2013), p. 155134. ISSN: 1098-0121, 1550-235X. DOI: 10.1103/PhysRevB.87.155134. URL: https://link.aps.org/doi/10.1103/PhysRevB.87.155134 (visited on 08/27/2021).

[135] Oleksiy Kashuba, Herbert Schoeller, and Janine Splettstoesser. "Nonlinear adiabatic response of interacting quantum dots". In: *EPL (Europhysics Letters)* 98.5 (June 1, 2012), p. 57003. ISSN: 0295-5075, 1286-4854. DOI: 10.1209/0295-5075/98/57003. URL: https://iopscience.iop.org/article/10.1209/0295-5075/98/57003 (visited on 08/27/2021).

[136] Michele Filippone, Karyn Le Hur, and Christophe Mora. "Giant Charge Relaxation Resistance in the Anderson Model". In: *Physical Review Letters* 107.17 (Oct. 17, 2011), p. 176601. ISSN: 0031-9007, 1079-7114. DOI: 10.1103/PhysRevLett.107.176601. URL: https://link.aps.org/doi/10.1103/PhysRevLett.107.176601 (visited on 08/27/2021).

[137] Michele Filippone, Karyn Le Hur, and Christophe Mora. "Admittance of the SU(2) and SU(4) Anderson quantum R C circuits". In: *Physical Review B* 88.4 (July 3, 2013), p. 045302. ISSN: 1098-0121, 1550-235X. DOI: 10.1103/PhysRevB.88.045302. URL: https://link.aps.org/doi/10.1103/PhysRevB.88.045302 (visited on 08/27/2021).

[138] M. Moskalets, P. Samuelsson, and M. Büttiker. "Quantized Dynamics of a Coherent Capacitor". In: *Physical Review Letters* 100.8 (Feb. 26, 2008), p. 086601. ISSN: 0031-9007, 1079-7114. DOI: 10.1103/PhysRevLett.100.086601. URL: https://link.aps.org/doi/10.1103/PhysRevLett.100.086601 (visited on 08/27/2021).

[139] S. Ol'khovskaya et al. "Shot Noise of a Mesoscopic Two-Particle Collider". In: *Physical Review Letters* 101.16 (Oct. 14, 2008), p. 166802. ISSN: 0031-9007, 1079-7114. DOI: 10.1103/PhysRevLett.101.166802. URL: https://link.aps.org/doi/10.1103/PhysRevLett.101.166802 (visited on 08/27/2021).

[140] Janine Splettstoesser et al. "Electron counting with a two-particle emitter". In: *Physical Review B* 78.20 (Nov. 17, 2008), p. 205110. ISSN: 1098-0121, 1550-235X. DOI: 10.1103/PhysRevB.78.205110. URL: https://link.aps.org/doi/10.1103/PhysRevB.78.205110 (visited on 08/27/2021).

[141] G. Haack, M. Moskalets, and M. Büttiker. "Glauber coherence of single-electron sources". In: *Physical Review B* 87.20 (May 17, 2013), p. 201302. ISSN: 1098-0121, 1550-235X. DOI: 10.1103/PhysRevB.87.201302. URL: https://link.aps.org/doi/10.1103/PhysRevB.87.201302 (visited on 08/27/2021).

[142] Michael Moskalets, Géraldine Haack, and Markus Büttiker. "Single-electron source: Adiabatic versus nonadiabatic emission". In: *Physical Review B* 87.12 (Mar. 29, 2013), p. 125429. ISSN: 1098-0121, 1550-235X. DOI: 10.1103/PhysRevB.87.125429. URL: https://link.aps.org/doi/10.1103/PhysRevB.87.125429 (visited on 08/27/2021).

[143] María Florencia Ludovico et al. "Dynamical energy transfer in ac-driven quantum systems". In: *Physical Review B* 89.16 (Apr. 21, 2014), p. 161306. ISSN: 1098-0121, 1550-235X. DOI: 10.1103/PhysRevB.89.161306. URL: https://link.aps.org/doi/10.1103/PhysRevB.89.161306 (visited on 08/27/2021).

[144] María Florencia Ludovico et al. "Dynamics of energy transport and entropy production in ac-driven quantum electron systems". In: *Physical Review B* 94.3 (July 21, 2016), p. 035436. ISSN: 2469-9950, 2469-9969. DOI: 10.1103/PhysRevB.94.035436. URL: https://link.aps.org/doi/10.1103/PhysRevB.94.035436 (visited on 08/17/2021).

[145] María Ludovico et al. "Periodic Energy Transport and Entropy Production in Quantum Electronics". In: *Entropy* 18.11 (Nov. 23, 2016), p. 419. ISSN: 1099-4300. DOI: 10.3390/e18110419. URL: http://www.mdpi.com/1099-4300/18/11/419 (visited on 08/27/2021).

[146] J. Keeling, A. V. Shytov, and L. S. Levitov. "Coherent Particle Transfer in an On-Demand Single-Electron Source". In: *Physical Review Letters* 101.19 (Nov. 7, 2008), p. 196404. ISSN: 0031-9007, 1079-7114. DOI: 10.1103/PhysRevLett.101.196404. URL: https://link.aps.org/doi/10.1103/PhysRevLett.101.196404 (visited on 08/27/2021).

[147] Daniel Litinski, Piet W. Brouwer, and Michele Filippone. "Interacting mesoscopic capacitor out of equilibrium". In: *Physical Review B* 96.8 (Aug. 21, 2017), p. 085429. ISSN: 2469-9950, 2469-9969. DOI: 10.1103/PhysRevB.96.085429. URL: https://link.aps.org/doi/10.1103/PhysRevB.96.085429 (visited on 08/27/2021).

[148] M. I. Alomar, Jong Soo Lim, and David Sánchez. "Coulomb-blockade effect in nonlinear mesoscopic capacitors". In: *Physical Review B* 94.16 (Oct. 19, 2016), p. 165425. ISSN: 2469-9950, 2469-9969. DOI: 10.1103/PhysRevB.94.165425. URL: https://link.aps.org/doi/10.1103/PhysRevB.94.165425 (visited on 08/27/2021).

[149] Javier I. Romero et al. "Nonlinear charge and energy dynamics of an adiabatically driven interacting quantum dot". In: *Physical Review B* 95.23 (June 8, 2017), p. 235117. ISSN: 2469-9950, 2469-9969. DOI: 10.1103/PhysRevB.95.235117. URL: http://link.aps.org/doi/10.1103/PhysRevB.95.235117 (visited on 08/27/2021).

[150] D. J. Thouless. "Quantization of particle transport". In: *Physical Review B* 27.10 (May 15, 1983), pp. 6083–6087. ISSN: 0163-1829. DOI: 10.1103/PhysRevB.27.6083. URL: https://link.aps.org/doi/10.1103/PhysRevB.27.6083 (visited on 08/17/2021).

[151] B. Spivak, F. Zhou, and M. T. Beal Monod. "Mesoscopic mechanisms of the photovoltaic effect and microwave absorption in granular metals". In: *Physical Review B* 51.19 (May 15, 1995), pp. 13226–13230. ISSN: 0163-1829, 1095-3795. DOI: 10.1103/PhysRevB.51.13226. URL: https://link.aps.org/doi/10.1103/PhysRevB.51.13226 (visited on 03/04/2022).

[152] H. Pothier et al. "Single electron pump fabricated with ultrasmall normal tunnel junctions". In: *Physica B: Condensed Matter* 169.1 (Feb. 1991), pp. 573–574. ISSN: 09214526. DOI: 10.1016/0921-4526(91)90332-9. URL: https://linkinghub.elsevier.com/retrieve/pii/0921452691903329 (visited on 03/14/2022).

[153] P. W. Brouwer. "Rectification of displacement currents in an adiabatic electron pump". In: *Physical Review B* 63.12 (Mar. 5, 2001), p. 121303. ISSN: 0163-1829, 1095-3795. DOI: 10.1103/PhysRevB.63.121303. URL: https://link.aps.org/doi/10.1103/PhysRevB.63.121303 (visited on 03/14/2022).

[154] Joseph E. Avron, Daniel Osadchy, and Ruedi Seiler. "A Topological Look at the Quantum Hall Effect". In: *Physics Today* 56.8 (Aug. 2003), pp. 38–42. ISSN: 0031-9228, 1945-0699. DOI: 10.1063/1.1611351. URL: http://physicstoday.scitation.org/doi/10.1063/1.1611351 (visited on 08/17/2021).

[155] Di Xiao, Ming-Che Chang, and Qian Niu. "Berry phase effects on electronic properties". In: *Reviews of Modern Physics* 82.3 (July 6, 2010), pp. 1959–2007. ISSN: 0034-6861, 1539-0756. DOI: 10.1103/RevModPhys.82.1959. URL: https://link.aps.org/doi/10.1103/RevModPhys.82.1959 (visited on 08/17/2021).

[156] Liliana Arrachea. "Energy dynamics, heat production and heat-work conversion with qubits: towards the development of quantum machines". In: (2022). Publisher: arXiv Version Number: 1. DOI: 10.48550/ARXIV.2205.14200. URL: https://arxiv.org/abs/2205.14200 (visited on 08/23/2022).

[157] T. Schmiedl and U. Seifert. "Efficiency at maximum power: An analytically solvable model for stochastic heat engines". In: *EPL (Europhysics Letters)* 81.2 (Jan. 2008), p. 20003. ISSN: 0295-5075, 1286-4854. DOI: 10.1209/0295-5075/81/20003. URL: https://iopscience.iop.org/article/10.1209/0295-5075/81/20003 (visited on 02/16/2022).

[158] Ronnie Kosloff and Yair Rezek. "The Quantum Harmonic Otto Cycle". In: *Entropy* 19.4 (Mar. 23, 2017), p. 136. ISSN: 1099-4300. DOI: 10.3390/e19040136. URL: http://www.mdpi.com/1099-4300/19/4/136 (visited on 02/11/2022).

[159] Paolo Abiuso and Vittorio Giovannetti. "Non-Markov enhancement of maximum power for quantum thermal machines". In: *Physical Review A* 99.5 (May 6, 2019), p. 052106. ISSN: 2469-9926, 2469-9934. DOI: 10.1103/PhysRevA.99.052106. URL: https://link.aps.org/doi/10.1103/PhysRevA.99.052106 (visited on 02/16/2022).

[160] Vasco Cavina et al. "Maximum-power heat engines and refrigerators in the fast-driving regime". In: *Physical Review A* 104.3 (Sept. 30, 2021), p. 032226. ISSN: 2469-9926, 2469-9934. DOI: 10.1103/PhysRevA.104.032226. URL: https://link.aps.org/doi/10.1103/PhysRevA.104.032226 (visited on 02/16/2022).

[161] Bibek Bhandari et al. "Geometric properties of adiabatic quantum thermal machines". In: *Physical Review B* 102.15 (Oct. 8, 2020), p. 155407. ISSN: 2469-9950, 2469-9969. DOI: 10.1103/PhysRevB.102.155407. URL: https://link.aps.org/doi/10.1103/PhysRevB.102.155407 (visited on 02/16/2022).

[162] Ronnie Kosloff. "A quantum mechanical open system as a model of a heat engine". In: *The Journal of Chemical Physics* 80.4 (Feb. 15, 1984), pp. 1625–1631. ISSN: 0021-9606, 1089-7690. DOI: 10.1063/1.446862. URL: http://aip.scitation.org/doi/10.1063/1.446862 (visited on 08/17/2021).

[163] Tova Feldmann and Ronnie Kosloff. "Performance of discrete heat engines and heat pumps in finite time". In: *Physical Review E* 61.5 (May 1, 2000), pp. 4774–4790. ISSN: 1063-651X, 1095-3787. DOI: 10.1103/PhysRevE.61.4774. URL: https://link.aps.org/doi/10.1103/PhysRevE.61.4774 (visited on 08/17/2021).

[164] Marlan O. Scully. "Quantum Afterburner: Improving the Efficiency of an Ideal Heat Engine". In: *Physical Review Letters* 88.5 (Jan. 23, 2002), p. 050602. ISSN: 0031-9007, 1079-7114. DOI: 10.1103/PhysRevLett.88.050602. URL: https://link.aps.org/doi/10.1103/PhysRevLett.88.050602 (visited on 08/17/2021).

[165] Bihong Lin and Jincan Chen. "Performance analysis of an irreversible quantum heat engine working with harmonic oscillators". In: *Physical Review E* 67.4 (Apr. 11, 2003), p. 046105. ISSN: 1063-651X, 1095-3787. DOI: 10.1103/PhysRevE.67.046105. URL: https://link.aps.org/doi/10.1103/PhysRevE.67.046105 (visited on 08/17/2021).

[166] Tien D. Kieu. "The Second Law, Maxwell's Demon, and Work Derivable from Quantum Heat Engines". In: *Physical Review Letters* 93.14 (Sept. 29, 2004), p. 140403. ISSN: 0031-9007, 1079-7114. DOI: 10.1103/PhysRevLett.93.140403. URL: https://link.aps.org/doi/10.1103/PhysRevLett.93.140403 (visited on 08/17/2021).

[167] Yair Rezek and Ronnie Kosloff. "Irreversible performance of a quantum harmonic heat engine". In: *New Journal of Physics* 8.5 (May 31, 2006), pp. 83–83. ISSN: 1367-2630. DOI: 10.1088/1367-2630/8/5/083. URL: https://iopscience.iop.org/article/10.1088/1367-2630/8/5/083 (visited on 08/17/2021).

[168] H. T. Quan et al. "Quantum thermodynamic cycles and quantum heat engines". In: *Physical Review E* 76.3 (Sept. 7, 2007), p. 031105. ISSN: 1539-3755, 1550-2376. DOI: 10.1103/PhysRevE.76.031105. URL: https://link.aps.org/doi/10.1103/PhysRevE.76.031105 (visited on 08/17/2021).

[169] M. J. Henrich, F. Rempp, and G. Mahler. "Quantum thermodynamic Otto machines: A spin-system approach". In: *The European Physical Journal Special Topics* 151.1 (Dec. 2007), pp. 157–165. ISSN: 1951-6355, 1951-6401. DOI: 10.1140/epjst/e2007-00371-8. URL: http://link.springer.com/10.1140/epjst/e2007-00371-8 (visited on 08/17/2021).

[170] JiZhou He, Xian He, and Wei Tang. "The performance characteristics of an irreversible quantum Otto harmonic refrigeration cycle". In: *Science in China Series G: Physics, Mechanics and Astronomy* 52.9 (Sept. 2009), pp. 1317–1323. ISSN: 1672-1799, 1862-2844. DOI: 10.1007/s11433-009-0169-z. URL: http://link.springer.com/10.1007/s11433-009-0169-z (visited on 08/17/2021).

[171] A. del Campo, J. Goold, and M. Paternostro. "More bang for your buck: Super-adiabatic quantum engines". In: *Scientific Reports* 4.1 (May 2015), p. 6208. ISSN: 2045-2322. DOI: 10.1038/srep06208. URL: http://www.nature.com/articles/srep06208 (visited on 08/17/2021).

[172] A Alecce et al. "Quantum Otto cycle with inner friction: finite-time and disorder effects". In: *New Journal of Physics* 17.7 (July 9, 2015), p. 075007. ISSN: 1367-2630. DOI: 10.1088/1367-2630/17/7/075007. URL: https://iopscience.iop.org/article/10.1088/1367-2630/17/7/075007 (visited on 08/17/2021).

[173] Bruno Leggio and Mauro Antezza. "Otto engine beyond its standard quantum limit". In: *Physical Review E* 93.2 (Feb. 16, 2016), p. 022122. ISSN: 2470-0045, 2470-0053. DOI: 10.1103/PhysRevE.93.022122. URL: https://link.aps.org/doi/10.1103/PhysRevE.93.022122 (visited on 08/17/2021).

[174] B. Karimi and J. P. Pekola. "Otto refrigerator based on a superconducting qubit: Classical and quantum performance". In: *Physical Review B* 94.18 (Nov. 9, 2016), p. 184503. ISSN: 2469-9950, 2469-9969. DOI: 10.1103/PhysRevB.94.184503. URL: https://link.aps.org/doi/10.1103/PhysRevB.94.184503 (visited on 08/17/2021).

[175] Gentaro Watanabe et al. "Quantum Performance of Thermal Machines over Many Cycles". In: *Physical Review Letters* 118.5 (Feb. 2, 2017), p. 050601. ISSN: 0031-9007, 1079-7114. DOI: 10.1103/PhysRevLett.118.050601. URL: https://link.aps.org/doi/10.1103/PhysRevLett.118.050601 (visited on 08/17/2021).

[176] Michele Campisi and Rosario Fazio. "The power of a critical heat engine". In: *Nature Communications* 7.1 (Sept. 2016), p. 11895. ISSN: 2041-1723. DOI: 10.1038/ncomms11895. URL: http://www.nature.com/articles/ncomms11895 (visited on 08/17/2021).

[177] Andrea Solfanelli, Marco Falsetti, and Michele Campisi. "Nonadiabatic single-qubit quantum Otto engine". In: *Physical Review B* 101.5 (Feb. 25, 2020), p. 054513. ISSN: 2469-9950, 2469-9969. DOI: 10.1103/PhysRevB.101.054513. URL: https://link.aps.org/doi/10.1103/PhysRevB.101.054513 (visited on 02/11/2022).

[178] Jong-Min Park et al. "Quantum mechanical bound for efficiency of quantum Otto heat engine". In: *Physical Review E* 100.1 (July 30, 2019), p. 012148. ISSN: 2470-0045, 2470-0053. DOI: 10.1103/PhysRevE.100.012148. URL: https://link.aps.org/doi/10.1103/PhysRevE.100.012148 (visited on 08/17/2021).

[179] D. von Lindenfels et al. "Spin Heat Engine Coupled to a Harmonic-Oscillator Flywheel". In: *Physical Review Letters* 123.8 (Aug. 22, 2019), p. 080602. ISSN: 0031-9007, 1079-7114. DOI: 10.1103/PhysRevLett.123.080602. URL: https://link.aps.org/doi/10.1103/PhysRevLett.123.080602 (visited on 02/10/2022).

[180] R Gallego, A Riera, and J Eisert. "Thermal machines beyond the weak coupling regime". In: *New Journal of Physics* 16.12 (Dec. 10, 2014), p. 125009. ISSN: 1367-2630. DOI: 10.1088/1367-2630/16/12/125009. URL: https://iopscience.iop.org/article/10.1088/1367-2630/16/12/125009 (visited on 08/17/2021).

[181] Sai Vinjanampathy and Janet Anders. "Quantum thermodynamics". In: *Contemporary Physics* 57.4 (Oct. 2016), pp. 545–579. ISSN: 0010-7514, 1366-5812. DOI: 10.1080/00107514.2016.1201896. URL: https://www.tandfonline.com/doi/full/10.1080/00107514.2016.1201896 (visited on 08/17/2021).

[182] José P. Palao, Ronnie Kosloff, and Jeffrey M. Gordon. "Quantum thermodynamic cooling cycle". In: *Physical Review E* 64.5 (Oct. 30, 2001), p. 056130. ISSN: 1063-651X, 1095-3787. DOI: 10.1103/PhysRevE.64.056130. URL: https://link.aps.org/doi/10.1103/PhysRevE.64.056130 (visited on 02/16/2022).

[183] M. Youssef, G. Mahler, and A.-S. F. Obada. "Quantum optical thermodynamic machines: Lasing as relaxation". In: *Physical Review E* 80.6 (Dec. 23, 2009), p. 061129. ISSN: 1539-3755, 1550-2376. DOI: 10.1103/PhysRevE.80.061129. URL: https://link.aps.org/doi/10.1103/PhysRevE.80.061129 (visited on 02/16/2022).

[184] Nicolas Brunner et al. "Virtual qubits, virtual temperatures, and the foundations of thermodynamics". In: *Physical Review E* 85.5 (May 14, 2012), p. 051117. ISSN: 1539-3755, 1550-2376. DOI: 10.1103/PhysRevE.85.051117. URL: https://link.aps.org/doi/10.1103/PhysRevE.85.051117 (visited on 02/16/2022).

[185] Raam Uzdin, Amikam Levy, and Ronnie Kosloff. "Equivalence of Quantum Heat Machines, and Quantum-Thermodynamic Signatures". In: *Physical Review X* 5.3 (Sept. 29, 2015), p. 031044. ISSN: 2160-3308. DOI: 10.1103/PhysRevX.5.031044. URL: https://link.aps.org/doi/10.1103/PhysRevX.5.031044 (visited on 08/17/2021).

[186] Kay Brandner, Keiji Saito, and Udo Seifert. "Thermodynamics of Micro- and Nano-Systems Driven by Periodic Temperature Variations". In: *Physical Review X* 5.3 (Aug. 19, 2015), p. 031019. ISSN: 2160-3308. DOI: 10.1103/PhysRevX.5.031019. URL: https://link.aps.org/doi/10.1103/PhysRevX.5.031019 (visited on 08/17/2021).

[187] J. Onam González et al. "Classical emulation of quantum-coherent thermal machines". In: *Physical Review E* 99.6 (June 3, 2019), p. 062102. ISSN: 2470-0045, 2470-0053. DOI: 10.1103/PhysRevE.99.062102. URL: https://link.aps.org/doi/10.1103/PhysRevE.99.062102 (visited on 02/11/2022).

[188] Francesco Campaioli et al. "Enhancing the Charging Power of Quantum Batteries". In: *Physical Review Letters* 118.15 (Apr. 12, 2017), p. 150601. ISSN: 0031-9007, 1079-7114. DOI: 10.1103/PhysRevLett.118.150601. URL: http://link.aps.org/doi/10.1103/PhysRevLett.118.150601 (visited on 08/17/2021).

[189] Felipe Barra. "Dissipative Charging of a Quantum Battery". In: *Physical Review Letters* 122.21 (May 30, 2019), p. 210601. ISSN: 0031-9007, 1079-7114. DOI: 10.1103/PhysRevLett.122.210601. URL: https://link.aps.org/doi/10.1103/PhysRevLett.122.210601 (visited on 08/17/2021).

[190] J. M. Luttinger. "Theory of Thermal Transport Coefficients". In: *Physical Review* 135.6 (Sept. 14, 1964), A1505–A1514. ISSN: 0031-899X. DOI: 10.1103/PhysRev.135.A1505. URL: https://link.aps.org/doi/10.1103/PhysRev.135.A1505 (visited on 08/17/2021).

[191] Gen Tatara. "Thermal Vector Potential Theory of Transport Induced by a Temperature Gradient". In: *Physical Review Letters* 114.19 (May 14, 2015), p. 196601. ISSN: 0031-9007, 1079-7114. DOI: 10.1103/PhysRevLett.114.196601. URL: https://link.aps.org/doi/10.1103/PhysRevLett.114.196601 (visited on 08/17/2021).

[192] Henrik Bruus and Karsten Flensberg. *Many-body quantum theory in condensed matter physics: an introduction*. Oxford graduate texts. OCLC: ocm56694794. Oxford ; New York: Oxford University Press, 2004. 435 pp. ISBN: 978-0-19-856633-5.

[193] Vasco Cavina, Andrea Mari, and Vittorio Giovannetti. "Slow Dynamics and Thermodynamics of Open Quantum Systems". In: *Physical Review Letters* 119.5 (Aug. 2, 2017), p. 050601. ISSN: 0031-9007, 1079-7114. DOI: 10.1103/PhysRevLett.119.050601. URL: http://link.aps.org/doi/10.1103/PhysRevLett.119.050601 (visited on 08/17/2021).

[194] Doron Cohen. "Quantum pumping in closed systems, adiabatic transport, and the Kubo formula". In: *Physical Review B* 68.15 (Oct. 3, 2003), p. 155303. ISSN: 0163-1829, 1095-3795. DOI: 10.1103/PhysRevB.68.155303. URL: https://link.aps.org/doi/10.1103/PhysRevB.68.155303 (visited on 08/17/2021).

[195] Alex Kamenev. *Field Theory of Non-Equilibrium Systems*. 1st ed. Cambridge University Press, Sept. 8, 2011. ISBN: 978-0-521-76082-9 978-1-139-00366-7. DOI: 10.1017/CBO9781139003667. URL: https://www.cambridge.org/core/product/identifier/9781139003667/type/book (visited on 03/06/2023).

[196] Gianluca Stefanucci and Robert van Leeuwen. *Nonequilibrium Many-Body Theory of Quantum Systems: A Modern Introduction*. 1st ed. Cambridge University Press, Mar. 7, 2013. ISBN: 978-0-521-76617-3 978-1-139-02397-9. DOI: 10.1017/CBO9781139023979. URL: https://www.cambridge.org/core/product/identifier/9781139023979/type/book (visited on 03/06/2023).

[197] Liliana Arrachea and Michael Moskalets. "Relation between scattering-matrix and Keldysh formalisms for quantum transport driven by time-periodic fields". In: *Physical Review B* 74.24 (Dec. 19, 2006), p. 245322. ISSN: 1098-0121, 1550-235X. DOI: 10.1103/PhysRevB.74.245322. URL: https://link.aps.org/doi/10.1103/PhysRevB.74.245322 (visited on 02/17/2022).

[198] M. Moskalets and M. Büttiker. "Floquet scattering theory of quantum pumps". In: *Physical Review B* 66.20 (Nov. 26, 2002), p. 205320. ISSN: 0163-1829, 1095-3795. DOI: 10.1103/PhysRevB.66.205320. URL: https://link.aps.org/doi/10.1103/PhysRevB.66.205320 (visited on 08/18/2021).

[199] M. Moskalets and M. Büttiker. "Floquet scattering theory for current and heat noise in large amplitude adiabatic pumps". In: *Physical Review B* 70.24 (Dec. 6, 2004), p. 245305. ISSN: 1098-0121, 1550-235X. DOI: 10.1103/PhysRevB.70.245305. URL: https://link.aps.org/doi/10.1103/PhysRevB.70.245305 (visited on 08/17/2021).

[200] Michael V Moskalets. *Scattering Matrix Approach to Non-Stationary Quantum Transport*. IMPERIAL COLLEGE PRESS, Sept. 2011. ISBN: 978-1-84816-834-3 978-1-84816-835-0. DOI: 10.1142/p822. URL: https://www.worldscientific.com/worldscibooks/10.1142/p822 (visited on 08/18/2021).

[201] Ralf Bulla, Theo A. Costi, and Thomas Pruschke. "Numerical renormalization group method for quantum impurity systems". In: *Reviews of Modern Physics* 80.2 (Apr. 2, 2008), pp. 395–450. ISSN: 0034-6861, 1539-0756. DOI: 10.1103/RevModPhys.80.395. URL: https://link.aps.org/doi/10.1103/RevModPhys.80.395 (visited on 04/21/2022).

[202] Kenneth G. Wilson. "The renormalization group: Critical phenomena and the Kondo problem". In: *Reviews of Modern Physics* 47.4 (Oct. 1, 1975), pp. 773–840. ISSN: 0034-6861. DOI: 10.1103/RevModPhys.47.773. URL: https://link.aps.org/doi/10.1103/RevModPhys.47.773 (visited on 04/21/2022).

[203] H. Krishna-murthy, J. Wilkins, and K. Wilson. "Renormalization-group approach to the Anderson model of dilute magnetic alloys. I. Static properties for the symmetric case". In: *Physical Review B* 21.3 (Feb. 1980), pp. 1003–1043. ISSN: 0163-1829. DOI: 10.1103/PhysRevB.21.1003. URL: https://link.aps.org/doi/10.1103/PhysRevB.21.1003 (visited on 04/21/2022).

[204] R Bulla, Th Pruschke, and A C Hewson. "Anderson impurity in pseudo-gap Fermi systems". In: *Journal of Physics: Condensed Matter* 9.47 (Nov. 24, 1997), pp. 10463–10474. ISSN: 0953-8984, 1361-648X. DOI: 10.1088/0953-8984/9/47/014. URL: https://iopscience.iop.org/article/10.1088/0953-8984/9/47/014 (visited on 04/21/2022).

[205] Rok Žitko and Thomas Pruschke. "Energy resolution and discretization artifacts in the numerical renormalization group". In: *Physical Review B* 79.8 (Feb. 11, 2009), p. 085106. ISSN: 1098-0121, 1550-235X. DOI: 10.1103/PhysRevB.79.085106. URL: https://link.aps.org/doi/10.1103/PhysRevB.79.085106 (visited on 03/16/2023).

[206] Axel Freyn and Serge Florens. "Optimal broadening of finite energy spectra in the numerical renormalization group: Application to dissipative dynamics in two-level systems". In: *Physical Review B* 79.12 (Mar. 19, 2009), p. 121102. ISSN: 1098-0121, 1550-235X. DOI: 10.1103/PhysRevB.79.121102. URL: https://link.aps.org/doi/10.1103/PhysRevB.79.121102 (visited on 03/16/2023).

[207] Roman-Pascal Riwar and Janine Splettstoesser. "Charge and spin pumping through a double quantum dot". In: *Physical Review B* 82.20 (Nov. 8, 2010), p. 205308. ISSN: 1098-0121, 1550-235X. DOI: 10.1103/PhysRevB.82.205308. URL: https://link.aps.org/doi/10.1103/PhysRevB.82.205308 (visited on 08/17/2021).

[208] Liliana Arrachea and Rosa López. "Anomalous Joule law in the adiabatic dynamics of a quantum dot in contact with normal-metal and superconducting reservoirs". In: *Physical Review B* 98.4 (July 5, 2018), p. 045404. ISSN: 2469-9950, 2469-9969. DOI: 10.1103/PhysRevB.98.045404. URL: https://link.aps.org/doi/10.1103/PhysRevB.98.045404 (visited on 08/27/2021).

[209] H. Shiba. "The Korringa Relation for the Impurity Nuclear Spin-Lattice Relaxation in Dilute Kondo Alloys". In: *Progress of Theoretical Physics* 54.4 (Oct. 1, 1975), pp. 967–981. ISSN: 0033-068X, 1347-4081. DOI: 10.1143/PTP.54.967. URL: https://academic.oup.com/ptp/article-lookup/doi/10.1143/PTP.54.967 (visited on 08/27/2021).

[210] Massimiliano Esposito, Maicol A. Ochoa, and Michael Galperin. "Quantum Thermodynamics: A Nonequilibrium Green's Function Approach". In: *Physical Review Letters* 114.8 (Feb. 25, 2015), p. 080602. ISSN: 0031-9007, 1079-7114. DOI: 10.1103/PhysRevLett.114.080602. URL: https://link.aps.org/doi/10.1103/PhysRevLett.114.080602 (visited on 08/27/2021).

[211] Anton Bruch et al. "Quantum thermodynamics of the driven resonant level model". In: *Physical Review B* 93.11 (Mar. 30, 2016), p. 115318. ISSN: 2469-9950, 2469-9969. DOI: 10.1103/PhysRevB.93.115318. URL: https://link.aps.org/doi/10.1103/PhysRevB.93.115318 (visited on 08/27/2021).

[212] Patrick Haughian, Massimiliano Esposito, and Thomas L. Schmidt. "Quantum thermodynamics of the resonant-level model with driven system-bath coupling". In: *Physical Review B* 97.8 (Feb. 26, 2018), p. 085435. ISSN: 2469-9950, 2469-9969. DOI: 10.1103/PhysRevB.97.085435. URL: https://link.aps.org/doi/10.1103/PhysRevB.97.085435 (visited on 08/27/2021).

[213] María Florencia Ludovico et al. "Probing the energy reactance with adiabatically driven quantum dots". In: *Physical Review B* 97.4 (Jan. 31, 2018), p. 041416. ISSN: 2469-9950, 2469-9969. DOI: 10.1103/PhysRevB.97.041416. URL: https://link.aps.org/doi/10.1103/PhysRevB.97.041416 (visited on 08/27/2021).

[214] F. Covito et al. "Transient Charge and Energy Flow in the Wide-Band Limit". In: *Journal of Chemical Theory and Computation* 14.5 (May 8, 2018), pp. 2495–2504. ISSN: 1549-9618, 1549-9626. DOI: 10.1021/acs.jctc.8b00077. URL: https://pubs.acs.org/doi/10.1021/acs.jctc.8b00077 (visited on 08/27/2021).

[215] Phillip Weinberg et al. "Adiabatic perturbation theory and geometry of periodically-driven systems". In: *Physics Reports* 688 (May 2017), pp. 1–35. ISSN: 03701573. DOI: 10.1016/j.physrep.2017.05.003. URL: https://linkinghub.elsevier.com/retrieve/pii/S0370157317301412 (visited on 08/27/2021).

[216] Raúl A. Bustos-Marún. "Geometric rectification for nanoscale vibrational energy harvesting". In: *Physical Review B* 97.7 (Feb. 12, 2018), p. 075412. ISSN: 2469-9950, 2469-9969. DOI: 10.1103/PhysRevB.97.075412. URL: https://link.aps.org/doi/10.1103/PhysRevB.97.075412 (visited on 08/27/2021).

[217] Ivar Martin, Gil Refael, and Bertrand Halperin. "Topological Frequency Conversion in Strongly Driven Quantum Systems". In: *Physical Review X* 7.4 (Oct. 16, 2017), p. 041008. ISSN: 2160-3308. DOI: 10.1103/PhysRevX.7.041008. URL: https://link.aps.org/doi/10.1103/PhysRevX.7.041008 (visited on 08/27/2021).

[218] Alexander Cyril Hewson. *The Kondo Problem to Heavy Fermions*. 1st ed. Cambridge University Press, Jan. 28, 1993. ISBN: 978-0-521-36382-2 978-0-521-59947-4 978-0-511-47075-2. DOI: 10.1017/CBO9780511470752. URL: https://www.cambridge.org/core/product/identifier/9780511470752/type/book (visited on 08/27/2021).

[219] Rok Zitko. *NRG Ljubljana*. Version 8f90ac4. May 29, 2021. DOI: 10.5281/ZENODO.4841076. URL: https://zenodo.org/record/4841076 (visited on 08/27/2021).

[220] L. D. Landau and E. M. Lifshitz. *Statistical Physics: Volume 5*. 3rd ed. ISBN: 978-0-08-057046-4.

[221] Kerson Huang. *Statistical mechanics*. 2nd ed. New York: Wiley, 1987. 493 pp. ISBN: 978-0-471-81518-1.

[222] Liliana Arrachea, Michael Moskalets, and Luis Martin-Moreno. "Heat production and energy balance in nanoscale engines driven by time-dependent fields". In: *Physical Review B* 75.24 (June 18, 2007), p. 245420. ISSN: 1098-0121, 1550-235X. DOI: 10.1103/PhysRevB.75.245420. URL: https://link.aps.org/doi/10.1103/PhysRevB.75.245420 (visited on 08/17/2021).

[223] Michael Tomka et al. "Geodesic Paths for Quantum Many-Body Systems". In: *arXiv:1606.05890 [cond-mat, physics:quant-ph]* (July 19, 2016). arXiv: 1606.05890. URL: http://arxiv.org/abs/1606.05890 (visited on 02/11/2022).

[224] Michael Kolodrubetz, Vladimir Gritsev, and Anatoli Polkovnikov. "Classifying and measuring geometry of a quantum ground state manifold". In: *Physical Review B* 88.6 (Aug. 19, 2013), p. 064304. ISSN: 1098-0121, 1550-235X. DOI: 10.1103/PhysRevB.88.064304. URL: https://link.aps.org/doi/10.1103/PhysRevB.88.064304 (visited on 08/17/2021).

[225] Raúl Bustos-Marún, Gil Refael, and Felix von Oppen. "Adiabatic Quantum Motors". In: *Physical Review Letters* 111.6 (Aug. 5, 2013), p. 060802. ISSN: 0031-9007, 1079-7114. DOI: 10.1103/PhysRevLett.111.060802. URL: https://link.aps.org/doi/10.1103/PhysRevLett.111.060802 (visited on 08/17/2021).

[226] Liliana Arrachea and Felix von Oppen. "Nanomagnet coupled to quantum spin Hall edge: An adiabatic quantum motor". In: *Physica E: Low-dimensional Systems and Nanostructures* 74 (Nov. 2015), pp. 596–602. ISSN: 13869477. DOI: 10.1016/j.physe.2015.08.031. URL: https://linkinghub.elsevier.com/retrieve/pii/S1386947715301740 (visited on 08/17/2021).

[227] Lucas J. Fernández-Alcázar, Horacio M. Pastawski, and Raúl A. Bustos-Marún. "Dynamics and decoherence in nonideal Thouless quantum motors". In: *Physical Review B* 95.15 (Apr. 7, 2017), p. 155410. ISSN: 2469-9950, 2469-9969. DOI: 10.1103/PhysRevB.95.155410. URL: http://link.aps.org/doi/10.1103/PhysRevB.95.155410 (visited on 08/17/2021).

[228] María Florencia Ludovico and Massimo Capone. "Enhanced performance of a quantum-dot-based nanomotor due to Coulomb interactions". In: *Physical Review B* 98.23 (Dec. 5, 2018), p. 235409. ISSN: 2469-9950, 2469-9969. DOI: 10.1103/PhysRevB.98.235409. URL: https://link.aps.org/doi/10.1103/PhysRevB.98.235409 (visited on 08/17/2021).

[229] Anton Bruch et al. "Interacting adiabatic quantum motor". In: *Physical Review B* 97.19 (May 9, 2018), p. 195411. ISSN: 2469-9950, 2469-9969. DOI: 10.1103/PhysRevB.97.195411. URL: https://link.aps.org/doi/10.1103/PhysRevB.97.195411 (visited on 08/17/2021).

[230] Xiao-Liang Qi, Taylor L. Hughes, and Shou-Cheng Zhang. "Fractional charge and quantized current in the quantum spin Hall state". In: *Nature Physics* 4.4 (Apr. 2008), pp. 273–276. ISSN: 1745-2473, 1745-2481. DOI: 10.1038/nphys913. URL: http://www.nature.com/articles/nphys913 (visited on 08/17/2021).

[231] Niels Bode et al. "Current-induced switching in transport through anisotropic magnetic molecules". In: *Physical Review B* 85.11 (Mar. 27, 2012), p. 115440. ISSN: 1098-0121, 1550-235X. DOI: 10.1103/PhysRevB.85.115440. URL: https://link.aps.org/doi/10.1103/PhysRevB.85.115440 (visited on 08/17/2021).

[232] Qinglei Meng, Smitha Vishveshwara, and Taylor L. Hughes. "Spin-transfer torque and electric current in helical edge states in quantum spin Hall devices". In: *Physical Review B* 90.20 (Nov. 6, 2014), p. 205403. ISSN: 1098-0121, 1550-235X. DOI: 10.1103/PhysRevB.90.205403. URL: https://link.aps.org/doi/10.1103/PhysRevB.90.205403 (visited on 08/17/2021).

[233] Antonio Ros. "The isoperimetric problem". In: *Global theory of minimal surfaces* 2 (2001), pp. 175–209.

[234] Enea Parini. "An introduction to the Cheeger problem". In: *Surveys in Mathematics and its Applications* 6 (2011), pp. 9–21.

[235] Gian Paolo Leonardi. "An Overview on the Cheeger Problem". In: *New Trends in Shape Optimization*. Ed. by Aldo Pratelli and Günter Leugering. Vol. 166. Series Title: International Series of Numerical Mathematics. Cham: Springer International Publishing, 2015, pp. 117–139. ISBN: 978-3-319-17562-1 978-3-319-17563-8. DOI: 10.1007/978-3-319-17563-8_6. URL: http://link.springer.com/10.1007/978-3-319-17563-8_6 (visited on 02/04/2022).

[236] Viktor Blåsjö. "The Isoperimetric Problem". In: *The American Mathematical Monthly* 112.6 (June 2005), pp. 526–566. ISSN: 0002-9890, 1930-0972. DOI: 10.1080/00029890.2005.11920227. URL: https://www.tandfonline.com/doi/full/10.1080/00029890.2005.11920227 (visited on 02/17/2022).

[237] Hugh Howards, Michael Hutchings, and Frank Morgan. "The Isoperimetric Problem on Surfaces". In: *The American Mathematical Monthly* 106.5 (May 1999), pp. 430–439. ISSN: 0002-9890, 1930-0972. DOI: 10.1080/00029890.1999.12005065. URL: https://www.tandfonline.com/doi/full/10.1080/00029890.1999.12005065 (visited on 02/17/2022).

[238] Frank Morgan. "Manifolds with density". In: *Notices of the AMS* 52.8 (2005), pp. 853–858.

[239] César Rosales et al. "On the isoperimetric problem in Euclidean space with density". In: *Calculus of Variations and Partial Differential Equations* 31.1 (Sept. 27, 2007), pp. 27–46. ISSN: 0944-2669, 1432-0835. DOI: 10.1007/s00526-007-0104-y. URL: http://link.springer.com/10.1007/s00526-007-0104-y (visited on 02/17/2022).

[240] Colin Carroll et al. "The isoperimetric problem on planes with density". In: *Bulletin of the Australian Mathematical Society* 78.2 (Oct. 2008), pp. 177–197. ISSN: 0004-9727, 1755-1633. DOI: 10.1017/S000497270800052X. URL: https://www.cambridge.org/core/product/identifier/S000497270800052X/type/journal_article (visited on 02/17/2022).

[241] R. Landauer. "Irreversibility and Heat Generation in the Computing Process". In: *IBM Journal of Research and Development* 5.3 (July 1961), pp. 183–191. ISSN: 0018-8646, 0018-8646. DOI: 10.1147/rd.53.0183. URL: http://ieeexplore.ieee.org/document/5392446/ (visited on 02/17/2022).

[242] Rolf Landauer. "Dissipation and noise immunity in computation and communication". In: *Nature* 335.6193 (Oct. 1988), pp. 779–784. ISSN: 0028-0836, 1476-4687. DOI: 10.1038/335779a0. URL: http://www.nature.com/articles/335779a0 (visited on 02/17/2022).

[243] Antoine Bérut et al. "Experimental verification of Landauer's principle linking information and thermodynamics". In: *Nature* 483.7388 (Mar. 2012), pp. 187–189. ISSN: 0028-0836, 1476-4687. DOI: 10.1038/nature10872. URL: http://www.nature.com/articles/nature10872 (visited on 02/17/2022).

[244] Yonggun Jun, Momčilo Gavrilov, and John Bechhoefer. "High-Precision Test of Landauer's Principle in a Feedback Trap". In: *Physical Review Letters* 113.19 (Nov. 4, 2014), p. 190601. ISSN: 0031-9007, 1079-7114. DOI: 10.1103/PhysRevLett.113.190601. URL: https://link.aps.org/doi/10.1103/PhysRevLett.113.190601 (visited on 02/17/2022).

[245] Fatemeh Hajiloo et al. "Detailed study of nonlinear cooling with two-terminal configurations of topological edge states". In: *Physical Review B* 102.15 (Oct. 30, 2020), p. 155434. ISSN: 2469-9950, 2469-9969. DOI: 10.1103/PhysRevB.102.155434. URL: https://link.aps.org/doi/10.1103/PhysRevB.102.155434 (visited on 02/17/2022).

[246] Juan Herrera Mateos et al. "Thermoelectric cooling properties of a quantum Hall Corbino device". In: *Physical Review B* 103.12 (Mar. 3, 2021), p. 125404. ISSN: 2469-9950, 2469-9969. DOI: 10.1103/PhysRevB.103.125404. URL: https://link.aps.org/doi/10.1103/PhysRevB.103.125404 (visited on 02/17/2022).

[247] Liliana Arrachea. "dc response of a dissipative driven mesoscopic ring". In: *Physical Review B* 70.15 (Oct. 21, 2004), p. 155407. ISSN: 1098-0121, 1550-235X. DOI: 10.1103/PhysRevB.70.155407. URL: https://link.aps.org/doi/10.1103/PhysRevB.70.155407 (visited on 08/27/2021).

[248] Olivier Maillet et al. "Optimal Probabilistic Work Extraction beyond the Free Energy Difference with a Single-Electron Device". In: *Physical Review Letters* 122.15 (Apr. 18, 2019), p. 150604. ISSN: 0031-9007, 1079-7114. DOI: 10.1103/PhysRevLett.122.150604. URL: https://link.aps.org/doi/10.1103/PhysRevLett.122.150604 (visited on 08/27/2021).

[249] Juzar Thingna, Massimiliano Esposito, and Felipe Barra. "Landau-Zener Lindblad equation and work extraction from coherences". In: *Physical Review E* 99.4 (Apr. 26, 2019), p. 042142. ISSN: 2470-0045, 2470-0053. DOI: 10.1103/PhysRevE.99.042142. URL: https://link.aps.org/doi/10.1103/PhysRevE.99.042142 (visited on 08/27/2021).

[250] R. Sampaio et al. "Contributions to single-shot energy exchanges in open quantum systems". In: *Physical Review E* 99.6 (June 25, 2019), p. 062131. ISSN: 2470-0045, 2470-0053. DOI: 10.1103/PhysRevE.99.062131. URL: https://link.aps.org/doi/10.1103/PhysRevE.99.062131 (visited on 08/27/2021).

[251] Inbal Oz, Oded Hod, and Abraham Nitzan. "Evaluation of dynamical properties of open quantum systems using the driven Liouville-von Neumann approach: methodological considerations". In: *Molecular Physics* 117.15 (Aug. 18, 2019), pp. 2083–2096. ISSN: 0026-8976, 1362-3028. DOI: 10.1080/00268976.2019.1584338. URL: https://www.tandfonline.com/doi/full/10.1080/00268976.2019.1584338 (visited on 08/27/2021).

[252] Pengpeng Diao et al. "Shortcuts to adiabaticity in Fermi gases". In: *New Journal of Physics* 20.10 (Oct. 15, 2018), p. 105004. ISSN: 1367-2630. DOI: 10.1088/1367-2630/aae45e. URL: https://iopscience.iop.org/article/10.1088/1367-2630/aae45e (visited on 08/27/2021).

[253] Ayoti Patra and Christopher Jarzynski. "Shortcuts to adiabaticity using flow fields". In: *New Journal of Physics* 19.12 (Dec. 14, 2017), p. 125009. ISSN: 1367-2630. DOI: 10.1088/1367-2630/aa924c. URL: https://iopscience.iop.org/article/10.1088/1367-2630/aa924c (visited on 08/27/2021).

[254] Esteban Calzetta. "Not-quite-free shortcuts to adiabaticity". In: *Physical Review A* 98.3 (Sept. 12, 2018), p. 032107. ISSN: 2469-9926, 2469-9934. DOI: 10.1103/PhysRevA.98.032107. URL: https://link.aps.org/doi/10.1103/PhysRevA.98.032107 (visited on 08/27/2021).

[255] Antti O. Niskanen, Jukka P. Pekola, and Heikki Seppä. "Fast and Accurate Single-Island Charge Pump: Implementation of a Cooper Pair Pump". In: *Physical Review Letters* 91.17 (Oct. 24, 2003), p. 177003. ISSN: 0031-9007, 1079-7114. DOI: 10.1103/PhysRevLett.91.177003. URL: https://link.aps.org/doi/10.1103/PhysRevLett.91.177003 (visited on 02/17/2022).

[256] Mikko Möttönen, Juha J. Vartiainen, and Jukka P. Pekola. "Experimental Determination of the Berry Phase in a Superconducting Charge Pump". In: *Physical Review Letters* 100.17 (Apr. 28, 2008), p. 177201. ISSN: 0031-9007, 1079-7114. DOI: 10.1103/PhysRevLett.100.177201. URL: https://link.aps.org/doi/10.1103/PhysRevLett.100.177201 (visited on 09/11/2021).

[257] Nathanaël Cottet et al. "Observing a quantum Maxwell demon at work". In: *Proceedings of the National Academy of Sciences* 114.29 (July 18, 2017), pp. 7561–7564. ISSN: 0027-8424, 1091-6490. DOI: 10.1073/pnas.1704827114. URL: http://www.pnas.org/lookup/doi/10.1073/pnas.1704827114 (visited on 02/17/2022).

[258] Jorden Senior et al. "Heat rectification via a superconducting artificial atom". In: *Communications Physics* 3.1 (Dec. 2020), p. 40. ISSN: 2399-3650. DOI: 10.1038/s42005-020-0307-5. URL: http://www.nature.com/articles/s42005-020-0307-5 (visited on 02/17/2022).

[259] Rishabh Upadhyay et al. "Robust strong coupling architecture in circuit quantum electrodynamics". In: *arXiv:2107.11135 [cond-mat, physics:quant-ph]* (July 23, 2021). arXiv: 2107.11135. URL: http://arxiv.org/abs/2107.11135 (visited on 02/17/2022).

[260] Andrew Guthrie et al. "A Cooper-Pair Box Architecture for Cyclic Quantum Heat Engines". In: *arXiv:2109.03023 [cond-mat, physics:quant-ph]* (Sept. 7, 2021). arXiv: 2109.03023. URL: http://arxiv.org/abs/2109.03023 (visited on 02/17/2022).

[261] N. Ares et al. "Resonant Optomechanics with a Vibrating Carbon Nanotube and a Radio-Frequency Cavity". In: *Physical Review Letters* 117.17 (Oct. 21, 2016), p. 170801. ISSN: 0031-9007, 1079-7114. DOI: 10.1103/PhysRevLett.117.170801. URL: https://link.aps.org/doi/10.1103/PhysRevLett.117.170801 (visited on 02/17/2022).

[262] Roger Balian. *From Microphysics to Macrophysics*. Berlin, Heidelberg: Springer Berlin Heidelberg, 1991. ISBN: 978-3-662-21916-4 978-3-540-45475-5. DOI: 10.1007/978-3-540-45475-5. URL: http://link.springer.com/10.1007/978-3-540-45475-5 (visited on 02/12/2022).

[263] R. Kawai, J. M. R. Parrondo, and C. Van den Broeck. "Dissipation: The Phase-Space Perspective". In: *Physical Review Letters* 98.8 (Feb. 22, 2007), p. 080602. ISSN: 0031-9007, 1079-7114. DOI: 10.1103/PhysRevLett.98.080602. URL: https://link.aps.org/doi/10.1103/PhysRevLett.98.080602 (visited on 08/17/2021).

[264] Jordan Horowitz and Christopher Jarzynski. "Illustrative example of the relationship between dissipation and relative entropy". In: *Physical Review E* 79.2 (Feb. 5, 2009), p. 021106. ISSN: 1539-3755, 1550-2376. DOI: 10.1103/PhysRevE.79.021106. URL: https://link.aps.org/doi/10.1103/PhysRevE.79.021106 (visited on 08/17/2021).

[265] Massimiliano Esposito, Katja Lindenberg, and Christian Van den Broeck. "Entropy production as correlation between system and reservoir". In: *New Journal of Physics* 12.1 (Jan. 15, 2010), p. 013013. ISSN: 1367-2630. DOI: 10.1088/1367-2630/12/1/013013. URL: https://iopscience.iop.org/article/10.1088/1367-2630/12/1/013013 (visited on 08/17/2021).